OPTIMIZATION OF ENERGY EFFICIENCY OF AIR-COOLED CHILLERS USING WATER MIST PRE-COOLING

YANG JIA

Ph.D

The Hong Kong Polytechnic University

2013

OPTIMIZATION OF ENERGY EFFICIENCY OF AIR-COOLED CHILLERS USING WATER MIST PRE-COOLING

Yang Jia

A thesis submitted in partial fulfilment of the requirements for the Degree of Doctor of Philosophy

Department of Building Services Engineering

The Hong Kong Polytechnic University

April, 2012

Certificate of Originality

I hereby declare that this thesis is my own work and that, to the best of my knowledge and belief, it reproduces no material previously published or written nor material that has been accepted for the award of any other degree or diploma, except where due acknowledgement has been made in the text.

_____ (Signed)

Yang Jia _____ (Name of student)

Abstract

Air-cooled chillers are widely used to provide space cooling in air-conditioned buildings due to their flexibility. The operation of chillers usually takes up the highest proportion of the total electricity consumption of buildings. Low operational efficiency and undesirable control are part of the reasons for such high energy consumption. The deficient performance of air-cooled chillers is mainly due to the traditional head pressure control (HPC) under which the condensing temperature is kept high. To improve energy efficiency, chiller systems should be properly operated to meet the cooling load under external and internal conditions with the least energy consumption.

This research focuses on the optimal operation of water mist assisted air-cooled chillers under variable condensing temperature control (CTC), using numerical simulation, artificial neural network (ANN) and genetic algorithm (GA). The optimization problem is formulated and solved to find the optimal set point of condensing temperature and optimal water mist generation rate under various conditions with least chiller energy consumption. To achieve this objective, a combination of field investigation, experimentation and system simulation was conducted.

Field investigation was conducted to identify the operating characteristics and energy performance of two existing chiller plants with and without water mist pre-cooling. With the operating characteristics of the studied chillers, the thermodynamic models for the air-cooled chillers with twin refrigeration circuits with and without water mist system were developed using TRNSYS and validated using a wide range of operating data. With the validated model, simulation analyses were carried out to

determine viable energy saving measures for the chiller plant, including optimal circuit loading sequence (CLS), CTC, variable speed condenser fans (VSF) and water mist pre-cooling of the entering condenser air stream. In order to study the year-round energy consumption, representative office and hotel buildings and their air-conditioning systems were modeled using EnergyPlus. With the chiller models and the building models, the load-frequency and weather-load profiles of the buildings were established, and the energy savings potentials of individual and mixed uses of the measures were assessed.

Due to the complex nonlinear characteristics of chiller systems, this research presents an intelligent control technique, including neural networks and genetic algorithms, for the optimal control of the air-cooled chillers under various operating conditions. This control involves identifying the optimal set points of condensing temperature, condenser fans operation and the optimal water mist generation rate, which results in the least electricity consumption by the compressors and condenser fans. ANN is used to model the operation of air-cooled chillers, and GA is adopted in searching optimal set points of condensing temperature and optimal water mist generation rate based on the predicted fitness values. The results show that this control technique enabled optimal condensing temperature control successfully, and the chiller performance could be improved considerably, and its control performance is superior to the conventional control.

The main contribution to knowledge of this research is the development of an optimal operation method for water mist assisted air-cooled chillers under variable condensing temperature control, which is applicable to improve the energy efficiency of air-cooled chillers. This research also develops an artificial intelligent system based on the ANN and GA to simulate the chiller operation and find the optimal

solution for the optimal control of air-cooled chillers, aiming to provide a practical control technique for the chiller operation. Building services engineers will benefit from the results of this research on how to design and efficiently operate multiple air-cooled chillers with water mist system to cut down electricity bills. The results of this study will also be helpful for chiller manufacturers to apply variable condensing temperature control and artificial intelligent control in their development of more efficient chiller products.

List of Publications

Journal Papers

Yang J., Chan K.T., Wu X.S., et al. (2011), Experimental study on the air-cooled chiller with water mist, *Heating Ventilating & Air Conditioning*, 41(10, Supplement):180-184 (In Chinese).

Yang J., Chan K.T., Wu X.S., et al. (2012), Optimal control for screw chillers with multiple compressors, *Journal of Logistical Engineering University*, 28(1): 65-70 (In Chinese).

Yang J., Chan K.T., Wu X.S., et al. (2012). Performance enhancement of air-cooled chillers with water mist: Experimental and analytical investigation, *Applied Thermal Engineering,* 40: 114 -120.

Yang J., Chan K.T., Wu X.S., et al. (2012). An analysis on the energy efficiency of air-cooled chillers with water mist system, *Energy and Buildings,* 55: 273 -284.

Chan K.T., Yang J., Wu X.S., et al. Advanced control for air-cooled chillers with multiple compressors and twin refrigeration circuits (Manuscripts).

Yang J., Chan K.T., Wu X.S., et al. An intelligent control of condensing temperature for air-cooled chillers (Manuscripts).

Conference Papers

Yang, J., Chan, K.T., and Wu, X.S. (2008). Chiller load profile modeling using artificial neural networks, *9th International Symposium on Building and Urban Environmental Engineering*, Hong Kong.

Yang, J., Chan, K.T., and Wu, X.S. (2008). Development and analysis of the chiller model, *16th National Academic Conference on Heating, Ventilation, Air-Conditioning and Refrigeration*, Chongqing: 274 (In Chinese).

Yang J., Chan K.T., Wu X.S. (2009). Optimum operation of air-cooled chillers with multiple refrigeration circuits, *Proceedings - 6th International Symposium on Heating, Ventilating and Air Conditioning, ISHVAC 2009*, Vol. 1, Nanjing: 460-467.

Yang, J., Chan, K.T., and Wu, X.S. (2009). Application of water mist pre-cooling on air-cooled chillers," *Building Simulation 2009*, Glasgow, Scotland: 2204-2211.

Yang, J., Chan, K.T., and Wu, X.S. (2009). Improved chiller efficiency under condensing temperature control using neural network, *1st International Postgraduate Conference on Infrastructure and Environment*, Hong Kong: 23-30.

Yang, J., Chan, K.T., and Wu, X.S. (2010). Experimental studies of energy performance of air-cooled chillers with water mist system, *2nd International Postgraduate Conference on Infrastructure and Environment*, Hong Kong: 21-30.

Yang, J., Chan, K.T., and Wu, X.S. (2010). Modelling and analysis of air-cooled chillers with water mist system using neural networks, *the First International Conference on Sustainable Urbanization (ICSU)*, Hong Kong: 1871-1878.

Yang, J., Chan, K.T., and Wu, X.S. (2010). Modelling of chiller performance using artificial neural networks, *2010 International conference on information security and artificial intelligence*, Vol. 3, Chengdu, China: 419-422.

Yang, J., Chan, K.T., and Wu, X.S. (2010). Advanced condenser fans control for air-cooled chillers using neural networks, *Clima 2010,* Antalya, Turkey, Paper No.: R1-TS57-OP06 (Ref.0626).

Chan, K.T., Yu F.W. and Yang, J. (2010). Improving energy efficiency of air-cooled chillers with water mist, *The 10th International Symposium on Building and Urban Environmental Engineering (BUEE2010)*, Seoul, Korea: 39-45.

Chan, K.T., Yang, J., and Yu F.W. (2011). Energy performance of chillers with water mist assisted air-cooled condensers. *Building simulation 2011*. Sydney, Australia: 2088-2095.

Acknowledgements

I would like to express my sincere gratitude and profound respect to my chief supervisor, Prof. Chan Kwok Tai, for his valuable and constructive suggestions, guidance and encouragement throughout this research work, and to my co-supervisor, Prof. Wu Xiangsheng, for his encouragement and valuable comments.

I would like to thank Dr. Yu Fu Wing, for his help and valuable recommendations and comments for the chiller model development.

I would also like to acknowledge the financial support from the central research grant of the Hong Kong Polytechnic University.

My grateful thanks are extended to the staff of the Facility Management Office at The Hong Kong Polytechnic University for helping me to set up the experiment on the chillers with water mist pre-cooling and to collect the chiller plant data.

I am thankful to my friends and colleagues for their support and inspiration. Finally, I would like to extend special thanks to my family for their great love and encouragement.

Table of Contents

Certificate of Originality ..... **I**

Abstract ..... **II**

List of Publications ..... **V**

Acknowledgements ..... **VII**

Table of Contents ..... **VIII**

List of Figures ..... **XII**

List of Tables ..... **XVII**

Nomenclature ..... **XIX**

Chapter 1 Introduction **1**

1.1 Background *1*

1.2 Optimal control for air-cooled chillers *7*

1.2.1 Optimal control method 8

1.2.2 Optimization techniques 10

1.3 Aim, objectives and scope of works *12*

1.3.1 Aim and objectives 12

1.3.2 Scope of works 12

1.4 Organization of the Thesis *13*

Chapter 2 Literature Review **16**

2.1 State-of-the-art technologies for air-cooled chillers *16*

2.1.1 Variable condensing temperature control 16

2.1.2 Variable speed control of condenser fans 21

2.1.3 Evaporative cooling for air-cooled condensers 23

2.2 Artificial neural networks *25*

2.2.1 Artificial neural network architectures 26

2.2.2 Learning methods in neural networks 29

2.2.3 Back-propagation ANNs 33

2.2.4 Development of ANN models 36

2.2.4.1 Selection of input and output variables 38

2.2.4.2 Data pre-processing 39

2.2.4.3 Selection of BP algorithm 41

2.2.4.4 Optimization of the ANN structure 41

2.2.5 Performance of the neural network 44

2.3 Genetic algorithm *46*

2.3.1 GA procedure 48
2.3.2 Elements of the genetic algorithm 50

2.4 Hybrid artificial neural networks-genetic algorithms technique 56

Chapter 3 Building System and Simulation Platform 60

3.1 Building and system description 60
3.1.1 Description of generic reference buildings 61
3.1.2 Zones and system description 64

3.2 Development of the simulation platform 67
3.2.1 EnegyPlus and its applications 67
3.2.2 Building modelling 70
3.2.3 Cooling load profile of office and hotel buildings 71

3.3 Summary 76

Chapter 4 Modelling and Simulation of Chiller Systems 77

4.1 Field investigation into the performance of chilled water plants 77
4.1.1 Description of the buildings studied and their chiller plants 77
4.1.2 Evaluation of operating variables 81

4.2 Modelling and simulation of the chilled water plant 82
4.2.1 Chiller model 87
4.2.2 Condenser fans control 94
4.2.2.1 Control algorithm of constant speed condenser fans 96
4.2.2.2 Control algorithm of variable speed condenser fans 98
4.2.2.3 Control of condenser fans under CTC 99
4.2.3 Procedure to evaluate operating variables of the model chiller 101
4.2.4 Model validation 107

4.3 Chiller COP with various set points of condensing temperature 109

4.4 Optimum set points of condensing temperature 113

4.5 Chiller COP under four strategies 116
4.5.1 Chiller COP 117
4.5.2 COP Improvements 119

4.6 Optimal load sharing between refrigeration circuits 122
4.6.1 Circuit loading sequence 122
4.6.1.1 Constant speed fan control 123
4.6.1.2 Variable speed fan control 126
4.6.2 Potential benefits from optimal circuit loading sequence 128

4.7 Summary 129

Chapter 5 Experimental and Simulation Study on Water Mist System 131

5.1 Description of water mist system 131

5.2 Description of studied chiller coupling water mist 133

5.3 Experimental study of the chiller with water mist system 136
5.3.1 Experiment setup and data acquisition 136
5.3.2 Experiment results analysis 139
5.3.2.1 Temperature drop 139
5.3.2.2 Condensing temperature 142

5.3.2.3 Thermal Effectiveness 144
5.3.2.4 Chiller COP 147
5.3.2.5 Water consumption 150

5.4 Integrated chiller model with water mist 151
5.4.1 Water mist system model 151
5.4.2 Integrated chiller model 154
5.4.3 Validation of the integrated chiller model 157

5.5 Performance of the chiller with HPC and mist pre-cooling 159
5.5.1 Thermal properties of air entering the condenser 161
5.5.2 Condensing temperature 162
5.5.3 Chiller COP 165

5.6 Effect of mist pre-cooling on the chiller with variable speed condenser fans 168
5.6.1 Thermal properties of air entering the condenser 170
5.6.2 Condensing temperature 171
5.6.3 Chiller COP 174

5.7 Improved chiller COP with CTC and water mist 176
5.7.1 Optimal set point of condensing temperature 176
5.7.2 Improved chiller COP with enhanced condenser features 183

5.8 Energy savings of enhanced condenser features 191

5.9 Evaluation of chiller energy saving potential in the local building sector 198

5.10 Summary 202

Chapter 6 Neural Network Based Optimal Control of Air-Cooled Chillers 203

6.1 Optimization method 204
6.1.1 Formulation of optimization problem 205
6.1.2 Process of the hybrid ANN–GA optimization algorithm 206

6.2 Optimization case studies 207
6.2.1 CTC with VSF 209
6.2.1.1 Neural network construction 209
6.2.1.2 Performance analysis of MLP neural network 214
6.2.1.3 Formulation of optimization problem 220
6.2.1.4 Optimization results by GA 221
6.2.1.5 Verification of the optimization result 223
6.2.2 CTC with VSF and optimal waster mist 225
6.2.2.1 Neural network construction 225
6.2.2.2 Performance analysis of MLP neural network 227
6.2.2.3 Formulation of optimization problem 230
6.2.2.4 Optimization results by GA 231
6.2.2.5 Verification of the optimization result 233

6.3 Sensitivity analysis 235

6.4 Summary 238

Chapter 7 Conclusions and Recommendations 240

7.1 Conclusions 240

7.2 Recommendations 244

Appendix A - Chiller Model under HPC 246

Appendix B - Chiller Model under CTC with Water Mist Pre-cooling..... 258

References 275

List of Figures

Figure 2.1 Multilayer feed-forward neural network 28
Figure 2.2 Recurrent neural network 28
Figure 2.3 Block diagram of learning with a teacher 30
Figure 2.4 Block diagram of reinforcement learning 32
Figure 2.5 Block diagram of unsupervised learning 32
Figure 2.6 Classification of learning algorithms 33
Figure 2.7 Two basic signal flows in a MFNN: forward propagation of function signals and back-propagation of error signals 34
Figure 2.8 ANN design flow process 38
Figure 2.9 Neural network with a pre-processing and post-processing block 40
Figure 2.10 Selection of optimum network architecture 43
Figure 2.11 A basic genetic algorithm 49
Figure 2.12 Chromosomal representation 51
Figure 2.13 Roulette wheel selection 53
Figure 2.14 Two point crossover of binary strings 54
Figure 2.15 Mutation 55
Figure 2.16 Optimization strategy 59
Figure 3.1 Typical floor plan and thermal zones of the office building 62
Figure 3.2 Hotel configuration 63
Figure 3.3 Floor plan and thermal zones of the tower block and podium block 63
Figure 3.4 Zoning arrangements in the hotel building (plan view) 65
Figure 3.5 3D view of office building and hotel building model 70
Figure 3.6 Weather load profile of the representative office building 72
Figure 3.7 Weather load profile of the representative hotel building 73
Figure 4.1 Schematic of the chiller system 78
Figure 4.2 A photo of the studied chiller 78
Figure 4.3 Graphical screen of the chiller plant 80
Figure 4.4 Flow diagram of modelling the chiller under TRNSYS 85
Figure 4.5 Vapour compression cycle of the model chiller 86
Figure 4.6 Schematic of the air-cooled chiller 87
Figure 4.7 Flow chart of the chiller model with constant speed fans under HPC 104

Figure 4.8 Flow chart of the chiller model with variable speed fans under HPC 105
Figure 4.9 Flow chart of the chiller model with constant speed fans under CTC.... 106
Figure 4.10 Flow chart of the chiller model with variable speed fans under CTC .. 107
Figure 4.11 Comparison between the modelled and measured chiller COP..... 108
Figure 4.12 Variations in chiller COP with the set points of condensing temperature for chillers using constant speed condenser fans under different outdoor temperature 111
Figure 4.13 Variations in chiller COP with the set points of condensing temperature for chillers using variable speed condenser fans under different outdoor temperature 112
Figure 4.14 Variations in the optimum set point of condensing temperature ($T_{cdsp,op}$)..... 115
Figure 4.15 Variations in the difference between the optimum set point of condensing temperature ($T_{cdsp,op}$) and the outdoor temperature (T_{db}).. 115
Figure 4.16 COP percentage change compared with the algorithm of Eq.(4.55) 116
Figure 4.17 Chiller COP curves for four strategies of condenser fan control..... 119
Figure 4.18 Percentage change in chiller COP under HPC with variable speed condenser fans..... 120
Figure 4.19 Percentage change in chiller COP under CTC with constant speed condenser fans..... 121
Figure 4.20 Percentage change in chiller COP under CTC with variable speed condenser fans..... 122
Figure 4.21 Percentage change of chiller COP relative to CSF1 under different CLSs 125
Figure 4.22 Percentage change of chiller COP relative to VSF1 under different CLSs 127
Figure 5.1 Schematic of the water mist system..... 132
Figure 5.2 Vapour compression cycle of the refrigeration circuit 132
Figure 5.3 Arrangement of the chilled water system 134
Figure 5.4 Graphic interface of the chiller monitor system 134
Figure 5.5 Schematic of the air-cooled chiller 135
Figure 5.6 Photograph of the water mist system with data loggers 138
Figure 5.7 Data loggers for the experiments..... 138
Figure 5.8 Psychrometric chart for evaporative cooling process..... 141

Figure 5.9 Impact of ambient air WBD on temperature change of entering condenser air due to water mist pre-cooling 141
Figure 5.10 Change in refrigerant condensing temperature (ΔT) due to water mist pre-cooling at part load ratios of 0.4–0.5 (Circuit 2) 144
Figure 5.11 Change in refrigerant condensing temperature (ΔT) due to water mist pre-cooling at part load ratios of 0.9–1.0 144
Figure 5.12 Variation of approach temperature with thermal effectiveness 146
Figure 5.13 Chiller COP percentage change at various conditions due to water mist pre-cooling 150
Figure 5.14 Flow chart of the water mist model 154
Figure 5.15 Flow chart of the chiller model with water mist and CSF under HPC . 156
Figure 5.16 Comparison between the modeled and measured chiller COP 157
Figure 5.17 Comparison between the modeled and measured DBT and RH of entering condenser air 158
Figure 5.18 Procedure for evaluating optimal water mist generation rate 160
Figure 5.19 Chiller performance curves for scheme CS1 161
Figure 5.20 Temperature change of air entering the condenser for scheme CS2 162
Figure 5.21 Condensing temperature change for scheme CS2 164
Figure 5.22 Condensing temperature change for scheme CS3 165
Figure 5.23 Chiller COP change for scheme CS2 167
Figure 5.24 Chiller COP change for scheme CS3 168
Figure 5.25 Chiller performance curves for scheme VS1 169
Figure 5.26 Temperature change of air entering the condenser for scheme VS2 171
Figure 5.27 Condensing temperature change for scheme VS2 172
Figure 5.28 Condensing temperature change for scheme VS3 173
Figure 5.29 Fan speed change for scheme VS2 173
Figure 5.30 Fan speed change for scheme VS3 174
Figure 5.31 COP change for scheme VS2 175
Figure 5.32 COP change for scheme VS3 175
Figure 5.33 Variations in the $T_{cdsp,op}$ with designed water mist generation rate and CSF 178
Figure 5.34 Variations in the difference between $T_{cdsp,op}$ and the outdoor WBT with designed water mist generation rate and CSF 178

Figure 5.35 Variations in the optimum set point of condensing temperature ($T_{cdsp,op}$) with designed water mist generation rate and VSF 180
Figure 5.36 Variations in the $T_{cdsp,op}$ with optimal water mist generation rate and VSF 180
Figure 5.37 Variations in the difference between $T_{cdsp,op}$ and the outdoor WBT with designed water mist generation rate andVSF 182
Figure 5.38 Variations in the difference between $T_{cdsp,op}$ and the outdoor WBT with optimal water mist generation rate and VSF 182
Figure 5.39 COP curves of the chiller with different control strategies 185
Figure 5.40 Percentage change in chiller COP under various conditions in relation to the HPC case (RH=50%) 189
Figure 5.41 Percentage change in chiller COP under various conditions in relation to the HPC case (RH=80%) 190
Figure 5.42 Schedule of staging chillers in the office building 192
Figure 5.43 Schedule of staging chillers in the hotel building..... 192
Figure 5.44 Monthly total electricity consumption of chillers serving the typical buildings with each condenser feature 194
Figure 5.45 Variation of chiller COP in reference buildings 195
Figure 5.46 Variation of the total stock of offices in Hong Kong ($\times 10^3$ m^2)..... 201
Figure 6.1 Hybrid intelligent control using ANN and GA 205
Figure 6.2 Flowchart of optimization scheme based on combined ANN-GA algorithm 207
Figure 6.3 ANN architecture for Case 1 210
Figure 6.4 The networks performance MSE against neurons in the hidden layer .. 214
Figure 6.5 The converging trends of training, validation and testing subsets..... 216
Figure 6.6 Training state of the ANN model 217
Figure 6.7 Performance of the ANN model (Case 1)..... 218
Figure 6.8 Comparison of ANN modeled and TRNSYS simulated values for Case 1 219
Figure 6.9 The convergence curve of the GA search for case 1 225
Figure 6.10 ANN architecture for Case 2 227
Figure 6.11 Convergence of training, validation and testing subsets for Case 2 228
Figure 6.12 Training state of the ANN model for Case 2 228
Figure 6.13 Performance of the ANN model (Case 2)..... 229

Figure 6.14 Comparison of ANN modeled and TRNSYS simulated values for Case 2 230
Figure 6.15 The convergence curve of the GA search for case 2 233
Figure 6.16 Sensitivity influence coefficients..... 238

List of Tables

Table 3.1 Basic characteristics and design criteria of office and hotel examples..... 64
Table 3.2 Construction of fabric and internal structure of the office building 66
Table 3.3 Construction of fabric and internal structure of the hotel building..... 67
Table 3.4 Occupancy density, lighting load profiles and operating schedule of ventilating fans in the office building 68
Table 3.5 Occupancy density, lighting and equipment load profiles and the operating schedule of ventilating fans of guestrooms in the hotel building 69
Table 3.6 Occupancy density, lighting and equipment load profiles and the operating schedule of ventilating fans of shops and restaurants in the hotel building 69
Table 3.7 Frequency distribution of hourly office building cooling loads 71
Table 3.8 Frequency distribution of hourly hotel building cooling loads..... 72
Table 3.9 Frequency distribution of the hourly data of chiller loads (Hotel) 74
Table 3.10 Frequency distribution of the hourly data of chiller loads (Office building)..... 75
Table 4.1 Details of the chiller model..... 79
Table 4.2 Error analysis of operating variables 82
Table 4.3 Operating schemes for the chiller with constant speed fans 124
Table 4.4 Operating schemes for the chiller with variable speed fans..... 126
Table 4.5 Energy performance of chillers under different control strategies 129
Table 5.1 Details of the chiller model..... 135
Table 5.2 Case study of individual and mixed condenser features..... 183
Table 5.3 Energy performance of chillers under different control strategies (Office)..... 197
Table 5.4 Energy performance of chillers under different control strategies (Hotel) 197
Table 5.5 Summary of energy use of office buildings from 1985 to 2009 199
Table 5.6 Electricity savings of air-cooled chillers in new offices and hotels due to improved condenser features in 2012-2016 202
Table 6.1 Comparison of the candidate network structures..... 213
Table 6.2 Comparison of ANN-GA with TRNSYS results (Case 1)..... 224
Table 6.3 Comparison of ANN-GA with TRNSYS results (Case 2)..... 234

Table 6.4 Variable list and input ranges for sensitivity analysis and IC (PLR=1). . 237
Table 6.5 Variable list and input ranges for sensitivity analysis and IC (PLR=0.3). 237

Nomenclature

AU	overall heat transfer coefficient, kW/°C
BCL	building cooling load, kW
COP	coefficient of performance of chiller
CR	compression ratio
CTC	variable condensing temperature control
C_{pa}	specific heat capacity of air, assumed to be 1.02 kJ/(kg·K)
C_{pw}	specific heat capacity of water, assumed to be 4.19 kJ/(kg·K)
C_{prg}	specific heat capacity of vapour refrigerant at evaporator, kJ/(kg·K)
C_{prl}	specific heat capacity of liquid refrigerant at condenser, kJ/(kg·K)
E	power input, kW
$E_{cf,ea}$	rated power of one condenser fan, kW
HPC	traditional head pressure control
h_i	specific enthalpy of refrigerant at state "i" (state 1: compressor suction; state 2: compressor discharge; state 3: condenser discharge or expansion valve inlet; state 4: expansion valve outlet or evaporator suction), kJ/kg
K_{ex}	charateristic constant of expansion valve
LMTD	log mean temperature difference, °C
m_r	refrigerant mass flow per compressor, kg/s
m_w	mass flow rate of chilled water, kg/s
N_{cc}	number of staged compressors
N_{cf}	number of staged condenser fans
N_{ch}	number of staged chillers
n_i	index of reversible polytropic expansion
P	saturated refrigerant pressure of the refrigeration circuit, kPa

PLR	chiller part load ratio, given by Q_{cl}/Q_{cr}
Q_{cd}	heat rejection, kW
Q_{cl}	cooling capacity, kW
Q_{cr}	nominal cooling capacity, kW
q_{rf}	refrigeration effect, kJ/kg
R_{cf}	rotating speed of staged condenser fans, rps
R_{cfr}	full speed of condenser fans, rps
R^2	coefficient of determination
RMSE	absolute root-mean-square error
T	temperature of saturated refrigerant within the refrigeration circuit, °C
T_{cdae}	temperature of air entering the condenser or outdoor temperature, °C
T_{cdal}	temperature of air leaving the condenser, °C
T_{cdsc}	degree of subcooling, °C
T_{cdsp}	set point of condensing temperature, °C
T_{chwr}	temperature of return chilled water, °C
T_{chws}	temperature of supply chilled water, °C
T_{evsh}	degree of superheat, °C
T_{db}	dry-bulb temperature of the ambient air, °C
T_{wb}	wet-bulb temperature of the ambient air, °C
V_a	airflow provided by staged condenser fans, m^3/s
V_{ar}	rated airflow of a variable speed condenser fan, m^3/s
V_{vd}	volumetric displacement of each compressor, m^3/s
v_r	specific volume of refrigerant at compressor suction, m^3/kg
v_1,	specific volume of saturated vapour refrigerant at evaporator, m^3/kg
w_{in}	isentropic work input to compressor, kJ/kg
η_{isen}	isentropic efficiency

η_{cc}	combined motor and transmission efficiency
η_{ec}	cooling effectiveness of an water mist system
η_v	volumetric efficiency
ρ_a	air density, kg/m^3
δW_a	addition of humidity ratio, kg/(kg dry air)
h	specific enthalpy of the moist air, kJ/(kg dry air)
φ	relative humidity
μ	degree of saturation
W	air humidity ratio, kg/(kg dry air)

Subscripts

cc	compressor
cd	condenser
cf	condenser fan
ch	chiller
ev	evaporator
max	maximum
op	optimum
tot	total
pump	high pressure pump
s	saturation water vapor
w	water vapor
1	circuit 1 of the chiller
2	circuit 2 of the chiller
11	first section of evaporator of refrigeration circuit 1
12	second section of evaporator of refrigeration circuit 1

Chapter 1 Introduction

This chapter provides background information about the operation and energy performance of air-cooled chillers in chilled water systems, presents a review of the optimization techniques and outlines the aims and objectives of this study. The air-cooled chillers are regarded as energy inefficient due to the conventional head pressure control (HPC), and variable condensing temperature control (CTC) is proposed as an alternative for HPC to improve chiller efficiency. This study aims to develop an optimum operating strategy with variable condensing temperature control and water mist pre-cooling to improve the coefficient of performance (COP) of air-cooled chillers.

1.1 Background

There have been growing concerns about energy consumption and its implications for the environment and the ecosystem. With high economic growth, Hong Kong has seen a dramatic increase in energy consumption in recent years, particularly electricity use in commercial and residential buildings. It was found that the local building stocks accounted for nearly half of the total primary energy requirement (Lam, Li et al. 2003), and buildings worldwide shared a substantial responsibility for the greenhouse gases emissions consequent to electricity generation (Yik, Burnett et al. 2001). For modern cities in the tropical and sub-tropical regions, air-conditioning systems are the dominant consumer of energy in buildings, and the energy consumption of air-conditioning systems accounts for nearly 60% of the total annual electricity for office buildings (Lam 2000) and 30-50% of the total annual electricity for hotel buildings (Deng and Burnett 2000; Yu and Chan 2005a). Chillers are the vital part in a central air conditioning system, which are commonly used for

providing cooling energy in the form of chilled water in most commercial buildings. Chillers consume about 60% of the total annual electricity use for air-conditioning systems (Lam 2000; Yik, Burnett et al. 2001; Yu and Chan 2005a). Therefore, chiller systems play a significant role in the building energy savings, and this underlines the opportunity to take energy efficiency measures for chillers to reduce the electricity consumption of commercial buildings.

The energy performance of chillers is of paramount concern in respect of building energy efficiency. It hinges on the heat rejection process in which the refrigerant rejects heat to condensing media. There are three major types of liquid chillers, including air-cooled chillers, water-cooled chillers and evaporative cooled chillers. Air-cooled chillers make use of ambient air as the condensing medium, while water-cooled chillers use fresh water or sea water for heat rejections. Considering the constraints on using fresh water and sea water, air-cooled chillers are commonly installed in local commercial buildings (Lam 2000; Yik 2001). Although the government intends to widen the application of cooling towers in air-conditioning systems for energy efficiency (EMSD 2008), there are arguments why air-cooled chillers should not be phased out. As far as the medium of heat rejection is concerned, outdoor air is free, unlimited and readily available. Fresh water is a scarce resource, and sea water is not readily available except for buildings close to the sea. The operation of water-cooled chillers with cooling towers hinges on the availability of water supply and the treatment of fresh water. It may be feasible to implement water cooling systems in new commercial buildings, accounting for a small percentage of the building stock. However, in most cases, it is difficult or even impossible to retrofit the existing air-cooled chiller plants with water-cooled chillers, as there is a problem of finding spaces for installing cooling towers and their auxiliary equipment in existing buildings. Therefore, air-cooled chillers should not be phased out. The

popularity of air-cooled chillers also is due to the ease of installation, the simplicity of operation and maintenance, and the lower installation and maintenance costs as compared to water-cooled chillers (Yip and Hui 1991; Zhang, You et al. 2000).

Water-cooled chillers normally have an efficiency advantage over air-cooled chillers. At the full load condition, the coefficient of performance (COP) of air-cooled chillers is 2.4–4.2 while that of water-cooled chillers is usually well above 4.2. Their difference in COP is primarily associated with the fact that air-cooled chillers and water-cooled chillers have different levels of condensing temperature due to different temperatures of the heat rejection mediums (air or water), and water-cooled chillers can take advantage of lower condensing temperatures than air-cooled chillers. As to water-cooled chillers, the temperature of supply condenser water is designed to be 29°C along with a condensing temperature of 40°C (Dossat and Horan 2002), and the condensing temperature tends to drop considerably at part load conditions. Air-cooled chillers, by contrast, are designed with an 11–14°C difference between condensing temperature and ambient air temperature (ARI 1998). In Hong Kong, air-cooled chillers are designed to operate at an outdoor temperature of 35°C due to the hot summers. The deficient performance of air-cooled chillers is mainly due to the traditional head pressure control (HPC), whereby minimal condenser fans are staged to control the condensing temperature to float around a high set point of 50°C. Using a high set point of condensing temperature calls for lower heat rejection airflow and hence the least fan power, but the compressor power is kept high. This control cannot bring about maximum chiller COP under part load conditions with moderate outdoor temperatures. The use of HPC is also due to a convention that the proper function of thermostatic expansion valves needs a high pressure differential of at least 690 kPa to control refrigerant flow properly. The use of electronic expansion valves enables the

required differential pressure to be as low as 290 kPa for ensuring compressor lubrication (Yu, Chan et al. 2006).

As far as medium sized chillers are concerned, each includes a shell-and-tube type evaporator, single or multiple compressors, and an air-cooled condenser with multiple fans. Each chiller also comprises one or more refrigeration circuits and for each circuit, there is one expansion valve of either the thermostatic or electronic type to regulate refrigerant fed into the evaporator. Each chiller contains a microprocessor to control the staging of compressors and condenser fans. The chillers operate typically under traditional head pressure control, which causes a considerable decrease in COP when the chiller operates under part load conditions. Considering that chillers tend to operate frequently at part load to meet the changing building cooling load (Browne and Bansal 1998; Browne and Bansal 2001b; Roper 2000), improving their part load performance is vital for building energy efficiency (Chow and Chan 1995; Lee and Yik 2002).

As HPC is regarded as energy inefficient, variable condensing temperature control (CTC) is proposed as an alternative to HPC to lower the condensing temperature for air-cooled chillers (Manske, Reindl et al. 2001; Yu and Chan 2006b). Under CTC, the condenser fans are staged as many as possible in most operating conditions to enhance the heat rejection airflow to decrease the condensing temperature, allowing the condensing temperature to approach its lower boundary. This causes an increase in the fan power, but the compressor power can be minimized. There is a trade off between the compressor's operation at lower discharge pressures and additional condenser fan energy consumption. CTC can minimize the sum of compressor power and condenser fan power for all operating conditions, and hence the chiller COP is improved. Since there may be many control settings that meet these environmental

requirements, there exists an opportunity to find a set of optimal control settings that minimize energy costs. However, optimizing the trade-off between a compressor's reduced power consumption and additional condenser fan energy consumption at lower head pressures has been a challenge. Considering that air-cooled chillers are still popular in many buildings in subtropical regions, it is crucial to improve their COP through enhancing the design and operation of their condensers, and investigate how the condensing temperature can be better controlled in order to minimize the sum of compressor power and condenser fan power to maximize the chiller COP.

Over the last decades, there has been considerable amount of interest in developing effective building operation strategies to achieve maximum energy savings. Various optimal or near-optimal operating strategies have been investigated for different types of heating, ventilating, and air conditioning (HVAC) systems. The HVAC system is a complicated, nonlinear and discrete system involving many strongly coupled subsystems and numerous constrains. Therefore, it poses a big challenge for system modelling and optimization (Kusiak and Li 2010). The conventional methodologies for optimal control of the chiller system are studied by using a mathematical model or experimental practices. Although some mathematical models and empirical methods related to central cooling plant had been developed, but the analyses of the research on chiller optimization encountered complex thermodynamic phenomena and relied on a series of simplifying assumptions. The mathematical methods and/or empirical methods may not describe the system well, and they cannot handle a complex system with high noise, external disturbance and high nonlinearity. In addition, these models need a robust numerical solver and are time-consuming to solve, which is not suitable for optimization and process control.

To alleviate the drawbacks, an alternative method needs to be developed and applied in order to predict the results and to find the optimal values for the controllable variables. Artificial intelligence (AI) is appropriate for such complex and ill-defined problems as an alternative approach to conventional techniques. AI is the use of computers to emulate the reasoning and decision-making processes of humans. AI techniques emerged as a computer science discipline in the mid 1950s, and there is recently a growing interest in the application of AI techniques in various areas, such as engineering (Chan and Huang 2003; Peng, Zhang et al. 2010; Pham and Pham 1999), building (Dounis 2010), renewable energy system (Mellit, Kalogirou et al. 2009), HVAC system (Nguyen and Chan 2006), supervisory control (Uraikul, Chan et al. 2007), particularly in areas with huge amounts of data but very little theory. Numerous applications of AI techniques have been shown to be effective in decision making and optimization. AI systems comprise of five major branches, i.e. expert systems (ES), artificial neural networks (ANNs), genetic algorithms (GAs), fuzzy logic (FL) and various hybrid systems, which are combinations of two or more of the branches mentioned previously (Kalogirou 2003).

Despite convincing results in many areas, little has been done using neural networks to model the air-cooled chiller under CTC. The chiller system is a complex, nonlinear, discrete system involving numerous constrains. Therefore, it poses a big challenge for system modelling and optimization. Unlike many studies are centered on mathematical models and simulation approaches, this research presents AI techniques for chiller model and control.

As chiller operation causes an upward trend in electricity use for the increasing number of buildings in Hong Kong, it is essential to develop better plant controls for efficient operation of cooling plant. The long-term significance of this project rests

on its contribution to energy conservation in the building sector of Hong Kong. The outcome is a method of optimal operation for water mist assisted air-cooled chillers under variable condensing temperature control, using AI techniques on the optimum set point of condensing temperature and load sharing strategies at part load conditions.

1.2 Optimal control for air-cooled chillers

Optimization is a scientific area that offers a wide variety of methods with great potential for the solution of complicated decision problems (Diakaki, Grigoroudis et al. 2008). The difference between normal operation and optimal operation is that in optimal operation, the system is controlled to minimize or maximize the cost function while satisfying certain physical constraints, which is a function of controlled and uncontrolled variables(Ning and Zaheeruddin 2010). The optimal control for chiller plants is to determine the optimal operation mode and set points that minimize overall system energy consumption or operating cost while still meeting the building cooling load. For the chiller system, the uncontrolled variables are those such as the chiller load, ambient air conditions. Control variables include the continuous control variables and discrete control variables that are set points and operating mode minimizing the total system cost. The continuous control variables are those, such as chilled water temperature, chilled water flow rate, and set point of condensing temperature, which can vary continuously over the control range. The discrete control variables are those that have discrete settings, such as high and low fan speed, the number of operating chillers, and the number of operating condenser fans.

1.2.1 Optimal control method

The optimization algorithm is a numerical method for finding the values of the optimal solutions, and it is common to apply a suitable simulation–optimization technique to model the system to determine the required operation parameters. It comprises of two sections: control methods and optimization techniques. The control methods can simulate or properly predict the behavior of complex systems, and the optimization techniques are used to find optimal control solutions for a system. The optimal control in HVAC systems can be divided into four categories, including model-based supervisory control method, hybrid supervisory control method, performance map-based supervisory control method, and model-free supervisory control method (Wang and Ma 2008). The selection of the control methods for an optimal control application is crucial to the development of an effective control strategy.

Model-free supervisory control methods, including expert systems and reinforcement learning approach, do not require a "model" of the targeted system. Expert systems can imitate human reasoning to make decisions and deduce the reasonable solutions for a given working condition, and reinforcement learning approach can be applied to find the optimal or near-optimal solutions for the control problem without any prior knowledge of the environment. However, model-free supervisory control depends on the richness of the knowledge database, and it takes a long time for the controllers to learn. These features hinder the implement of model-free supervisory control in practice (Henze and Schoenmann 2003; Liu and Henze 2006).

According to the knowledge of the system utilized to formulate the models, the model-based supervisory control can be further divided into three groups: physical model-based supervisory control, gray-box model-based supervisory control, and

black-box model-based supervisory control (Wang and Ma 2008). Physical model-based supervisory control is based on fundamental laws of energy, mass, heat transfer, momentum, and flow balance, etc., and a set of mathematical equations can be derived and solved. Generally, physical models have excellent performance in prediction and high control reliabilities since the basic assumptions and physical laws utilized in the model development are effective and valid within the allowed working conditions. However, most physical models are rather complicated, and an iteration process is always required. These characteristics may seriously prevent their online optimal control. Considering the drawbacks of the physical models, gray-box models consisting of a combination of empirical and physical models are commonly employed for the chiller system (Browne and Bansal 1998; Ding 2007). The main advantages of gray-box models are that the complexity and computational requirements to achieve the optimal solutions are reduced greatly; however, gray-box models strongly depend on the richness of data used to train the models.

Black-box models are composed entirely of empirical models and therefore do not generally utilize parameters that have physical meaning. Typical black-box models are polynomial curve fits and artificial neural networks (ANNs). Black-box models are simple enough without requiring the detailed physical knowledge of the system, and they do not generally utilize parameters that have physical meaning. They can map the performance of a tested system, and provide very fast execution speeds compared to gray or physical models. As a result, black-box models are generally utilized in system simulation programs (Reddy and Andersen 2002; Swider 2003). The accuracy of these models depends on the size of data used to train the models. Artificial neural networks are capable of powerful universal function approximation (Haider and Zeng 2009; Iannella and Back 2001; Maass 1997; Shin 1998). Theoretically, an ANN model with a proper configuration is able to map any

complicated functional relationship between dependent and independent variables without the need for a preconceived function form and prior knowledge of the regularities in the data. ANNs can generalize from previous examples and modify their behaviour in response to the environment. Recently, ANN models have demonstrated advantages over the traditional methods (Bechtler, Browne et al. 2001a; Chow, Zhang et al. 2002; Hosoz and Ertunc 2006; Hosoz, Ertunc et al. 2008; Swider, Browne et al. 2001; Wu, Zhang et al. 2011). The excellent capability of ANNs in function approximation inspired the development of ANN-based function approximation of chiller models in this study, identifying the functional mapping between specific outputs and controllable and non-controllable inputs of the chillers.

1.2.2 Optimization techniques

When the appropriate optimal control method is selected, the method used for finding the optimal control variables is equally important in realizing the optimal control strategy. Many optimization techniques have been developed in the past decades, and they could be summarized into two categorizes: linear optimization techniques and nonlinear optimization techniques (Wang and Ma 2008). The linear optimization technique is the most simple and straightforward technique, including direct search methods (Wright and Hanby 1987; Yao and Chen 2010), gradient-based methods (Chang, Chan et al. 2010; Ilhan 2012).

As the optimization problems related to optimal control of HVAC systems are often complicated, nonlinear and discrete system should be utilized to deal with such problems. Nonlinear optimization techniques are more complex and sophisticated than linear optimization techniques, and they can be further subdivided into two categories, including nonlinear local optimization techniques and nonlinear global optimization techniques (Wang and Ma 2008). Nonlinear local optimization

techniques include direct search techniques, gradient-based optimization techniques, etc. Nonlinear global optimization techniques include simulated annealing, branch and bound, evolutionary algorithm (EA), tabu search, etc. Evolutionary algorithms include evolution strategy (ES), evolutionary programming (EP), genetic algorithm (GA), and genetic programming (GP). Gradient-based optimization techniques are effective in search for the optimum for a particular and simple optimization problem, but they would likely get trapped at the local optimal values, and the convergence speed is strongly dependent on the initial guess of optimal variables (Wang and Jin 2000). To overcome this shortcoming, nonlinear global optimization techniques should be applied for the nonlinear and complicated optimization problems in HVAC systems. Global optimization techniques depend on heuristic methods rather than derivatives to search for the optimal solutions, and they can explore the overall search space and can avoid to get trapped at the local optimal values. EA has been found to be more advantageous over the traditional and other heuristic methods for HVAC optimization problems (Fong, Hanby et al. 2009). Among all of these optimization techniques, GA is more attractive than other optimization algorithms. GA is a result-based method, and no derivatives are required during the calculation since it is independent of the function gradient. In addition, GA has implicit parallel computation features, which make it more efficient than the exhaustive search methods. These features make it feasible to solve the complicated and global optimization problems, and GA has been widely used in building thermal system (Wright, Loosemore et al. 2002), control of HVAC system (Chow, Zhang et al. 2002; Huang and Lam 1997; Lu, Cai et al. 2005a; Nassif, Kajl et al. 2005; Wang and Jin 2000; Zhou and Haghighat 2009), building design optimization (Magnier and Haghighat 2010; Wang, Zmeureanu et al. 2005), solar energy (Kalogirou 2004;

Varun and Siddhartha 2010), heat exchanger (Allen, Savard-Goguen et al. 2009; Xie, Sunden et al. 2008), etc.

1.3 Aim, objectives and scope of works

1.3.1 Aim and objectives

With a view to operating air-cooled chillers more efficiently, the aim of this research is to investigate the composite methodologies for improving air-cooled chiller performance, including variable condensing temperature control, variable speed condenser fans and water mist pre-cooling. The objectives of this research are:

- to identify the operating characteristics and performance of air-cooled chillers with and without water mist pre-cooling under local climatic conditions;
- to develop the control strategy of variable set point of condensing temperature for the air-cooled chillers combined with the enhanced condenser features;
- to propose a hybrid ANN–GA strategy to facilitate modeling and optimization of the air-cooled chillers; and
- to evaluate the potential electricity savings of chillers with variable condensing temperature control, water mist pre-cooling and other enhanced condenser features in Hong Kong.

1.3.2 Scope of works

The objectives are achieved through a combination of field investigation, experimentation and system simulation.

- A field investigation is carried out on existing chiller plants with air-cooled screw chillers to identify their operating characteristics and performance of air-cooled chillers under local climatic conditions.

- Experimental study on the air-cooled chillers with water mist system is conducted. The operating data are used to furnish parameters of a chiller's mathematical models and to validate the models.
- Detailed chiller models with or without water mist pre-cooling are developed, which form the basis for the simulation analysis of variable condensing temperature control. Extensive simulations are performed on the enhanced condenser features, including variable condensing temperature control, variable speed condenser fans and water mist pre-cooling, and the potential benefits of air-cooled chillers with different condenser feathers are studied.
- This research proposes a hybrid ANN–GA strategy to facilitate modeling and optimization of the air-cooled chillers. It can be expressed in two parts: first an ANN model is needed that can act like the real system; second, based on the ANN model, the control methodology using GA is developed that can find the optimal solution from the solution space of simulation model. This hybrid method can be considered to be an optimization technique that uses GA to find the optimal solution from the solution space generated by the previously trained neural network.
- Representative office building and hotel buildings in Hong Kong are modelled. The model buildings are used for ascertaining the cooling load profiles which constitute the inputs of the chiller models to be developed in this research. The energy saving potential for the commercial building sector in Hong Kong will be evaluated with the proposed optimal control strategies.

1.4 Organization of the Thesis

This research aims to develop an optimal operation method for water mist assisted air-cooled chillers under variable condensing temperature control, and propose a

robust and efficient simulation-based optimization technique combining GA and ANN for air-cooled chillers, so as to meet the required chiller load with minimum energy consumption. Before implementation of energy saving measures in a chiller plant, it is worth characterizing the performance of current chiller products and the related specifications and requirements. It is also necessary to analyze chiller performance by simulation to assess energy effectiveness relating to various energy saving measures and to ascertain the control requirements.

Chapter 1 provides background information about the operation and energy performance of air-cooled chillers in air-conditioned buildings, the optimization methods and optimization techniques, and outlines the aims and objectives of this study.

Chapter 2 reviews the variable condensing temperature control and other advanced condenser features for enhancing the COP of air-cooled chillers. The fundamental of neural networks, genetic algorithms and neural control concepts are also reviewed.

Chapter 3 presents the generic reference buildings including a representative office building and a hotel building, and the characteristics of the load-frequency and weather-load profiles of such buildings.

Chapter 4 develops the models of the air-cooled screw chiller with twin refrigeration circuits. This chapter investigates how variable condensing temperature control and variable speed condenser fans can be applied to enhance the chiller COP. It also presents the investigation on the optimal load sharing between refrigeration circuits in the air-cooled chillers.

Chapter 5 describes the experiment on an air-cooled screw chiller with water mist system and the development of the integrated models for the air-cooled chiller with water mist system. The composite methodologies for improving air-cooled chiller

performance are investigated, including variable condensing temperature control, variable speed condenser fans and water mist pre-cooling. The findings of experimental and simulation studies on the air-cooled screw chiller with water mist are presented. Detailed analyses on the energy saving potential of the chillers serving the typical office building and the hotel building with improved efficiency of air-cooled chillers are reported.

Chapter 6 presents the implementation of the optimal control using neural network and genetic algorithm for air-cooled chillers.

Chapter 7 gives conclusions and recommendations for future work.

Chapter 2 Literature Review

This chapter reviews the measures to improve chiller performance, especially the variable condensing temperature control (CTC) and the other advanced condenser features for enhancing the COP of air-cooled chillers, including variable speed condenser fans and water mist pre-cooling. The fundamental of neural networks, genetic algorithms and neural control concepts are also presented.

2.1 State-of-the-art technologies for air-cooled chillers

2.1.1 Variable condensing temperature control

It is important to understand the control of condensing temperature for air-cooled chillers because this influences greatly how their COP changes at different operating conditions. Compared with water-cooled chillers using evaporative cooling towers, air-cooled chillers are less-efficient. According to many studies (Chan and Yu 2002; Love, Cleland et al. 2005; Manske, Reindl et al. 2001; Smith and King 1998), the deficient performance of air-cooled chillers is mainly due to the traditional head pressure control (HPC) under which the condensing temperature floats around a high set point of 50°C based on a design outdoor temperature of 35°C, irrespective of different chiller loads and weather conditions. In general, chiller microprocessors are equipped with a control algorithm to stage the constant speed fans, which is based on settings (set point, high setting and low setting point) for the condensing temperature. The conventional control of air-cooled chillers is not intended to control the condensing temperature at its set point precisely, but allow the condensing temperature to hover above the outdoor temperature by various degrees. The difference between the condensing temperature and its set point depends mainly on

the outdoor temperature, chiller load and the differential pressure requirement of an expansion valve. The controllability of condensing temperature dictates the trade-off between compressor power and condenser fan power and, in turn, influences the way to maximize the chiller COP in any given operating condition.

For air-cooled chillers, the condenser fan power under HPC can be kept low, but the compressor power remains to be considerable with higher condensing temperature. The pitfalls of conventional HPC have been highlighted. To overcome this, proper control of condensing temperature should be developed to optimize the trade-off between the compressor power and condenser fan power, given that the condensing temperature can vary widely in response to the outdoor temperature and chiller load. Variable condensing temperature control (CTC) is proposed as an alternative to HPC to lower the condensing temperature to improve chiller efficiency (Brownell, Klein et al. 1999; Hosoz and Ertunc 2006; Love, Cleland et al. 2005; Manske, Reindl et al. 2001).

The lowering of condensing temperature is constrained mainly by the required pressure differential across the expansion valve. The flow of refrigerant within a chiller is traditionally controlled by using a thermostatic expansion valve (TEV) which throttles a proper amount of liquid refrigerant from the condenser to the evaporator and creates a certain differential between the condensing pressure and evaporating pressure for allowing heat rejection to take place (Yu, Chan et al. 2006). If a thermostatic expansion valve (TEV) is used, the potential to reduce the condensing temperature is low at high chiller loads even with reduced outdoor temperatures based on the physical characteristics of a TEV, because a high differential between the condensing pressure and evaporating pressure is required for the valve to provide sufficient refrigerant flow to satisfy the loads. The proper

function of thermostatic expansion valves conventionally needs a high pressure differential of at least 690 kPa to control refrigerant flow properly (ARI 1998; Brownell, Klein et al. 1999; Yu, Chan et al. 2006). The condensing temperature is raised along with the high pressure differential. Therefore, traditional head pressure control has been adopted to maintain the condensing temperature at a high level in regardless of variations in outdoor temperature and cooling load.

Electronic expansion valves (EEVs), on the other hand, help relieves the constraint, and the required differential pressure can be as low as 290 kPa for ensuring compressor lubrication (Yu, Chan et al. 2006), which is much lower than that normally required for TEVs. EEVs enable the lower limit of the condensing temperature to drop, and they are the pre-requisite for the implementation of variable condensing temperature control (CTC). Each EEV includes a PID controller to compute its open position based on the set point of the degree of superheat, which is superior to TEVs in the refrigerant flow control. Refrigerant flow is directly proportional to the open position of an EEV and is independent of the pressure differential across the valve. When the degree of superheat exceeds its set point, the electronic expansion valve begins to open wider to call for more refrigerant to be fed into the evaporator, and hence the degree of superheat is restored to its set point. It is desirable to use EEVs to provide accurate control of the degree of superheat to meet the changing chiller load when the condensing temperature varies with the outdoor temperature from time to time (Finn and Doyle 2000; Outtagarts, Haberschill et al. 1997; Tassou and Al-Nizari 1993).

The extent to which the compressor power can drop hinges on the lowest condensing temperature that is achievable at a given evaporating temperature. The lower boundary of condensing temperature is dictated by the differential pressure

requirement of expansion valves, the heat rejection capacity of condensers and the free flow of oil for proper compressor lubrication. The differential pressure requirement can be relieved by using electronic expansion valves. Experimental tests on an air-cooled reciprocating chiller confirmed that lubricant could return properly to the compressors operating with oil level regulators even when the condensing temperature dropped down to 20°C (Yu, Chan et al. 2006).

It is questionable how a fixed set point of condensing temperature can be used in all operating conditions to minimize the sum of compressor power and condenser fan power. According to recent research, the set point of condensing temperature should be reset in response to changes in outdoor temperature and chiller part load ratios in order to maximize chiller COP in various operating conditions (Manske, Reindl et al. 2001; Yu and Chan 2006b). To successfully implement CTC, the chiller microprocessor should contain an algorithm to carry out the reset strategy for the set point of condensing temperature. Yet there is little proof about the capability of adjusting the set point of condensing temperature via the existing chiller microprocessors.

Floating head pressure control (FHPC) has been emerged as a basic energy saving technology in industrial refrigeration systems serving supermarkets (Khattar and Henderson 2000). FHPC is an analogue of CTC because its implementation means that the set point of condensing temperature should be adjusted in response to the outdoor temperature and chiller load. There are many researches on the use of floating head pressure control. Brownell (1998) made a comparison between the fixed and floating head pressure control for a refrigeration system serving the Madison ice arena. To implement floating head pressure, he recommended that the condensing pressure should be adjusted as a function of the ambient web bulb

temperature for water-cooled chillers or evaporative condensers, which resulted in an increase of 23% in the COP of the refrigeration system. He did not describe in detail what modification should be made on the control system of chillers in order to realize the floating head pressure control. Various fan control strategies were investigated in a refrigeration thermal test centre (Edison 2007), which showed that various degrees of energy savings could be achieved by using variable condensing temperature set points and variable speed condenser fans. Another research on energy savings in refrigeration plants with floating head pressure control was reported (Singh 2007). There were electronic controllers to permit refrigeration system operation at the lowest condenser pressure possible, and the control of condenser fans was based on the temperature difference between the outdoor temperature and condensing temperature. An overall 13.95% energy saving could be achieved when variable speed along with floating condensing pressure control strategies were employed.

While CTC can be a standard feature for new refrigeration systems and can be retrofitted in existing refrigeration systems, it is hardly found in air-cooled chiller products available in the market. There is little technical difficulty in implementing CTC in air-cooled chillers, but hardly any manufacturers have attempted to retrofit their chiller products with this advanced control, which involved in adding a controller capable of automatically adjusting the set point of condensing temperature in response to variations in the outdoor temperature and chiller load. There is also little proof about the capability of adjusting the set point of condensing temperature via the existing chiller microprocessor.

2.1.2 Variable speed control of condenser fans

Variable speed technology has long been a workable energy-efficient feature to enhance the energy performance of chiller systems. Considering a chilled water system with air cooled chillers, variable speed control is confined to the compressors, condenser fans and chilled water pumps.

Many studies have demonstrated that variable speed control for chiller compressors or cooling tower fans could save power when chillers operate at part load (Aprea, Mastrullo et al. 2004; Hartman 2001; Koury, Machado et al. 2001; Qureshi and Tassou 1996; Tassou and Qureshi 1998). The power saving is due to the improved efficiency of the motors when operating at a lower speed under part-load conditions. While variable speed compressors are increasingly used for chillers, there is limited evidence to support the use of variable speed condenser fans for the heat rejection system of air-cooled chillers.

There is a convention among engineers that variable speed control for condenser fans has an insignificant effect on saving chiller power, as the nominal fan power accounts for less than one-tenth of the nominal compressor power. Although variable speed control of condenser fans can bring a lot of benefits in respect of operation and energy efficiency, it is still not a standard feature for air-cooled chillers (Holden 2005). Variable speed control for condenser fans is superior to cycling constant speed condenser fans in steps with regard to the controllability of condensing temperature. With regard to energy savings, considerable power can be saved because of the cube relationship between power and speed when the fans operate at reduced speed to meet the required heat rejection airflow for any given cooling capacity. Furthermore, the variable speed fans are able to better control the condensing temperature at any given reduced set point. Existing air-cooled chillers

normally contain multiple condenser fans, and the constant speed fans are staged in steps to maintain the required condensing temperature or pressure. Such the step-by-step variation of heat rejection airflow could cause a serious fluctuation in the condensing temperature and hence the COP when its set point is adjusted from time to time in response to the ambient and load conditions. When a variable frequency drive is applied to control the speed of all the condenser fans in parallel, they can operate altogether at the required speed to maintain the set point of the condensing temperature.

The fan speed may increase by up to 20% if the variable frequency drive is properly sized. Depending on the condenser design, this helps further lower the condensing temperature, even at high outdoor temperatures. Considering that all the variable speed condenser fans need to operate, the control of fan cycling in steps can be waived. This helps moderate the wear and tear problem resulting from frequent switching of the fans. The noise emitted from air-cooled chillers can be reduced when the fans are able to operate at lower speed. This can help eliminate the need to build an acoustic enclosure for the chillers which could cause ineffective heat rejection with increased energy consumption.

If variable speed control is applied to condenser fans, each of them can operate at a lower speed with much reduced power while the condensing temperature is maintained at its set point. Simulation analyses on air-cooled reciprocating and screw chillers (Chan and Yu 2002; Yu and Chan 2006b) confirmed that variable speed condenser fans and electronic expansion valves should be used to complement CTC to increase the chiller COP by up to 127.5%. The heat rejection airflow could be modulated smoothly by the variable speed fans with reduced power to enhance the controllability of condensing temperature. It was reported that the implementation of

CTC was economically viable, with very short paybacks of 0.38-1.07 years when used in chiller systems serving local commercial buildings (Yu and Chan 2006a).

2.1.3 Evaporative cooling for air-cooled condensers

As air-cooled chillers apply condenser fans to force ambient air to condense and slightly sub-cool the refrigerant, the extent of the condensing temperature drop is constrained by the dry bulb temperature (DBT) of ambient air. Evaporative cooling could decrease the temperature of ambient air, and is effective for pre-cooling the entering condenser air so as to improve the performance of the air-cooled chillers. This concept is enhanced at present in consideration of energy saving and environmental protection.

Refrigeration systems with evaporative condensers have been applied for years. However, using evaporative pre-coolers to enhance the COP of air-cooled chillers is not common, even though the concept is not new. For the evaporative pre-coolers, ambient air is drawn or blown through a porous wetted surface with a film of cool water. The air stream is cooled by the evaporation of water when leaving the pre-cooler, and its DBT drops to approach its wet bulb temperature (WBT). The pre-coolers enable the condensing temperature to drop in response to a reduction of air temperature entering condensers, which results in a decrease of the compressor power. However, additional fan power is required for the evaporative condenser to draw or blow air through the porous surface due to the pressure drop across the pre-coolers, which results in the beneficial trade off. The pre-coolers, when installed in front of air-cooled condensers, can pre-cool the outdoor air before entering the condensers while consuming less than 15% of the cooling water required by cooling towers and evaporative condensers (Bom, Foster et al. 1999; Zhang, You et al. 2000).

The potential and benefits of using evaporative pre-coolers hinge on the extent to

which the condensing temperature can drop and whether the decrease in compressor power due to this drop can outweigh the additional fan power. Zhang et al. (Zhang, You et al. 2000) have indicated that the use of evaporative pre-coolers can bring about a 14.7% increase in the COP of air-cooled chillers working under the climatic conditions of Tianjin of China. According to a simulation study conducted by Yu and Chan (2005b), a 1.4–14.4% decrease in chiller power and a 1.3–4.6% increase in the refrigeration effect could be achieved when an air-cooled reciprocating chiller with an evaporative pre-cooler operated under head pressure control. When the condensing temperature control replaced the head pressure control, the chiller power could further reduce by 1.3–4.3% in certain operating conditions. The pre-coolers are expected to have a high effectiveness when cooling outdoor air in a hot and dry climate, but they can function properly even when the climate is hot and humid. The combined use of CTC and evaporative pre-coolers is an economically viable option for chiller performance improvements (Yu and Chan 2006a). However, this technology has some side effects including the risk of mineral deposits and corrosion of the condenser coils, which will reduce the cooling efficiency with time.

Due to the side effects of evaporative pre-coolers, an alternative for evaporative cooling is proposed, which is to install water mist system to pre-cool the air entering condensers. The system produces a mist of 10-micron water droplets via atomization nozzles, which allows the ambient air entering the condenser to cool from its dry-bulb temperature to wet-bulb temperature while the droplets are fully vaporized. The water mist pre-cooling system is not a new concept, and it has been applied successfully in the industries (Cheung, Santos et al. 2006; Hsieh and Yao 2006; Zhang, Fang et al. 2007). However, the application of water-mist pre-cooling associated with a chiller system is uncommon. The water mist system has advantage over the evaporative condenser because, firstly, it has no additional air pressure loss

through the wetted media and hence no additional fan power will be incurred. Although the water mist pump will operate to deliver water at a high pressure of around 70 bars, the water flow rates are very low and hence a small amount of power to drive the high pressure pumps is the only additional power to be considered. Secondly, it is simple and convenient to install a mist system, which is advantageous in retrofitting for the existing hundreds of thousands of air-cooled chillers. Due to the remarkable advantage of water mist system, it is expected to be widely applied. Yu and Chan (2009) studied the application of water mist system by simulation. Yet there is a lack of field investigations for the air-cooled chillers with water mist system, and there is a lack of research into how to reap the benefits of water mist pre-cooling with CTC and other advanced condenser features.

2.2 Artificial neural networks

Artificial neural networks (ANNs) are computing systems made up of a number of simple and highly interconnected neurons (also called nodes or processing elements), which represents information and processes information according to methods inspired by current knowledge of brain structure and brain function (Richard M 1997). ANN is a computational mechanism which, given a set of data, is able to acquire, represent, and compute a mapping from one multivariate space of information to another (Garrett 1994). Information is passed through the neurons along interconnections. An incoming connection has two values associated with it, an input value and a weight. The output of the unit is a function of the summed value.

A typical artificial neural network is comprised of one input layer, one output layer and one or more hidden layers. Each layer consists of many interconnected neurons, each of which is connected to other neurons in the following layer. ANNs are models which map from a set of given patterns (input patterns) to an associated set of known

values (target output) and learn the relationship between the controlled and uncontrolled variables by studying previously recorded data. They are trained with respect to data sets until they learn the patterns presented to them. When ANNs are trained properly with a sufficient data set and learning period, each ANN will adjust to establish the best non-linear relationship possible for its own unique architecture, then they can be used for prediction, classification or control.

The main advantages of ANNs over other modeling techniques are their abilities to map complex and nonlinear functions, to learn and generalize by experience, as well as to handle multivariable problems without having to assume the form of the relationship between input and output variables, instead of complex rules and mathematical routines. ANN can operate as a black box model, which requires no detailed information about the system and sophisticated mathematical knowledge, obviating the need to use complex mathematically explicit formulas, computer models, or impractical and costly physical models (Mellit and Kalogirou 2008). In addition, neural networks are fault tolerant, robust, and noise immune. With the capability of an ANN to cope with uncertainty in complex situations, there has been a substantial increase in a wide range of applications in recent years, and they have been applied for process modeling, pattern classification, clustering, expert rules extraction, forecasting, prediction, optimization and control (Basheer and Hajmeer 2000; Bechtler, Browne et al. 2001b; Gandhidasan and Mohandes 2011; Kalogirou 2003; Kavchak and Budman 1999; Song, Baek et al. 2005; Soteris A 2000). From the control theory viewpoint, the capability of neural networks to deal with nonlinear system is most significant.

2.2.1 Artificial neural network architectures

Multiple neurons are interconnected to form a neural network to facilitate parallel-

distributed computing. A number of ANN architectures and algorithms have been developed and applied for solving different problems (Haykin 1999; Pham and Pham 1999). ANNs can be classified in many different ways according to their relevant features. The classification of ANNs can be based on the their function (e.g., pattern association, clustering), the type of learning algorithm, the learning rule (the driving engine of the learning algorithm), the degree of learning supervision, etc. (Basheer and Hajmeer 2000). Generally, ANNs are classified according to the direction of flow of information within the neural network, and they are feed-forward neural networks and recurrent neural networks (or feedback networks). In the feed-forward neural network, information or signals move in only one direction from the input nodes to output nodes, and there is no feedback (loops) in the network. Feed-forward ANNs tend to be straightforward networks that associate inputs with outputs. Generally, a feed-forward neural network consists of multiple layers, including one input layer, one output layer, and one or more hidden layers, therefore, it is called multilayer feed-forward neural network (MFNN). Figure 2.1 shows the typical configuration of multilayer feed-forward neural network. Each single neuron is connected to other neurons of a previous layer through adaptable synaptic weights, and the signal traveling along the link is multiplied by the connection weight. In subsequent layers, each unit sums its inputs and a bias or threshold term, and an output of each unit can be produced with the activation function. Multiple layers of neurons with nonlinear transfer functions allow the network to learn linear and nonlinear relationships between input and output vectors. The number of hidden layers in a neural network greatly affects its performance. By adding one or more hidden layers, the network is enabled to extract higher-order statistics, which causes the network to become more complicated and incurs more computing time. There is a trade-off between accuracy of the neural network, the structural complexity and

hence the computing time.

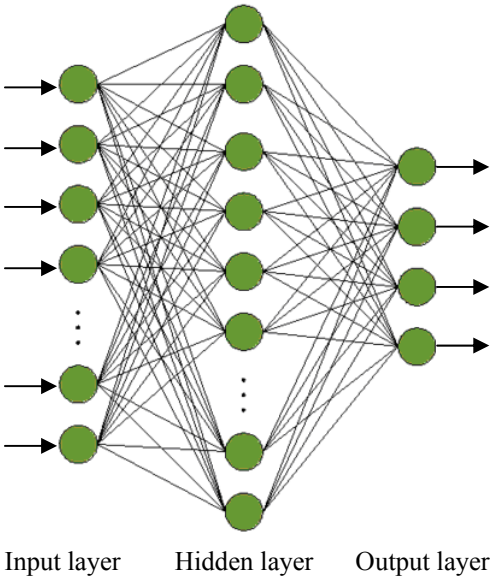

Figure 2.1 Multilayer feed-forward neural network

Contrary to feed-forward networks, recurrent neural networks (RNNs) are models with bi-directional data flow. A recurrent neural network distinguishes itself from a feed-forward neural network in that it has at least one feedback loop. While a feed-forward network propagates data only from input to output, RNNs can have signals traveling in both directions by introducing loops in the network. Figure 2.2 demonstrates the configuration of recurrent neural network. Computations derived from earlier input are fed back into the network, which gives them a kind of memory. The presence of feedback loop in the RNNs has a profound impact on the learning capability of the network and on its performance, which results in a nonlinear dynamical behavior (Haykin 1999).

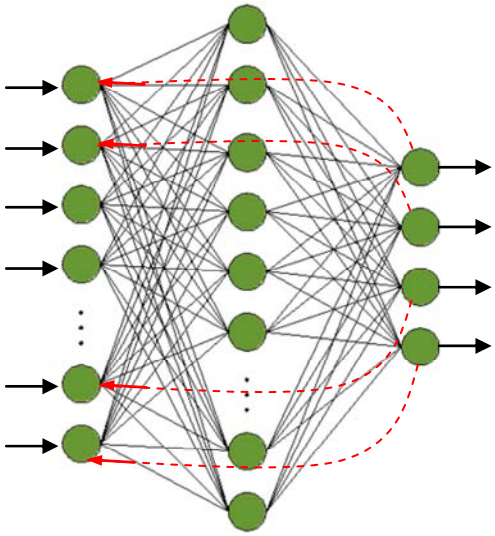

Figure 2.2 Recurrent neural network

2.2.2 Learning methods in neural networks

Analogous to the learning process of human brain, an ANN learns from the data provided. This learning process is also referred to as ‘training”. The most significant property for a neural network is the ability to learn from its environment, and improve the performance through learning. A neural network learns about its environment through an interactive process of adjustments applied to its synaptic weights and bias levels. Ideally, the network becomes more knowledgeable about its environment after each iteration of the learning process (Haykin 1999). A prescribed set of well-defined rules for the solution of a learning problem is called a learning algorithm. There is a diverse variety of learning algorithms, and each offers advantages of its own. Basically, learning algorithms differ from each other in the way in which the adjustment to a synaptic weight of a neuron is formulated. Generally, based on presence or absence of a teacher, there are three types of learning algorithms: unsupervised learning, supervised learning and reinforced learning

(Haykin 1999).

Supervised learning is also referred to as learning with a teacher. Figure 2.3 shows a block diagram of learning with a teacher. In supervised learning, both the inputs and the outputs are provided, and supervised learning employs a “teacher” to assist in training by telling the network what the desired response should be for a given input. The network processes the inputs and compares its resulting outputs against the desired outputs, and then the supervised learning algorithms use the difference between the predicted and desired response to adjust the weights of the network to improve prediction capabilities (McCord-Nelson and Illingworth 1991). It is a closed-loop feedback system, but the unknown environment is not in the loop. The important principle is that supervised learning requires an input and a corresponding desired output. Given an algorithm designed to minimize the cost function, an adequate set of input-output examples, and enough time permitted to do the training, a supervised learning system is usually able to perform such tasks as pattern classification and function approximation (Haykin 1999; Priddy and Keller 2005).

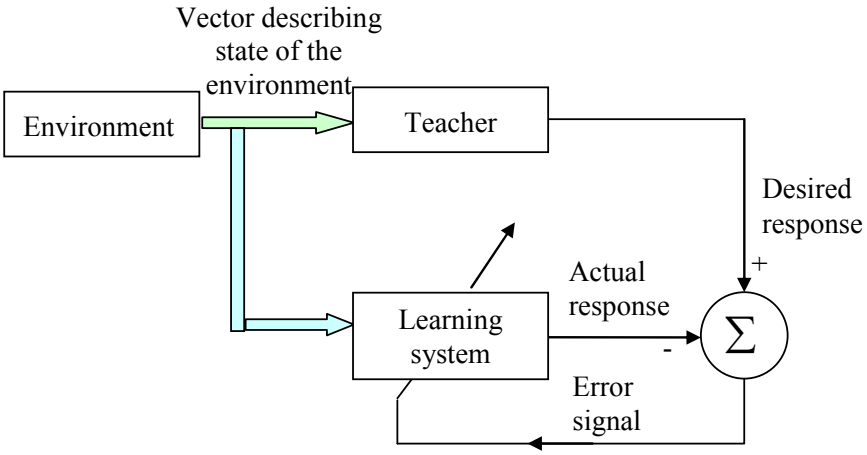

Figure 2.3 Block diagram of learning with a teacher

In supervised learning, the learning process acts as a teacher. However, there is no teacher employed in the learning process for the algorithm of ‘learning without a

teacher'. It is analogous to students learning a lesson on their own. Under the paradigm of learning without a teacher, two subdivisions are identified: reinforcement learning and unsupervised learning. In reinforcement learning, the learning of an input-output mapping is performed through continuous interaction with the environment in order to minimize a scalar index of performance. Figure 2.4 shows the block diagram of one form of reinforced learning system built around a critic that converts a primary reinforcement signal received from the environment into a higher quality reinforcement signal called the heuristic reinforcement signal, both of which are scalar inputs. Reinforcement learning is closely related to dynamic programming. In unsupervised learning, there is no external teacher or critic to oversee the learning process to adjust the weights, rather there is an internal monitoring of performance, as indicated in Figure 2.5. The learning process is an open loop with a set of adaption rules that govern general behavior. The learning system receives stimulus from the environment, produces a response and, along with the adaption rule, adjusts the weights of the neural network to obtain the desired performance. The adaption rule in the unsupervised algorithm performs the error-signal generation role the teacher performs in the supervised learning system. Once the network has become tuned to the statistical regularities of the input data, it develops the ability to form internal representations for encoding features of the input and thereby to create new classes automatically (Haykin 1999; McCord-Nelson and Illingworth 1991; Priddy and Keller 2005).

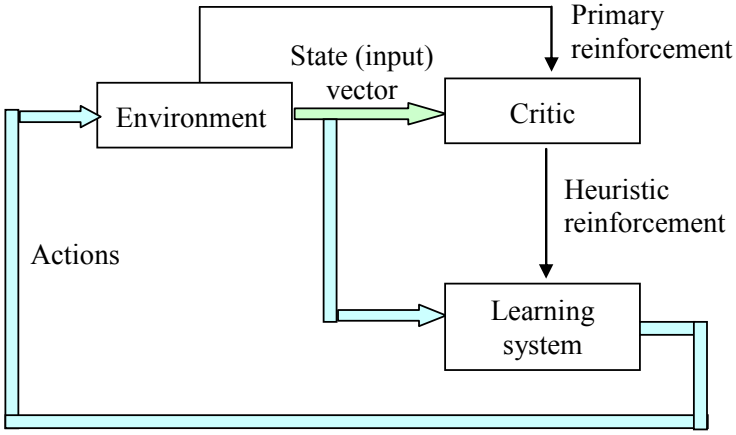

Figure 2.4 Block diagram of reinforcement learning

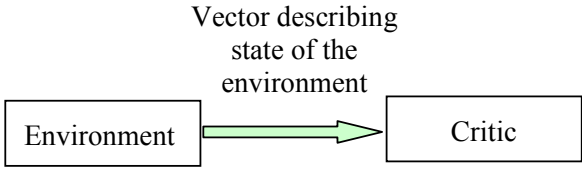

Figure 2.5 Block diagram of unsupervised learning

These learning algorithms can be further categorized based on the learning rules used. A learning rule defines how exactly the network weights should be adjusted or updated between successive training cycles (epochs). The unsupervised learning algorithms include Hebbian and competitive learning algorithm, and supervised learning algorithms include stochastic learning and gradient descent learning. Gradient descent learning is further categorized as least mean square algorithm and back propagation. Figure 2.6 shows the classification of the learning algorithms. Generally, several of the algorithms are used to achieve the minimum error in the shortest time. There are also alternative forms of neural network systems being constantly developed, including new or modifications of existing ones. For specific problems, the decision as to which network works better for a given problem depends strictly on the problem logistics. For example, a clustering problem requires a Kohonen network, and a mapping problem may be modeled using a variety of ANNs such as BP and radial basis function (RBF) networks. The suitability of an

appropriate paradigm and strategy for application is very much dependent on the type of the problem to be solved (Kalogirou 2003).

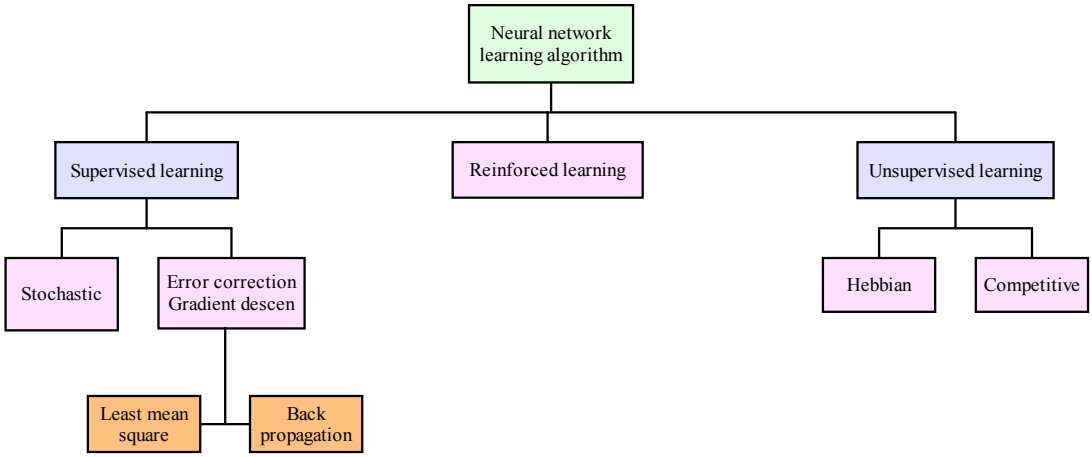

Figure 2.6 Classification of learning algorithms

2.2.3 Back-propagation ANNs

Despite the diversity of ANN algorithms, the back-propagation (BP) algorithm and its variants are the most popular learning algorithms in neural networks (Besaw, Rizzo et al. 2010; Kalogirou 2003; Mohanraj, Jayaraj et al. 2012). BP networks are known for their ability to generalize well on a wide variety of problems. BP networks belong to a supervised type of networks, i.e. trained with both inputs and outputs. Due to its popularity, flexibility and adaptability, BP has been widely applied in many application areas as it tends to generalize well.

Multilayer feed-forward neural networks consist of units arranged in layers with only forward connections to units in subsequent layers, as shown in Figure 2.1. The connections have weights associated with them. Each signal traveling along the link is multiplied by a connection weight. The first layer is the input layer, and the input units distribute the inputs to units in subsequent layers. In subsequent layers, each unit sums its inputs, adds a bias or threshold term to the sum and nonlinearly transforms the sum to produce an output. This nonlinear transformation is called the

activation function of the unit. The output layer units often have linear activations. The layers between the input layer and output layer are called hidden layers and units in hidden layers are called hidden units (Mellit and Kalogirou 2008).

The training of all patterns of a training data set is called an epoch. The training set has to be a representative collection of input–output examples. Figure 2.7 depicts a portion of a multilayer feed-forward ANN trained with BP algorithm. Two kinds of signals are identified in this network: function signals and error signals. A function signal propagates forward (neuron by neuron) through the neural network, and emerges at the output end of the network as an output signal. An error signal originates at an output neuron of the neural network, and propagates backward (layer by layer) through the network.

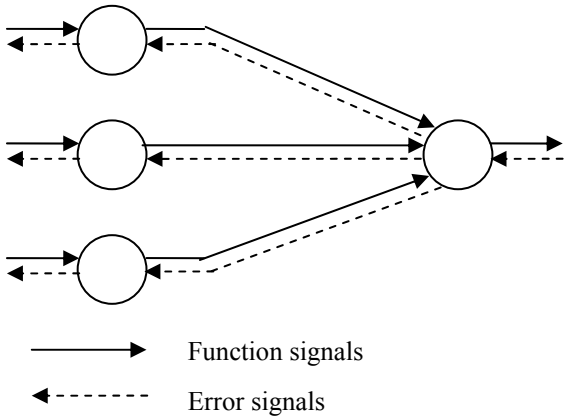

Figure 2.7 Two basic signal flows in a MFNN: forward propagation of function signals and back-propagation of error signals

BP training is a gradient descent algorithm. It tries to improve the performance of the neural network by reducing the total error by changing the weights along its gradient (Haykin 1999). Suppose the *i*th element of the input vector (pattern) is denoted by $x_i(n)$, $y_j(n)$ refers to the function signal appearing at the output of neuron *j* at iteration *n*, and $W_{ji}(n)$ denotes the synaptic weight connecting the output of neuron *i* to the input of neuron *j* at iteration *n*, and the correction applied to this weight at

iteration n is denoted by $\Delta W_{ji}(n)$.

In any interlayer, a typical neuron j integrates the signals, y_j, impinging onto it, and produces a net effect, ξ_j, according to the neuron dynamics,

$$\xi_j(n) = \sum_i W_{ji}(n) x_i(n)) \tag{2.1}$$

The corresponding activation, $y_j(n)$, of the neuron is determined using a transfer function, f, which converts the total signal into a real number from a bounded interval:

$$y_j(n) = f(\xi_j(n)) = f(\sum_i W_{ji}(n) x_i(n))) \tag{2.2}$$

One popular function used in BP is the basic continuous sigmoid:

$$f(\xi) = \frac{1}{1+e^{-\xi}} \tag{2.3}$$

where $-\infty < \xi < +\infty$, and $0 \le f \le 1$.

The error signal at the output of neuron j at iteration n is defined by

$$e_j(n) = d_j(n) - y_j(n) \tag{2.4}$$

Defining the instantaneous value of the error function for neuron j as $\frac{1}{2}e_j^2(n)$, the total error function J of a multiple feed-forward neural network can be written as

$$J(n) = \frac{1}{2}\sum_j e_j^2(n) \tag{2.5}$$

BP is based on searching an error surface (error as a function of ANN weights) using gradient descent for point(s) with minimum error. Each iteration in BP constitutes two sweeps: a forward activation to produce a solution, and a backward propagation

of the computed error to modify the weights. Based on this, the derivative of SSE with respect to weights can be calculated to adjust each weight. The correction $\Delta W_{ji}(n)$, which is defined by the data rule, is used to adapt (Haykin 1999).

$$\Delta W_{ji}(n) = -\eta \frac{\partial J(n)}{\partial w_{ji}(n)} \tag{2.6}$$

where η is the learning rate of the back-propagation algorithm. The use of the minus sign in Eq.(2.6) accounts for the gradient descent in weight space.

In any interlayer, an arbitrary weight $W_{ji}(n)$ at iteration (n) will be updated from its previous state (n-1) value according to

$$W_{ji}(n) = W_{ji}(n-1) + \Delta W_{ji}(n) \tag{2.7}$$

This back-propagation technique propagates backward the errors from the output layer through the hidden layer to the input layer with the modified delta rule until the stop criteria is satisfied.

The key distinguishing characteristic of the multilayer feed-forward neural networks with back-propagation learning algorithm is that it forms a nonlinear mapping from a set of input stimuli to a set of outputs using features extracted from the data patterns. The neural network can be designed and trained to accomplish a wide variety of nonlinear mappings, even for the very complex problems (Mellit and Kalogirou 2008).

2.2.4 Development of ANN models

Artificial neural networks are capable of powerful universal function approximation, modeling the complex problems with many variables easily (Chow, Zhang et al. 2002; Ekici and Aksoy 2009; Esen, Inalli et al. 2008; Wang and Chen 2002; Zhou and Haghighat 2009), which is the advantage of ANN from other methods. In this

research, the objective function is built by ANN technique to map the complex non-linear relationship between working conditions and the chiller outputs. Traditional modeling methods for chillers mostly relied on the assumptions for model simplifications, and thus may lead to inaccurate results. The characteristic of the ANN technique make it suitable for modeling the chiller performance, and therefore is utilized in this research as the modeling tool.

The performance of ANN is affected by the characteristic of the network, such as training algorithm and neural network architecture. Neural network architecture refers to the arrangement of neurons into layers and the connection patterns within and between layers. The ANN model and its architecture determine how an ANN transforms its inputs to outputs. Once the architecture has been determined, the network is trained and then tested.

The main steps involved in developing an ANN to model air-cooled chillers are data pre-processing and neural network construction. Data pre-processing includes data specification, organization and analysis. Neural network construction involves designing a preliminary model, building the model and optimizing the network architecture during the training process by selecting the appropriate architecture and the suitable learning rate, momentum and the activation function. If the neural network does not reach an acceptable error during training, the data pre-processing step may need to be revisited to improve the training. The procedure for developing ANN models for air-cooled chillers is shown in Figure 2.8.

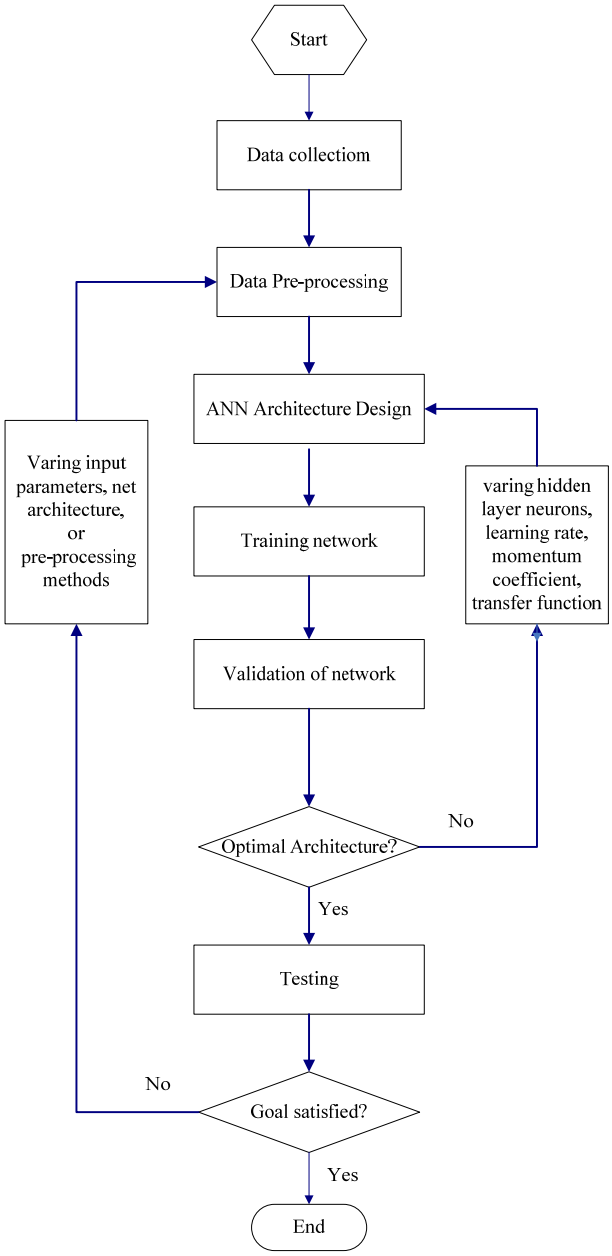

Figure 2.8 ANN design flow process

2.2.4.1 Selection of input and output variables

When building ANN models, the system has to be identified with respect to the input and output variables that characterize the system. Proper selection of input variables for accurate prediction of a set of output variables is vital for modeling of any system using ANN (Fast, Assadi et al. 2009), because they significantly affect the performance of the weight adaptation algorithm used for the ANN models. System knowledge to identify the interrelation between the input and output parameters helps

in this respect. The inputs include the uncontrolled variables specific to the environment and controlled variables modified by the operators. In the present case for the air-cooled chillers, the inputs that can influence the performance of chiller under investigation are outdoor conditions, chiller load, set points of controlled variables and characteristic parameters of the chiller. The outputs are the related chiller outputs.

2.2.4.2 Data pre-processing

In this research, one typical meteorological year's simulation data were obtained for different condenser features, respectively, and the simulation period covered the complete operating seasons of the chiller plant of a building, so that the annual variations could be learned. The lower and upper boundaries of the cases were covered in a typical meteorological year's working conditions. It was important to cover the lower and upper extreme conditions of the cases investigated, as the neural network learned all the range of possible values and thus extrapolation was not needed.

The data required for the off-line training of the ANN model were produced using the TRNSYS simulation. A preliminary analysis of the data would identify any obvious errors due to equipment or simulation failure. The available simulation data of each case were randomly divided into three subsets: training (60%), validating (20%) and testing data (20%) (Beale, Hagan et al. 2011). The first subset was used to perform the training of the network, computing the gradient and updating the network weights and biases. The second subset was applied to evaluate the performance of the network during training. Training continued as long as the network continued improving on the validation set. The test subset was used for estimating the performance of the trained network on new data, which was never seen by the

network during the training. The test set provided a completely independent evaluation of the ANN accuracy.

Generally, for the neural network, there are a pre-processing block between the input and the first layer of the network and a post-processing block between the last layer of the network and the output, as shown in Figure 2.9.

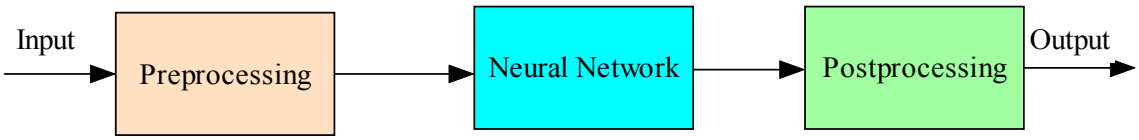

Figure 2.9 Neural network with a pre-processing and post-processing block

Data pre-processing for an ANN involves normalizing the input data and reducing its dimensionality. Each value of input and output is normalized to ensure all input parameters initially have the same relative influence on the output of the network, so that no one set of values dominates the solution. Without normalization, input variables with a little change could produce significantly different results (Massie, White et al. 2002). The scaling used is either in the range -1 to 1 or in the range 0 to 1 depending on the type of data and the activation function used (Kalogirou 2003). One of the simplest and most common methods to normalize data is through a simple linear rescaling. In this research, to enhance the adaptability of the neural network, all the input and output values were normalized so that they fell in the interval [-1, 1] using the following equation (Hosoz, Ertunc et al. 2007):

$$p_n = 2\frac{p - \min(p)}{\max(p) - \min(p)} - 1 \tag{2.8}$$

where p_n is the normalized form of vector p.

When the training completes, the outputs from the neural networks corresponded to the normalized targets, and the corresponding de-normalization manipulations should

be reverse transformed back into the units of the original target data when the network is put to use in the field.

2.2.4.3 Selection of BP algorithm

ANN is based on the working process of human brain in decision making. The most popular learning algorithms are the backpropagation (BP) and its variants, and the BP algorithm is one of the most powerful learning algorithms in neural networks (Kalogirou 2003). During the course of training, many training functions can be adopted, such as Levenberg-Marquardt backpropagation, batch gradient descent with momentum, variable learning rate backpropagation, BFGS quasi-Newton backpropagation, Bayesian regulation backpropagation. In order to achieve the best result, different training options should be attempted. Improving of the generalization should be attempted by means of regularization and early stopping. Compared with other training methods, the Levenberg–Marquardt algorithm gives the fastest response with a minimum convergence error. The Bayesian regularization approach involves modifying the usually used objective function, and it forces the network response to be smoother and less likely to overfit, and hence provides the training algorithm with a superior generalization capability. Therefore, Bayesian regularization in combination with Levenberg–Marquardt training was chosen for this research.

2.2.4.4 Optimization of the ANN structure

The architecture of an ANN is usually divided into three parts: an input layer, hidden layer(s) and an output layer. The information contained in the input layer is mapped to the output layer through the hidden layers. The neuron number of the input layer of the ANN model is determined by the number of input variables selected, and the neurons of the output layer is determined by the number of the output variables

selected. It has been proved that in most function approximation problems, one hidden layer may be sufficient to map an arbitrary function to any degree of accuracy (Al-Shareef, Mohamed et al. 2008; Xin 1996; Zhang and Morris 1998). In fact, neural networks with more than one hidden layer are more complex and time consuming. Adding additional layers can allow for greater flexibility in the model, which may increase the learning capacity. However, too many hidden layers will result in overtraining and a loss in generalization capability, and it will also increase the training time (Nannariello and Fricke 2001). In a Feed-forward neural network, the hidden layer is made up of sigmoid functions which are capable of simulating the nonlinear effects, and hence it is sufficient to include one single hidden layer. In this research three-layer BP neural networks with one hidden layer will be considered. Next, the number of neurons in the hidden layer is determined.

Generally, the error on training data decreases with increasing number of hidden neurons or training cycles, as shown in Figure 2.10 (Basheer and Hajmeer 2000). The initial large decrease in the error is due to learning, but the subsequent slow reduction in error may be attributed to memorization resulting from the excessively training, or overfitting due to a large number of hidden neurons. During ANN training, the error on test subsets also generally shows an initial reduction and a subsequent increase due to memorization and overtraining of the trained ANN model. The optimal neural network architecture is obtained with minimum error for test data set.

One method for improving network generalization is to use a network that is just large enough to provide an adequate fit. To determine the required number of hidden neurons for sufficient training, many different rules have been proposed. Although the formulas will suggest different optimal number of hidden neurons in a feed-forward neural network, they can provide a reference for the possible range of the

optimal number of hidden neurons. For the ANN model with only one hidden layer, the number of neurons in the hidden layer is defined by Eq. (2.9) (Xie 2003).

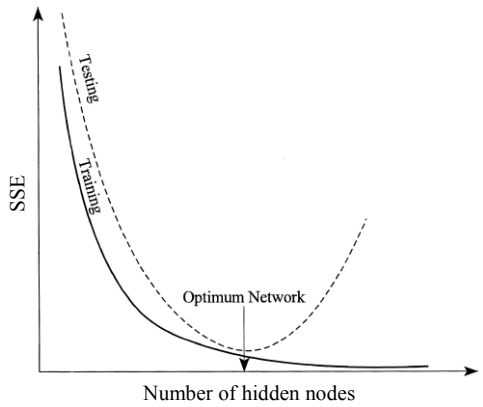

Figure 2.10 Selection of optimum network architecture

$$n = \sqrt{mn_1} \tag{2.9}$$

Yao and Wang (2002) put forward another empirical formula to determine the number of neurons in the hidden layer as follow.

$$n = \sqrt{0.13mn_1 + 0.12m^2 + 2.54n_1 + 0.77m + 0.86} \tag{2.10}$$

Two formulas were suggested (Xin 2000) to calculate the required number of neurons in the hidden layer.

$$n = \sqrt{n_1 + m} + c \tag{2.11}$$

$$n = \log_2 n_1 \tag{2.12}$$

Xu and Chen (2008) proposed an approach for determining the optimal number of hidden nodes in a feed-forward neural network as shown in Eq. (2.13).

$$n = C_f (N/(d \log N))^{1/2} \tag{2.13}$$

In the above five formulas, n is the number of hidden neurons, n_1 is the number of neurons in the input layer, m is the number of neurons in the output layer, c is a constant which belongs to [1, 10], d is the input dimension of the target function f, N

is the number of training pairs, and C_f is the first absolute moment of the Fourier magnitude distribution of the target function *f*.

2.2.5 Performance of the neural network

As the initial weights are randomly given, the outputs of the neural network will be different from the desired ones each time. With training, the weights of the neural network are continually updated to reduce the difference between the outputs and the desired response, which is regarded as the error and can be measured in different ways. The most common indicator is the mean squared errors (MSE), which is the square difference between the network's output and the desired response, as defined in Eq. (2.14).

$$MSE = \frac{1}{N}\sum_{i=1}^{N}(t_i - a_i)^2 \tag{2.14}$$

where t_i is the target value, a_i is the network output and N is number of input – output data pairs.

Overfitting is a major problem that occurs during the neural network training. If a neural network overfits or memorizes the training data, its generalized performance is likely to be severely compromised and the error becomes larger. The MSE minimization procedure by itself does not ensure that the trained neural network will possess the desired generalization ability. To improve the generalization capability, the performance function of the feedforward neural network model should be modified by adding a term that consists of the mean squares of the network weights and biases (MSW), and the new error function is called the generalized error function (MSEREG) defined as follow (Beale, Hagan et al. 2011).

$$MSW = \frac{1}{N}\sum_{i=1}^{N} w_i^2 \tag{2.15}$$

$$MSEREG = \gamma MSE + (1-\gamma)MSW \tag{2.16}$$

where w_i is the weight vector, and parameter γ is the performance ratio.

This modified performance function causes the neural network to have smaller weights and biases, which forces the neural network to response smoother and is less likely to overfit. It is difficult to determine the optimum value for the performance ratio parameter. It is desirable to determine the optimal regularization parameters in an automated fashion. Bayesian framework can determine the optimal regularization function parameters automatically (Beale, Hagan et al. 2011).

Early stopping is also a recommended criterion for stopping the training of a neural network to improve its generalization and prevent overfitting, which is beneficial to the network performance (Beale, Hagan et al. 2011; Nguyen, Abbass et al. 2005). It should be noted that a neural network will always learn the training data set better as the training is sufficient. Generally, the training set error decreases with increasing iterations. However, it is not always guaranteed better performance in the test. If the neural network is trained too much, the neural network memorizes the training patterns and does not generalize well. Therefore, the criterion to early stop training should be well determined. In the technique of early stopping, the validation error normally decreases during the initial phase of training, as does the training set error. However, when the neural network starts to overfit the data, the error on the validation set typically begins to rise. When the validation error increases for a specified number of iterations, the training is stopped, and the weights and biases at the minimum of the validation error are returned (Beale, Hagan et al. 2011).

The performance of the ANN based prediction is evaluated by a regression analysis between the network outputs and the corresponding targets. In addition to the generalized error function (MSEREG), the correlation coefficient (R), mean relative

error and absolute fraction of variance (R^2) can be used for assessing the error of the neural network. The correlation coefficient is a measure of how well the variation in the output is explained by the targets, which is defined as follows (Hosoz, Ertunc et al. 2007):

$$R(a,p) = \frac{\mathrm{cov}(a,p)}{\sqrt{\mathrm{cov}(a,a)\,\mathrm{cov}(p,p)}} \tag{2.17}$$

where cov(a, p) is covariance between a and p sets that refer to the actual output and the predicted output sets, respectively. Similarly, cov(a, a) and cov(p, p) are the auto covariances of a and p sets, respectively. The correlation coefficient evaluates the degree to which two variables are linearly related, which ranges between -1 and 1. The R values closer to 1 indicate a stronger agreement of training and predicted values, while the R values closer to -1 indicate a stronger negative relationship.

The absolute fraction of variance (R^2) is determined from Eq.(2.18) (Hosoz, Ertunc et al. 2007).

$$R^2 = 1 - \frac{\sum_{i=1}^{N}(a_i - p_i)^2}{\sum_{i=1}^{N} P_i^2} \tag{2.18}$$

where a_i is the actual output, N is the number of points in data set, p_i is the predicted output. The R^2 values range between 0 and 1. A very good fit yields a R^2 value of 1, whereas a poor fit results in a value near 0.

2.3 Genetic algorithm

Genetic algorithms (GAs) are stochastic global search and optimization methods that mimic the process of natural evolution. In the early 1970s, John Holland, one of the founders of evolutionary computation, introduced the concept of genetic algorithms (Holland 1992), and he published the book *Adaptation in Natural and Artificial*

Systems in 1975, which described a general framework for understanding the mechanisms responsible for natural adaptation and designing biologically-inspired artificial systems in a variety of systems over a broad range of timescales (Booker and Riolo 2000).

GA is based on Darwin's theories of natural evolution and natural genetics for the design and implementation of robust adaptive systems. Over the last decades, GA has received much attention due to its potential as optimization techniques and GA turns out to be one of the most promising approaches for dealing with complex systems (Oswaldo 2005). To date, GAs have been successfully applied to an extensive number of applications in machine learning (Chi, Ersoy et al. 2007; Sette and Boullart 2000) and data mining (Koonce and Tsai 2000; Sikora and Piramuthu 2007; Sörensen and Janssens 2003), most notably classification (Hu 2005; Sarkar, Sana et al. 2011; Yamany, Khiani et al. 1997), pattern recognition (Alsultanny and Aqel 2003; P.N 2002; Polat and Yıldırım 2008), reinforcement learning (Kamei and Ishikawa 2006; Koulouriotis and Xanthopoulos 2008) and various complex optimization (Cook, Ragsdale et al. 2000; Morimoto, De Baerdemaeker et al. 1997; Shen, Wang et al. 2007). GA is one of the most common global optimization methods in building applications, including building design optimization (Caldas and Norford 2002; Ooka and Komamura 2009; Wright, Loosemore et al. 2002), optimal control of HVAC systems (Chang 2005; Chow, Zhang et al. 2002; Lu, Cai et al. 2005b; Mossolly, Ghali et al. 2009; Wang and Xu 2006; Zhou and Haghighat 2009), renewable and sustainable energy (Kalogirou 2004; Varun and Siddhartha 2010). GA is capable of dealing with multi-objectives optimization with discontinuous variables and multi-modal problems, and is tolerant to noise, and hence it is robust (Huang and Lam 1997; Znouda, Ghrab-Morcos et al. 2007). In addition, it is highly efficient and is easy to use.

GAs are search or optimizing algorithms based on the mechanics of natural selection and natural genetics. They are guided randomized procedures that efficiently exploit historical information to speculate on the new search points with expected improved performance. GAs differ substantially from traditional search and optimization methods in four ways (Goldberg 1989):

(1) GAs search from a population of points in parallel, not a single point, many of which are likely to provide alternatives to the "best" individuals of the population.

(2) GAs only use the objective function and corresponding fitness levels to determine the directions of search instead of requiring derivatives or other auxiliary knowledge.

GAs do not require the calculation of the objective function gradient with respect to the design variables, and continuity of differentiability of problem functions is neither required nor used in calculations of a GA. This feature is particularly helpful in some cases such as for multi-objective problems and mixed integer non-linear programming.

(3) GAs use probabilistic transition rules instead of deterministic rules. Due to the probabilistic nature, the initial guess has a low incidence on the final result of the optimization, and GAs are unlikely to converge to a local optimum.

(4) GAs work on an encoding of the parameter set, not the parameter set itself.

2.3.1 GA procedure

Genetic algorithms are typically implemented using computer simulations in which an optimization problem is specified. In a genetic algorithm, a population of strings (called chromosomes), which encode candidate solutions (called individuals) to an optimization problem, evolves toward better solutions. Based on the idea of "survival of the fittest" and "natural selection", GA is a class of parallel iterative algorithm

with certain learning ability (Goldberg 1989). The implementation of the most traditional genetic algorithm can be briefly illustrated with Figure 2.11.

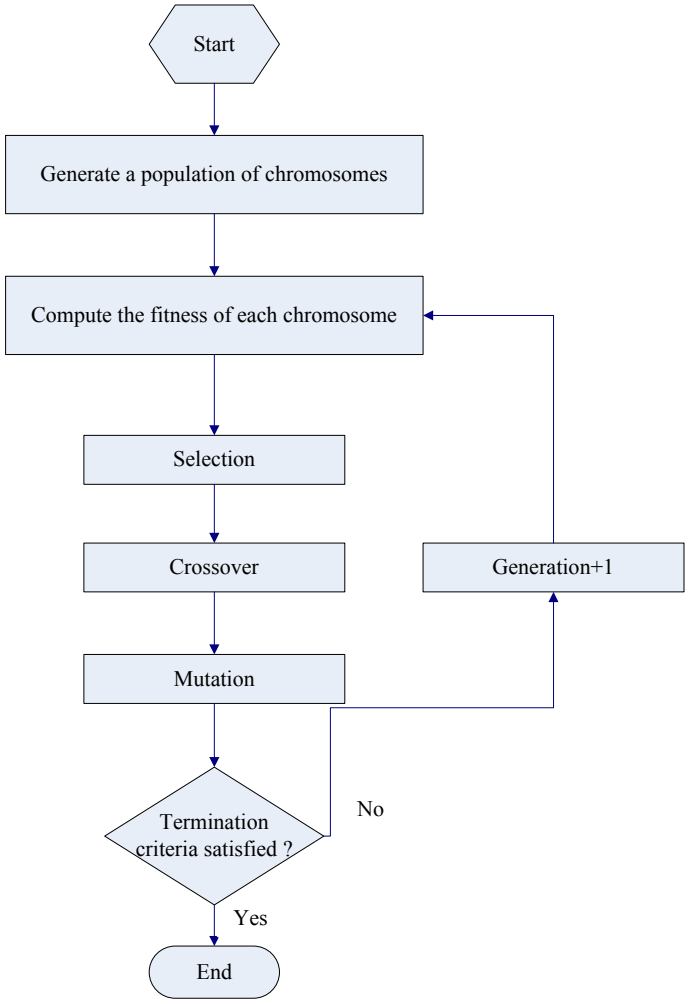

Figure 2.11 A basic genetic algorithm

It starts from an initial population of individuals randomly generated according to some probability distribution. The fitness of each individual chromosome is then calculated and evaluated, and multiple individuals are randomly selected from the current population. Then, GA applies the genetic operators to form a new population, including selection, crossover and mutation. The process is repeated until the termination criterion is satisfied. GA operates on a population of potential solutions following the principle of survival of the fittest to produce better and better approximations to a solution.

It can be identified that a GA represents an iterative process. Each iteration of this process is called a generation. A typical number of generations for a simple GA can range from 50 to 500 or more (Mitchell 1996). The entire set of generations is called a run. At the end of a run, it is expected to find one or more highly fit chromosomes in the population.

2.3.2 Elements of the genetic algorithm

Population representation

GAs operate on a number of potential solutions, called a population, consisting of some individuals simultaneously. The utilization of populations is one of the most important features of GAs. Increasing the population size enables the genetic algorithm to search more points and thereby obtain a better result. However, the larger the population size, the longer the genetic algorithm takes to compute each generation. Typically, a population size of between 30 and 100 is recommended (Chipperfield, Fleming et al. 2001).

Each chromosome represents a legal solution to the problem and is encoded of a string of genes. For most GAs, the candidate solutions are represented by chromosomes coded by either a binary number system or a real decimal number system. GAs using binary strings as the chromosomes are called binary-coded GAs. Whereas GAs using real-number representation of solutions are called real-coded GAs. The most commonly used representation in GAs is the binary alphabet (0, 1) (as shown in Figure 2.12 a) but sometimes, depending on the application, integers or real numbers (as shown in Figure 2.12 b) are used. Any representation can be used and enables a solution to be encoded as a finite length string. If a numerical optimization problem has a real value in nature, a real-coded genetic algorithm perform better than a binary-coded GA in terms of consistency, precision, and faster

execution (Lin, Li et al. 2000), which increases the level of possible exploration of the search space without adversely affecting the convergence characteristics (Chipperfield, Fleming et al. 2001). In this research, real-coded GA is used, and the variable values are represented as floating-point numbers. This is because the problems use continuous variables, and it seems more natural to use the real-coded GA.

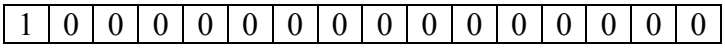

(a) binary representation

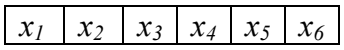

(b) real number representation

Figure 2.12 Chromosomal representation

Fitness functions

A fitness function is used to measure the chromosome's performance or fitness for the problem to be solved. The more suitable is the solution, the better is the fitness. The GA uses a measure of fitness of individual chromosomes to carry out reproduction (Negnevitsky 2005). The fitness function greatly affects the convergence speed of a GA process. To drive the GA search process towards the best solution, the fitness function should be able to reflect the key properties of the model. If the fitness function contains inadequate information about the model, it cannot identify a chromosome (solution) with superior characters, the convergence will be very slow, and the search process will not be able to find the best solution in an acceptable time period (Chen, Worden et al. 2007). Therefore, the definition of the fitness function is crucial for the problem to be solved. In addition, the fitness function has to make the evaluation of each chromosome in an efficient manner due to a large number of times the function will be called during the execution of the

genetic algorithm. According to the rule of the GA, the fitness function should be no less than zero.

GA operators

GA is an optimum search technique based on the concepts of natural selection and survival of the fittest. During the process of evolution, a population of potential solutions, termed as chromosomes/individuals, is evolved over successive generations using three main types of operators: selection, crossover and mutation. First of all, the selection operator is applied to select chromosomes to be part of a reproduction process based on fitness evaluation. In the reproduction process, new individuals of the next generation are created through crossover and mutation operators. Crossover and mutation do not always occur, and they do with some probability.

Selection This operator selects relatively 'fit' chromosomes in the population for reproduction based on the fitness criterion. The fitter an individual, the larger the probability it is likely to be selected to reproduce. There are various existing types of selection operators, including roulette wheel selection, sequential selection, tournament selection, dominant selection, hybrid selection and kin selection operators. One of the most frequently used chromosome selection techniques is the roulette wheel selection (Goldberg 1989; Lipowski and Lipowska 2012). Figure 2.13 illustrates the roulette wheel, and each chromosome is given a slice of a circular roulette wheel equal in area to the chromosome's fitness, and the fitness determines the chromosome's chance of being selected for mating. It is like spinning a roulette wheel where each chromosome has a segment on the wheel proportional to its fitness. When the roulette wheel is spun, the arrow comes to rest on one of the segments, and the corresponding chromosome is selected.

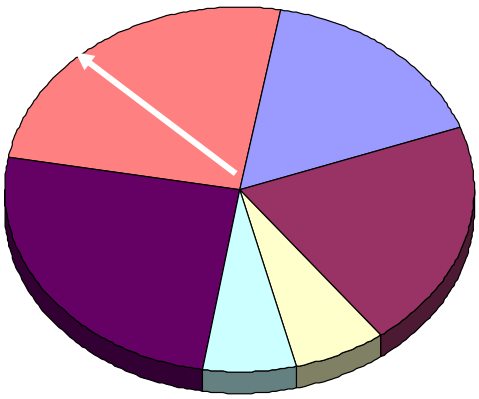

Figure 2.13 Roulette wheel selection

Considering N individuals, each is characterized by its fitness. The selection probability $p_s(X_i)$ of the i-th individual is defined as follows (Wang 2005).

$$p_s(X_i) = \frac{f(X_i)}{\sum_{j=1}^{N} f(X_j)} \tag{2.19}$$

where $f(X_i)$ is the fitness value of the individual X_i, $i = 1, 2, \ldots, N$.

Then proportional selection (e.g. round roulette selection) will be used to select designs. That is, individual X_i will be selected if a uniformly random number ζ in (0, 1) satisfies

$$\sum_{j=0}^{i-1} p_s(X_j) < \xi \le \sum_{j=0}^{i} p_s(X_j)$$

where $p_s = 0$ for $j = 0$.

Crossover Crossover is an efficient way of adapting the population based on the crossover probability. The crossover operator randomly chooses a crossover point where two parent chromosomes 'break', and then exchanges the subsequences before and after that locus between two chromosomes to create two offspring as shown in Figure 2.14, which combines the features of two parent structures. One-point crossover or two-point crossover is commonly used as the crossover method. The

crossover point is randomly selected. The purpose of crossover operator is to produce new chromosomes that are distinctly different from their parents, yet contain some of their parents' characteristics (Anijdan, Bahrami et al. 2006). Without the operator of crossover, the chromosome cloning takes place, and the offsprings are created as exact copies of their parents. The crossover operator roughly mimics biological recombination between two single-chromosome (haploid) organisms (Mitchell 1996), and blends the genetic information between chromosomes to explore the search space.

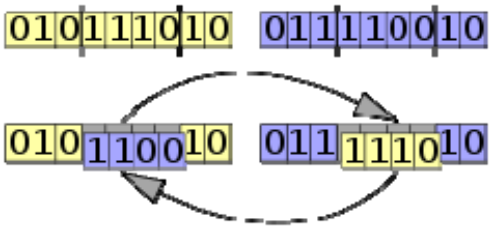

Figure 2.14 Two point crossover of binary strings

The crossover operation only occurs when the crossover probability is greater or equal to the randomly generated number between 0 and 1. In binary-coded GA, the crossover operation can be implemented by using methods like one-point crossover or two-point crossover. However, in real-coded GA, the blending methods give better results in crossover operation. In blending method, two individuals are randomly chosen among the population, and they will perform crossover with crossover probability p_c, and then the new generations are produced as the combination of the variable values from the two parents into new variable values in the offspring as follows (Randy and Sue 2004):

$$X' = \lambda X + (1-\lambda)Y \tag{2.20}$$

$$Y' = (1-\lambda)X + \lambda Y \tag{2.21}$$

where λ is a number randomly generated between 0 and 1, X and Y are the parent chromosomes, and X' and Y' are the next generation chromosomes.

Once the crossover operator is complete, the parenting pool with unchanged and recombined individuals becomes the offspring population.

Mutation The operation of mutation has the potential to change a gene. The mutation operator randomly flips some of the bits in a chromosome as shown in Figure 2.15, which represents a change in the gene. Mutation is used to maintain adequate diversity in the population of chromosomes to avoid premature convergence and trapping on a local optimum, which may lead to a significant improvement in fitness of the individual, but sometimes these random changes will have some harmful results for some conditions. Without mutation, the population tends to converge to a homogeneous state where individuals are just slightly different from each other. Mutation can occur at any gene in a chromosome with some probability, and the probability of a mutation is equal to the mutation rate. Since mutation rate is very small in natural evolution, the probability applied for the mutation operator in GAs is kept quite low, typically ranging from 0.001 to 0.01(Negnevitsky 2005).

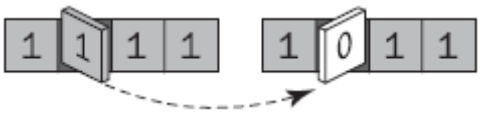

Figure 2.15 Mutation

For the real-coded GA, mutation operator is often performed in the following way by adding certain random number (Wang 2005).

$$x_{\text{new}} = x_{\text{old}} + \zeta \tag{2.22}$$

where ζ is a random number subject to normal distribution $N(0, 1)$.

2.4 Hybrid artificial neural networks-genetic algorithms technique

The greatest advantage of ANNs over other modeling techniques is their capability to model complex, non-linear processes without having to assume the form of the relationship between input and output variables (Tiwari, Dubey et al. 2009). As a developing and promising technology, ANNs have been widely used in building industry. GAs are gradient-free, parallel optimization algorithms based on the concepts of natural selection and survival of the fittest, which are capable of handling non-linear, complex and irregular solution spaces and are very efficient tools for optimization. The main drawback of GAs is the computational time to reach optimal solutions, which hinders GAs for building applications. As the commonly used simulation programs such as EnergyPlus, TRNSYS or ESP-r are time consuming to operate. Therefore, it is necessary to take full advantage of GA capabilities while keeping a reasonable computation time.

Finding the solution to an optimal control problem is generally difficult and time-consuming even in the presence of complete and correct knowledge of the system dynamics. Many practical optimization problems have no explicitly known forms of objective functions, so that they require considerably expensive computational time or some complicated analysis to evaluate the objective value. Due to their advantages of ANN and GA, the combination of ANN and GA has been used for integrated process modeling and optimization. If a hybrid artificial neural networks-genetic algorithms (ANN-GA) strategy is proposed, where ANN is used as fitness approximation and GA is applied to perform effective and robust evolutionary optimization, this hybrid technique will guarantee the efficiency of genetic search and the optimal solutions.

The hybrid ANN-GA strategy has been applied for prediction of electrical energy

consumption (Azadeh, Ghaderi et al. 2007; Li and Su 2010), optimization of solar systems (Mellit, Kalogirou et al. 2010; Soteris A 2004), optimization of ventilation systems (Zhou and Haghighat 2009), building design (Magnier and Haghighat 2010; Sun, Fang et al. 2010), and optimization of building central cooling systems (Chow, Zhang et al. 2002; Gibson 1997). These studies confirm that the integrated algorithm of artificial neural network and genetic algorithm is powerful and efficient in the building field, which can save a significant amount of computation time while keeping the optimization reliable.

Chiller system optimization control is a complicated nonlinear system. In the past, many optimization control studies related to central cooling plant had been reported, but the analyses of the research on chiller optimization encountered complex thermodynamic phenomena and relied on a series of simplifying assumptions. Such analysis needs a robust numerical solver and is time-consuming to solve under the diverse weather and operating conditions, and hence is not suitable for rapid prediction in optimization and process control. The GA and ANN are appropriate to tackle the chiller system control problems, and the hybrid ANN−GA technique is a powerful method for process modeling and optimization, which can take full advantage of ANN and GA capabilities (Chow, Zhang et al. 2002). In this study, a hybrid ANN–GA strategy is proposed to facilitate modeling and optimization of the air-cooled chillers, where ANN learns the nonlinear mapping and is used as fitness approximation, and GA is applied to perform effective and robust evolutionary optimization to find the global optimum in a bounded parametric searching space.

One of the objectives in this research is to develop the optimal control strategy using a hybrid ANN and GA under variable condensing temperature control, but there is a lack of the chiller operating data under variable condensing temperature control.

Currently nearly all the air-cooled chillers are operating under HPC, there is no reset for set point of condensing temperature when chiller are operating at various conditions. In order to study how the set points of condensing temperature influence the performance of air-cooled chillers, even establish the scheme for optimum set point of condensing temperature, the detailed simulation of chiller plant is needed. The simulation results will be treated as database for ANN models to train and test. When the manufactures do the experiments under CTC, and the related operating data are recorded, the operating data will easily replace the simulation data and be used as the database for the ANN models, as the methodologies are the same.

The general approach for the simulation-based optimization strategy of this study is illustrated in Figure 2.16. It is divided in three sequential steps. First the representative office building and hotel building models and chiller models are developed using EnergyPlus and TRNSYS, and the chiller models are validated using measured operating data. Then, sufficient simulations using these models are conducted to generate a database under normal operating conditions. Once the database is created, the simulation results will be used to train and validate the ANN models. After training and validation, the ANN models are then integrated into the genetic algorithm serving as the evaluation function, and GA can search for the optimal or near-optimal controlled variables to operate the chillers efficiently.

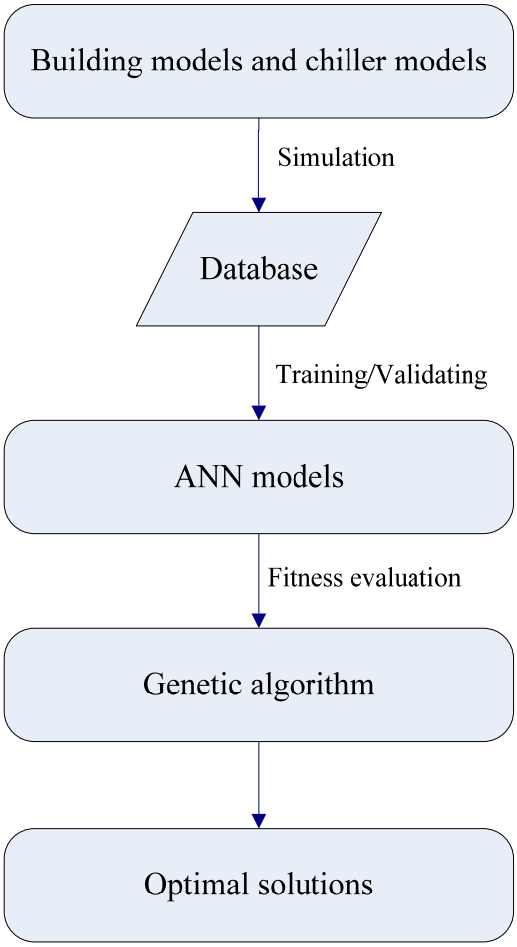

Figure 2.16 Optimization strategy

Chapter 3 Building System and Simulation Platform

This chapter presents the generic reference buildings including a representative office building and a hotel building, and the characteristics of the load-frequency and weather-load profiles of such buildings. It outlines how these load profiles can be used to evaluate the numbers of chillers in the chilled water plants serving the buildings. The representative hotel and office buildings are mainly used to ascertain the cooling demand for the typical commercial buildings and investigate the developed optimal strategies in terms of energy performances under various operating conditions.

3.1 Building and system description

It is widely recognized that commercial buildings account for major electricity consumption and this strongly influences the environment and world ecosystem (Lam 2000; Lam, Li et al. 2003; Yu and Chan 2005a). The majority of buildings in Hong Kong are high-rise and large portion of the total building stocks are commercial buildings, including office buildings and hotels. These account for considerable energy consumption in the building sector in Hong Kong. According to surveys of the electricity consumption of local hotels and office buildings (Deng and Burnett 2000; Yik, Burnett et al. 2001), hotels have an average energy use intensity (EUI) of 406 kWh/m^2 to 427 kWh/m^2 which is nearly double the amount consumed by office buildings. The amount of electrical energy consumed by the central chillers is large, which accounts for as much as 35-40% of the annual total electricity in Hong Kong (Chan and Yu 2002). Therefore, it is worth investigating the electricity end-use characteristics of the commercial buildings.

To formulate strategies for optimizing the efficiency of chilled water plants in commercial buildings, it is important to understand the interaction between building cooling load and chiller load profiles. Two buildings are modelled in this research: one is a representative office building in Hong Kong, and the other is an existing five star hotel which is representative of the trade. The model buildings are aimed at ascertaining the cooling load profiles which constitute the inputs of the chiller model developed in this research.

3.1.1 Description of generic reference buildings

The characteristics of building cooling load greatly influence the determination of chillers and how these chillers should be staged in implementing chiller sequencing.

As there are various buildings with different designs, shapes and scales, and each type of building has its own feature such as occupancy schedules, the internal heat gains, and the requirements for air-conditioning and the chiller system. With regard to the investigation into the impacts of the chiller power consumption of buildings with various control strategies, it would be extremely time-consuming and tedious if the different cooling load patterns of all different types of building are simulated. Therefore, generic office and hotel buildings are needed to serve as a basis for comparison and evaluation. The generic buildings should incorporate most of the design features common in local commercial buildings.

According to a survey of 64 commercial buildings in Hong Kong (Chan and Chow 1998), the construction characteristics of high-rise office buildings in Hong Kong were identified and a reference building was developed as the basis for simulation. The reference office building is 40-storey high with building parameters commonly found in the surveyed buildings. It has a dimension of 36 m × 36 m with curtain-wall construction and a centralized HVAC system. Figure 3.1 shows the plan of the model

building, which has a 3.2 m floor-to-floor height and a window height of 1.6 m. This represents a window-to-wall ratio (WWR) of 50%.

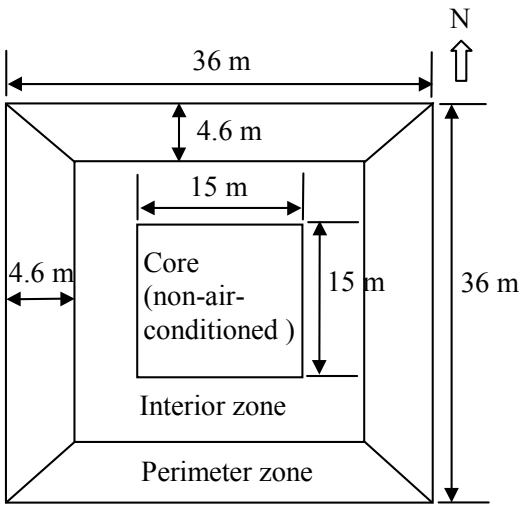

Figure 3.1 Typical floor plan and thermal zones of the office building

As for hotel buildings, the representative hotel building is based on an existing hotel in Hong Kong. According to the energy surveys for the local hotel sector (Deng and Burnett 2000), the hotel building adopted in this study has average characteristics in terms of the number of guestrooms, total floor area and annual electricity consumption per unit floor area of the building. It is expected that the hotel has representative cooling requirement and energy performance for a large group of local hotels. Figures 3.2 and 3.3 show the hotel configuration and the floor plan. Table 3.1 summarizes the general features of the representative office and hotel buildings.

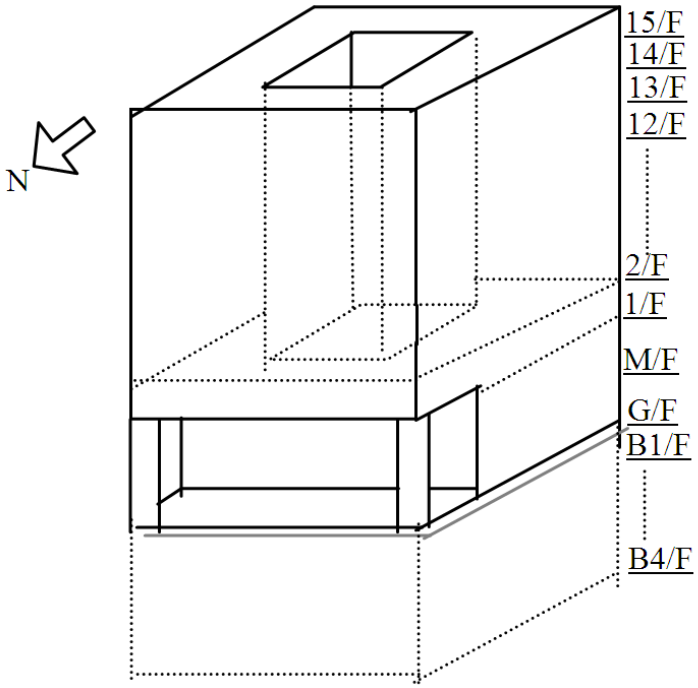

Figure 3.2 Hotel configuration

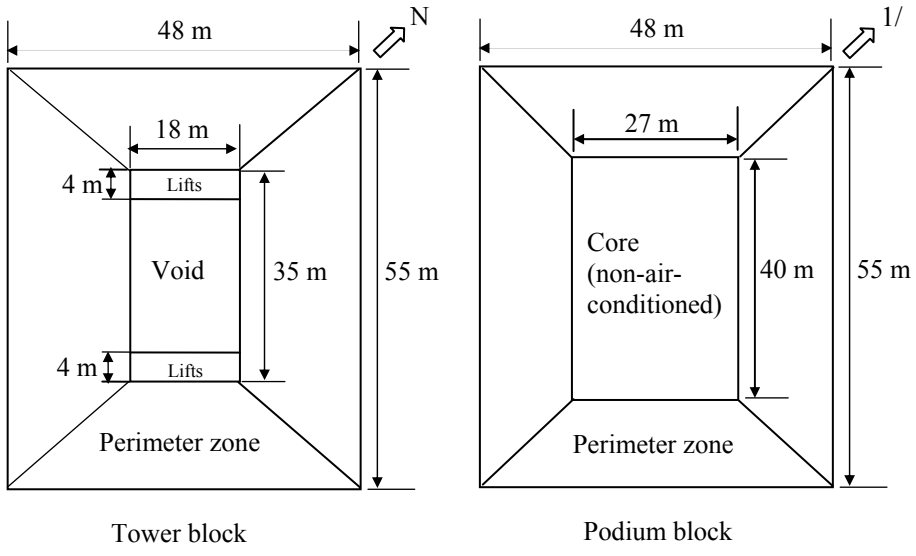

Figure 3.3 Floor plan and thermal zones of the tower block and podium block in the hotel building

Table 3.1 Basic characteristics and design criteria of office and hotel examples

Building	Office	Hotel	
General	Tower	Tower	Podium
Area	Office	Guestrooms	Shops and restaurants
Floor Dimension (L x W) (m)	36 x 36	55 x 48 with a central void of 18 x 27	55 x 48
Area per floor (m^2)	1296	2154	2640
Air-conditioned area per floor (m^2)	1071	2010	1560
Number of floors	40	17	4
Floor to floor height (m)	3.2	2.6	3.9
Total air-conditioned area (m^2) (%GFA)	42840 (82.6)	42420 (85.9)	
Gross floor area (GFA) (m^2)	51840	49332	
Orientation	N/E/S/W	NW/NE/SE/SW	
Aspect ratio	1.0	1.1	
Construction Details			
Window to wall ratio	0.5	NW/SE: 0.6, SW/NE: 0.3	
U-value (Wall) ($W/m^2 \cdot °C$)	2.3	1.9	
U-value (Window) ($W/m^2 \cdot °C$)	5.7	5.4	
U-value (Roof) ($W/m^2 \cdot °C$)	0.7	0.7	
Glass shading coefficient	0.45	0.55	
Design Criteria			
Area	Office	Guestrooms	Shops and restaurants
Temperature (°C)	24	24	22
Relative humidity (%)	50	50	50
Ventilation rate (L/s/person)	10	7.5	5
Occupancy (m^2/person)	9	18	5
Equipment load (W/m^2)	25	12	50
Lighting load (W/m^2)	20	18	35
Occupied periods			
Weekdays	0900–1700	0100–2400	0800–2300
Saturdays	0900–1300	0100–2400	0800–2300
Sundays	Unoccupied	0100–2400	0800–2300

3.1.2 Zones and system description

Due to the complexity of the representative office and hotel buildings, the buildings are divided into multi-zones, as illustrated in Figure 3.1, Figure 3.3 and Figure 3.4. The detailed information about the construction of the office and hotel buildings is shown in Table 3.2 and Table 3.3. After each thermal zone was constructed, the parameters influencing its thermal environment were specified, namely, infiltration, ventilation, heating, cooling, and heat gains due to occupancy, computer equipment, artificial lighting and other heat generating appliances.

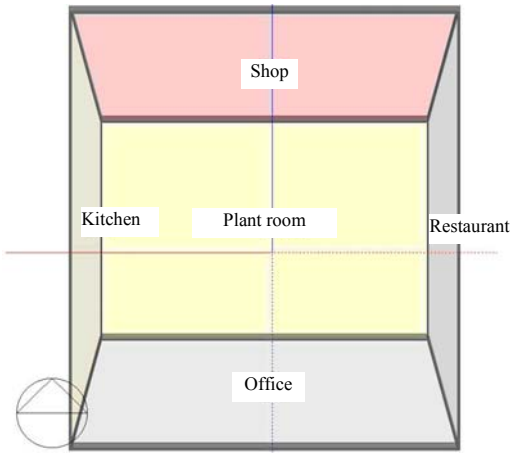

(a) Basement

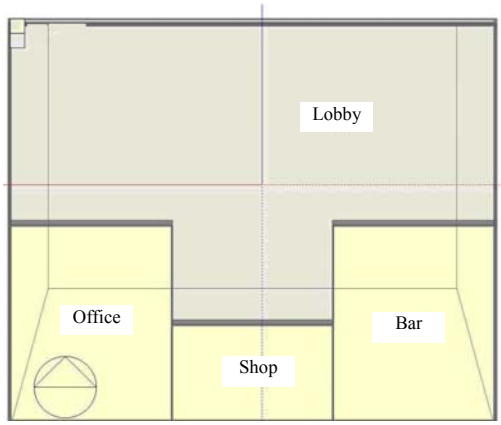

(b) Ground floor

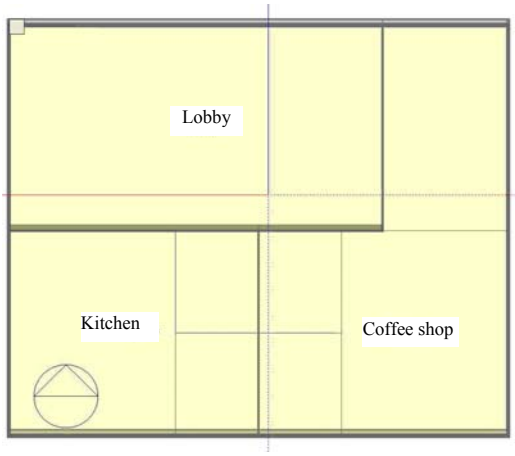

(c) Mezzanine floor

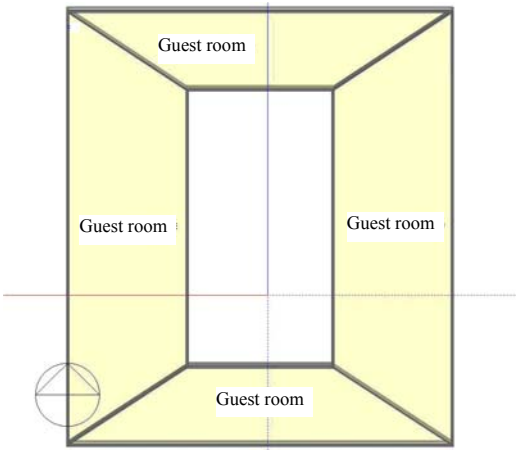

(d) Typical floor

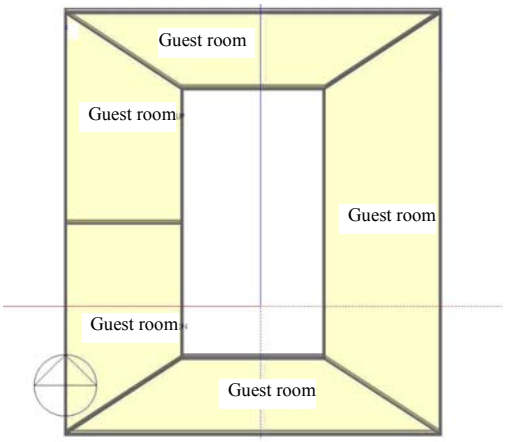

(e) 14th floor

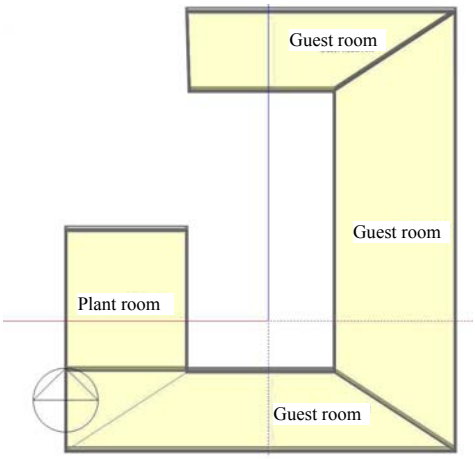

(f) 15th floor

Figure 3.4 Zoning arrangements in the hotel building (plan view)

Table 3.2 Construction of fabric and internal structure of the office building

Layer Material*	Thickness (mm)	Thermal conductivity (W/m·°C)	Density (kg/m^3)	Specific heat (J/kg· °C)	Thermal resistance (m^2·°C /W)
External wall					
Granite panel	25	1.802	2242	837	-
Air layer	50	-	-	-	0.156
Concrete	100	1.731	2243	840	-
Plaster	20	0.38	1120	840	-
Roof					
Screeding	25	0.721	1858	837	-
Polystyrene Insulation	37	-	-	-	1.07
Asphalt	30	-	-	-	0.026
Screeding	25	0.721	1858	837	-
Concrete	100	1.731	2243	840	
Floor					
Vinyl tile	-	-	-	-	0.0088
Screeding	25	0.721	1858	837	-
Concrete	50	1.731	2243	840	-
Ceiling					
Concrete	50	1.731	2243	840	-
Screeding	25	0.721	1858	837	-
Vinyl tile	-	-	-	-	0.0088
Partition					
Gypsum board	15	0.16	950	840	-
Air layer	50	-	-	-	0.156
Gypsum board	15	0.16	950	840	-
Core wall					
Plaster	20	0.727	1602	840	-
Concrete	250	1.731	2243	840	-
Plaster	20	0.727	1602	840	-
Window					
6 mm reflective glass, single pane, shading coefficient = 0.45, U-value = 5.5 W/(m^2·°C)					

* Layer sequence: top to bottom = outside to inside

Table 3.3 Construction of fabric and internal structure of the hotel building

Layer Material*	Thickness (mm)	Thermal conductivity (W/m·°C)	Density (kg/m^3)	Specific heat (J/kg·°C)	Thermal resistance (m^2·°C /W)
External wall					
Granite panel	25	1.802	2242	837	-
Air layer	50	-	-	-	0.156
Concrete	200	1.731	2243	840	-
Plaster	20	0.38	1120	840	-
Roof					
Screeding	25	0.721	1858	837	-
Polystyrene Insulation	37	-	-	-	1.07
Asphalt	30	-	-	-	0.026
Screeding	25	0.721	1858	837	-
Concrete	100	1.731	2243	840	
Floor					
Vinyl tile	-	-	-	-	0.0088
Screeding	25	0.721	1858	837	-
Concrete	50	1.731	2243	840	-
Ceiling					
Concrete	50	1.731	2243	840	-
Screeding	25	0.721	1858	837	-
Vinyl tile	-	-	-	-	0.0088
Partition					
Gypsum board	15	0.16	950	840	-
Air layer	50	-	-	-	0.156
Gypsum board	15	0.16	950	840	-
Core wall					
Plaster	20	0.727	1602	840	-
Concrete	150	1.731	2243	840	-
Plaster	20	0.727	1602	840	-
Window					
6 mm tinted glass, single pane, shading coefficient = 0.55, U-value = 5.38 W/m^2·°C					

* Layer sequence: top to bottom = outside to inside

3.2 Development of the simulation platform

3.2.1 EnegyPlus and its applications

Computer simulation is commonly used to determine the thermal performance of buildings. Among various simulation programs, EnergyPlus is a new building energy simulation program (Crawley, Lawrie et al. 2001) that combines the strengths of two widely used programs, namely BLAST (Al-Rabghi and Hittle 2001) and DOE-2 (Andolsun, Culp et al. 2011), and it represents a significant step forward in terms of computational techniques and program structures. For the simulation of the thermal behaviour of the representative buildings under climate change, EnergyPlus has many desirable features and is employed as the simulation tool in this research.

The models of the representative office building and hotel building were developed to ascertain the cooling demand for these typical buildings with the simulation program EnergyPlus. In the calculation of hourly building cooling loads, detailed features of these buildings were compiled, including the materials, orientation, construction, ventilation and air-conditioning requirements, occupancy, equipment power density and operating schedules, which were set according to EMSD's recommendations (EMSD 2007). The schedules for occupancy density, lighting density and ventilation are presented in Tables 3.4, 3.5 and 3.6, whereby the variations of cooling demand and heat gains in different periods can be precisely described.

Table 3.4 Occupancy density, lighting load profiles and operating schedule of ventilating fans in the office building

Hour	Occupancy*	Lighting* (Perimeter)	Lighting* (Interior)	Ventilating fans
		Weekdays		
1-7	0.0	0.05	0.05	Off
8	0.05	0.1	0.1	Off
9	0.4	0.5	0.5	On
10	0.95	0.9	1.0	On
11	0.95	0.9	1.0	On
12	0.95	0.9	1.0	On
13	0.95	0.9	1.0	On
14	0.45	0.8	0.9	On
15	0.95	0.9	1.0	On
16	0.95	0.9	1.0	On
17	0.95	0.9	1.0	On
18	0.5	0.8	0.8	On
19	0.25	0.5	0.5	On
20	0.1	0.3	0.3	Off
21	0.05	0.2	0.2	Off
22-24	0.0	0.05	0.05	Off
		Saturday		
1-7	0.0	0.05	0.05	Off
8	0.05	0.1	0.1	Off
9	0.3	0.5	0.5	On
10-13	0.6	0.75	0.8	On
14-17	0.1	0.2	0.2	Off
18	0.05	0.1	0.1	Off
19-24	0.0	0.05	0.05	Off
		Sunday		
1-9	0.0	0.05	0.05	Off
10-17	0.05	0.1	0.1	Off
18-24	0.0	0.05	0.05	Off

* Values denote fractions of maximum occupancy and lighting power.

Table 3.5 Occupancy density, lighting and equipment load profiles and the operating schedule of ventilating fans of guestrooms in the hotel building

Hour	Occupancy*	Lighting*	Equipment*	Ventilating fans
		Weekdays		
1-8	1.0	0.05	0.05	On
9-21	0.3	0.3	0.3	On
22-24	1.0	0.05	0.05	On
		Saturday		
1-8	1.0	0.05	0.05	On
9-21	0.3	0.3	0.3	On
22-24	1.0	0.05	0.05	On
		Sunday		
1-8	1.0	0.05	0.05	On
9-21	0.3	0.3	0.3	On
22-24	1.0	0.05	0.05	On

* Values denote fractions of maximum occupancy, lighting power and equipment power.

Table 3.6 Occupancy density, lighting and equipment load profiles and the operating schedule of ventilating fans of shops and restaurants in the hotel building

Hour	Occupancy*	Lighting*	Equipment*	Ventilating fans
		Weekdays		
1-7	0.1	0.05	0.05	Off
8-16	0.8	0.8	0.8	On
17-23	0.7	0.8	0.8	On
23-24	0.1	0.05	0.05	Off
		Saturday		
1-7	0.1	0.05	0.05	Off
8-16	0.8	0.8	0.8	On
17-23	0.7	0.8	0.8	On
23-24	0.1	0.05	0.05	Off
		Sunday		
1-7	0.1	0.05	0.05	Off
8-16	0.8	0.8	0.8	On
17-23	0.7	0.8	0.8	On
23-24	0.1	0.05	0.05	Off

* Values denote fractions of maximum occupancy, lighting power and equipment power.

Since the developed optimal control strategies mainly focus on optimizing the control of multiple chiller systems to improve the chiller efficiency, the thermal balance is of major concern; therefore, the following simplifications have been made in the construction of the building models.

(a) The cooling loads calculated from EnergyPlus are simply the idealized energy required to maintain indoor temperature set points and the results are not system-specific.

(b) It is assumed that every piece of air-handling equipment is capable of delivering the cooling energy required to meet the cooling demand for the thermal conditions specified in each zone and that the operation of chillers with different arrangements is able to satisfy perfectly the changing building cooling load.

(c) The controllability and dynamic response of the airside and water equipment are disregarded in this steady-state performance analysis.

3.2.2 Building modelling

Google Sketchup is employed to generate building geometry for the EnergyPlus model, which is a user-friendly 3-D drawing interface. OpenStudio, a plug-in for Google SketchUp, is an extension to Google's popular 3D modeling tool that adds EnergyPlus context to the SketchUp program. The Plug-in allows users to quickly create geometry for EnergyPlus using the built-in functionality of Google SketchUp including existing drawing tools, integration with Google Earth, Building Maker, and Photo Match. Figure 3.5 shows the EnergyPlus building models using Google SketchUp for the office building and the hotel building, respectively.

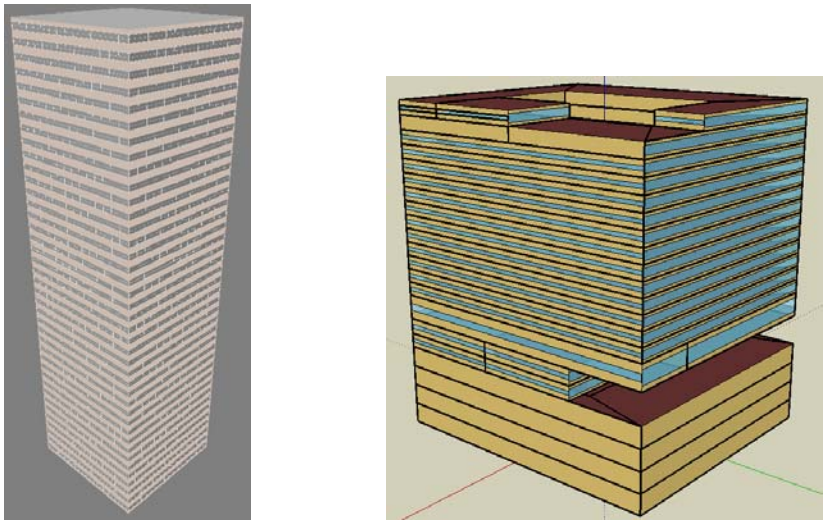

(a) Office building (b) Hotel building

Figure 3.5 3D view of office building and hotel building model

3.2.3 Cooling load profile of office and hotel buildings

Based on the hourly weather data of an Example Weather Year, there are 3051 cooling hours for the office building, which account for 97.8% of the total 3120 office hours. Table 3.7 shows the frequency distribution of hourly building load ratios (BLRs) in different ranges of outdoor temperatures for the office building, which is a ratio to the peak building cooling load. Load-frequency means the percentage of total operating hours at a given range of building load ratios. The chillers and pumps have to operate at a building load ratio of below 0.5 for 67.7% of the total cooling hours. The peak load range of 0.9 to 1 accounts for only 1.0% of the total cooling hours.

For the representative hotel building, there are 8551 cooling hours which accounted for 97.6% of the total 8760 hours per year. Table 3.8 shows the frequency distribution of the hourly building cooling load ratios in different ranges of outdoor temperatures. The chillers and pumps have to operate at a building load ratio of below 0.5 for 55.9% of the total cooling hours. The peak load range of 0.9 to 1 accounts for only 0.6% of the total cooling hours.

Table 3.7 Frequency distribution of hourly office building cooling loads

Outdoor temperature (°C)	Building load ratio (Building cooling load expressed as a ratio of its peak value)										
	0–0.1	0.1–0.2	0.2–0.3	0.3–0.4	0.4–0.5	0.5–0.6	0.6–0.7	0.7–0.8	0.8–0.9	0.9–1	Subtotal
11–13	2	0	0	0	0	0	0	0	0	0	2
13–15	81	0	0	0	0	0	0	0	0	0	81
15–17	158	59	0	0	0	0	0	0	0	0	217
17–19	14	244	37	0	0	0	0	0	0	0	295
19–21	0	113	205	24	0	0	0	0	0	0	342
21–23	0	17	199	108	20	0	0	0	0	0	344
23–25	0	7	63	137	84	16	0	0	0	0	307
25–27	0	1	32	70	121	120	37	1	0	0	382
27–29	0	0	23	35	99	93	109	48	5	0	412
29–31	0	0	8	26	60	24	145	146	71	6	486
31–33	0	0	0	5	12	3	24	48	58	25	175
33–35	0	0	0	0	0	0	2	2	3	1	8
Subtotal	255	441	567	405	396	256	317	245	137	32	3051

Table 3.8 Frequency distribution of hourly hotel building cooling loads

Outdoor temperature (°C)	Building load ratio (Building cooling load expressed as a ratio of its peak value)										
	0–0.1	0.1–0.2	0.2–0.3	0.3–0.4	0.4–0.5	0.5–0.6	0.6–0.7	0.7–0.8	0.8–0.9	0.9–1	Subtotal
11–13	82	1	0	0	0	0	0	0	0	0	83
13–15	321	81	0	0	0	0	0	0	0	0	402
15–17	143	546	25	0	0	0	0	0	0	0	714
17–19	0	409	443	9	0	0	0	0	0	0	861
19–21	0	30	614	335	10	0	0	0	0	0	989
21–23	0	0	135	411	212	35	0	0	0	0	793
23–25	0	0	3	216	410	303	56	2	0	0	990
25–27	0	0	0	15	286	413	318	117	6	0	1155
27–29	0	0	0	0	47	277	454	424	256	8	1466
29–31	0	0	0	0	0	74	300	180	248	34	836
31–33	0	0	0	0	0	10	144	70	21	9	254
33–35	0	0	0	0	0	0	6	2	0	0	8
Subtotal	546	1067	1220	986	965	1112	1278	795	531	51	8551

The characteristics of the building cooling load were expressed as a weather–load profile, which shows how the hourly building cooling load (expressed as a ratio to its peak value) changes in response to outdoor temperature throughout a year. Figures 3.6 and 3.7 show the weather-load profiles of the typical office building and hotel building, respectively. As illustrated in these figures, the building load ratio increase closely with the outdoor temperature. The weather-load profile of a building could be used for demonstrating a weather dependent load and an internal load (weather independent load), and the proportion of the internal load could be separate from the weather-dependent load by analyzing the weather load profile.

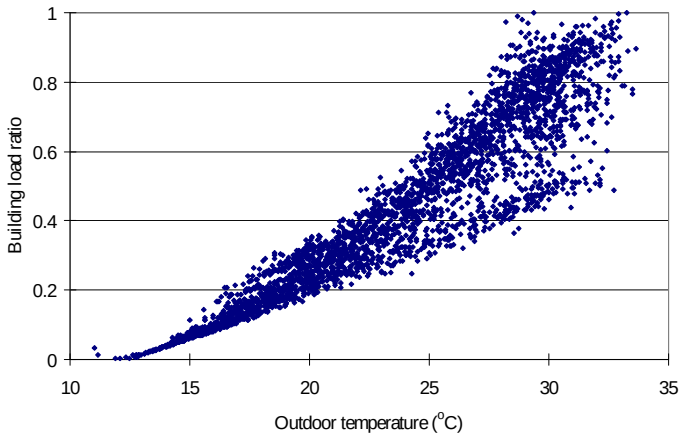

Figure 3.6 Weather load profile of the representative office building

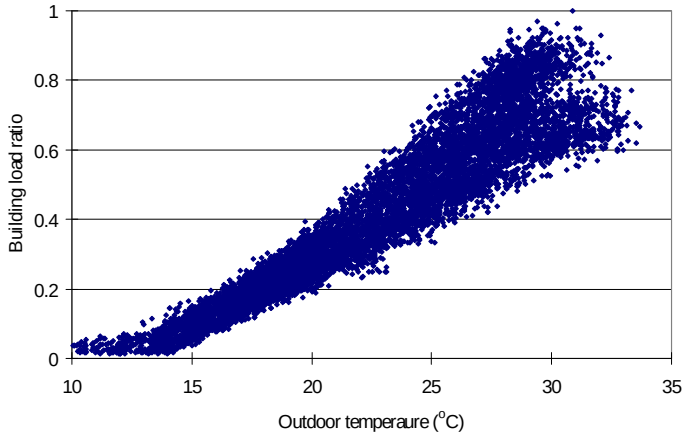

Figure 3.7 Weather load profile of the representative hotel building

Based on the weather-load and load-frequency profiles, the hourly building cooling load is used to determine how many chillers needed to be staged and the operating conditions of chillers. To meet the peak cooling load of 7253 kW, the chiller plant of the office building is designed with seven air-cooled screw chillers, each of which has a nominal cooling capacity of 1116 kW. The size of these chillers is comparable to that of the investigated chiller. The use of equally-sized chillers within a multiple chiller system can facilitate easier implementation of a control strategy and provide more flexible operation and maintenance (ASHRAE. 2007). As the peak cooling load of the hotel building is 4476 kW, the hotel building's chiller plant is designed with four air-cooled screw chillers, each of which had a nominal cooling capacity of 1116 kW, and also the cooling capacity is compatible to the studied chiller in this research.

To highlight the chiller load profiles, the conventional chiller sequence of a multiple-chiller system is considered in this study, which is to operate the minimum number of evenly loaded chillers to meet the required cooling load. With this chiller sequence, all the staged chillers are operating at the same load, and no additional chillers started to operate until each of the running chillers is operating at full load. This means that two, three, and four chillers would operate when the building

cooling load exceeded 1116, 2232 and 3348 kW for the hotel building, respectively. It is important to look at how often the chillers operated at or near full load. Table 3.9 demonstrates how the hourly data of chiller part load ratios of the hotel building are distributed in different ranges of outdoor temperatures, given the schedule of staging chillers and the hourly building cooling load data shown in Table 3.8. Under the multiple chiller arrangement, each chiller operates at higher load ratios and 68.2% of the total chiller load data are at part load ratios of 0.7–1. Furthermore, the chillers are able to work at a part load ratio of 0.9–1 with outdoor temperatures ranging between 11–35°C for over 18.6% of the operating time.

Table 3.9 Frequency distribution of the hourly data of chiller loads (Hotel)

Outdoor temperature (°C)	Chiller part load ratio									
	0.1–0.2	0.2–0.3	0.3–0.4	0.4–0.5	0.5–0.6	0.6–0.7	0.7–0.8	0.8–0.9	0.9–1	Subtotal
11–13	48	33	1	1	0	0	0	0	0	83
13–15	110	101	108	64	16	3	0	0	0	402
15–17	3	31	108	154	175	138	80	23	2	714
17–19	0	0	0	15	187	147	194	193	125	861
19–21	0	0	0	0	368	256	114	107	144	989
21–23	0	0	0	0	126	245	202	125	95	793
23–25	0	0	0	0	3	118	395	256	218	990
25–27	0	0	0	0	0	108	361	357	329	1155
27–29	0	0	0	0	0	53	447	600	366	1466
29–31	0	0	0	0	0	1	134	484	217	836
31–33	0	0	0	0	0	0	29	136	89	254
33–35	0	0	0	0	0	0	1	4	3	8
Subtotal	161	165	217	234	875	1069	1957	2285	1588	8551

Table 3.10 shows how the hourly data of chiller part load ratios of the office building are distributed in different ranges of outdoor temperatures. Given seven steps of staging chillers to meet the changing building cooling load, the opportunity to operate the chillers at higher loads increases considerably. 79.3% of the total chiller load data are at part load ratios of 0.7–1 for the entire range of outdoor temperatures.

Furthermore, the chillers are able to work at a part load ratio of 0.9–1 with outdoor temperatures ranging between 11–35°C for over 31.4% of the operating time.

Table 3.10 Frequency distribution of the hourly data of chiller loads (Office building)

Outdoor temperature (°C)	Chiller part load ratio									
	0.1–0.2	0.2–0.3	0.3–0.4	0.4–0.5	0.5–0.6	0.6–0.7	0.7–0.8	0.8–0.9	0.9–1	Subtotal
11–13	1	0	1	0	0	0	0	0	0	2
13–15	27	32	18	3	1	0	0	0	0	81
15–17	0	1	42	58	51	24	20	15	6	217
17–19	0	0	0	0	81	44	55	60	55	295
19–21	0	0	0	0	57	73	71	78	63	342
21–23	0	0	0	0	6	62	94	92	90	344
23–25	0	0	0	0	1	34	105	77	90	307
25–27	0	0	0	0	0	7	82	151	142	382
27–29	0	0	0	0	0	6	29	208	169	412
29–31	0	0	0	0	0	2	38	216	230	486
31–33	0	0	0	0	0	0	3	63	109	175
33–35	0	0	0	0	0	0	0	4	4	8
Subtotal	28	33	61	61	197	252	497	964	958	3051

The cooling load profiles of these representative commercial buildings are used to:

- explore the relationship between building cooling load and chiller load;
- ascertain the conditions in which the staging of multiple chillers can be optimized;
- as an input to a chiller system model to analyse the year-round energy consumption of chillers under head pressure control and various energy saving measures.
- develop a benchmark for chiller efficiency under condensing temperature control.

3.3 Summary

This chapter describes the details of a representative office and a hotel building and their central HVAC systems concerned in this research. Based on these details, the representative office and hotel building models were developed with necessary simplifications. This chapter also explains how the load-frequency and weather-load profiles of the office building and hotel buildings varied. Having identified the operating conditions of the chillers in terms of the weather-load and load-frequency profiles, the building models together with the chiller models can be used for evaluating the robustness and energy efficiency of the control strategies which are reported in the following chapters.

Chapter 4 Modelling and Simulation of Chiller Systems

This chapter provides information about the chiller plant studied in an institutional building complex and the evaluation of the operating variables. It describes the development of a model of the air-cooled screw chiller with twin refrigeration circuits, which is validated with a wide range of operating data. This chiller model forms the basis for the comparison of different control strategies and the development of optimum chiller control strategy. This chapter then investigates how variable condensing temperature control and variable speed condenser fans can be applied to enhance the chiller COP. It also presents the investigation on the optimal load sharing between refrigeration circuits in an air-cooled chiller.

4.1 Field investigation into the performance of chilled water plants

4.1.1 Description of the buildings studied and their chiller plants

In order to identify the operating characteristics and efficiency of air-cooled chillers, one existing chilled water plant installed in an institutional complex was investigated at length. The chilled water plant includes five identical air-cooled screw chillers, which are connected in parallel as shown in Figure 4.1. The chillers operate under HPC, and heat rejection is regulated by staging minimal number of condenser fans to maintain the condensing temperature at a high level in most operating conditions. As shown in Figure 4.1, the chilled water distribution system of the plant is a two-loop pumping system. Each of the five chillers operates in conjunction with a dedicated constant speed primary-loop chilled water pump, while three identical variable-speed chilled water pumps are provided in the secondary-loop for distributing chilled water to air-side equipments. The rated flow rate and pumping pressure of the primary-loop

pumps are respectively 50 l/s and 200 kPa, and those of the secondary-loop pumps are 125 l/s and 430 kPa. Figure 4.2 is a photo of one of the studied chiller of the chiller plant. To meet the changing building cooling load, conventional chiller sequencing is implemented so that all the operating chillers share the load equally, and no additional chiller is started until each of the running chillers is operating at full load.

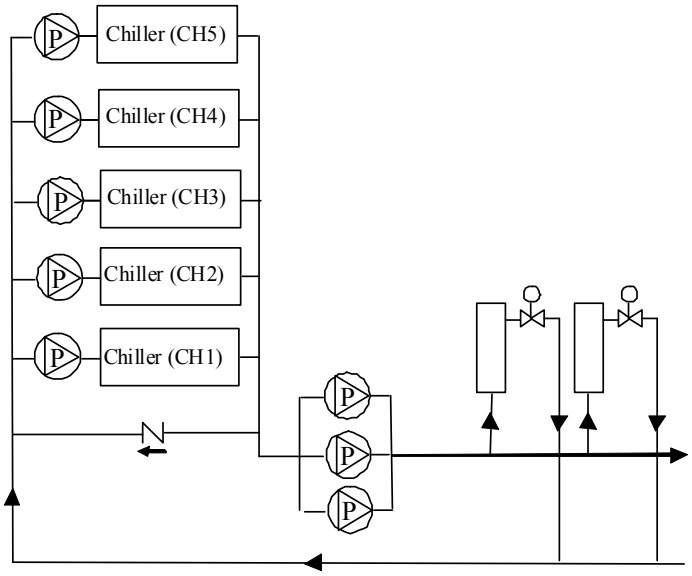

Figure 4.1 Schematic of the chiller system

Figure 4.2 A photo of the studied chiller

For this chiller plant, using refrigerant R134a, each chiller has a nominal cooling capacity of 1116 kW rated under the operating conditions of entering condenser air temperature at 35°C, entering/leaving chilled water temperatures at 12°C/7°C and chilled water flow rate at 50 l/s. The chiller comprises two refrigeration circuits in parallel and each circuit includes one evaporator, one condenser, one electronic expansion valve and two screw compressors. The air-cooled condenser contains 16 identical condenser fans to deliver a total airflow rate of 85.5 m^3/s by eight groups of condenser fans, and each refrigeration circuit is equipped with four groups of condenser fans. The power of each fan is 2.4 kW and the total fan power is 38.4 kW when all the fans are operating. The rated electric power demand of each chiller is 398 kW, and the COP at full load is 2.8. The detailed physical data of the studied chillers are shown in Table 4.1.

Table 4.1 Details of the chiller model

Refrigerant type	HFC-134a
Nominal cooling capacity (kW)	1116
Nominal power input (kW)	398
Refrigerant charge (kg)	
Circuit 1	156
Circuit 2	157
Compressors	
No. in circuit 1	2
No. in circuit 2	2
No. of control steps	10
Minimum step capacity (%)	10
Evaporator	
Type	Shell-and-tube flooded
Evaporating temperature (°C)	5
Temperature of supply chilled water (°C)	7
Max. water side operating pressure	1000
Condensers	
Condenser fans quantity	16
Fan speed (r/s)	15.8
Total air flow (m^3/s)	85.5

To investigate the performance of the air-cooled chiller, the operating data of the chiller plant were monitored year-round by a building management system, and were

compiled to provide a basis for the chiller model development and for verification of the chiller models. The operating data were monitored and logged by the building management system at one hour intervals over the experimental period. Figure 4.3 shows the graphical screen of the studied chiller plant.

The measured variables included outdoor temperature (T_{db}), evaporating temperature and pressure (T_{ev} and P_{ev}), condensing temperature and pressure (T_{cd} and P_{cd}) of each refrigeration circuit, power of each compressor (E_{cc}), chilled water flow rate (m_w), temperatures of supply and return chilled water (T_{chws} and T_{chwr}), condenser fan power of each circuit (E_{cf}), compressor power (E_{cc}). Resistance type temperature sensors were used to measure the temperature of chilled water at an uncertainty of ±0.1°C of readings. The chilled water flow rate was measured by ultrasonic flow meters with an uncertainty of ±1.5% of the flow rate. Compressor power and condenser fan power were metered by power meters with an uncertainty of ±1% of reading. The chiller COP was calculated by the chiller load divided by the overall power input, including power input to the compressors and condenser fans.

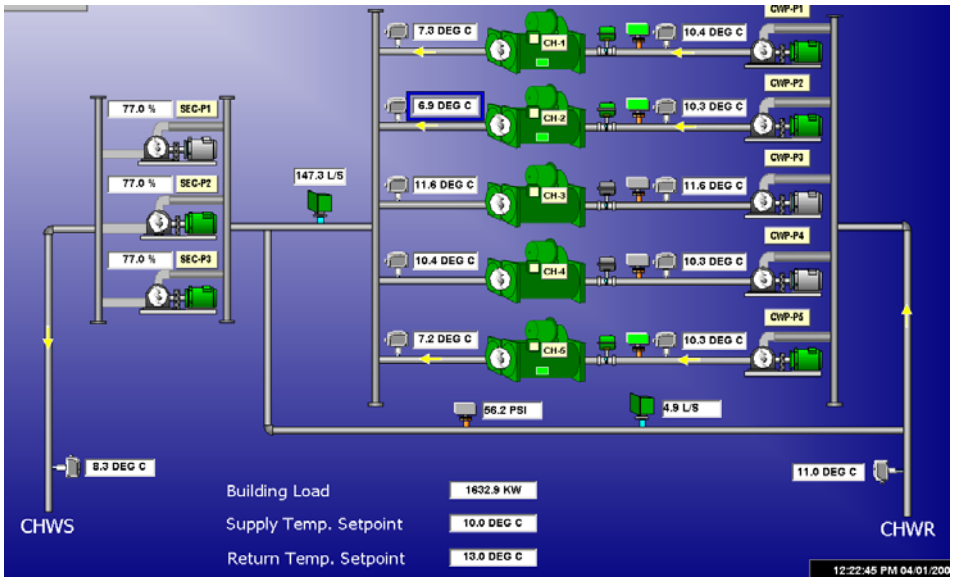

Figure 4.3 Graphical screen of the chiller plant

4.1.2 Evaluation of operating variables

It is expected that experimental data are subject to variability due to errors in their measurement, and this may influence the accuracy of the chiller model when these data serve as input of a model to evaluate its undetermined coefficients. An error analysis was therefore implemented to ascertain how these experimental errors influenced the modelled results and whether the assumptions made in the chiller model were adequate.

The chiller COP was not directly measured, but values of several associated variables were measured. ASHRAE Guideline 2 (ASHRAE 2010) provides a guideline for reporting uncertainty in results of experimental data as applied to HVAC equipment. An experimental result denoted as Y is determined from a set of independently measured variables x_i, where i = 1 to n, and n is the number of measurements related to Y.

$$Y = f(x_1, x_2, \cdots x_n) \tag{4.1}$$

Due to the accuracy of measured variables, the uncertainty associated with COP is determined by the single sample analysis (ASHRAE 2010), as shown in Eq. (4.2).

$$\delta COP_{(rms)} = \sqrt{\sum_{i=1}^{n} \left[\delta x_i \cdot (\partial COP / \partial x_i) \right]^2} \tag{4.2}$$

where x_i is the ith independent variable, and δx_i is the uncertainty of the variable x_i.

Table 4.2 shows the error analysis of operating variables relating to chiller COP. The root sum square error of chiller COP ($\delta COP_{(rms)}$) due to all the uncertainties of the individual variables was evaluated to be 0.088 in a COP value of 2.8, and the uncertainty of COP was 3.1%. This was mainly due to the uncertainties in the chilled water supply and return temperatures.

Table 4.2 Error analysis of operating variables

Measured variable x_i	Rated condition	Partial derivative $\partial COP / \partial x_i$	Uncertainty δx_i	Square of product $\left[\delta x_i \cdot (\partial COP / \partial x_i)\right]^2$	$\delta COP_{(rms)}$
T_{chwr} (°C)	12	0.525126	±0.1℃	0.002758	
T_{chws} (°C)	7	-0.52513	±0.1℃	0.002758	
E_{ch} (kW)	398	-0.0066	3.98kW (1%)	0.000689	
m_w (kg/s)	50	0.052513	0.75 kg/s (1.5%)	0.001551	
total				0.007756	0.088066

4.2 Modelling and simulation of the chilled water plant

Computer simulation is an invaluable tool to investigate the performance of chillers over a wide range of conditions, and it provides a means of optimizing the operation of the system and implementing fault detection and diagnosis (Jia and Reddy 2003; Wang, Wang et al. 2000). Many chiller models have been developed using different principles and approaches, and the various models can generally be divided into three main categories: empirical models, physical steady state models and physical dynamic models (Browne and Bansal 2001a).

Empirical models rely heavily on experimental data, and they are 'black-box' or 'grey-box' models based on curve-fit or thermodynamic models. Empirical models (Khan and Zubair 1999; King and Potter 1998; Phelan, Brandemuehl et al. 1997; Yik and Lam 1998) are relatively straightforward to establish but their application is limited to the specific chillers from which the empirical data are obtained. Physical steady state models (Browne and Bansal 1998; Ding and Fu 2005; Jia and Reddy 2003; Solati, Zmeureanu et al. 2003) are based on first-principles approaches with equations for mass and energy conservation, and they are more detailed and more widely applicable, but they are also more difficult to establish and use, as they usually involve a wide range of characteristic parameters of the modeled chiller

which are difficult to quantify. Steady-state models are useful under many conditions; however, dynamic simulation models are preferable under strongly dynamic conditions that are often seen in real-life operation. Physical dynamic models (Browne and Bansal 2002; Haberschill, Gay et al. 2003; Wang 1998; Wang, Wang et al. 2000) also consider the conservation of energy and mass, and take into account the rate of change of the system variables with time. For dynamic simulation, the chiller model is much more sophisticated and usually contains a system of differential equations, which need to be solved by using numerical integration techniques.

As both the building cooling load and the weather conditions did not change over minutes but longer, Chan and Yu (2006) stated that the time constant of the variation in a building's cooling-load was large when compared to that of the dynamic response to a chiller system, and it was reasonable to assume the chiller operation to be quasi-steady-state (Jia and Reddy 2003). Therefore, steady-state models are sufficient for the evaluation of the operating variables of chillers.

To improve the performance of air-cooled chillers, some of them are designed with multiple and separate refrigerant circuits, and each refrigeration circuit has one or more compressors. This design of multiple refrigerant circuits is to enhance the reliability and standby capacity, decrease in-rush current at system start-up. Such design also reduces the power consumption at part load condition and improves the overall chiller performance. Although a large variety of chiller models have been developed, very few of these are specifically developed for air-cooled screw chillers with multiple refrigeration circuits in detail. Gan (2000) investigated the benefits of using two separate refrigeration cycles to meet demands for both the freezer and fresh food compartments in domestic refrigerators. Swider (2003) considered a

single-circuited centrifugal chiller and a twin-circuited screw chiller and presented a comprehensive comparison of empirically based models. Yu and Chan (2006b) developed an air-cooled screw chiller model with four refrigeration circuits to analyze the chiller performance under CTC, in which the chiller with multiple refrigeration circuits was treated as a chiller with just one refrigeration circuit. Lee (2010) investigated the performance of air-cooled twin-circuit screw chiller based on the assumption that the two circuits shared the same cooling output and the overall heat transfer coefficients of the two sections of the evaporator A were equal. Almost none of the previous research has investigated the energy efficiency of air-cooled screw chillers with multiple refrigeration circuits under various operating conditions and how the performance of these chillers can be improved with variable condensing temperature control and variable speed condenser fans in response to changes in outdoor temperature and building cooling load. In this research, a steady-state thermodynamic model for an air-cooled chiller with two separate refrigerant circuits is presented, which serves for the analysis on various control strategies.

The simulation program TRNSYS 15 (Solar Energy Laboratory 2000) was used for the building and chiller system simulation in this study. TRNSYS is a complete and extensible simulation environment for the transient simulation of thermal energy systems, whose modular system approach makes it one of the most flexible tools available. The chiller components are modeled based on a modular approach and coded in the form of FORTRAN subroutines. By creating an input file of program, component subroutines are linked up to form the existing chiller. The outputs are operating variables within the components of compressors, the evaporator and condenser. They are solved by the different sets of algebraic equations through iterative procedure. The chiller model, comprising of inputs, constant parameters and outputs, was developed following the format of standard components in TRNSYS 15.

Figure 4.4 shows the flow diagram of modeling the chiller under TRNSYS (Yu and Chan 2007). The data file contained various set points and weather-load conditions at which the chiller operated, and each set of data comprised inputs to the chiller components: an evaporator, a compressor, an expansion valve and a condenser. These inputs were outdoor temperature (T_{db}), the part-load ratio (PLR) of the chiller, chilled water flow (m_w), the temperature of supply chilled water (T_{chws}), the degree of subcooling (T_{cdsc}), the degree of superheating (T_{evsh}) and the set point of condensing temperature (T_{cdsp}) (T_{cdsp} was used to determine the number of staged condenser fans). To evaluate the thermodynamic properties of the refrigerant R134a, the physical coefficients and equations given by Bourdouxhe et al. (1999) were incorporated into the model. The outputs were operating variables within the evaporator, compressors, expansion valve and condenser.

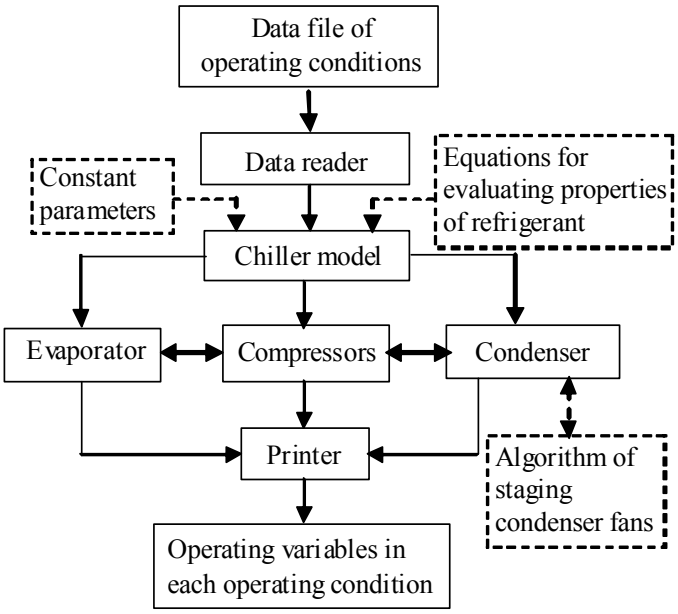

Figure 4.4 Flow diagram of modelling the chiller under TRNSYS

The following assumptions were made in the development of the chiller model:

- The model chiller operated under the standard vapour compression cycle as shown in Figure4.5.

- Heat transfer between the chiller system and its surrounding was negligible.
- The mass flow rate of the refrigerant was the same throughout the chiller and equaled to the mass flow rate through the staged compressors.
- Pressure losses in the heat exchangers and the refrigerant pipelines were negligible.
- The flow of refrigerant could be controlled perfectly to meet any given cooling capacity.
- The throttling of refrigerant across the expansion valve was isenthalpic.
- The degree of evaporator superheat (T_{evsh}) and that of condenser subcooling (T_{cdsc}) were assumed to be 8°C and 3°C in all operating conditions, respectively, given their possible variations (T_{evsh}: 4–9.5°C; T_{cdsc}: 1–6°C) would only cause uncertainty of chiller COP up to 0.16% (Yu and Chan 2006b).
- Changes in the calculated operating variables were independent of time and that meant the chiller operated in the steady state.

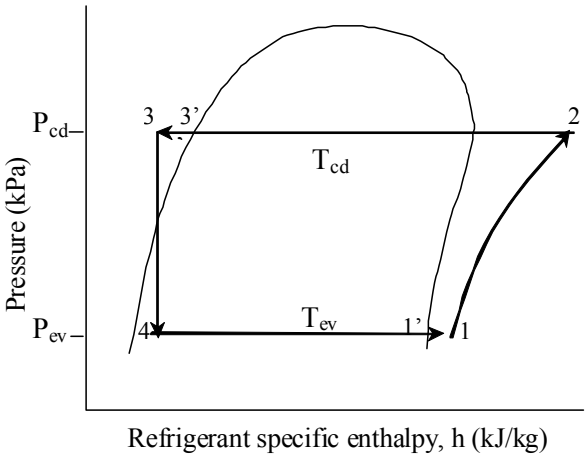

Figure 4.5 Vapour compression cycle of the model chiller

4.2.1 Chiller model

The model was based on an air-cooled chiller with constant speed screw compressors operating under head pressure control, which had the same configuration as the experimental chiller. The schematic of the air-cooled chiller with two refrigeration circuits was shown in Figure 4.6. Each refrigeration circuit of the chiller was equipped with two compressors, a condenser, an expansion valve and an evaporator. Though the refrigeration circuits were detached, there was only one chilled water circuit, and the chilled water passed serially through the respective evaporators of the first and second circuits. The number of passes directly affects the performance of a direct expansion shell and tube evaporator. To enhance the heat transfer, tubes were designed as a two-pass arrangement for chilled water. In this dual-circuit chiller, the chilled water passed first through the evaporator of circuit 1, then passed into the evaporator of circuit 2, and then back through the evaporator of circuit 1.

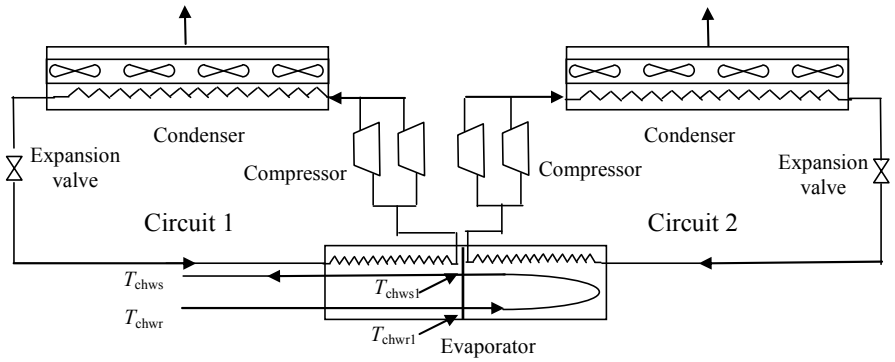

Figure 4.6 Schematic of the air-cooled chiller

The models considered the real process phenomena, including the capacity control of compressors and variations in the overall heat transfer coefficients of an evaporator and a condenser. The modeled components of the chiller were the compressors, the evaporators, the condensers and the expansion valves. To realize variable condensing temperature control for air-cooled screw chillers, it was important to identify the operating variables of chillers with some realism, and the mechanistic relations

between chiller components should be taken into account. The mass balance of refrigerant and energy balance at an evaporator, compressors, an expansion valve and a condenser have to be satisfied. To control the condensing temperature, an algorithm to determine the number or speed of staged condenser fans by a set point of condensing temperature (T_{cdsp}) was introduced and incorporated into the chiller model, which was important for variable condensing temperature control. The outputs were the operating variables of the chiller components and the chiller COP. They were determined by solving a set of equations in the component models through an iterative procedure.

For the air-cooled chiller with twin refrigeration circuits, there existed three operation modes (operation of circuit 1, operation of circuit 2 or operation of both circuits). As the two refrigerate circuits were identical, the models for the chiller components of one refrigerate circuit were applicable to the corresponding components of the other refrigeration circuit.

Evaporator

For the dual-circuit chiller with two-pass arrangement, the chilled water passed first through the evaporator of circuit 1, then passed into the evaporator of circuit 2, and then got back through the evaporator of circuit 1. According to the chilled water flow path, the heat transfer in the evaporator was modeled by three heat exchange sections in series, and there were two sections for circuit 1 and one section for circuit 2, respectively. The evaporating temperature and pressure were same for the two heat exchange sections of circuit 1. The cooling capacity of circuit 1, therefore, was the sum of the cooling load of the two heat exchange sections of circuit 1. The evaporator and condenser were simulated using the classical heat exchanger efficiency method.

For the evaporator model, the energy balance and cooling output of the chiller is expressed by the following equations.

$$Q = m_w \cdot c_{pw} \cdot (T_{chwr} - T_{chws}) \tag{4.3}$$

$$Q_1 = Q_{11} + Q_{12} \tag{4.4}$$

$$Q_{11} = m_w \cdot c_{pw} \cdot (T_{chwr} - T_{chwr1}) \tag{4.5}$$

$$Q_{12} = m_w \cdot c_{pw} \cdot (T_{chws1} - T_{chws}) \tag{4.6}$$

$$Q_2 = m_w \cdot c_{pw} \cdot (T_{chwr1} - T_{chws1}) \tag{4.7}$$

$$Q = Q_1 + Q_2 \tag{4.8}$$

where m_{w} is the chilled water mass flow rate, c_{pw} is the specific heat capacity of water, T_{chws1} and T_{chwr1} are the chilled water temperature entering and leaving refrigeration circuit 2, respectively.

The effectiveness of the evaporators (ε_{ev}) is used to simulate heat and mass transfer processes in the evaporator as in Eqs. (4.9-4.11). The evaporator overall heat transfer coefficients (AU_{ev}) of the three heat exchange sections of the evaporator are represented by mechanistic relation in Eqs. (4.12-4.14), respectively (Wang 1998), where c_1, c_2 and c_3 are characteristic parameters and have to be evaluated based on the performance data of the specific chiller to be modeled. The values of the heat transfer efficiency of the three heat exchange sections are expressed in Eqs. (4.15-4.17).

$$Q_{11} = \varepsilon_{ev11} \cdot m_w \cdot c_{pw} \cdot (T_{chwr} - T_{ev1}) \tag{4.9}$$

$$Q_{12} = \varepsilon_{ev12} \cdot m_w \cdot c_{pw} \cdot (T_{chws1} - T_{ev1}) \tag{4.10}$$

$$Q_2 = \varepsilon_{ev2} \cdot m_w \cdot c_{pw} \cdot (T_{chwr1} - T_{ev2}) \tag{4.11}$$

where

$$AU_{\text{ev11}} = \frac{1}{c_1 m_{\text{w}}^{-0.8} + c_2 Q_{\text{cl11}}^{-0.745} + c_3} \tag{4.12}$$

$$AU_{\text{ev12}} = \frac{1}{c_1 m_{\text{w}}^{-0.8} + c_2 Q_{\text{cl12}}^{-0.745} + c_3} \tag{4.13}$$

$$AU_{\text{ev2}} = \frac{1}{c_1 m_{\text{w}}^{-0.8} + c_2 Q_{\text{cl}_2}^{-0.745} + c_3} \tag{4.14}$$

$$\varepsilon_{\text{ev11}} = 1 - \exp(-\frac{AU_{ev11}}{m_w C_{pw}}) \tag{4.15}$$

$$\varepsilon_{\text{ev12}} = 1 - \exp(-\frac{AU_{ev12}}{m_w C_{pw}}) \tag{4.16}$$

$$\varepsilon_{\text{ev2}} = 1 - \exp(-\frac{AU_{ev2}}{m_w C_{pw}}) \tag{4.17}$$

The Clausius-Clapeyron equation gives the vapour pressure as a function of temperature.

$$P_{ev1} = \exp(a + \frac{b}{T_{ev1}}) \tag{4.18}$$

Compressors

The refrigerant mass flow rate through the compressors of circuit 1 is given by

$$m_{r1} = \frac{Q_1}{h_{11} - h_{14}} \tag{4.19}$$

$$m_{r1} = \frac{V_d \eta_{v1}}{v_{r1}} N_{cc1} \tag{4.20}$$

where V_{d} is the theoretical displacement volume of compressor, which is 0.12 m^3/s for the studied chiller according to the manufacture's performance data. η_{v1} is the volumetric efficiency of the compressor of circuit 1 estimated as a function of the compression ratio (CR), and they are determined by

$$\eta_{v1} = 1 - \frac{V_{cl}}{V_d}\left(CR_1^{\frac{1}{n_i}} - 1 \right) \tag{4.21}$$

$$CR_1 = \frac{P_{cd1}}{P_{ev1}} \tag{4.22}$$

The refrigerant mass flow rate through each compressor of circuit 1 is determined by Eqs. (4.23) and (4.24), respectively. The total refrigerant mass flow rate of circuit 1 is the sum of the refrigerant mass flow rate through the two compressors.

$$m_{r11} = \frac{Q_{cc11}}{h_{11} - h_{14}} \tag{4.23}$$

$$m_{r12} = \frac{Q_{cc12}}{h_{11} - h_{14}} \tag{4.24}$$

$$m_{r1} = m_{r11} + m_{r12} \tag{4.25}$$

The indicated compressor work per unit mass of refrigerant is given by

$$w_{in1} = P_{ev1}\, v_{1r} \frac{n_i}{n_i - 1}\left(CR_1^{\frac{n_i - 1}{n_i}} - 1 \right) \tag{4.26}$$

where v_r is the specific volume of superheated refrigerant at the compressor suction evaluated by Eq. (4.27) based on saturated specific volume of the refrigerant in the evaporator.

$$\frac{1}{v_{1r}} = \frac{1}{v_{11'}} - (-0.0007 + 0.0002\, P_{ev1})\, T_{evsh} \tag{4.27}$$

The power input to the staged compressors of circuit 1 (E_{cc1}) is the sum of the power of the two compressors, which can be calculated on the basis of the internal compression power (w_{in}).

$$E_{cc11} = m_{r11} \frac{w_{in1}}{\eta_{isen1}\ \eta_{cc11}} \tag{4.28}$$

$$E_{cc12} = m_{r12} \frac{w_{in1}}{\eta_{isen1}\ \eta_{cc12}} \tag{4.29}$$

$$E_{cc1} = E_{cc11} + E_{cc12} \tag{4.30}$$

where η_{isen1} is the isentropic efficiency determined by Eq. (4.31), and η_{cc11} and η_{cc12} are and the combined motor and transmission efficiency of the compressors given by Eqs. (4.32) and (4.33), respectively. Eq. (4.31) is based on the regression analysis (Solati, Zmeureanu et al. 2003), and the coefficients a_1 to a_8 are constants, which are –0.0316958, 2.90112, –0.0296849, –1.45279, 0.000321176, 0.00683086, 0.0170575 and –16.5018, respectively. The coefficients of Eqs. (4.32) and (4.33) have to be estimated by regression using chiller operating data, and PLR_{11} and PLR_{12} are the part load ratio of the two compressors in circuit 1, respectively.

$$\eta_{isen1} = 0.01(a_1 T_{cd1}^{\ 2} + a_2 T_{cd1} + a_3 T_{ev1}^{\ 2} + a_4 T_{ev1} + a_5 T_{cd1}^{\ 2} T_{ev1} + a_6 T_{cd1} T_{ev1} + a_7 Q_{cr1} + a_8) \tag{4.31}$$

$$\eta_{cc11} = b_1 + b_2 PLR_{11} + b_3 PLR_{11}^{\ 2} \tag{4.32}$$

$$\eta_{cc12} = b_1 + b_2 PLR_{12} + b_3 PLR_{12}^{\ 2} \tag{4.33}$$

The specific enthalpy of superheated refrigerant at the suction and discharge of the compressor (h_{11} and h_{12}) can be expressed using Eqs. (4.34) and (4.35). Eq. (4.36) describes the refrigerant enthalpy at the condenser discharge (h_{13}).

$$h_{11} = h_{11'} + C_{prg}\, T_{evsh} \tag{4.34}$$

$$h_{12} = h_{11} + \frac{w_{in1}}{\eta_{isen1}\eta_{cc1}} \tag{4.35}$$

$$h_{13} = h_{13'} - C_{prl}\, T_{cdsc} \tag{4.36}$$

Thermostatic Expansion valve

The studied chiller is equipped with an electronic expansion valve, which controls the refrigerant mass flow rate by sensing the degree of suction vapor superheat temperature. The expansion valve was modelled as an adiabatic process, so that the refrigerant enthalpy at the inlet and outlet of the expansion valve are equal. The refrigerant mass flow rate of circuit 1 through the valve is calculated by the following equation.

$$m_{r1} = K_{ex}\sqrt{\rho_{ex}\Delta P_{ex}} \tag{4.37}$$

where K_{ex} is a characteristic constant of the valve, ρ_{ex} is the refrigerant density at the inlet of the valve, and ΔP_{ex} is the inlet and outlet pressure difference of the expansion valve.

Condenser

Heat rejection involves the energy and mass balance in the condenser. Heat rejection of circuit 1 (Q_{cd1}) is described by the following equations

$$Q_{cd1} = Q_1 + E_{cc1} \tag{4.38}$$

$$Q_{cd1} = m_{r1}(h_{I2} - h_{I3}) \tag{4.39}$$

$$Q_{cd1} = V_{a1}\rho_a C_{pa}(T_{cdal1} - T_{cdae}) \tag{4.40}$$

$$Q_{cd1} = AU_{cd1}\,\mathrm{LMTD}_{cd1} \tag{4.41}$$

where

$$AU_{cd1} = \frac{1}{c_4 V_{a1}^{-0.5} + c_5\, m_{r1}^{-0.8} + c_6} \tag{4.42}$$

$$\mathrm{LMTD}_{cd1} = \frac{T_{cdal1} - T_{cdae}}{\ln\left(\frac{T_{cd1} - T_{cdae}}{T_{cd1} - T_{cdal1}}\right)} \tag{4.43}$$

The overall heat transfer coefficient of the condenser of circuit 1 (AU_{cd1}) shown in Eq. (4.42) (Yu and Chan 2006b), where c_4-c_6 can be determined by regression based

on the performance data of the chiller. Condensing temperature (T_{cd}) is correlated with the temperature of entering condenser air (T_{cdae}) and that leaving the condenser (T_{cdal}) by the log mean temperature difference ($LMTD_{cd}$) which is defined in Eq. (4.43), where ($T_{cdal1} - T_{cdae}$) and ($T_{cd1} - T_{cdal1}$) are the temperature difference between the entering and leaving condenser air, the temperature difference between the condensing temperature and leaving condenser air temperature, respectively.

The condensing pressure is estimated using the Clausius–Clapeyron equation.

$$P_{cd1} = \exp(a + \frac{b}{T_{cd1}}) \tag{4.44}$$

Chiller COP

The total power of the staged condenser fans (E_{cf}) is equal to the rated power of a condenser fan ($E_{cf,r}$) multiplied by the number of staged condenser fans (N_{cf}).

$$E_{cf} = N_{cf}\, E_{cf,r} \tag{4.45}$$

In order to characterize the performance of the chiller, the COP defined as the ratio of cooling capacity to the electrical power input is calculated, of which a higher value represents a higher efficiency of the system. It should be noted that the chiller power (E_{ch}) is the sum of compressor power (E_{cc}) and condenser fan power (E_{cf}).

$$COP = \frac{Q}{E_{ch}} = \frac{Q_1 + Q_2}{E_{ch1} + E_{ch2}} = \frac{m_{r1} \cdot (h_1 - h_2) + m_{r2} \cdot (h_1 - h_2)}{E_{ch1} + E_{ch2}} \tag{4.46}$$

4.2.2 Condenser fans control

Air-cooled chillers commonly operate under traditional head pressure control (HPC), and these chillers have long been considered energy inefficient. Under HPC, the set point of the condensing temperature (T_{cdsp}) is fixed at 45°C, preventing condensing the temperature (T_{cd}) from exceeding a maximum level of 52°C (Yu and Chan

2006b). The condensing temperature is kept high under HPC, and the heat rejection capacity of the air-cooled condenser is designed to control the condensing temperature at around 50°C when the outdoor temperature is 35°C. Considering a local outdoor temperature of 10-34°C, heat rejection airflow will vary for any given cooling capacity in order to maintain the condensing temperature at around its fixed set point of 45°C (Yu and Chan 2006b). HPC is incapable of lowering the condensing temperature to save compressor power, especially when the difference between T_{cdsp} and the outdoor temperature (T_{db}) is high.

For air-cooled chillers, different number of condenser fans are staged to control the condensing temperature and to achieve heat rejection. Heat rejection varies with the outdoor temperature and the chiller load. Under HPC, the control action is based on some settings of condensing temperature. For the air-cooled chillers with constant speed condenser fans, the condenser fans are cycled on or off with reference to a high and a low temperature settings under HPC. When the condensing temperature exceeds the high temperature setting, more condenser fans will be staged on group by group until the condensing temperature drops below the high condensing temperature setting. The number of staged condenser fans will remain unchanged as long as the condensing temperature is within the dead-band between the high and low condensing temperature settings. When the condensing temperature drops below the low temperature setting, the staged condenser fans will be switched off group by group to reduce the airflow rate, and hence, to raise the condensing temperature above the low setting. The high condensing temperature setting is 52°C (Yu and Chan 2006b) and low condensing temperature setting is 42°C (Lee, Yik et al. 2010). The lowest limit of the condensing temperature is 33°C, and it is due to a situation where thermostatic expansion valves require a minimum differential of 690 kPa for proper operation (Yu, Chan et al. 2006). For the chiller with electronic expansion

valves, the lowest limit is 20°C, which is intended for ensuring proper oil viscosity for compressor lubrication (Yu, Chan et al. 2006).

Chiller performance is greatly influenced by the condensing temperature, and the condensing temperature (T_{cd}) can be controlled by adjusting the heat rejection airflow (V_a). To control the condensing temperature, the set point of condensing temperature (T_{cdsp}) is introduced to determine the number and speed of staged condenser fans to modulate the heat rejection airflow. If the staged condenser fans are not sufficient to deliver the needed airflow to keep the condensing temperature within the dead band between the high and low condensing temperature settings, more or less condenser fans will be operated. This algorithm is particularly important in modelling precisely the heat-rejection characteristics of air-cooled condensers and in assessing the controllability of the condensing temperature under various operating conditions.

For any given cooling capacity (Q_{cl}), either the heat rejection airflow (V_a) or the set point of condensing temperature (T_{cdsp}) can be adjusted to minimize the chiller power which is equal to the sum of compressor power and condenser fan power. Inequality (4.48), obtained by transposing Eq. (4.47), shows how T_{cd} can be controlled by using T_{cdsp} for any given heat rejection (Q_{cd}). By transposing Inequality (4.47), Inequality (4.48) is established and used to determine the required V_a.

$$T_{cdal} = \frac{Q_{cd}}{V_a \rho_a C_{pa}} + T_{cdae} < T_{cd} \le T_{cdsp} \tag{4.47}$$

$$\frac{Q_{cd}}{\rho_a C_{pa} (T_{cdsp} - T_{cdae})} < V_a \tag{4.48}$$

4.2.2.1 Control algorithm of constant speed condenser fans

Eq. (4.49) gives the relationship between the required V_a and the number of staged

condenser fans (N_{cf}). The minimum N_{cf} for any given T_{cdsp} is determined using Inequality (4.50).

$$V_a = \frac{V_{a,tot}}{N_{cf,tot}} N_{cf} \tag{4.49}$$

$$\frac{N_{cf,tot}}{V_{a,tot}\ \rho_a\ C_{pa}} . \frac{Q_{cd}}{(T_{cdsp} - T_{cdae})} < N_{cf} \tag{4.50}$$

From inequality (4.50), it can be identified how the number of staged condenser fans varies according to different outdoor temperatures and different amounts of heat rejection. If the set point of condensing temperature (T_{cdsp}) is fixed at a high level, fewer condenser fans will be staged on when the chillers are operating at part load conditions with a low outdoor temperature. When more condenser fans are staged, the condensing temperature will drop. It is important to adjust the set point of condensing temperature by some algorithms so as to minimize the chiller power.

The working range of condensing temperature (T_{cd}) is governed by inequality (4.51), where the log mean temperature difference of the condenser ($LMTD_{cd}$) correlates with heat rejection (Q_{cd}) and the overall heat transfer coefficient of the condenser (AU_{cd}) by Eq. (4.52). T_{db} is the temperature of air entering the condenser, and T_{cdal} is the temperature of air leaving the condenser.

$$LMTD_{cd} + T_{db} < T_{cd} < LMTD_{cd} + T_{cdal} \tag{4.51}$$

$$Q_{cd} = AU_{cd}\ LMTD_{cd} \tag{4.52}$$

Referring to head pressure control, the set point of condensing temperature is fixed at a high level of 45°C, which corresponds to an outdoor temperature of 35°C plus a log mean temperature difference of around 10°C at the condenser side. This is a simple means to stage a minimum number of condenser fans, such that the condensing temperature complies with its higher boundary with a designed outdoor temperature

of 35°C in Inequality (4.51). However, maintaining this set point hinders the condensing temperature from reaching its lower boundary when the outdoor temperature is low or the condenser effectiveness can be enhanced at part load.

4.2.2.2 Control algorithm of variable speed condenser fans

Variable speed control for condenser fans is superior to cycling constant speed condenser fans in steps, with regard to the controllability of condensing temperature. The power of the condenser fans can drop considerably at lower speed while producing the required heat rejection airflow at part load operation.

For any given Q_{cd}, the required heat rejection airflow (V_a) was evaluated by using Eq. (4.49), regardless of the arrangement of condenser fans and whether the fans operated at a constant speed or a variable speed. This configuration of condenser fans should be changed in order to implement variable speed control. In the existing design of an air-cooled condenser with many groups of condenser fans, it would be difficult to decide whether to reduce the number or speed of the staged condenser fans if V_a drops under part load conditions. It would also be difficult to realize the actual power savings from the optimum trade-off between the compressor power and condenser fan power if the fans were improperly staged with inadequate rotating speed.

In order to tackle the difficulties, one variable speed condenser fan should be arranged for each refrigeration circuit. Given that the chiller studied had two refrigeration circuits, the condenser model contained two variable speed fans, each of which consumed the rated power of 19.2 kW and provided the rated airflow of 85.52 m^3/s at the full speed of 15.8 rps. The condenser fans could operate down to 10% of full speed to give a minimum airflow of 8.55 m^3/s. It was assumed that the variable

speed drive consumed 3% of the total power of the staged condenser fans at all speeds.

According to the fan law, the fan speed is directly proportional to the airflow and the fan power is directly proportional to the fan speed cubed. Eqs. (4.53) and (4.54) are derived from this law and used to calculate the rotating speed of each staged condenser fan (R_{cf}) and the total power of staged condenser fans (E_{cf}). It was assumed that all the staged condenser fans operated at the same speed and the same airflow.

$$R_{cf} = R_{cfr} \frac{V_a}{N_{cf} V_{ar}} \tag{4.53}$$

$$E_{cf} = N_{cf} E_{cf,ea} \left(\frac{V_a}{N_{cf} V_{ar}} \right)^3 \tag{4.54}$$

Using Eqs. (4.53) and (4.54), R_{cf} and E_{cf} are computed directly for any V_a determined based on a set point of condensing temperature (T_{cdsp}). The number of staged condenser fans (N_{cf}) is equal to that of the staged refrigeration circuits.

4.2.2.3 Control of condenser fans under CTC

Under head pressure control (HPC), T_{cdsp} is fixed at 45°C and the condensing temperature is prevented from exceeding the maximum level of 52°C (Yu and Chan 2006b). When the chiller is operating at part load at a low outdoor temperature, the condenser load (Q_{cd}) decreases while the the difference between T_{cdsp} and the outdoor temperature (T_{db}) increases. This results in a smaller number of staged condenser fans to enable the condensing temperature (T_{cd}) to float at slightly below 50°C. However, maintaining a fixed T_{cdsp} of 45°C cannot take full advantage of the opportunity to stage the condenser fans at optimal number and speed to minimize the sum of compressor power and condenser fan power for all operating conditions.

With the pitfalls of conventional head pressure control (HPC), the need to properly control the condensing temperature of air-cooled chillers is emphasized. It is desirable to lower T_{cdsp} to achieve maximum COP in all operating conditions, and the condensing temperature should vary in response to outdoor temperatures (Brownell, Klein et al. 1999; Love, Cleland et al. 2005; Manske, Reindl et al. 2001; Yu and Chan 2006b).

As HPC is regarded as energy inefficient, variable condensing temperature control (CTC) is proposed to be an alternative to HPC to considerably improve chiller efficiency. To implement CTC, the set point of condensing temperature should be reset according to the chiller load and the ambient air temperature. This reset enables the number or speed of the running condenser fans to be maximized, allowing condensing temperature to approach its lower boundary. The lowest possible T_{cdsp} is 20°C for ensuring proper lubrication for chillers with electronic expansion valves, given that the lubricant at a T_{cd} of below 20°C cannot be properly returned to the staged compressors (Yu, Chan et al. 2006).

For the air-cooled chillers with constant speed condenser fans, a straightforward approach to reset the set point of condensing temperature is proposed as Eq.(4.55) (Yu and Chan 2006b), in which T_{cdsp} is reset in response to T_{db}.

$$T_{cdsp} = \begin{cases} T_{db} + 5^{o}\text{C} & \text{for } T_{db} \geq 15^{o}\text{C} \\ 20^{o}\text{C} & \text{otherwise} \end{cases} \quad (4.55)$$

Resetting the set point of condensing temperature according to Eq. (4.55) allows T_{cd} to approach its lower boundary. However, this is not always true for all the operating conditions for the chillers with constant speed fans or variable speed fans. According to Eq. (4.47), the set point of condensing temperature (T_{cdsp}) influences directly the required heat rejection airflow and, in turn, the sum of compressor power input and

condenser fan power input. For the chillers with variable speed condenser fans, the maximum chiller COP may not be achieved from resetting the set point of the condensing temperature at its lower boundary when the fan power demand can drop considerably at lower speed. It is worth ascertaining an optimum T_{cdsp} to bring about maximum chiller COP at a given operating condition.

The strategy for implementing CTC is to adjust T_{cdsp} by a certain means, so that the trade-off between the compressor power and condenser fan power can be optimized for any given cooling capacity. Instead of using Eq. (4.55) to determine T_{cdsp}, a logical argument was included in the algorithm of controlling condenser fans to determine the optimum T_{cdsp} ($T_{cdsp,op}$) when CTC was used together with constant or variable speed condenser fans. This argument checked the change in chiller power when T_{cdsp} increased in steps of 0.05°C from its lower level of 20°C or (T_{db} + 3) °C, whichever was higher. These steps were small enough to trace the change of the chiller power due to the trade-off between the compressor power and condenser fan power. For each operating condition, the minimum chiller power along with the optimum T_{cdsp} was able to be identified by resetting T_{cdsp} varying from 20 to 45°C in steps of 0.05°C.

4.2.3 Procedure to evaluate operating variables of the model chiller

The whole model was programmed in Fortran 90, and the simulated system was constructed based on a transient simulation program TRNSYS. The flow chart in Figures 4.7-4.10 present the procedure to determine the operating variables of the chiller model with constant speed fans under HPC, variable speed fans under HPC, constant speed fans under CTC and constant speed fans under CTC, respectively. The programme started with the model initialization using the input data.

For the air-cooled chiller with twin refrigeration circuits, the cooling load of the chiller could be shared between the refrigeration circuits randomly. The strategy for the refrigeration circuit loading sequence (CLS) was specified first, and then one refrigeration circuit or both refrigeration circuits would be staged according to the total cooling load. Then, the evaporating temperature and pressure of circuits 1 and 2 (T_{ev1}, T_{ev2}, P_{ev1} and P_{ev2}) and the cooling loads of the three heat exchange sections of the evaporator (Q_{11}, Q_{12} and Q_2) were calculated through an iterative procedure by assuming a value for Q_{11} firstly. Once the model had determined the evaporating temperature and pressure of circuits 1 and 2, it evaluated the state variables of each refrigeration circuit. As the condensing temperature interacted between the compressor and condenser components, an iterative procedure was implemented to solve the operating variables of the two components simultaneously. To control the condensing temperature, there was another iterative loop for determining the number or speed of staged condensing fans. The number or speed of staged condenser fans and the corresponding airflow were computed according to a set point of condensing temperature.

The iterative procedure for estimating the heat rejection, the operating variables and the cooling capacity in both circuits of the chiller was similar. There were three logical arguments in the flow chart of the condenser model to ensure the reliability of all the calculated variables. In the first argument, if the temperature of air leaving the condenser (T_{cdal}) exceeded the high setting of the condensing temperature of 52°C, one more group of condenser fans would be added for chillers with constant speed fans or the speed of variable speed fans would increase to raise the airflow and to reduce the condensing temperature consequently. In the second argument, the convergence criterion for the cooling load shared by the first section of the heat exchanger in circuit 1 was 0.01 for the relative error. In the third argument, if the

difference between the condensing temperature and its previous value was within ±0.01°C, all variables would be solved in equilibrium; otherwise the next value of the condensing temperature would substitute for its previous one to perform the next iteration until the accuracy criteria were satisfied.

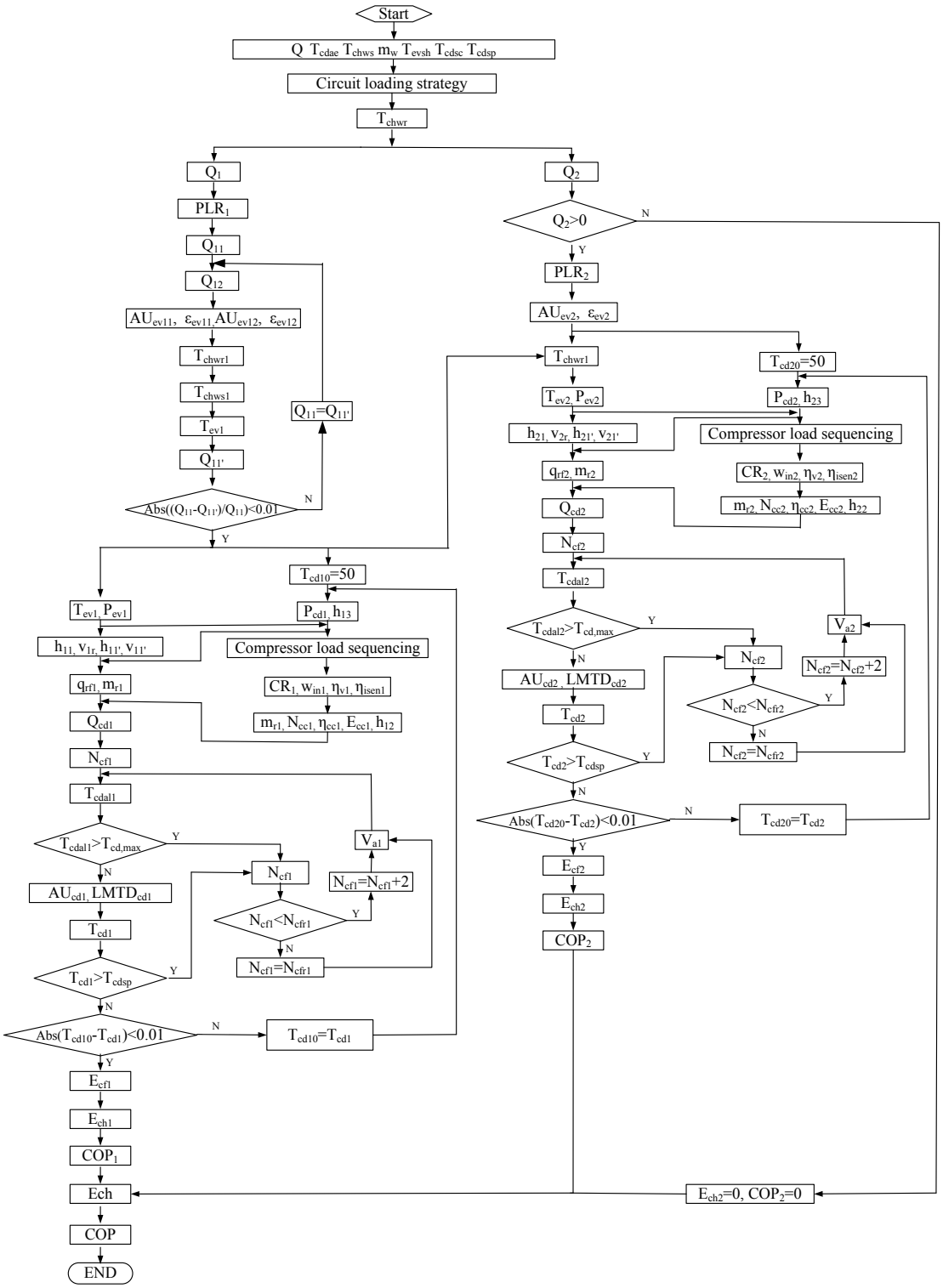

Figure 4.7 Flow chart of the chiller model with constant speed fans under HPC

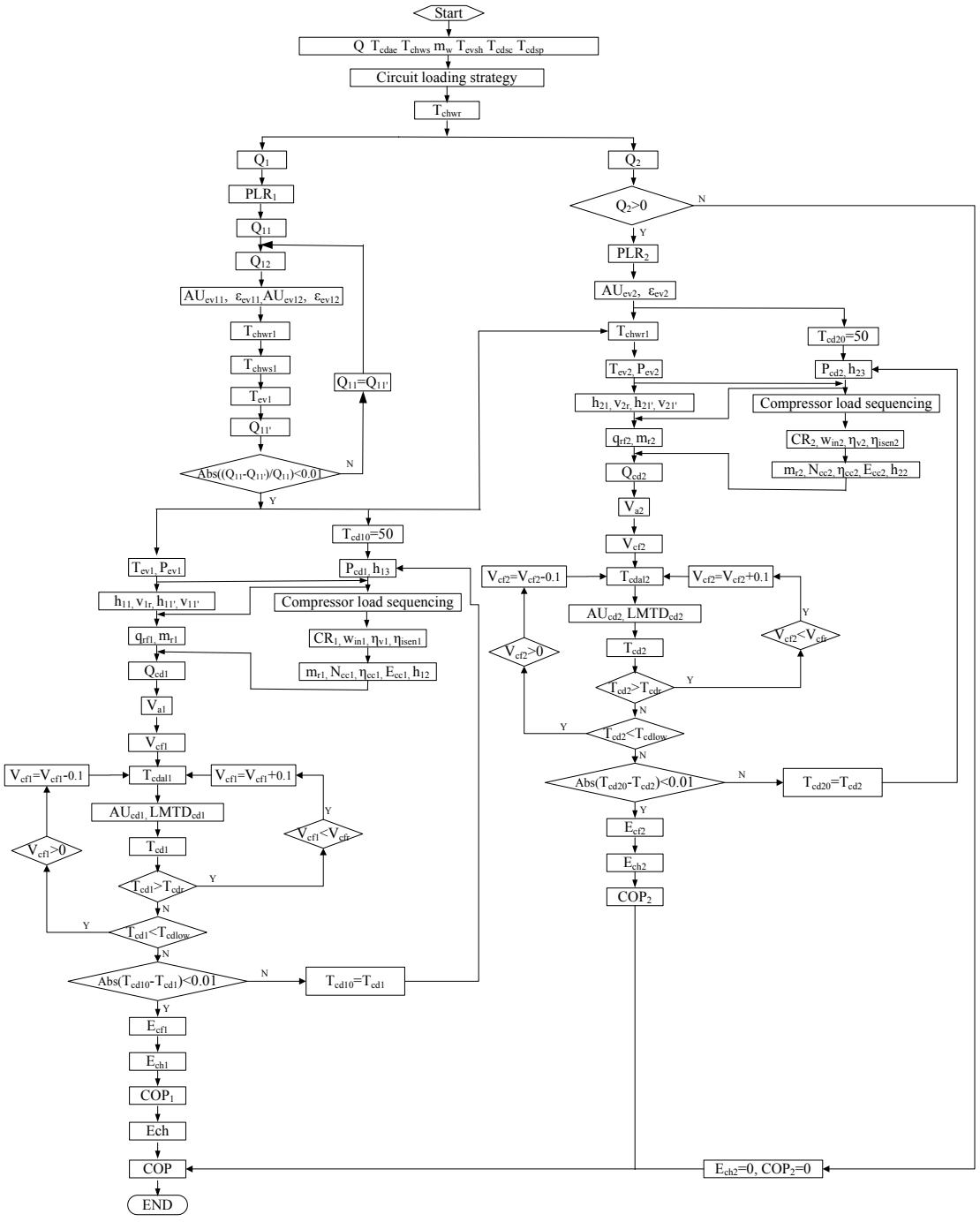

Figure 4.8 Flow chart of the chiller model with variable speed fans under HPC

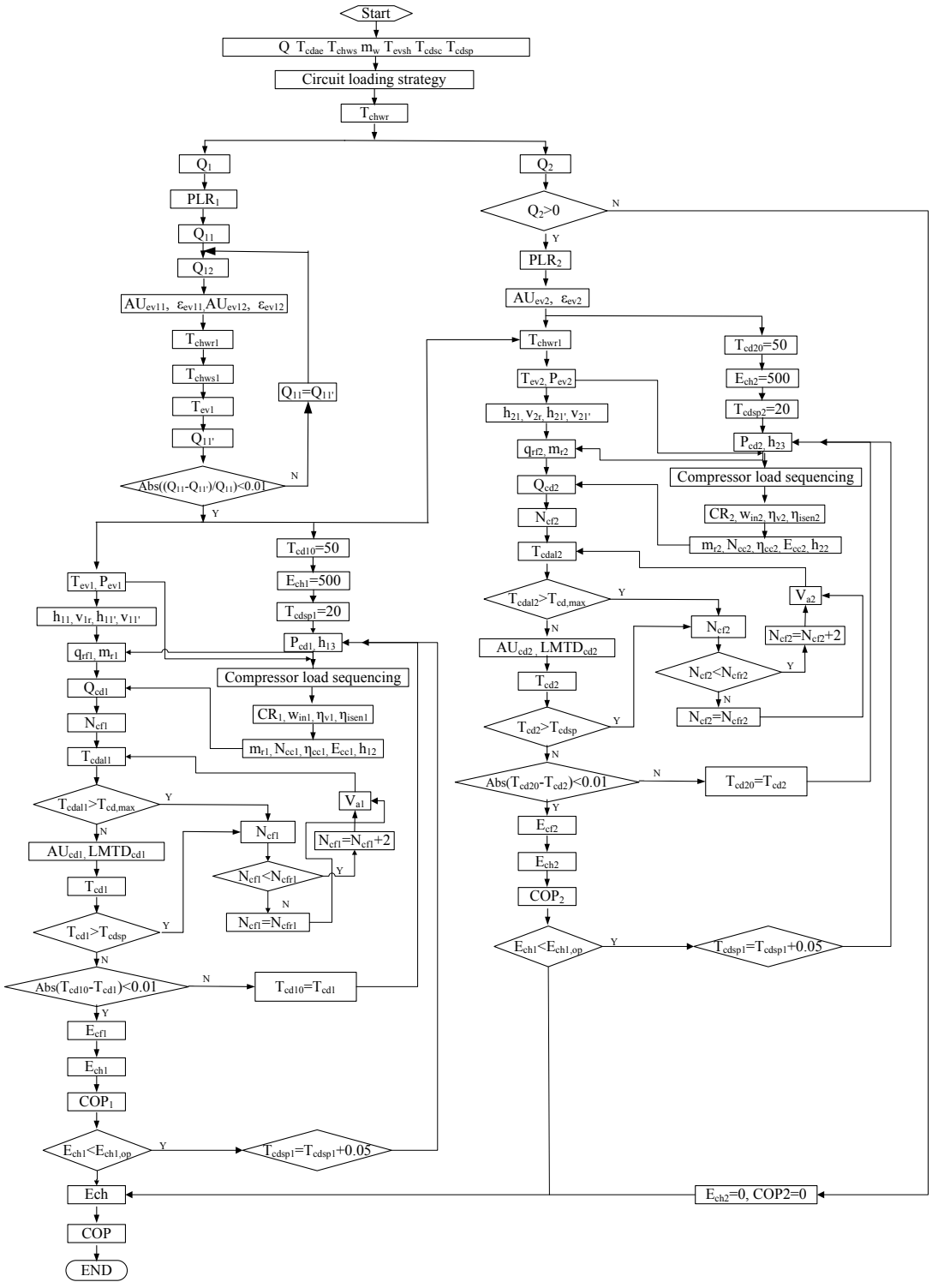

Figure 4.9 Flow chart of the chiller model with constant speed fans under CTC

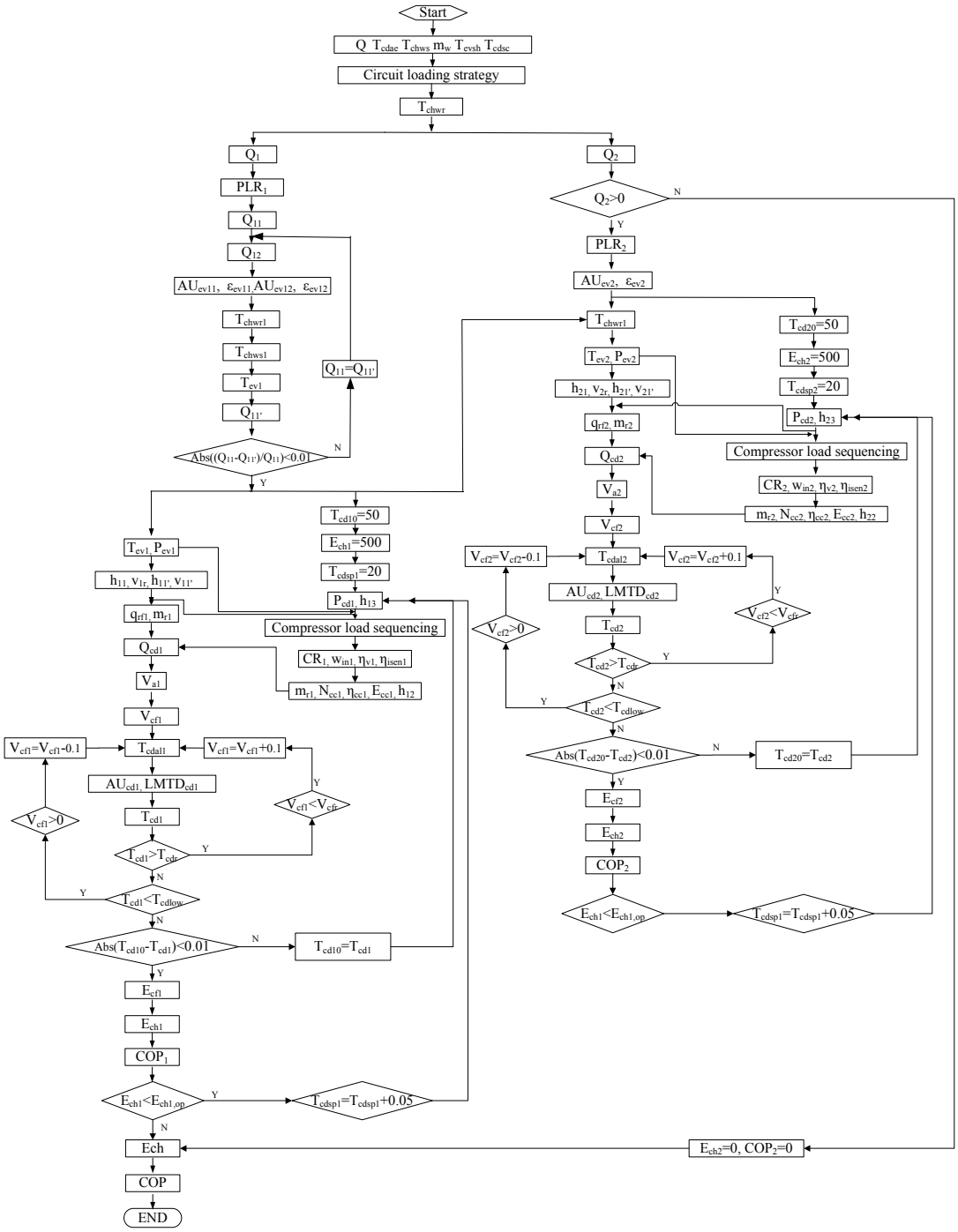

Figure 4.10 Flow chart of the chiller model with variable speed fans under CTC

4.2.4 Model validation

The primary purpose for the development of a chiller model is to provide a tool for investigating methods to optimize the performance of the chiller. An essential step prior to drawing conclusions from a model is to validate the model, which will provide confidence in the application of the model.

To verify the effectiveness of the developed modeling technique, the performance of the model was evaluated by comparing the modelled results with the operating data of the chiller. The measured data collected for validating the chiller model came from the chiller operating data under HPC. According to the scheme of load sharing between the two refrigeration circuits, the chiller model was simulated and the simulation results were compared with the corresponding experimental data. Figure 4.11 illustrates the comparison between the modeled and the measured chiller COP. There were two lines in the figure giving the boundary of ±10% deviation from the ideal case. For over 86% of the data, the uncertainty (the difference between the modeled value and the experimental value) of chiller COP was less than 10%.

Allowing for the experimental uncertainty of COP, being 3.1%, and the dead band for determining switching on one more or less group of condenser fans, which could result in the condensing temperature and the COP different from the measured ones, the deviations were within the allowable tolerance. Overall the chiller model was verified with an acceptable accuracy, and the simulation results were considered to be satisfactory. The validated model was used to investigate the chiller efficiency using different control strategies under various operating conditions.

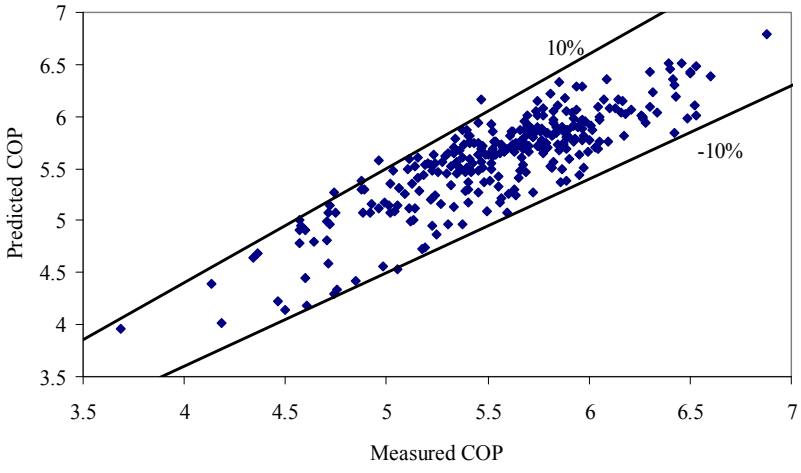

Figure 4.11 Comparison between the modelled and measured chiller COP

4.3 Chiller COP with various set points of condensing temperature

Variable condensing temperature control (CTC) was proposed as an alternative to HPC to lower the condensing temperature in response to changes of the ambient and load conditions (Yu and Chan 2006a), and the adjustment for T_{cdsp} should consider the constraints on compressor lubrication and the boundaries of the condensing temperature. The working range of condensing temperature (T_{cd}) was governed by Inequality (4.49). In this study, the lower limit for the set point of condensing temperature (T_{cdsp}) was 20°C or (T_{db} + 3) °C, whichever was higher. This limit is based on the boundaries of condensing temperature given in Inequality (4.51) and the requirement for ensuring the quality of oil viscosity for compressor lubrication (Yu, Chan et al. 2006). The highest T_{cdsp} is 45°C which is normally used under HPC. To implement variable condensing temperature control, electronic expansion valves (EXVs) are necessary to allow the condensing temperature to float freely above the outdoor temperature without any constraints from the differential pressure requirements.

As shown in Figure 4.12, the COP of the chiller with constant speed condenser fans varied with a range of condensing temperature set points, under various operating conditions in terms of combinations of outdoor temperatures (T_{db}: 15–35°C) and part load ratios (*PLR*: 0.125–1). The COP generally increased with the part load ratio of the compressors. The level of T_{cdsp} at which one more group of fans was consecutively staged varied, depending on the operating conditions. There was no regular trend in the change of chiller COP with the variation of T_{cdsp}. With the increase of the set point of condensing temperature from its lower boundary, the chiller COP increased in steps and then the maximum chiller COP could be achieved when T_{cdsp} increased to a level. Then the chiller COP decreased with further increase

of the set point of condensing temperature. There existed an optimal set point of condensing temperature for specific working conditions. However, for each operating condition, there could be two or more set points of condensing temperature at which the local maximum points of COP occurred. This was due to the change in the number of staged condenser fans across the range of T_{cdsp}. For the chiller with constant speed condenser fans, the condenser fans were cycled on or off group by group, and the COP remained unchanged when the number of staged condenser fans did not vary.

When the maximum COP was achieved, the level of T_{cdsp} signalled the staging of nearly all condenser fans. In this situation, the reduction of compressor power outweighed the additional fan power due to staging more condenser fans. All these findings confirmed the inadequacy of using HPC with a fixed T_{cdsp} of 45°C to control the staging of condenser fans.

According to the research by Yu and Chan (2006b), for the air-cooled chillers with constant speed fans, it was recommended to reduce the set point of condensing temperature to its lower limit in order to maximize chiller COP. The set point of condensing temperature (T_{cdsp}) should be adjusted following Eq. (4.55), of which the lower limit was 20°C or (T_{db} + 5) °C, whichever was higher. However, it was not always true for different air-cooled chillers with different control strategies. For certain conditions, the saving of the compressor power could not compensate for the increase of condenser fans power when the condensing temperature approached the lower boundary. Therefore, the optimum control strategy for the existing air-cooled may not to stage all the condenser fans to reach the lower boundary of condensing temperature all the time. As shown in Figure 4.12, the maximum COP could not be achieved by setting the set point of condensing temperature (T_{cdsp}) to the lower limit

as described in Eq. (4.55), and the maximum COP was achieved with various temperature differences between the optimal set point of condensing temperature and the outdoor temperature under different working conditions. It should be noted that this temperature difference was generally greater than 5°C. The relationship between the optimal set point of condensing temperature and the outdoor temperature could not be adequately described by Eq. (4.55) for all working conditions.

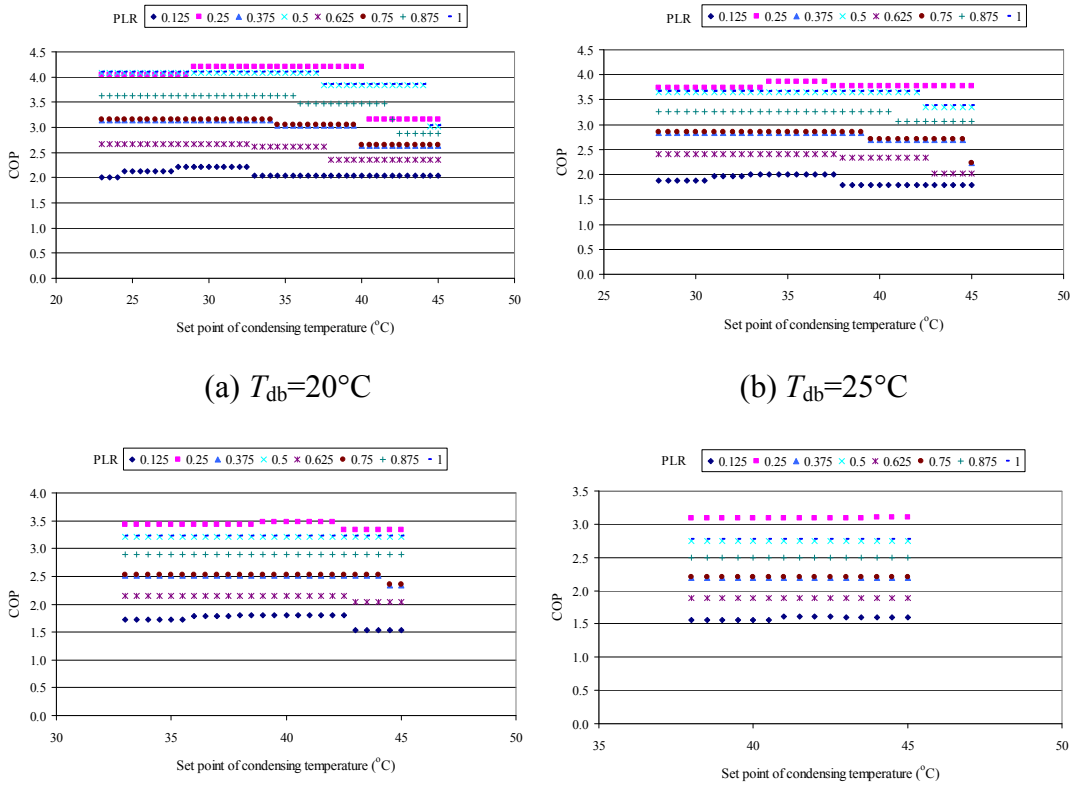

(a) T_{db}=20°C (b) T_{db}=25°C

(c) T_{db}=30°C (d) T_{db}=35°C

Figure 4.12 Variations in chiller COP with the set points of condensing temperature for chillers using constant speed condenser fans under different outdoor temperature

As shown in Figure 4.13, the COP varied more smoothly across the entire range of T_{cdsp} for the chiller with variable speed condenser fans. With the increase of the set point of condensing temperature from its lower boundary, the chiller COP increased to a maximum value and then decreased gently. The maximum COP could be achieved from an optimal set point of condensing temperature ($T_{cdsp,op}$). The locus of $T_{cdsp,op}$ for each outdoor temperature was plotted in Figure 4.13. It was identified that

the minimum chiller power could be achieved by lowering heat rejection airflow rather than maintaining the highest airflow for certain conditions, as the reduction of condenser fan power at lower fan speed could exceed the potential increase of compressor power under these conditions. Therefore, it was not appropriate to set the set point of the condensing temperature to its lower boundary for all operating conditions.

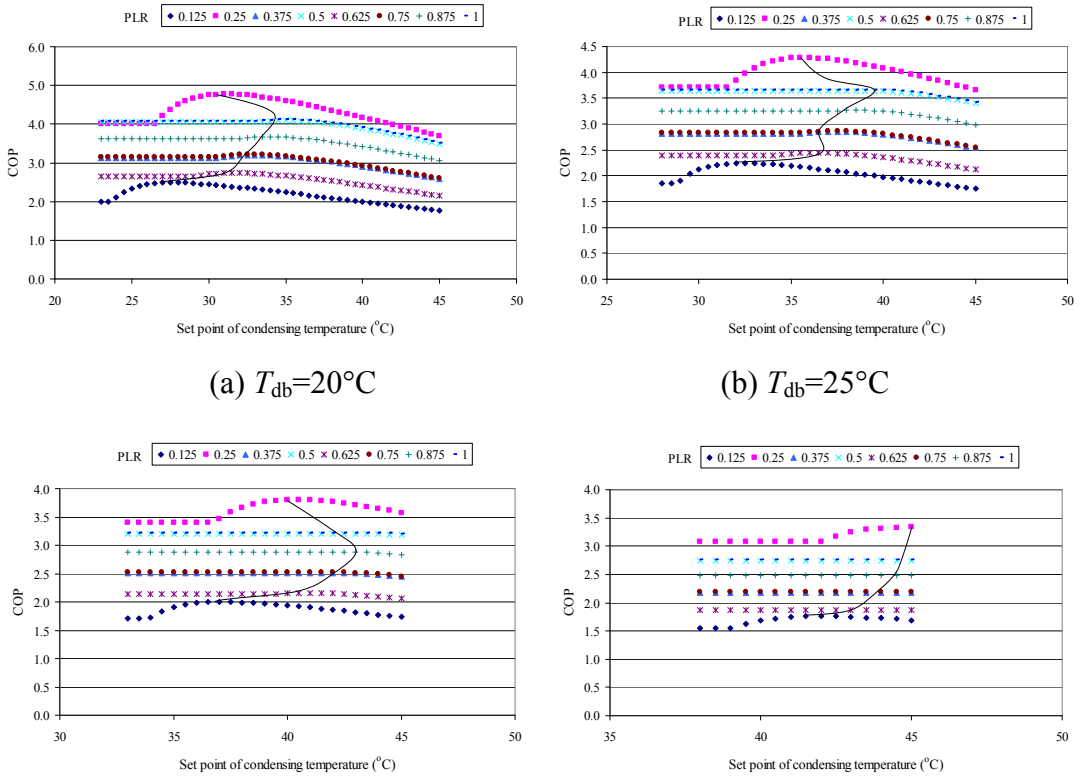

(a) T_{db}=20°C (b) T_{db}=25°C

(c) T_{db}=30°C (d) T_{db}=35°C

Figure 4.13 Variations in chiller COP with the set points of condensing temperature for chillers using variable speed condenser fans under different outdoor temperature

From Figures 4.12 and 4.13, it could be found that the chiller COP was best when PLR was 0.25. As the studied chiller had two refrigerant circuits, and each circuit was equipped with two compressors. According to the control strategy, when the chiller part load ratio is less than 0.25, only one compressor was staged. When the chiller part load ratio is 0.25, the staged compressor was at its full load, and the compressor efficiency was best. In addition, under such conditions, all the condenser

fans were available. To provide the needed condenser airflow, one more group of condenser fans could be staged for the air-cooled chillers with constant speed fans, and the condenser fans could be staged with larger speed than one fourth of the designed rotating speed. With higher compressor efficiency and sufficient condenser airflow rate, therefore, the best COP could be achieved at PLR of 0.25 for the studied air-cooled chillers with twin refrigeration circuits.

4.4 Optimum set points of condensing temperature

It has been confirmed that the use of HPC with a fixed T_{cdsp} of 45°C leads to a decline in chiller COP especially under partial load conditions. It is desirable to lower T_{cdsp} to attain maximum COP in all operating conditions, and it is worth ascertaining an optimum T_{cdsp} at a given operating condition.

When constant speed condenser fans were applied, it was adequate to adjust T_{cdsp} based on any given outdoor temperature alone, as shown in Eq. (4.55), which enabled the condensing temperature to approach its lower boundary. This adjustment was straightforward to ensure the highest number of condenser fans staged at any given chiller load. However, this set point of the condensing temperature may not be the optimal set point of condensing temperature for some operating conditions. Figures 4.12 and 4.13 reveal that maximum COP may not be achieved simply by setting the set point of condensing temperature according to Eq. (4.55), regardless of the chillers with constant speed fans or variable speed fans.

Having identified the pitfall of using Eq. (4.55) to evaluate maximum chiller COP, a logical argument was included in the algorithm of controlling condenser fans to determine the optimal set point of condensing temperature ($T_{cdsp,op}$) when CTC was applied with constant or variable speed condenser fans. For any given chiller part load ratio, it was possible to identify an optimal set point of condensing temperature

($T_{cdsp,op}$) for maximum COP by checking the variation in chiller COP throughout the T_{cdsp} range following the procedures in Figure 4.9. For each operating condition, this argument checked the difference in chiller COP when T_{cdsp} increased in steps of 0.05°C from its lower level of 20°C or (T_{db}+5) °C, whichever was higher. These steps were small enough to trace the change of COP, and the optimal T_{cdsp} could be identified along with the maximum chiller COP.

As shown in Figure 4.14, the $T_{cdsp,op}$ varied under different operating conditions for the air-cooled chiller with constant speed fans and variable speed fans. When using constant speed condenser fans, it was noted that there could be two or more set points of condensing temperature at which the local maximum points of COP occurred for each operating condition as shown in Figure 4.12. This was due to the change in the number of staged condenser fans across the T_{cdsp} range. In Figure 4.14 (a), just one of the set points of condensing temperature was presented at which the maximum COP was achieved. Figure 4.15 illustrates variation of the temperature difference between one of the optimal set points of condensing temperature and the outdoor temperature under various operating conditions. There was no regular trend for the optimal set point of condensing temperature of the chiller with constant speed fans, and it fluctuated widely for specific outdoor temperature. For the chiller with variable speed condenser fans, the optimal set point of condensing temperature increased closely with the chiller part load ratio for specific outdoor temperature as shown in Figure 4.14 (b), which indicated that $T_{cdsp,op}$ should be determined based on the outdoor temperature and the chiller part load ratio rather than on the outdoor temperature alone. For the maximum COP, the optimum set point of condensing temperature could be expressed as a function of outdoor temperature and chiller part load ratio, and it could be described as Eq. (4.56). It should be noted that the optimal set point of condensing temperature varied with the staging of the refrigeration

circuit(s).

$$T_{cdsp,op} = f(\text{PLR}, T_{db}) \tag{4.56}$$

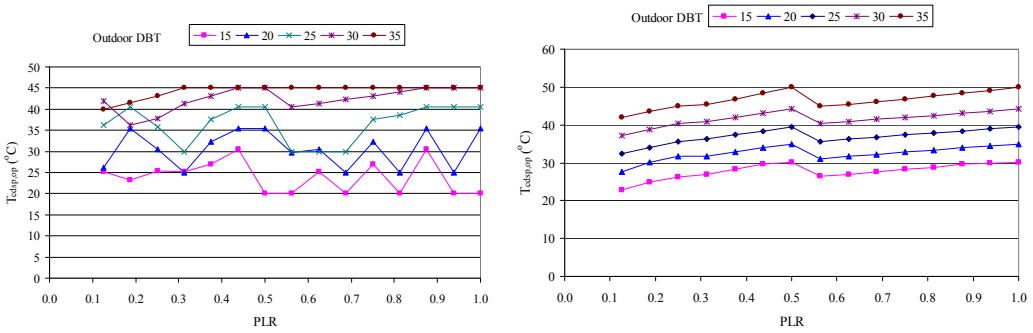

(a) Constant speed condenser fans (b) Variable speed condenser fans

Figure 4.14 Variations in the optimum set point of condensing temperature ($T_{cdsp,op}$)

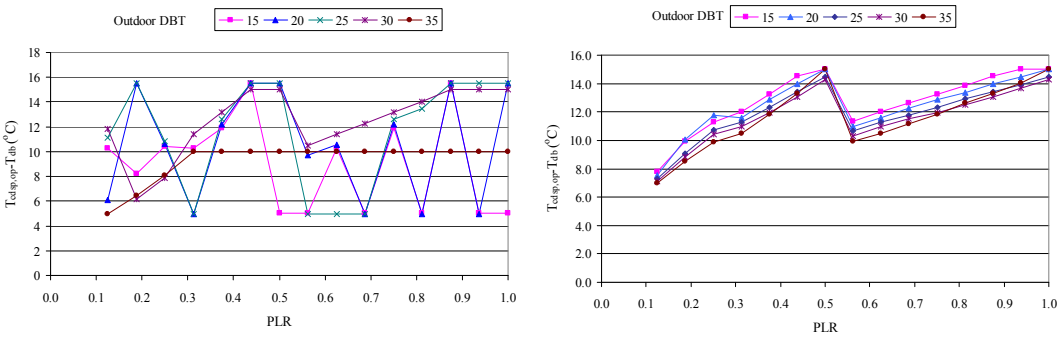

(a) Constant speed condenser fans (b) Variable speed condenser fans

Figure 4.15 Variations in the difference between the optimum set point of condensing temperature ($T_{cdsp,op}$) and the outdoor temperature (T_{db})

Heat rejection airflow (V_a) is conventionally modulated step by step via staging different numbers of condenser fans at a constant speed. This kind of condenser fan staging has long been implemented under HPC, resulting in the imprecise control of condensing temperature. The use of variable speed condenser fans, on the other hand, allows the heat rejection airflow to regulate smoothly and helps improve the controllability of the condensing temperature with reduced power at lower speed (Yu and Chan 2006b). Variable speed condenser fans can vary V_a continuously based on any given set point of condensing temperature (T_{cdsp}).

Under CTC, the set point of condensing temperature should be adjusted in response

to the outdoor temperature and the chiller load as the function shown in Eq. (4.56). The adjustment should consider the constraints on compressor lubrication and the boundaries of the condensing temperature. It was straightforward to adjust the set point of condensing temperature for the air-cooled chiller with constant speed fans using Eq. (4.55), but the set points by this algorithm may not be the optimal ones for certain conditions. The percentage change of the chiller COP with optimal set point of condensing temperature was shown in Figure 4.16, in relation to the chiller COP whose set point was reset based on Eq. (4.55). This figure demonstrated that the set point of condensing temperature based on Eq. (4.55) could be one of the optimal set points for most operating conditions. However, it was not true when the chiller part load ratios were less than 0.3, at which the chiller COP could be improved by up to 9.4% with optimal set point of condensing temperature. Therefore, it is desirable to adjust T_{cdsp} with a function of outdoor temperature and chiller PLR following the procedures in Figure 4.9.

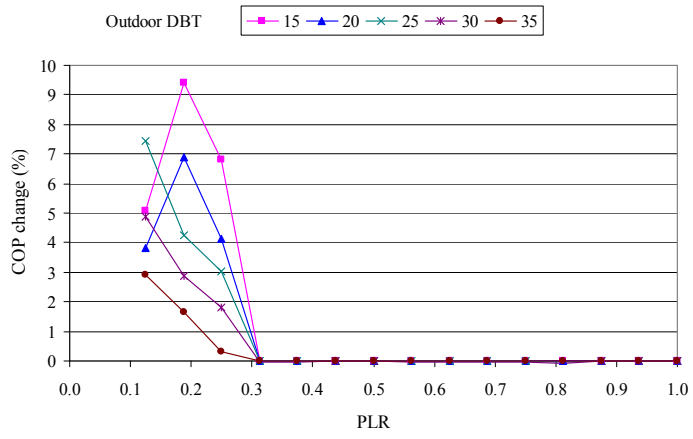

Figure 4.16 COP percentage change compared with the algorithm of Eq.(4.55)

4.5 Chiller COP under four strategies

In this section, the chiller operated at various outdoor temperatures and load conditions with operating schemes: (a) HPC with constant speed condenser fans; (b) HPC with variable speed condenser fans; (c) CTC with constant speed condenser

fans; (d) CTC with variable speed condenser fans.

4.5.1 Chiller COP

For any given operating condition, the chiller COP varied with different operating schemes because each scheme had its own unique modulation of heat rejection airflow based on a set point of condensing temperature. The chiller COP curves for the four operating schemes were shown in Figure 4.17, for outdoor temperature from 15 to 35°C at intervals of 5°C.

The chiller COP varied following the sequence of operating the two refrigerant circuits and the sequence of compressors in each refrigeration circuit of the chiller. This clearly revealed that the chiller COP dropped substantially when an additional compressor or refrigerant circuit was staged to cope with a rising load, because compressor efficiency dramatically decreased at low part load ratios under HPC. For each operating scheme, the chiller COP generally increased with the part load ratio of the staged compressors (PLR_{com}) and approached the highest level at a chiller part load ratio (PLR) of 0.25, 0.5 and 1 at any given outdoor temperature, as under such conditions the staged compressor(s) was/were full loaded. The highest chiller COP was due to the maximum compressor efficiency at its full load and the greatest overall heat transfer coefficient of the evaporator resulting from the maximum heat exchange effectiveness between the chilled water and refrigerant.

As shown in Figure 4.17(a), under HPC with constant speed condenser fans, the chiller COP fluctuated considerably because the heat rejection airflow varied step by step. It was difficult to assess the chiller COP precisely using a single performance curve as the curves crossed each other in some operating conditions. Similar findings were also observed from the evaluations of the existing plants with air-cooled screw chillers (Yu and Chan 2006a).

Figure 4.17(b) illustrates the variation of the chiller COP with variable speed condenser fans under HPC. The chiller COP could rise almost linearly with the increasing chiller load and varied following the staging of the refrigeration circuit and the compressor in each refrigeration circuit at any given outdoor temperature, which was different from the fluctuating COP when using HPC and constant speed fans. It was possible to use a single performance curve to assess its COP when the chiller operated under HPC with variable speed condenser fans. This was due to a situation where the condensing temperature could be controlled better at its set point by modulating the heat rejection airflow continuously. These findings indicated that a change in chiller COP was largely dependent on the type of condenser fans and on how condenser fans were controlled to provide the required heat rejection airflow for any given cooling load.

Unlike HPC under which the condensing temperature floated around its set point of 45°C regardless of outdoor temperatures, CTC was intended for enhancing heat rejection airflow, enabling the condensing temperature to float closely above the outdoor temperature. Although the increased heat rejection airflow caused an additional fan power, the decreased condensing temperature resulted in an increase in chiller COP because of a considerable reduction in compressor power. The extent of which in chiller COP could increase under CTC was identified by comparing the COP curves in Figure 4.17 (c) with Figure 4.17 (a) in the case of constant speed fans, or comparing the COP curves in Figure 4.17 (d) with Figure 4.17 (b) in the case of variable speed fans.

As illustrated in Figures 4.17 (c) and 4.17 (d), the chiller COP under CTC could be described by a set of part load performance curves, regardless of whether the condenser fans operated at constant or variable speed. These findings corroborate

Chan and Yu's results that a set of chiller performance curves should be used to assess the chiller COP at part load when the condensing temperature is controlled based on any given outdoor temperature (Yu and Chan 2006b). An upward shift in COP is found when the outdoor temperature drops. This indicates that chiller COP is greatly affected by the entering condenser air temperature.

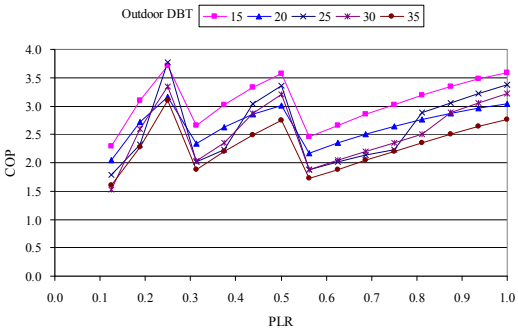

(a) HPC with constant speed fans

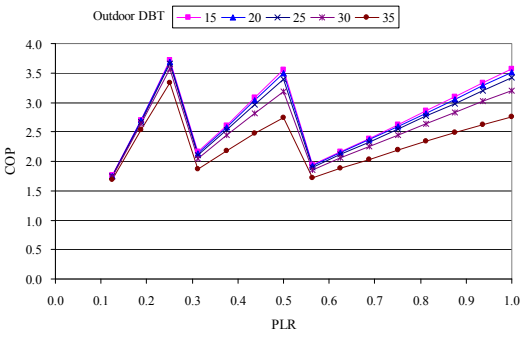

(b) HPC with variable speed fans

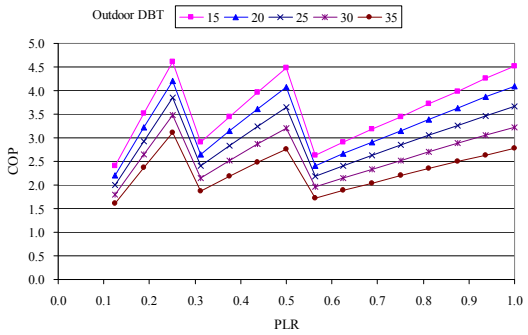

(c) CTC with constant speed fans

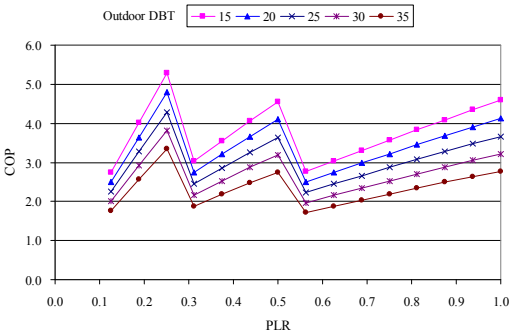

(d) CTC with variable speed fans

Figure 4.17 Chiller COP curves for four strategies of condenser fan control

4.5.2 COP Improvements

After identifying the optimum set point of condensing temperature, it affirmed worth assessing the potential improvements in chiller COP when CTC and variable speed condenser fans were applied to the existing air-cooled screw chillers. Comparing with the chiller performance with constant speed condenser fans under HPC, the COP with variable speed condenser fans under HPC could increase or reduce, depending on variations in the outdoor temperature and the chiller load, as shown in

Figure 4.18 in which an increase in chiller COP was expressed as a positive percentage.

With variable speed condenser fans under HPC, the COP increased by up to 17.1% when the outdoor temperature was 20°C and the part load ratio was 0.25. When the outdoor temperature was 35°C, the change of chiller COP was -0.3% to 10.8%. While the condensing temperature could be maintained close to its set point by using variable speed fans, the COP could comparatively decline to some extent due to the traditional head pressure control and the staging of the condenser fans group by group. The condensing temperature could drop below its set point when the heat rejection airflow provided by the constant speed fans exceeded the minimum airflow required to maintain the set point. Under these conditions, the compressor power was much less than that with variable speed condenser fans. In addition, the chiller COP drop was due to the fact that the variable speed drive consumed about 3% of the total power of the staged condenser fans. In general, it appears difficult to identify the potential benefits of using variable speed condenser fans under head pressure control.

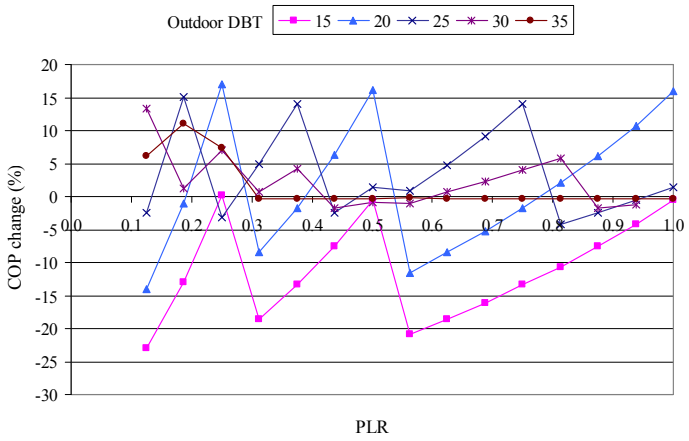

Figure 4.18 Percentage change in chiller COP under HPC with variable speed condenser fans

When the chiller operated under CTC with constant speed condenser fans, the chiller COP could be improved in all operating conditions up to 35.4%, as shown in Figure

4.19. It would be interesting to identify the extent to which the chiller COP could increase when CTC and variable speed condenser fans were applied. As illustrated in Figure 4.20, the use of variable speed condenser fans and CTC enabled the chiller COP to be improved by up to 51.8%. However, when the chiller operated at outdoor temperature of 35°C, the COP could slightly drop by up to 0.3% because there was a 3% increase in fan power due to the variable speed drive. The fan power was largest in this situation because all the condenser fans operated at full speed due to the use of lower set point of condensing temperature.

It should be noted that the chiller COP percentage change was based on the base case under HPC and constant speed condenser fans. As shown in Figure 4.17 (a), the chiller COP fluctuated considerably because the heat rejection airflow varied step by step, and the chiller COP for outdoor temperature 20°C was smaller than that for outdoor temperature 25°C and 30°C at some load conditions. Therefore, the chiller COP percentage change in outdoor temperature 20°C is the highest as shown in Figures 4.18, 4.19 and 4.20.

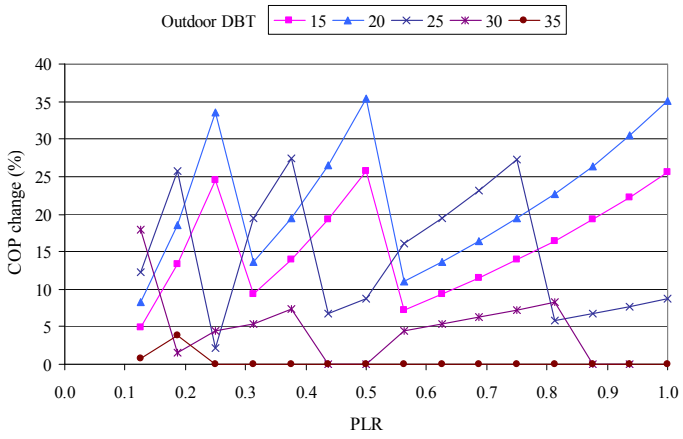

Figure 4.19 Percentage change in chiller COP under CTC with constant speed condenser fans

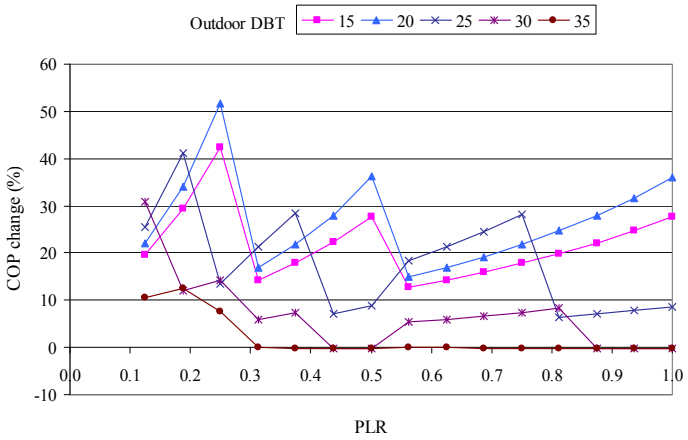

Figure 4.20 Percentage change in chiller COP under CTC with variable speed condenser fans

4.6 Optimal load sharing between refrigeration circuits

Many water chillers are designed with multiple refrigeration circuits connected in parallel, and each refrigeration circuit has one or more compressors. This design of multiple refrigerant circuits is to enhance the reliability and standby capacity, and it gives an opportunity to improve the chiller performance. As any one or more of the circuits in a chiller may be operated at a given conditions, the chiller performance would be different under different operating mode. This means that proper control strategy which is used to share the cooling load between the refrigeration circuits and sequence the compressors in each circuit is critical. For this reason, it is desirable to identify operating strategies on proper circuit loading sequence (CLS) that improve the efficiency of the chiller with multiple refrigeration circuits, which can minimize the sum of compressor power and condenser fan power of the staged chillers for all operating conditions.

4.6.1 Circuit loading sequence

For the chillers with multiple refrigeration circuits, there exist various modes of circuit staging which yield fluctuating efficiency under various cooling load conditions. As the chiller efficiency dramatically decreases at low part load ratios

under HPC, circuit sequencing is crucial to improve energy efficiency of chillers with multiple refrigeration circuits. If a chiller had two identical refrigeration circuits, as was the studied chiller, the cooling load could be shared by the two refrigeration circuits randomly; hence there existed an optimal load distribution between the refrigeration circuits rather than sharing the load equally. In this section, the simulation analysis considered both individual and mixed uses of three control schemes: circuit loading sequence, variable speed fan control and variable condensing temperature control.

4.6.1.1 Constant speed fan control

Circuit loading sequence (CLS) of the chillers with constant speed condenser fans was investigated firstly. Six operating schemes were considered for chillers with constant speed fans as shown in Table 4.3. Operating scheme CSF1 was the conventional circuit sequence control and served as the baseline. For the schemes CSF1 to CSF4, the two compressors in each refrigerate circuit operated with even load when the cooling load of the circuit was more than 25% of the rated chiller capacity, or one compressor operated in this refrigeration circuit.

Table 4.3 Operating schemes for the chiller with constant speed fans

Operating schemes	*Description*	*Notes*
CSF1	Loading priority was given to the lead circuit when chiller load was less than half of the rated chiller capacity, and kept the capacity of circuits 1 and 2 be equal when the total chiller load was more than half of the rated chiller capacity.	
CSF2	Balanced circuit loading that the control system kept the capacity of circuits 1 and 2 be equal at any time when the chiller operated.	
CSF3	Loading priority was given to the lead circuit until fully loaded, and then the other circuit met the balance of the load when the total chiller load was more than half of the rated chiller capacity	HPC
CSF4	Optimal CLS, in which cooling load was optimally shared by the two refrigeration circuits.	
CSF5	Optimal CLS and optimal compressor sequence, in which cooling load was optimally shared by the two refrigeration circuits, and also the load of each circuit was optimally shared by the two compressors in a refrigeration circuit.	
CSF6	CSF4+CTC	CTC

Figure 4.17(a) illustrates the chiller COP curves with constant speed condenser fans under HPC. Figure 4.21 shows the percentage change of chiller COP relative to scheme CSF1 under different circuit loading schemes. For the operating scheme CSF2, the chiller COP dropped significantly when the PLR was less than 0.25, and it could drop up to 54.3%. For PLR in the ranged of 0.25 to 0.5, chiller COP could be improved up to 12.9%. For the scheme CSF4, using optimal CLS, the chiller COP was improved when PLR was greater than 0.25, and it could be improved by various degrees up to 56.4%. It revealed that the optimal CLS could obviously improve the chiller COP for the chillers with multiple refrigeration circuits. When the operating scheme CSF5 was applied, the chiller COP could be improved further, especially when the PLR ranged from 0.5 to 0.75. Under such conditions, the load within one refrigeration circuit was optimally shared by the compressors in each refrigeration

circuit. There was no noticeable improvement when scheme CSF5 was compared with scheme CSF4. However, it was much more complicated and extremely time-consuming for implementing the two-level optimization in scheme CSF5. Considering the computation cost, it was recommended to implement scheme CSF4 with optimal CLS.

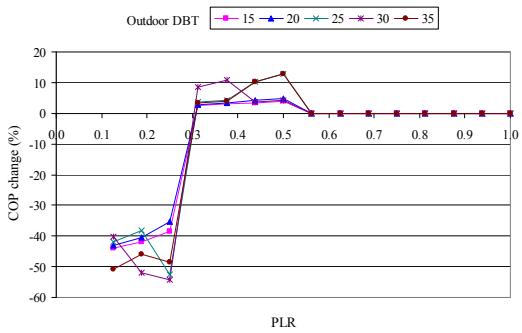

(a) CSF2

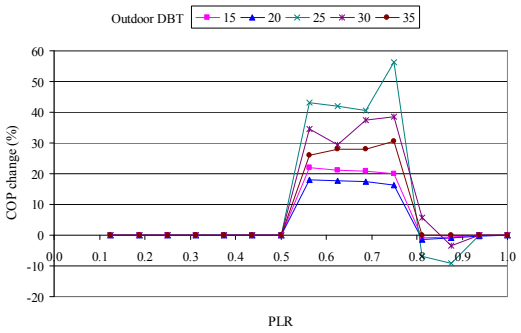

(b) CSF3

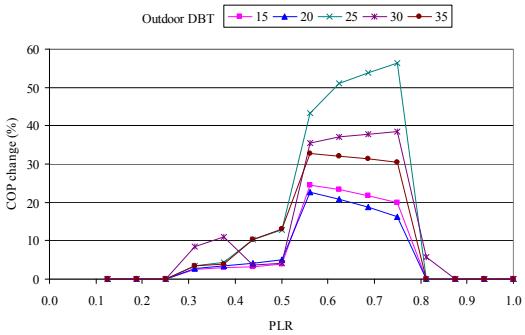

(c) CSF4

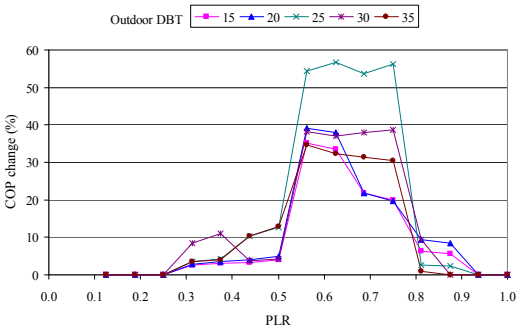

(d) CSF5

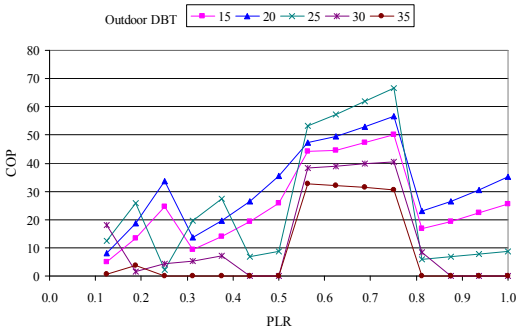

(e) CSF6

Figure 4.21 Percentage change of chiller COP relative to CSF1 under different CLSs

When the optimal CLS and variable condensing temperature control were applied together, the chiller COP could be obviously improved for all operating conditions

up to 66.7%. As shown in Figure 4.21 (e), the extent of improvement of the chiller COP was much larger for the range of PLR from 0.5 to 0.75, as under such conditions the optimal load sharing between the two refrigeration circuits could greatly improve the chiller efficiency.

4.6.1.2 Variable speed fan control

It would be interesting to investigate the effect of circuit loading sequence on the performance of chillers with variable speed condenser fans. There were also six operating schemes considered for the chiller with variable speed fans as shown in Table 4.4. Figure 4.22 demonstrates the percentage change of chiller COP relative to VSF1 under different circuit loading sequences. Similar to the results of the cases with constant speed condenser fans, the optimal CLS could obviously improve the chiller COP for chillers with multiple refrigeration circuits, and COP could be improved by up to 38.0% for scheme VSF4 as shown in Figure 4.22(c). When the operating scheme VSF5 was applied, the chiller COP could be improved further, but there was no significant improvement when comparing scheme VSF5 with scheme VSF4, and the computation in scheme VSF5 was very time-consuming. Considering the computation cost, VSF4 was preferred for the optimal load sharing between two refrigeration circuits if it was applied to on-line control.

Table 4.4 Operating schemes for the chiller with variable speed fans

Operating schemes	***Description***	***Notes***
VSF1	CSF1+VSF (baseline)	
VSF2	CSF2+VSF	
VSF3	CSF3+VSF	HPC
VSF4	CSF4+VSF	
VSF5	CSF5+VSF	
VSF6	CSF6+VSF	CTC

When the optimal CLS and variable condensing temperature control were applied together, the chiller COP could be improved further under operating scheme VSF6 as

shown in Figure 4.22 (e), especially when the PLR ranged from 0.5 to 0.75. Under such conditions, the optimal load sharing between the two refrigeration circuits and CTC enabled the chiller COP to improve considerably. Figure 4.22 (e) also revealed that the outdoor temperature had a great influence on the chiller performance and, the lower the outdoor temperature, the greater extent of the COP improvement could be achieved.

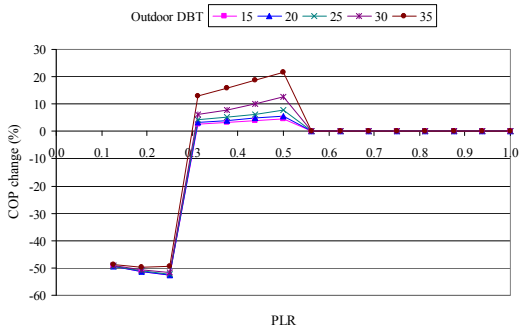

(a) VSF2

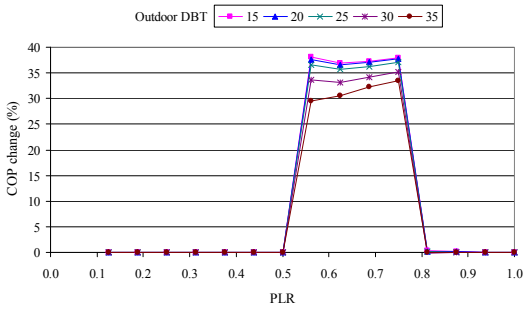

(b) VSF3

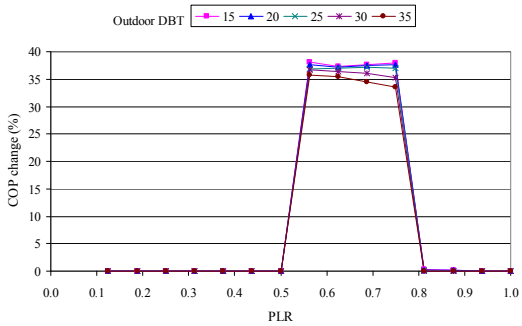

(c) VSF4

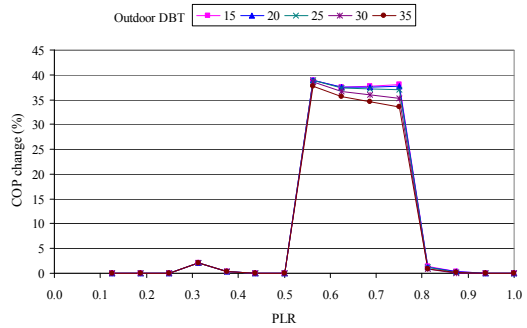

(d) VSF5

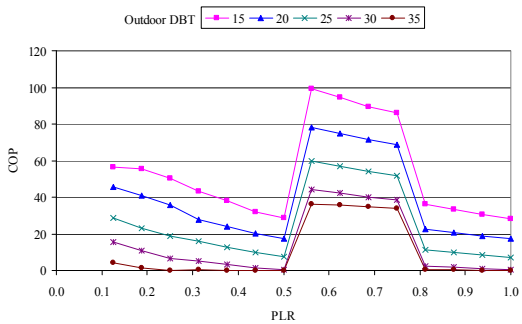

(e) VSF6

Figure 4.22 Percentage change of chiller COP relative to VSF1 under different CLSs

4.6.2 Potential benefits from optimal circuit loading sequence

From Figures 4.21 and 4.22, it was identified that the optimal CLS could obviously improve the chiller COP for the chillers with multiple refrigeration circuits. It was desirable to evaluate the cooling energy saving potential for a representative office building when different control strategies of CLS were implemented.

For the representative office building, the peak cooling load was 7338 kW as described in Chapter 3. To meet the peak cooling load, the office building's chiller plant was designed with seven air-cooled screw chillers, each of which had a nominal cooling capacity of 1116 kW. The size of these chillers was comparable to that of the model chiller. To highlight the effect of the CLS, the traditional chiller sequencing of a multiple-chiller system was considered in this study, which was to operate the minimum number of evenly loaded chillers to meet the required cooling load.

Having identified the cooling load profile of the office building and the scheme of staging chillers, it was possible to employ the chiller model to investigate the energy saving potential by the optimal CLS for air-cooled screw chillers with multiple refrigeration circuits.

The annual electricity consumption of the chillers under different control strategies was evaluated, as shown in Table 4.5. Average chiller COP was the annual cooling load divided by the annual chiller electricity consumption. The chiller performance under strategy CSF2 was inferior to that under CSF1 with annual electricity consumption increasing by 0.1%. For CSF4, optimal CLS enabled the total electricity consumption of the chillers to drop by 4.2%. When optimal CLS and optimal compressor sequence in a refrigeration circuit were implemented, as in scheme CSF5, 6.0% of the annual chiller electricity consumption was achieved. Based on the local weather, chillers operate in part load conditions with an outdoor

temperature of below 25°C for half of the time. Consequently, there is a considerable scope for lowering the condensing temperature. It was expected that the COP improvements would be more considerable with CLS and CTC. Under CTC with optimal CLS, substantial power consumption could be saved by 9.6% in the scheme CSF6.

When the studied air-cooled chillers were retrofitted with variable speed condenser fans replacing the constant speed fans, annual electricity consumption under VSF1 was saved only by 0.3% under CSF1, which mainly resulted from the traditional head pressure control. This indicated that HPC could not take full advantage of the energy saving potential of using variable speed condenser fans. It was desirable to operate the chiller with variable speed condenser fans under CTC. When the variable speed condenser fans and CTC were applied together to the studied chillers, it enabled the chiller plant to save annual electricity consumption up to 10.3%.

Table 4.5 Energy performance of chillers under different control strategies

Cases	*Annual electricity consumption (kWh)*	*Average COP*	*Energy saving (%)*	*Notes*
CSF1	3.52×10^6	2.86	-	Base case
CSF2	3.52×10^6	2.85	-0.1	
CSF3	3.42×10^6	2.94	2.7	
CSF4	3.37×10^6	2.98	4.2	
CSF5	3.31×10^6	3.04	6.0	
CSF6	3.18×10^6	3.16	9.6	
VSF1	3.51×10^6	2.86	0.3	
VSF2	3.51×10^6	2.86	0.2	
VSF3	3.40×10^6	2.96	3.5	
VSF4	3.39×10^6	2.96	3.5	
VSF5	3.37×10^6	2.98	4.2	
VSF6	3.16×10^6	3.18	10.3	

4.7 Summary

This chapter investigated the chiller plant in one institutional building complex, and the operating data were measured for validating the developed chiller model. The

sophisticated model of the air-cooled screw chiller with twin refrigeration circuits was developed, and it was validated with the operating data. The chiller model forms the basis for the comparison of different control strategies and the development of optimum chiller control strategy. This chapter then investigates how variable condensing temperature control and variable speed condenser fans can be applied to enhance the chiller COP. When the chiller operated under CTC with constant speed condenser fans, the chiller COP could be improved in all operating conditions up to 35.4%. The use of variable speed condenser fans and CTC enabled the chiller COP to be improved by up to 51.8%. The investigation on the optimal load sharing between refrigeration circuits in an air-cooled chiller was also presented. When the optimal CLS and variable condensing temperature control were applied together, the chiller COP could be obviously improved for all operating conditions up to 66.7%. When the variable speed condenser fans and CTC were applied together to the studied chillers, it enabled the chiller plant to save annual electricity consumption up to 10.3%.

Chapter 5 Experimental and Simulation Study on Water Mist System

This chapter outlines the methodologies of the experimental and simulation study on water mist system. It first describes how the experiment on an air-cooled screw chiller with water mist system is conducted, and the operating data are evaluated. It then presents the model of water mist, which is incorporated into the chiller model developed under the TRNSYS platform. The model for an air-cooled chiller with water mist system forms the basis for simulating and analysing the improvement of chiller efficiency with various control strategies. This chapter also reports a detailed analysis on the energy saving potential of the chillers serving the representative office building and hotel building with enhanced condenser features, and determines the possible contribution in reducing the total chiller electricity consumption of the building sector in Hong Kong.

5.1 Description of water mist system

Figure 5.1 illustrates a schematic of a typical water mist system, which comprises of a high pressure pump, a filter unit, atomization nozzles, high pressure and low pressure tubing. The high pressure pump can operate to deliver water at a high pressure of around 70 bars, and the water is forced through micro nozzles to create a mist of 10 micron droplets. When the tiny water droplets are sprayed into the atmosphere, they quickly absorb the heat in the environment and evaporate, and then the air temperature decreases due to evaporative cooling effect.

When the water mist system is coupled to an air-cooled chiller, the temperature of the entering condenser air will drop, which results in lowering the condensing

temperature and pressure, as shown in Figure 5.2. The refrigeration cycle of the chiller system with water mist system is changed from the cycle 1-2-3-4-1 to 1-2'-3'-4'-1. With the decrease of the condensing pressure, the compressor power is reduced. However, the cooling capacity increases, hence the COP of the chiller system will increase. Theoretically, the energy efficiency of air-cooled chillers coupling with a water mist system will be improved, but the degree of effectiveness is dependent on the climatic conditions, chiller load ratios and operational control strategies.

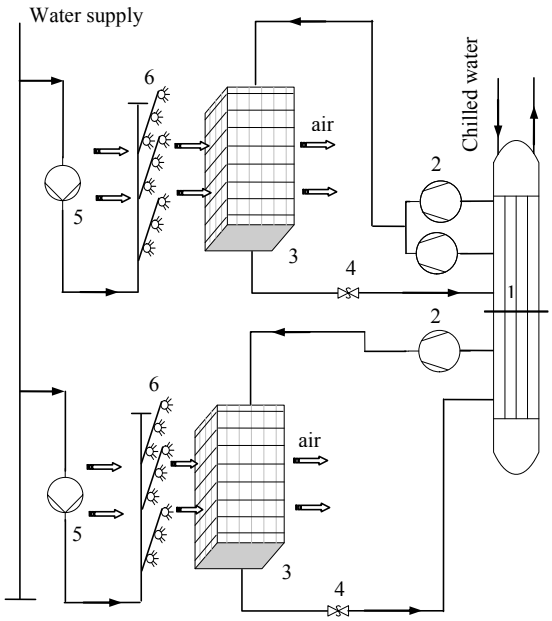

Figure 5.1 Schematic of the water mist system

1. Evaporator 2.Compressor 3.Condenser 4.Expansion valve 5.High pressure pump 6. Nozzles

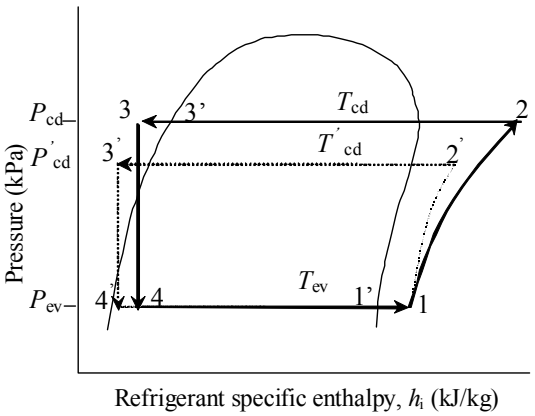

Figure 5.2 Vapour compression cycle of the refrigeration circuit

5.2 Description of studied chiller coupling water mist

One pragmatic approach to improving the chiller COP is to lower the condensing temperature to a level that enables the trade-off between compressor power and condenser fan power to be optimized. Using water mist pre-cooling to enhance the COP of air-cooled chillers is not common, even though the concept is not new.

In this research, an experiment was carried out on an air-cooled screw chiller to evaluate the improvement of chiller performance with water mist system. A chiller plant installed in an institutional complex comprising of three larger and one small screw chillers connected in parallel was investigated, in which the three lager chiller were identical. The arrangement of the chiller system was illustrated in Figure 5.3. A single-loop pumping system was used in which there was a differential pressure bypass pipe to balance the flow between the water side and air side system. There were four constant speed pumps, and each pump set delivered the design chilled water flow rate for an operating chiller operating matched to the pump. The chillers were staged one by one in response to the changing building cooling load, and the smaller chiller operates in the night mode, as shown in Figure 5.4.

One of the three greater chillers was investigated. The studied chiller had two refrigeration circuits as shown in Figure 5.5, namely circuit 1 and circuit 2, using refrigerant R134a. The chiller was equipped with one compressor for circuit 1 and two compressors for circuit 2. The nominal cooling capacity of the studied chiller was 705 kW, rated under the operating conditions of entering condenser air temperature at 35°C and entering/leaving chilled water temperatures at 12°C /7°C. The rated power of the studied chiller was 242 kW. The condensers comprised of 10 identical condenser fans arranged with a total air flow rate of 53.45 m^3/s, including four fans serving circuit 1 and six fans serving circuit 2. The fan speed was 15.8 r/s,

and each fan consumed a power of 2.4 kW. Table 5.1 shows the details of the chiller model.

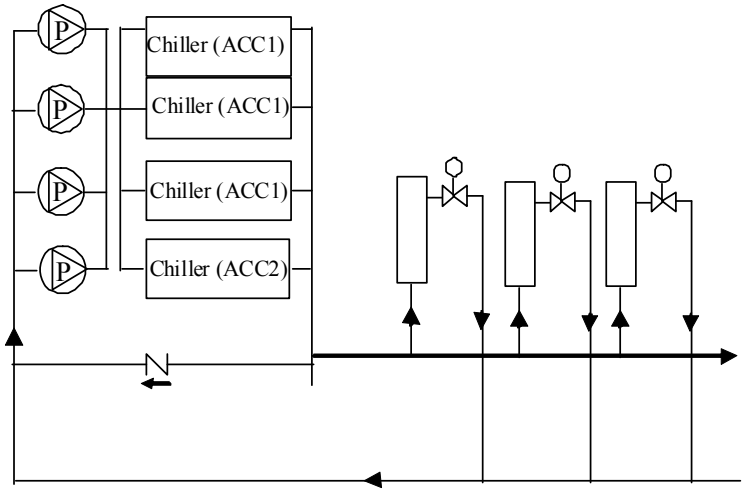

Figure 5.3 Arrangement of the chilled water system

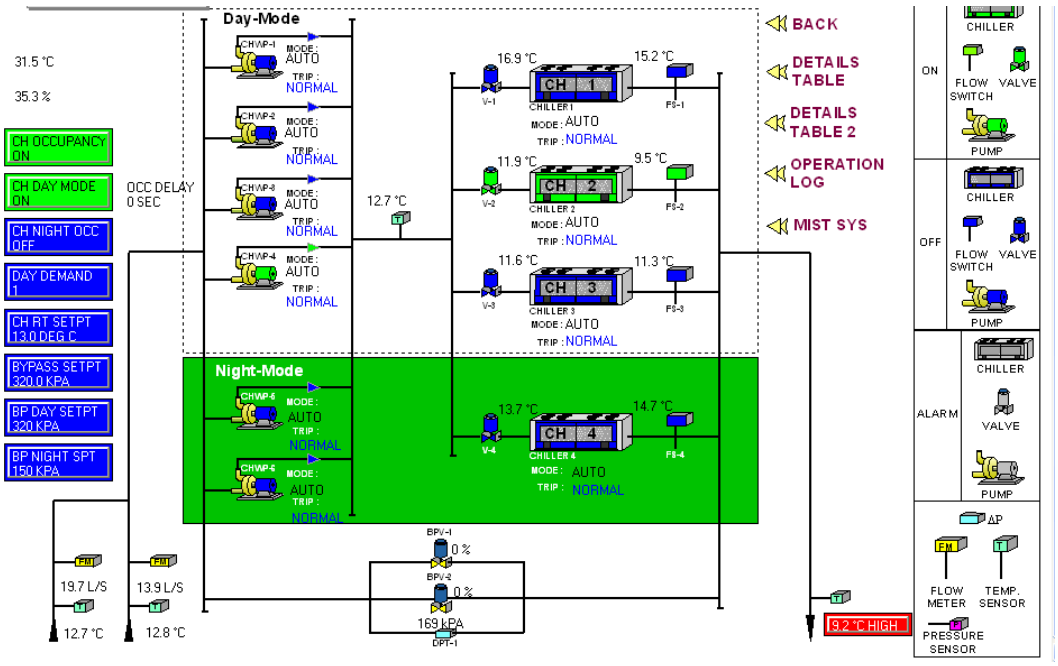

Figure 5.4 Graphic interface of the chiller monitor system

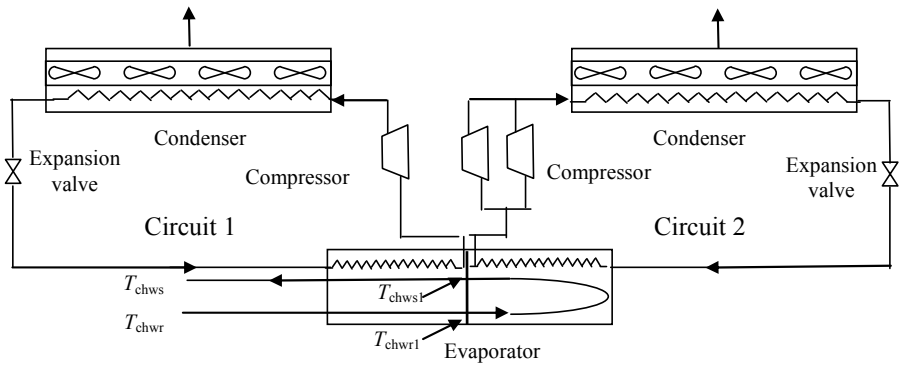

Figure 5.5 Schematic of the air-cooled chiller

Table 5.1 Details of the chiller model

Refrigerant type	HFC-134a
Nominal cooling capacity (kW)	705
Nominal power input (kW)	242
Refrigerant charge (kg)	
Circuit 1	81
Circuit 2	124
Compressors	
No. in circuit 1	1
No. in circuit 2	2
No. of control steps	8
Minimum step capacity (%)	16
Evaporator	
Type	Shell-and-tube flooded
Evaporating temperature (°C)	5
Temperature of supply chilled water (°C)	7
Max. water side operating pressure	1000
Condensers	
Condenser fans quantity	10
Fan speed (r/s)	15.8
Total air flow (m^3/s)	53.5

The air-cooled screw chiller plant was installed to provide space cooling several years ago. In order to improve the chiller efficiency, water mist systems were installed in July 2009. Each chiller was served by a separate water mist system comprising of two water mist circuits, as shown in Figure 5.1. The two water mist circuits contained high pressure pumps at rating of 0.75 kW and 1.25 kW dedicated for refrigeration circuits 1 and 2, respectively. The flow rate of the high pressure

pumps were 2 l/min and 4 l/min at 1500 rpm for circuit 1 and circuit 2, respectively, discharging through a total of 58 nozzles. According to the layout of the condenser coil, the nozzles were evenly distributed in front of the entire condenser surface to ensure better evaporative effect. The DBT and relative humidity (RH) of entering condenser air were measured with a data logger system, and the other variables related to chiller performance were recorded by the building management system (BMS). Figure 5.6 shows the experimental setup of the air DBT and RH sensors at the inlet to the condensers of the studied chiller. A distance of 750 mm was maintained between the nozzles and the condenser surface to ensure better cooling effect by full evaporation of water mist. The distance between the nozzles and the condenser face was determined based on the configuration of the condenser coil and preliminary on-site tests, which depended on the ambient air conditions, heat rejection airflow, water mist generation rate, layout of nozzles, etc. The numerical study by Tissot et al. (Tissot, Boulet et al. 2011) confirmed that almost all the sprayed water mist fully evaporated after a distance of 0.7 m from the injection point. The detailed experiment on the distance between the nozzles and the condenser face will be a future research work. With the water mist data and the chiller data, the chiller performance could be analyzed.

5.3 Experimental study of the chiller with water mist system

5.3.1 Experiment setup and data acquisition

The studied air-cooled screw chiller was operated under head pressure control. Experiments were conducted to investigate the performance of the air-cooled chiller with or without water mist system over a representative range of ambient temperature (T_{db}: 23.8–33.5°C), relative humidity (RH: 31.3–90.1%) and part load ratios (PLRs: 0.1–1.0) in the local climate, over a period of 4 months from July to

November 2009. The experimental data were used to determine the parameters of equations in the chiller model and to verify the developed chiller model incorporating the water mist model.

To investigate the performance of the air-cooled chiller with or without water mist system, there were many parameters needed to be measured, including evaporating temperature (T_{ev}) and condensing temperature (T_{cd}) of each refrigeration circuit, power of each compressor (E_{cc}), condenser fan power of each circuit (E_{cf}), chilled water flow rate (m_w), temperatures of supply and return chilled water (T_{chws} and T_{chwr}), water mist generation rate (m_{wm}), condenser air temperature and relative humidity at 3 locations: before the water mist (ambient air), at the inlet of the condenser coil and leaving the condenser coil. The operating data were monitored and logged at 10-minute or 15-minute intervals over the experimental period. Resistance type temperature sensors were used to measure the temperature of chilled water with an uncertainty of ±0.1°C. The chilled water flow rate was measured by an ultrasonic flow meter with an uncertainty of ±0.5% of the measured value. Compressor power (E_{cc}), condenser fan power (E_{cf}) and high pressure pump power (E_{hp}) were metered by power analysers with an uncertainty of ±0.1 kW. The DBT and RH of ambient air were monitored by a transmitter with an uncertainty of ±0.1°C for air temperature and ±2% for relative humidity, which were used to control the operation of the water mist systems. To measure the DBT and RH of entering condenser air, data loggers were installed at the inlet of the condenser as shown in Figure 5.6, which were weatherproof sensors with an uncertainty of ±0.2°C for air temperature and ±3% for relative humidity. One data logger was installed at the condenser outlet to measure the DBT and RH of the air leaving the condenser, whose uncertainty was ±0.3°C for air temperature and ±2.5% for relative humidity. Figure 5.7 shows some of the data loggers used in the experiments.

Figure 5.6 Photograph of the water mist system with data loggers

Figure 5.7 Data loggers for the experiments

As the chiller COP was not directly measured but calculated from the measured variables, an uncertainty analysis on the chiller COP was carried out. The chiller load (Q) could be calculated by Eq. (5.1). The chiller COP was calculated by the chiller load divided by the total power input, including the chiller power (E_{ch}) and high pressure pump power (E_{hp}) for generating water mist, and it was described as Eq. (5.2). The chiller power included the compressor power (E_{cc}), condenser fan power (E_{cf}) and lubrication pump power (E_{lp}). As the lubrication pump power was very

small, it was included in the measured compressor power.

$$Q = m_{\mathrm{w}} \cdot C_{\mathrm{pw}} \cdot (T_{\mathrm{chwr}} - T_{\mathrm{chws}}) \tag{5.1}$$

$$COP = Q/(E_{ch} + E_{hp}) = m_w \cdot C_{pw}(T_{chwr} - T_{chws})/(E_{cc} + E_{cf} + E_{hp}) \tag{5.2}$$

ASHRAE Guideline 2 (ASHRAE 2010) provides a guideline for reporting uncertainty in results of experimental data as applied to HVAC equipment. An experimental result denoted as Y is determined from a set of independently measured variables x_{i}, where i = 1 to n, and n is the number of measurements related to Y.

$$Y = f(x_1, x_2, \cdots x_n) \tag{5.3}$$

Due to the accuracy of measured variables, the uncertainty associated with COP was determined by the single sample analysis (ASHRAE 2010), as shown in Eq. (5.4).

$$\delta COP_{(rms)} = \sqrt{\sum_{i=1}^{n} \left[\delta x_i \cdot (\partial COP / \partial x_i)\right]^2} \tag{5.4}$$

where x_{i} is the ith independent variable, δx_{i} is the uncertainty of the variable x_{i}.

Using Eqs. (5.1) to (5.4), the root sum square error of chiller COP ($\delta COP_{(\mathrm{rms})}$) due to all the uncertainties of the individual variables was evaluated to be 0.099 in a COP value of 2.9 at the design condition, and the uncertainty of COP was 3.4%. This was mainly due to the uncertainties in the chilled water supply and return temperature.

5.3.2 Experiment results analysis

A detailed analysis is reported in the following section on how water mist pre-cooling improve the performace of air-cooled chillers and what parameters should be considered to optimize the operation of the mist system coupled to the chiller.

5.3.2.1 Temperature drop

The thermodynamic properties of the entering condenser air are vital for analyzing the performance of water mist system. Water mist pre-cooling system lowers the entering condenser air temperature, and the psychrometric chart shown in Figure 5.8 illustrates the evolution of condenser air through the water mist system and the condenser coil. The evaporative cooling process by the water mist is assumed to be adiabatic. Therefore, the process can be expressed as from Point A to Point B in Figure 5.8, which follows a constant wet-bulb temperature line. Points A, B and C represent the state of the outdoor air, the state of the entering condenser air and the wet-bulb temperature of the outdoor air, respectively. The wet bulb temperature approximates the temperature of adiabatic saturation and so is the lowest temperature that can be achieved by spraying water mist into the air. As shows in Figure 5.8 as point D, the temperature and RH of air leaving the condenser are also monitored to evaluate the operating balance on heat rejection of the condenser. The process from Point B to Point D represents the change of state of the entering condenser air from the inlet to outlet of the condenser, carrying away heat of condensation from the refrigerant.

When the water mist system was operated, the evaporative cooling effect reduced the temperature of the entering condenser air. Figure 5.9 shows the temperature change of the entering condenser air against the wet bulb depression (WBD) which is the difference between DBT and WBT of the ambient air. The scattered points are grouped with different levels of approach to WBT (at 1 K interval). Approach is the temperature difference between the dry bulb temperature of entering condenser air (T_{ecd}) and the wet bulb temperature of ambient air (T_{wb}), which can be as low as 0.5 K. It illustrates that the air temperature may decrease by varying degrees up to 9.4 K. It was observed that the WBD had a great impact on the temperature drop. The greater the WBD of the ambient air was, the greater the temperature drop could be

achieved when water mist was operated. When the DBT was high and RH was low, the temperature could drop more, as the evaporation process occurred intensively under such conditions. Therefore, water mist system is especially suitable for dry and hot area, and can be sized smaller for a given heat load under such weather conditions.

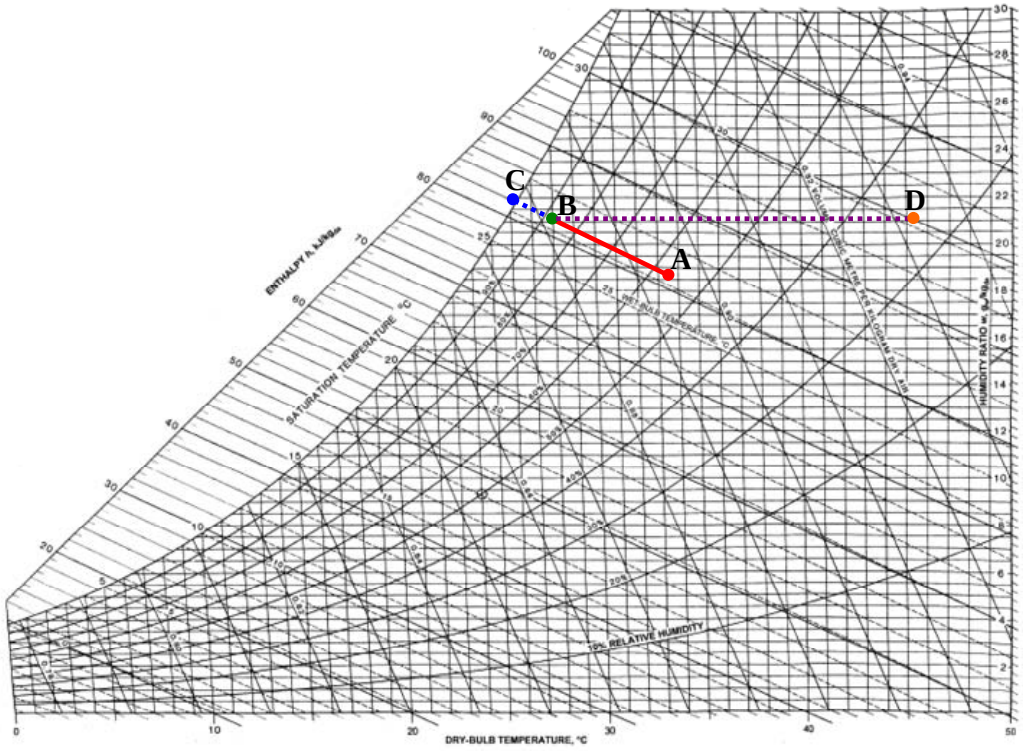

Figure 5.8 Psychrometric processes for the condenser air stream

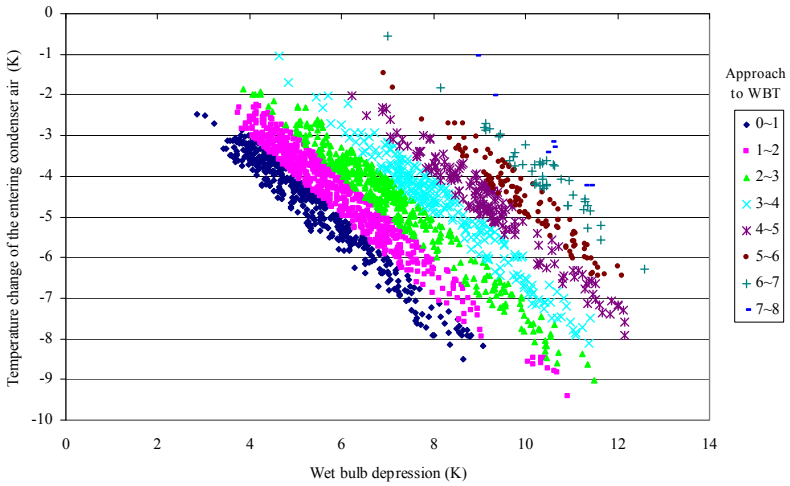

Figure 5.9 Impact of ambient air WBD on temperature change of entering condenser air due to water mist pre-cooling

5.3.2.2 Condensing temperature

For any given cooling capacity, the condensing temperature depends on the chiller load, heat rejection airflow and ambient air temperature. When the chiller operated without water mist, the condensing temperature was above 50°C for more than half of the operating conditions during the experimental period. When water mist system was operated, the condensing temperature was less than 55°C for all operating conditions and was below 45°C for more than half of the time. The lowest condensing temperature was 37.8°C during the experimental period. Figures 5.10 and 5.11 show the change of refrigerant condensing temperature with the ambient air temperature under different range of RH at part load ratios of 0.4-0.5 and 0.9-1.0 for circuits 1 and 2 respectively, which was due to the effect of water mist pre-cooling. The positive numbers represent a condensing temperature increase while the negative numbers represent a condensing temperature drop. According to the control strategy of the studied chiller, only circuit 2 was operated at part load ratios of 0.4–0.5. For refrigeration circuit 1, the condensing temperature drop varied regularly by up to 7.2 K. When the RH was lower, the condensing temperature drop could be larger. However, for refrigeration circuit 2, the condensing temperature varied irregularly, which could increase by up to 3.3 K or drop by up to 5.6 K during the experimental period. The variation of the condensing temperature changes was caused by the HPC with constant speed condenser fans and the specific configuration of the studied chiller having two refrigeration circuits. Circuit 1 was simpler and equipped with one compressor only. It was more complicated to control circuit 2 which was equipped with two compressors and six condenser fans. Under HPC with constant speed condenser fans, the condensing temperature could fluctuate considerably because the heat rejection airflow varied in steps by staging pairs of condenser fans.

When the condensing temperature exceeded the high condensing temperature setting, one more group of condenser fans would be switched on to increase heat rejection airflow, which enabled the condensing temperature to fall below the high setting. Because water mist pre-cooling would reduce the temperature of entering condenser air, the condensing temperature could fall below the high setting even if the number of staged condenser fans remained unchanged. For certain conditions, when the condensing temperature exceeded the high setting, both staging on more condenser fans and operating water mist could enable the condensing temperature to drop below the high setting, but the extent to which the condensing temperature could drop depended on the working conditions. As shown in Figure 5.10, when the ambient temperature varied from 31 to 33°C at part load ratios of 0.4-0.5, there was no obvious condensing temperature difference by staging on one more group of condenser fans and operating water mist, although the condensing temperature of chiller with mist pre-cooling could be slightly higher than that of chiller staging on more condenser fans without water mist when ambient DBT was 32°C and RH was above 70%.

In the case without water mist, when one more group of condenser fans was cycled on under some conditions, the heat rejection airflow provided by the constant speed fans could exceed the airflow required to maintain the set point of condensing temperature, and the reduction of the condensing temperature was more significant than that due to the evaporative cooling effect of water mist when the number of staged condenser fans remained unchanged. Hence the condensing temperature of the chiller with water mist could be higher than that of the chiller without water mist under HPC for certain conditions, as indicated by positive values of change of refrigerant condensing temperature in Figure 5.11 when ambient temperature varied from 27 to 30°C and chiller load ratios were close to one.

It should be noted that the condensing temperature dropped significantly for the chiller with water mist compared with the case without water mist, when the number of staged condenser fans were the same in both cases. These figures reveal that the condensing temperature of an air-cooled chiller with constant speed condenser fans may decrease or increase due to water mist pre-cooling under HPC, and the RH has a greater impact on the reduction of condensing temperature than the DBT of the ambient air. Compressor power can be saved by decreasing the condensing temperature, and the chiller performance is improved.

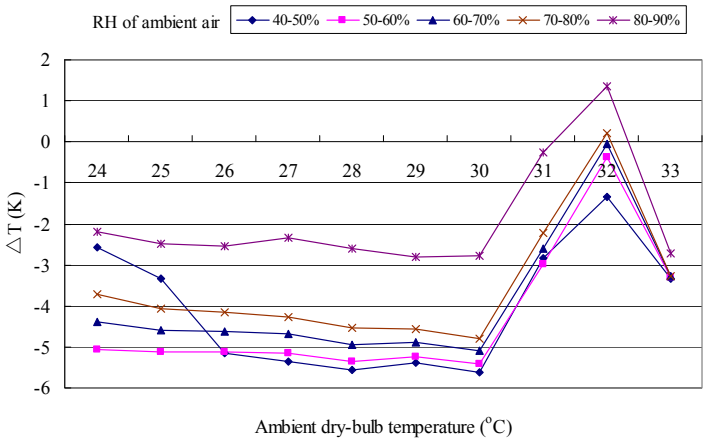

Figure 5.10 Change in refrigerant condensing temperature (ΔT) due to water mist pre-cooling at part load ratios of 0.4–0.5 (Circuit 2)

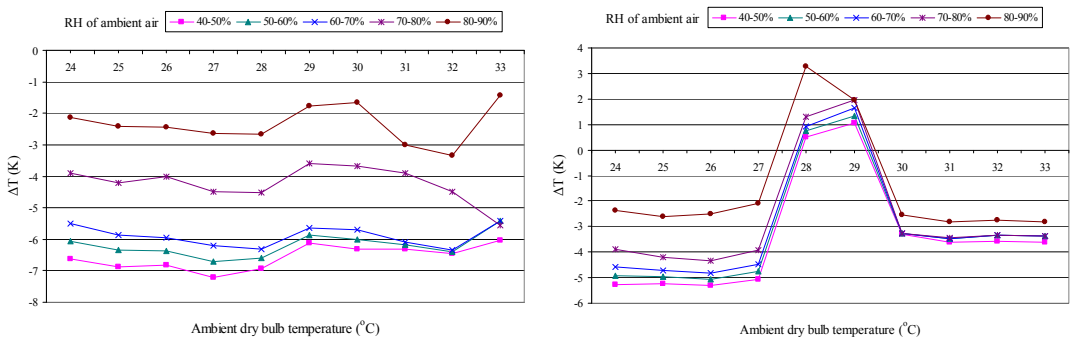

(a) Circuit 1 (b) Circuit 2

Figure 5.11 Change in refrigerant condensing temperature (ΔT) due to water mist pre-cooling at part load ratios of 0.9–1.0

5.3.2.3 Thermal Effectiveness

A suitable means of assessing the thermal performance of the water mist is the thermal effectiveness (ε), which is defined as a fraction of the maximum possible cooling of the ambient air, and is given by the following equation:

$$\varepsilon = \frac{T_{db} - T_{ecd}}{T_{db} - T_{wb}} \tag{5.5}$$

where T_{db} is the DBT of the ambient air, T_{ecd} is the DBT of entering condenser air, and T_{wb} is the WBT of the ambient air.

The thermal effectiveness involves both the approach and the range condition, as they are the two key determinants of energy performance. Range is the temperature difference between the ambient air and the entering condenser air. The thermal effectiveness can be expressed as Eq. (5.6).

$$\varepsilon = \frac{T_{db} - T_{ecd}}{(T_{db} - T_{ecd}) + (T_{ecd} - T_{wb})} = \frac{Range}{Range + Approach} \tag{5.6}$$

The 'Approach' is a better indicator of water mist performance, which is an important parameter in determining the capacity and optimizing the operation of the water mist system. Figure 5.12 shows the impact of thermal effectiveness on the approach to WBT for typical range temperatures at various operating conditions in this experimental investigation. The thermal effectiveness could be as high as 0.91 when the approach temperature was 0.5 K. For evaporative cooling, the ability to generate cooling medium approaching the WBT of ambient air is crucial. A well designed cooling tower can give an approach to WBT of 3 K. Costelloe et al. (Costelloe and Finn 2007) reported that a low primary approach temperature varying from 0.5 to 2.0 K could be achieved. The approach to WBT for both water mist system and cooling towers can be as low as 0.5 K, but the water mist system will give larger approach temperature in many conditions due to the designed water mist generation rate.

In this experiment, the water mist cooling could provide an approach to WBT as low as 0.5 K, and 52.3% of the approach temperatures were less than 2 K as shown in Figure 5.12. The thermal effectiveness of the water mist was higher than 0.6 for more than half of the working conditions during the experimental period. It was found that the thermal effectiveness could be lower than 0.4 due to the fact that the designed mist generation rate was much smaller than the required peak mist generation rate. If the water mist system was designed with larger water mist generation rate, there would be more chances to achieve higher thermal effectiveness.

It was reported that the thermal effectiveness of a direct evaporative pre-cooler with corrugated holed aluminum foil under the climatic conditions of Tianjin varied from 0.65 to 0.85 when the water sprinkling density increased from 0.2 to 1.2 Kg $m^{-2}s^{-1}$ (Zhang, You et al. 2000). The variation of the thermal effectiveness of water mist and an evaporative pre-cooler indicates that the effectiveness of evaporative cooling by both methods is greatly affected by the ambient air conditions, heat rejection airflow, design of the water mist system, water sprinkling intensity and water mist generation rate.

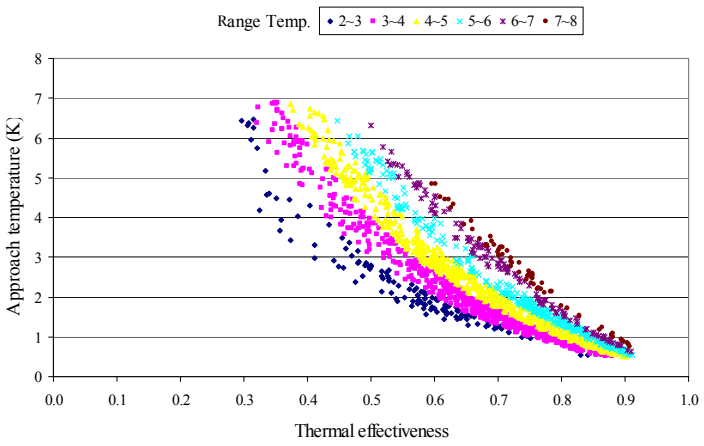

Figure 5.12 Variation of approach temperature with thermal effectiveness

It should be noted that thermal effectiveness of the water mist system coupling to the air-cooled chiller could be different with the same approach temperature, which was

greatly affected by the range temperature as shown in Figure 5.12. With a certain approach temperature, the thermal effectiveness would be higher with larger range temperature. To achieve certain thermal effectiveness with a low approach temperature, a relatively lower range temperature was required.

5.3.2.4 Chiller COP

The COP of the chiller operating with water mist pre-cooling was compared with the COP of the chiller without water mist pre-cooling under similar working conditions, and the chiller COP improvement resulting from the lower entering condenser air temperature and hence lower condensing temperature could be identified. Figure 5.13 illustrates the percentage change of the chiller COP under different RH ranges of ambient air at part load ratios of 0.4-0.5 and 0.9-1.0, relative to the base case without water mist pre-cooling. A positive number means a chiller COP increase while a negative number means a chiller COP reduction. It was observed that the chiller COP with water mist was improved noticeably from the baseline for most operating conditions, and could be improved in varying degrees by up to 18.6% when the reduction in compressor power exceeded the additional power of high pressure pump generating water mist. The chiller COP could be improved more when RH was lower, as shown in Figure 5.13, because evaporation was dependent on the RH of ambient air. With lower RH, evaporation process occurred more intensively, and a greater temperature drop could be achieved. Therefore, the improvement of chiller COP could be more significant for chillers operating in hot and arid regions.

However, the chiller COP could decrease by 3.8% when the staged condenser fans with water mist were more than that without water mist pre-cooling due to the traditional HPC. This indicated that water mist pre-cooling had both positive and

negative effects on chillers operating under HPC. The casual drop of the chiller COP was due to HPC and the extra pump power generating water mist. For the air-cooled chillers with constant speed condenser fans, the condenser fans would be cycled on and off with reference to a high and a low condensing temperature settings under HPC. For certain operating conditions, due to the pre-cooling effect, more groups of condenser fans would be staged without water mist to let the condensing temperature drop below the high setting than that operating with water mist. With more condenser fans, the reduction of the condensing temperature could be more significant than that due to the evaporative cooling effect of water mist when the number of staged condenser fans remained unchanged. Under such conditions, the compressor power without mist pre-cooling was less than that with water mist pre-cooling, and hence the chiller COP without water mist could be higher than that with water mist pre-cooling, as shown in Figure 5.13 when ambient temperature varied from 27 to 30°C at part load ratios of 0.9-1.0. To make maximum advantage of the water mist pre-cooling, it is undesirable to operate the air-cooled chiller under HPC, and HPC should be replaced by variable condensing temperature control (CTC), whereby the condensing temperature can approach its lower boundary via staging all condenser fans in most operating conditions. Under CTC, the sum of compressor power and condenser fan power can be minimized by staging condenser fans with optimal number or speed for all operating conditions. Variable speed control for condenser fans is another complement to water mist pre-cooling, which is superior to cycling constant speed condenser fans in steps, with regard to the controllability of condensing temperature. When the variable condensing temperature control and variable speed condenser fans are applied to air cooled screw chillers, the COP could increase by 4.0-127.5% (Yu and Chan 2006b). When the water mist system is

coupled to the air-cooled chillers with variable speed condenser fans and CTC, the chiller COP will be improved further.

Zhang et al. (2000) investigated the evaporative precooler filled with corrugated holed aluminum foil and reported that COP of the chiller could be improved by 14.7% under the climatic conditions of Tianjin. Hajidavalloo (Hajidavalloo and Eghtedari 2010) studied the effect of incorporating evaporative cooler in the window-air-conditioner by injecting water on the media pad installed in both sides of the air conditioner in very hot regions of about 50°C, and reported that the power consumption decreased by about 16% and the COP increased by about 55%. According to a reported simulation study (Yu and Chan 2009), the use of water mist pre-cooling enabled an increase of chiller COP in various degrees up to 7.7%, but it could drop from the baseline by up to 1.3% for an air-cooled screw chiller operating under HPC in subtropical regions. Compared with these studies on evaporative cooling, both the evaporative cooler device and the water mist system could improve the COP of air-cooled chillers, but the improvement of the chiller efficiency depended on the ambient air conditions, size of the evporative pre-cooler, design of the water mist system, layout of the mist nozzles, chiller load ratios and control strategies of the chillers.

The strategy to operate the water mist system is vital. It was suggested to operate the water mist system only when DBT was greater than 28°C and RH was less than 75%. Under this criteria, the chiller efficiency could be improved, but many operating hours were screened out. As shown in Figure 5.13, the water mist system worked effectively even when the chiller operated beyond the above criteria so as to maximize its energy saving potential. At RH of 80-90% and part load ratios of 0.9-1.0, the chiller COP could be improved by 6.6% and 9.8% when the chiller operated

at ambient temperatures of 24°C and 32°C, respectively. The criteria for operating air-cooled chillers with water mist system for optimal efficiency have to be investigated further with more experiments conducted at various combinations of PLR, weather parameters, water mist generation rates and droplet sizes.

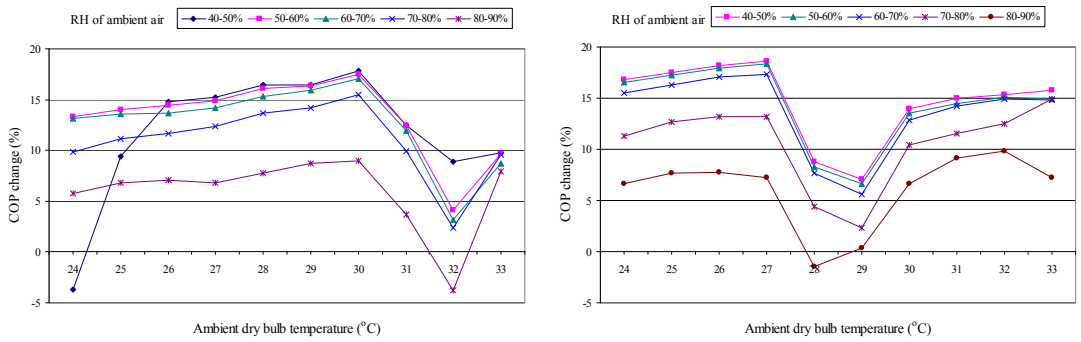

(a) at part load ratios of 0.4–0.5 (b) at part load ratios of 0.9–1.0

Figure 5.13 Chiller COP percentage change at various conditions due to water mist pre-cooling

5.3.2.5 Water consumption

The designed flow rate of each nozzle was 1.25×10^{-3} l/s when the high pressure pumps operated to deliver water through the tubing at a high pressure of 70 bars. The water mist system was designed to provide a total water mist generation rate of 0.073 l/s for the studied air-cooled screw chiller. For water-cooled chillers, the total water losses from cooling tower are the sum of drift losses, evaporation losses and blow down losses. According to Standard 550/590 (ARI 2003), the total water losses can be calculated based on an assumption that the water losses accounts for 1.5% of the cooling water flow rate, which is designed at 0.054 l/s per kW cooling capacity. For the water-cooled chiller with same cooling capacity as the studied air-cooled chiller, whose capacity is 708 kW, the designed cooling water flow rate is 38.2 l/s and the expected water loss is 0.57 l/s. Comparatively, the water consumption rate of the

water mist system is much smaller, and is about 9.5% of the water losses for an open-loop cooling tower serving a water-cooled chiller with same cooling capacity.

The advantages of applying water mist pre-cooling have been investigated for air-cooled chillers operating in a subtropical climate. As WBD is associated with the maximum possible lowering of air temperature, it is expected that energy savings from this technology are more significant when WBD of ambient air is higher during the cooling season. As the water mist system consumes less than 10% of the water losses required by an open-loop cooling tower system, this technology of water mist pre-cooling is beneficial for wide application, especially for cities challenged by shortage of water. It occupies an intermediate position between air-cooled chillers and water-cooled chillers, and is particularly applicable in a hot and arid environment where water is scarce and the WBD is significant.

In the condenser air stream, the water mist generated may not fully evaporate before entering the condenser coil, and the unevaporized or excessive mist may cause damping of the condenser fins and coil. On the other hand, any presence of water mist in the air stream passing through the condenser coil may provide further evaporation and reject more heat from the refrigerant. This is an unknown process which deserves further research.

5.4 Integrated chiller model with water mist

5.4.1 Water mist system model

To improve the chiller performance, a water mist system is coupled to the air-cooled condensers. When water mist is sprayed into the air stream entering the condenser, the air temperature will drop due to the evaporative cooling effect, and the RH and the humidity ratio of the air will increase, approaching saturation. At a given DBT and RH of the ambient air, the addition of moisture in the air sream due to water mist

spray is determined by Eq. (5.7). The humidity ratio of the ambient air is expressed as Eq. (5.8), then the humidity ratio of air at the inlet of condenser is computed by Eq. (5.9).

$$\delta W = m_{mist}/(V_a \rho_a) \tag{5.7}$$

$$W = 0.622 P_{ws}/(P - P_{ws}) \tag{5.8}$$

$$W' = W + \delta W \tag{5.9}$$

where W in kg/(kg dry air) is the air humidity ratio, δW is the additon of humidity ratio of the air in kg/(kg dry air), P is the total barometric pressure of the moist air in Pa, and P_{ws} is the saturation pressure of water vapor in Pa.

The saturation pressure of water vapor in relation to the temperature is given by (ASHRAE 2009)

$$\ln P_{ws} = C_1/T + C_2 + C_3 T + C_4 T^2 + C_5 T^3 + C_6 \ln T \tag{5.10}$$

where T is absolute temperature, K, and C_1, C_2, C_3, C_4, C_5, and C_6 are coefficients.

$C_1 = -5.800 \times 10^3$

$C_2 = 1.391$

$C_3 = -4.864 \times 10^{-2}$

$C_4 = 4.176 \times 10^{-5}$

$C_5 = -1.445 \times 10^{-8}$

$C_6 = 6.546$

The specific enthalpy of the moist air in kJ/(kg dry air) is

$$h = 1.006t + W(2501 + 1.86t) \tag{5.11}$$

where t is the DBT of outdoor air in °C.

As the evaporation of water mist into the air is adiabatic, the specific enthalpy of the moist air is constant, and the temperature of entering condenser air (T_{cdae}) is calculated as follow:

$$T_{cdae} = (h - 2501\ W')/(1.006+1.86\ W') \tag{5.12}$$

The relative humidity φ is a function of degree of saturation (μ) as follow:

$$\varphi = \mu / \left(1-(1-\mu)(P_w / P)\right) \tag{5.13}$$

where P_w is the partial pressure of water vapor in the moist air at the given temperature T_{cdae}.

Degree of saturation μ is the ratio of the humidity ratio W of moist air to the humidity ratio W_s of saturated moist air at same temperature and pressure:

$$\mu = W / W_s\big|_{t,p} \tag{5.14}$$

Before calculating the relative humidity φ of the air at the inlet of the condenser coil, the air humidity ratio W and the humidity ratio W_s of saturated air have to be calculated. The air humidity ratio W at the temperature of the air entering the condenser (T_{cdae}) is determined by Eq. (5.15) (ASHRAE 2009). The humidity ratio W_s of saturated air at the temperature of T_{cdae} is computed using Eqs. (5.8) and (5.10) based on the temperature T_{cdae}.

$$W = \frac{(2501-2.326T_{wb})T_{wb} - 1.006(T_{cdae} - T_{wb})}{2501+1.86T_{cdae} - 4.186T_{wb}} \tag{5.15}$$

When the calculated humidity ratio W is greater than the maximum allowable humidity ratio at the saturation state or the calculated relative humidity φ is greater than 1 or equal to 1, the air at the inlet of condenser becomes saturated and T_{cdae} is equal to WBT (T_{wb}). Under such conditions, the generation rate of the water mist

system is more than that needed, and the surplus water mist droplets will fall down to the ground or be carried to the condenser coil.

Figure 5.14 shows the procedure for computing the thermal properties of entering condenser air for the air-cooled chiller with water mist pre-cooling.

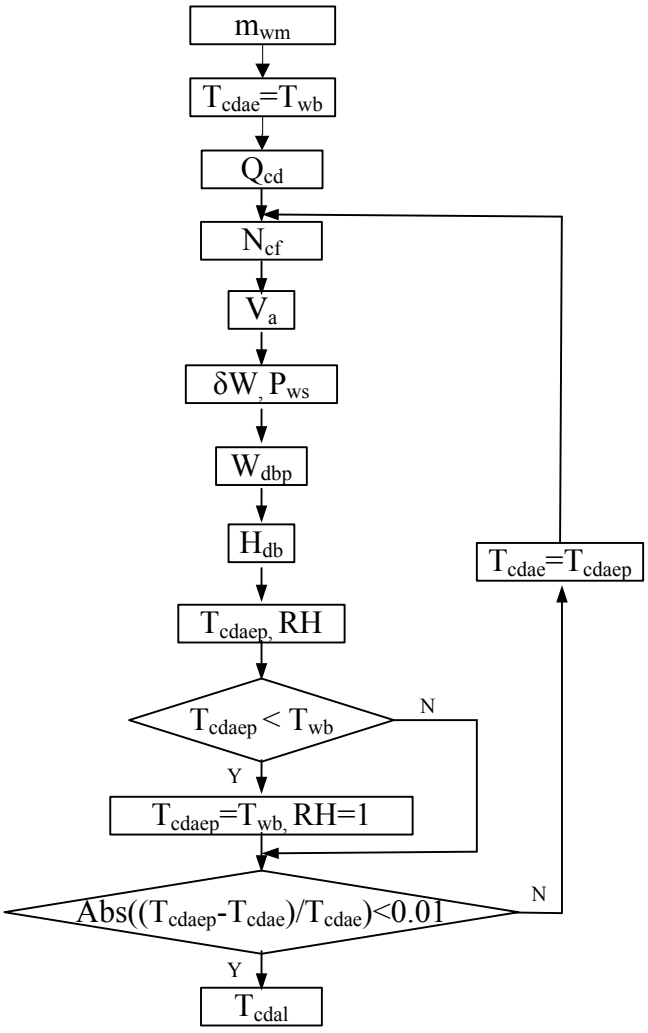

Figure 5.14 Flow chart of the water mist model

5.4.2 Integrated chiller model

Referring to Eq. (5.7), the increase of the air humidity ratio and the resulting air temperature T_{cdae} at the condenser inlet are related to the airflow rate passing through the condenser coil. To evaluate the chiller performance, the water mist model shown in Figure 5.14 was incorporated into the chiller model developed in Chapter 4 and

solved through an iterative procedure, as illustrated in Figure 5.15 for the chiller model with water mist and constant speed condenser fans under HPC. The integrated chiller model was programmed in Fortran 90, and the simulated system was constructed based on the transient simulation program TRNSYS. The programme started with the model initialization using the input data. For the air-cooled chiller with twin refrigeration circuits, the cooling load of the chiller could be shared within the refrigeration circuits randomly. The scheme for load sharing between the refrigeration circuits was specified first, and then one refrigeration circuit or both refrigeration circuits would be staged according to the total cooling load. Then, the evaporating temperature and pressure of circuits 1 and 2 (T_{ev1}, T_{ev2}, P_{ev1} and P_{ev2}) and the cooling loads of the three heat exchange sections of the evaporator (Q_{11}, Q_{12} and Q_2) were calculated through an iterative procedure by assuming an initial value of Q_{11}. Once the model had determined the evaporating temperature and pressure of circuits 1 and 2, it evaluated the other operating variables of each refrigeration circuit. As the condensing temperature interacted between the compressor and condenser components, an iterative procedure was implemented to solve the operating variables of the two components simultaneously. To control the condensing temperature, there was another iterative loop for computing the number of staged condensing fans. The number of staged condenser fans and the corresponding airflow were determined according to the set point of condensing temperature.

The iterative procedures to estimate the heat rejection, the operating variables and the cooling load in both refrigerant circuits of the chiller were similar. The convergence criterion for computing condensing temperature and evaporating temperature in this model was 0.01°C. When a converged solution was obtained, all the variables of the model would be computed with the required accuracy.

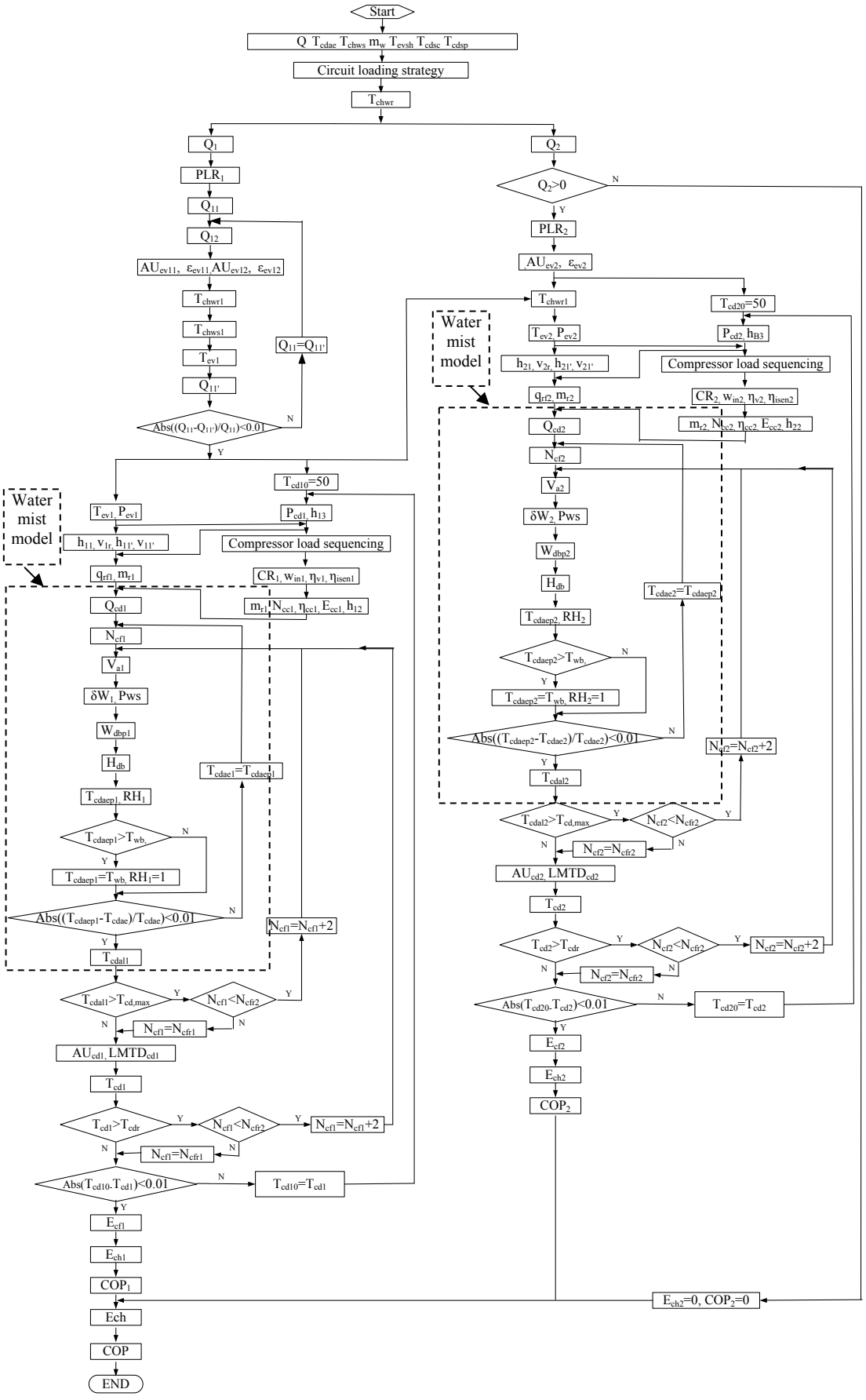

Figure 5.15 Flow chart of the chiller model with water mist and CSF under HPC

5.4.3 Validation of the integrated chiller model

An essential step prior to drawing conclusions from a model was to verify the model. To verify the effectiveness of the developed modeling technique, the performance of the model was evaluated by comparing the modeled results with the operating data of the chiller system. The measured data collected for validating the chiller model came from the chiller operating data under HPC. According to the scheme of load sharing between the two refrigeration circuits, the chiller model was simulated and the simulation results were compared with the corresponding experimental data. Figure 5.16 illustrates the comparison between the modeled and measured chiller COP. There were two lines in the figure giving the boundary of ±10% deviation from the ideal case. For over 86% of the data, the uncertainty (the difference between the modeled value and the experimental value) of chiller COP was less than 10%. With regard to the uncertainty of DBT of the entering condenser air, the uncertainty for more than 85% of the data was less than 5% as shown in Figure 5.17 (a), and the uncertainty for all the data was less than 10%. For the RH of the entering condenser air, more than 93% of the data lied within an error band of ±10% as shown in Figure 5.17 (b). The simulation results, therefore, were considered to be satisfactory.

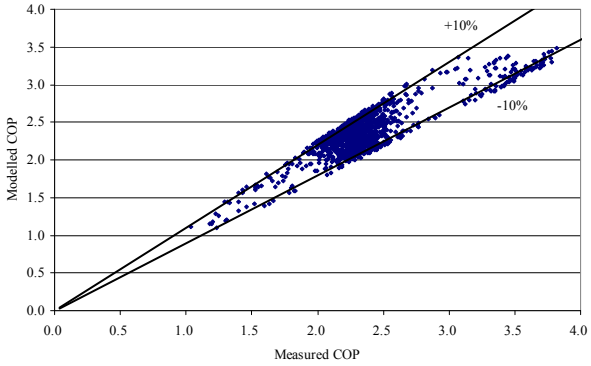

Figure 5.16 Comparison between the modeled and measured chiller COP

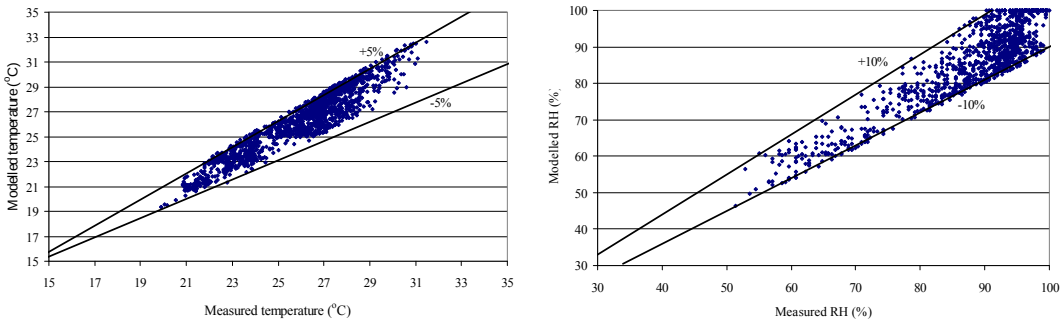

(a) DBT (b) RH

Figure 5.17 Comparison between the modeled and measured DBT and RH of entering condenser air

Drawing on the integrated chiller model, the validated chiller model was used to investigate how the individual and mixed condenser features of CTC and water mist pre-cooling influenced the chiller performance with respect to prevailing range of operating conditions. Each operating condition referred to a combination of chiller part load ratios (from 0.125 to 1 at 0.0625 intervals), dry bulb temperatures (T_{db} from 15 to 35°C at 5°C intervals) and relative humidity levels (RH from 40% to 90% at 10% intervals).

However, the experimentally investigated chiller with water mist was not a standard chiller, which included one compressor in refrigeration circuit 1 and two compressors in refrigeration circuit 2. For generality, the studied chiller should be more representative. The studied chiller shown in Figure 4.6 was more representative, as it comprised of two identical refrigeration circuits and each refrigeration circuit contain two identical compressors. In fact, water mist system was installed for the studied chiller reported in Chapter 4. However, the operating data for the water mist system of such chillers failed to be monitored due to the BMS system error. Fortunately, the operating data of the chillers before water mist installation was recorded and could be used to analyze the chiller performance without water mist pre-cooling, as described in Chapter 4.

As the water mist model developed had been validated satisfactorily, the water mist model could be incorporated to the chiller models developed in Chapter 4, and then the integrated model for the generic chiller with water mist was used to investigate the advanced control of condensing temperature (e.g. CTC) and alternative condenser designs using variable speed fans and water mist pre-cooling. To highlight the effect of water mist, the conventional refrigeration circuit sequence control was implemented in this paper, under which only circuit 1 was staged when the chiller load was less than half of the rated chiller capacity, and two circuits operated evenly when the chiller load was great than half of the rated chiller capacity.

5.5 Performance of the chiller with HPC and mist pre-cooling

Three operating schemes (CS1 to CS3) were considered. CS1 referred to the conventional HPC without water mist pre-cooling, which served as the baseline. Schemes CS2 and CS3 referred to different strategies for the air-cooled chiller: CS2 was HPC with designed water mist generation rate; CS3 was HPC with optimal water mist generation rate. A straightforward strategy to operate the water mist system was applied by interlocking the operation of the high pressure water pumps and the chillers for schemes CS2 and CS3. The pre-cooling effect produced by the water mist system is best when the DBT of ambient air approaches to WBT due to evaporation of water. Therefore, the optimal generation rate of water mist should vary in response to the working conditions to bring the DBT down to the WBT and no surplus water mist is generated.

Under the optimal water mist control, all the potential penalties associated with incomplete evaporation of mist were eliminated. To evaluate the optimal mist generation rate under HPC or CTC, the model first examined whether the RH of the entering condenser air pre-cooled by the designed water mist rate was greater than

one. If this was the case, the water mist generation rate reduced step by step to avoid surplus water mist. If the RH of the entering condenser air after mist pre-cooling was less than one, the water mist generation rate increased step by step to allow the pre-cooled dry bulb temperature to approach to the wet bulb temperature. Figure 5.18 illustrates the procedure for evaluating the optimal mist generation rate under HPC or CTC.

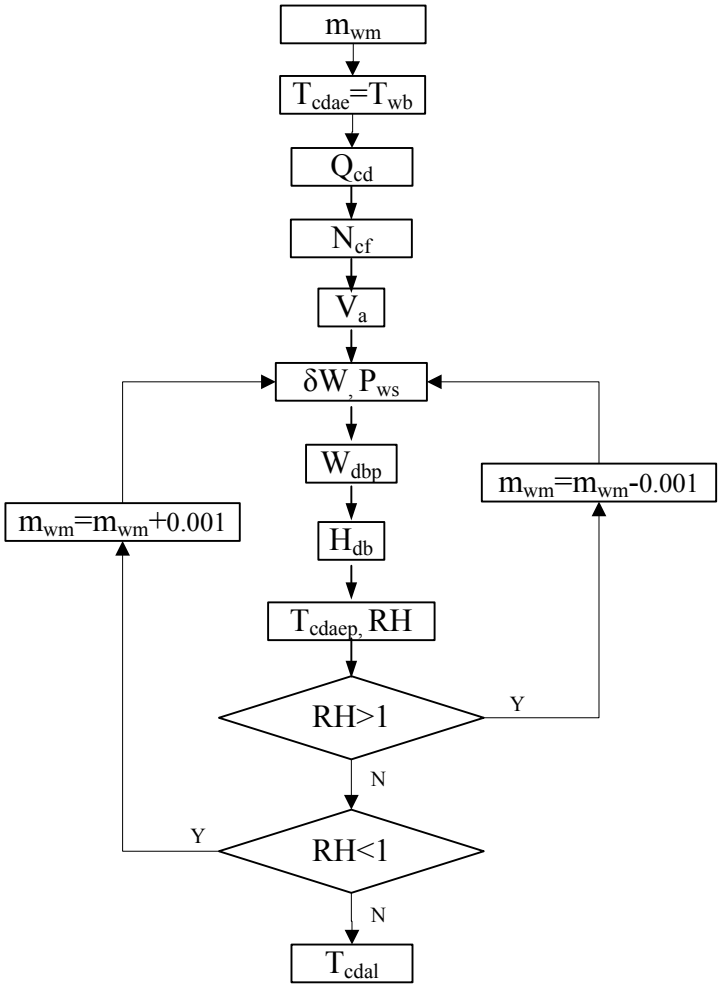

Figure 5.18 Procedure for evaluating optimal water mist generation rate

Figure 5.19 illustrates the part load performance curves for the chiller without water mist pre-cooling for the operating scheme CS1. The curves show how the chiller COP varies with different PLRs at outdoor temperature ranging from 15 to 35°C. Under HPC with constant speed condenser fans, the chiller COP fluctuated considerably because the heat rejection airflow varied by staging groups of

condenser fans step by step. Following the sequencing of the two refrigerant circuits and the compressors in each refrigeration circuit, the chiller COP dropped considerably when one more compressor or refrigeration circuit was staged due to the poor compressor efficiency at low part load ratios. It also revealed that the outdoor temperature greatly affected the chiller performance, and the chiller COP tended to be higher with lower outdoor temperature, which reinforced the need of water mist pre-cooling.

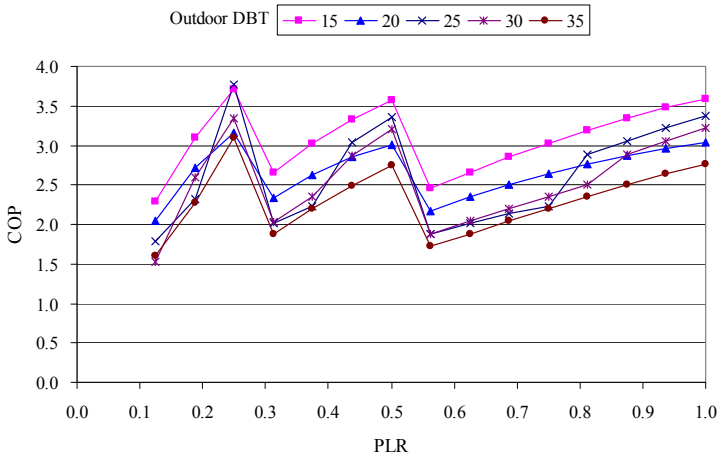

Figure 5.19 Chiller performance curves for scheme CS1

5.5.1 Thermal properties of air entering the condenser

Figure 5.20 shows the temperature change of the entering condenser air due to water mist evaporative cooling. As the two refrigeration circuits were identical, the thermal properties of air entering the condenser of refrigeration circuit 1 were analyzed. The temperature of the entering condenser air under scheme CS2 could drop by up to 6.5°C when only two condenser fans were staged with the designed water mist generation rate.

It was observed that the wet bulb depression (WBD) of ambient air had great influence on the cooling effect of the water mist system, and the temperature of the entering condenser air could drop more with greater WBD. In particular, when the

condenser airflow rate was low and WBD was less than 6.5°C, the temperature drop of the entering condenser air was linear with the WBD for scheme CS2. It should be noted that the temperature change of air entering the condenser was not only dependent on the WBD, but also on the condenser airflow rate, DBT and the water mist generation rate. As shown in Figure 5.20, the temperature drop of the entering condenser air tended to be smaller when more condenser fans were staged. Under such conditions, the airflow rate was larger, but the designed water mist generation rate was insufficient to bring the DBT of the entering condenser air to approach the WBT, hence the temperature drop was smaller.

With optimal water mist generation rate for scheme CS3, the DBT of the entering condenser air approached to the WBT under all working conditions, taking maximum advantage of the WBD. For scheme CS3, the temperature drop of the entering condenser air could be up to 8.8°C when outdoor RH was 50%.

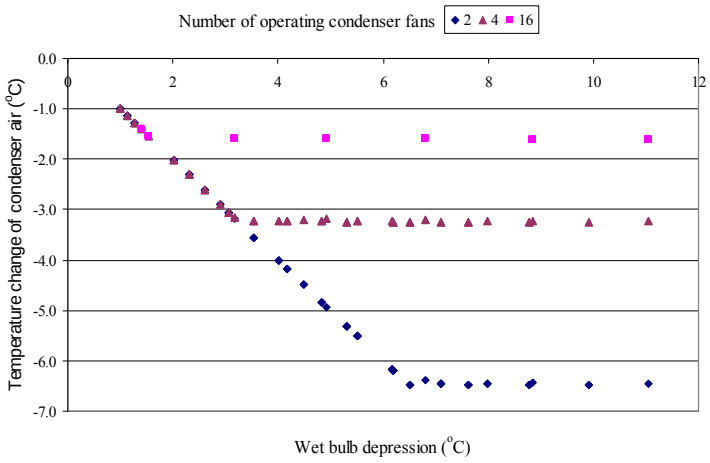

Figure 5.20 Temperature change of air entering the condenser for scheme CS2

5.5.2 Condensing temperature

For any given cooling capacity, the condensing temperature depends on the chiller load, heat rejection airflow and ambient air temperature. Owing to the evaporative

cooling effect of the water mist, the temperature of entering condenser air drops, and the condensing temperature of the chiller changes accordingly.

Figures 5.21 and 5.22 demonstrate the change of the condensing temperature under schemes CS2 and CS3 compared with that under scheme CS1, respectively. The positive numbers represent a condensing temperature increase while the negative numbers represent a condensing temperature drop. The condensing temperature could drop by up to 7.8°C when RH was 50% under scheme CS2. With optimal water mist generation rate, the condensing temperature could drop further, by up to 9.5°C when RH was 50% under scheme CS3. However, Figures 5.21 and 5.22 also indicated that the condensing temperature would casually increase for certain conditions up to 9.7°C. The increase of the condensing temperature was caused by the HPC with constant speed condenser fans. For the air-cooled chiller operating under HPC with constant speed fans, the condenser fans was staged group by group to meet the required heat rejection airflow, and the heat rejection airflow varied step by step, which resulted in fluctuation of the condensing temperature. The condenser fans would be cycled on and off with reference to a high and a low condensing temperature settings under HPC.

When the condensing temperature exceeded the high condensing temperature setting, one more group of condenser fans would be switched on to increase heat rejection airflow, which enabled the condensing temperature to fall below the high setting. Because water mist pre-cooling reduced the temperature of the entering condenser air, the condensing temperature would fall below the high setting even if the number of staged condenser fans remained unchanged.

For certain conditions, when the condensing temperature exceeded the high setting, both staging on more condenser fans and operating water mist caused the condensing

temperature to drop below the high setting, but the extent to which the condensing temperature could drop depended on the working conditions. In the case without water mist, when one more group of condenser fans was cycled on, the heat rejection airflow provided by the constant speed fans might exceed the airflow required to maintain the set point of condensing temperature, and the reduction of the condensing temperature was more significant than that due to the evaporative cooling effect of water mist when the number of staged condenser fans remained unchanged. Hence the condensing temperature of the chiller with water mist could sometimes be higher than that of the chiller without water mist under HPC.

From Figures 5.21 and 5.22, it was also observed that the extent of the condensing temperature drop was constrained by the temperature of entering condenser air. With lower relative humidity, the condensing temperature could drop more.

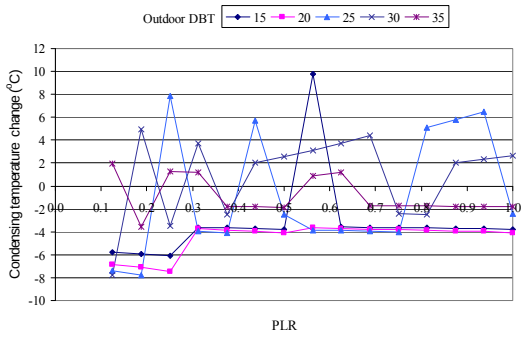

(a) RH=50%

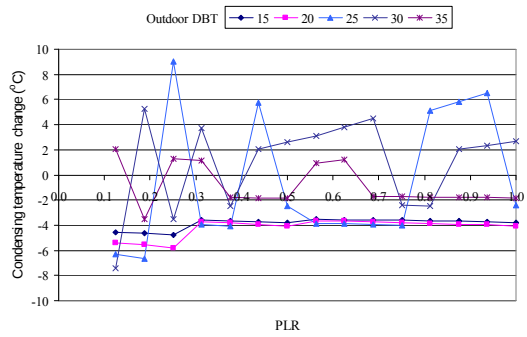

(b) RH=60%

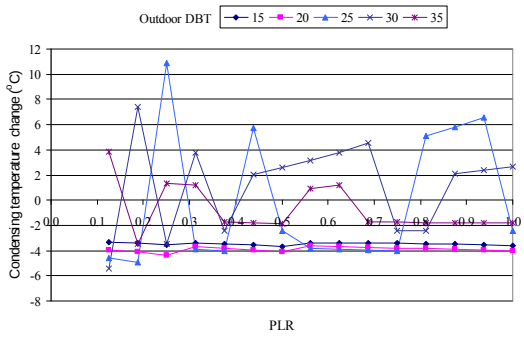

(c) RH=70%

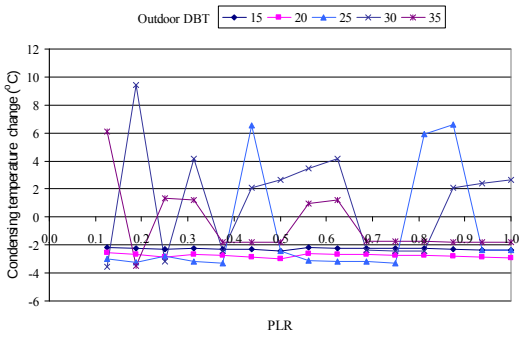

(d) RH= 80%

Figure 5.21 Condensing temperature change for scheme CS2

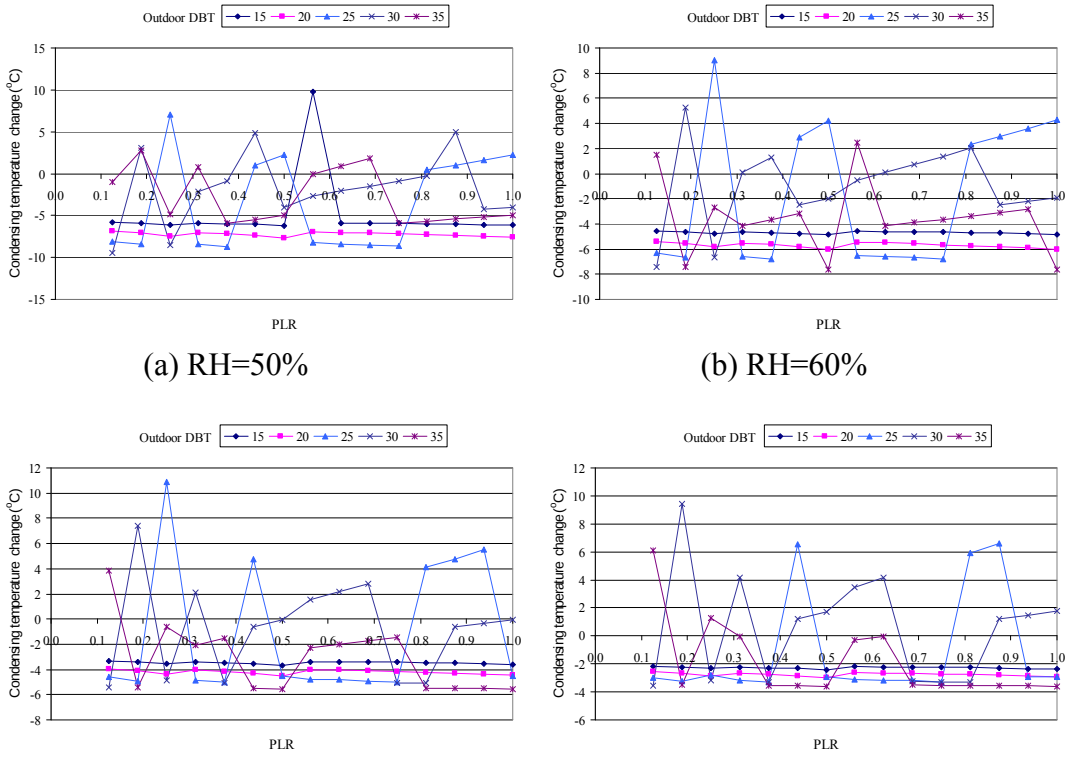

(a) RH=50% (b) RH=60%

(c) RH=70% (d) RH= 80%

Figure 5.22 Condensing temperature change for scheme CS3

5.5.3 Chiller COP

Water mist pre-cooling enabled a reduction of temperature of air entering condensers, and improved the chiller performance differently under various operating schemes. The potential benefits of each condenser feature were identified by a comparison on how the system COP varied under different operating schemes in relation to the baseline. A positive percentage meant a chiller COP increase while a negative percentage meant a chiller COP drop.

Figures 5.23 and 5.24 show the percentage change of COP of schemes CS2 and CS3 from the baseline under head pressure control, respectively. Chiller COP could increase or decrease relative to the baseline depending on the working conditions under HPC. When the chiller operated under HPC with designed water mist generation rate, the chiller COP would increase in varying degrees by up to 21.3% and 9.8% when the RH was 50% and 80%, respectively. With optimal water mist

generation rate, the chiller COP under HPC would increase in varying degrees by up to 25.8% and 10.9% when the RH was 50% and 80%, respectively. In such conditions, the additional power of high pressure pump generating water mist was insignificant comparing to the reduction in compressor power due to the drop of the entering condenser air temperature. These results revealed that there existed great potential to improve the chiller efficiency by coupling water mist system with air-cooled chillers, and the chiller performance could be improved more with optimal mist generation rate.

In contrary to the general trend of improved efficiency in schemes CS2 and CS3, there were casual occurrences of decreased chiller COP due to unfavourable fan staging under HPC and extra pump power consumed for generating water mist. The studied chiller was equipped with 8 pairs of constant speed fans which were staged by pair with reference to a high and a low condensing temperature settings under HPC. For certain operating conditions without water mist, more groups of condenser fans would be staged to drive the condensing temperature below the high setting than that operating with water mist. With more condenser fans, the reduction of the condensing temperature could be more significant than that due to the evaporative cooling effect of water mist but less staged fans. Under such conditions, the compressor power without mist pre-cooling was less than that with water mist pre-cooling, and hence the chiller COP without water mist could be higher than that with water mist pre-cooling. This indicated that HPC was energy inefficient, and it was undesirable to operate the chiller with water mist under HPC.

The impact of the ambient air RH on the improvement of chiller COP was revealed in Figures 5.23 and 5.24, indicating that the water mist system worked more effectively at lower levels of RH. The chiller COP increased more noticeably at

higher outdoor temperature and lower RH, as the water mist evaporated effectively to bring the DBT of the entering condenser air to approach the WBT. This, in turn, lowered the compressor power considerably. This indicates that water mist pre-cooling is especially suitable for dry and hot regions.

From Figures 5.23 and 5.24, it could be found that the chiller COP could be improved for most operating conditions, and the water mist system worked effectively at lower levels of relative humidity. Therefore, operating the water mist system was an efficient way to improve the COP of the air-cooled chiller. However, it was undesirable to operate the chiller with water mist under HPC, as the energy saving potential of mist pre-cooling could not be fully utilized of under HPC. Variable speed condenser fans and CTC are favorable complements to water mist pre-cooling.

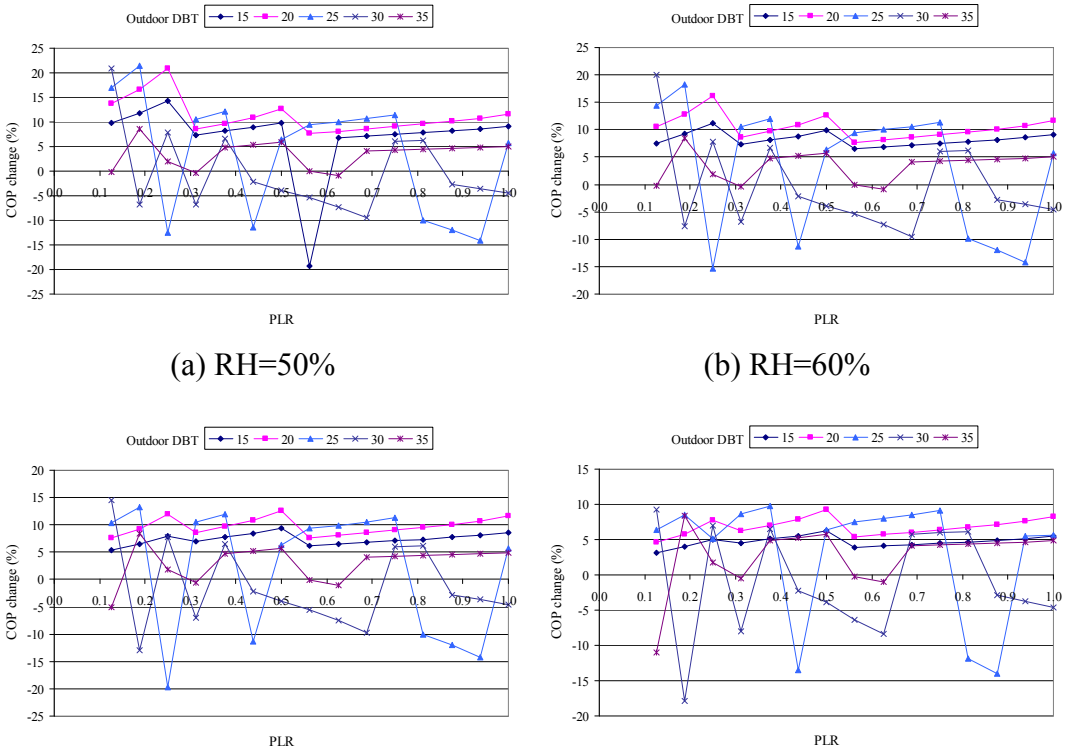

(a) RH=50%

(b) RH=60%

(c) RH=70%

(d) RH= 80%

Figure 5.23 Chiller COP change for scheme CS2

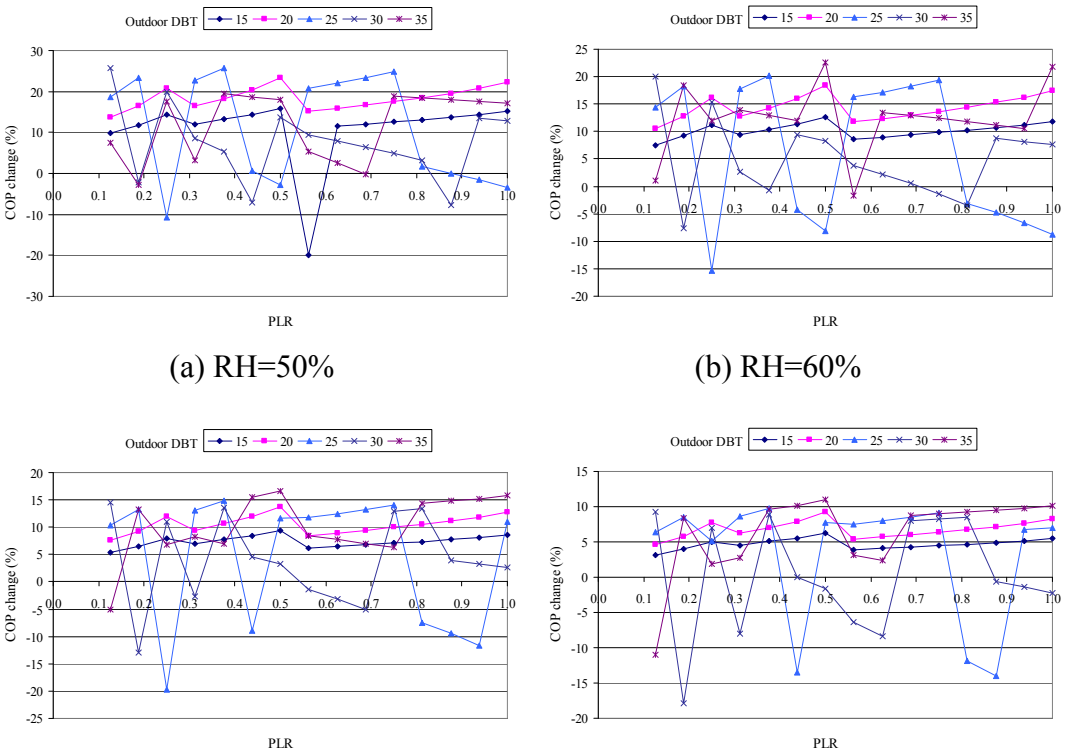

(a) RH=50%

(b) RH=60%

(c) RH=70%

(d) RH= 80%

Figure 5.24 Chiller COP change for scheme CS3

5.6 Effect of mist pre-cooling on the chiller with variable speed condenser fans

Variable speed control for condenser fans (VSF) is superior to cycling constant speed condenser fans in steps, with regard to the controllability of condensing temperature. The power of the condenser fans can drop considerably at lower speed while producing the required heat rejection airflow at part load operation. The use of VSF has a significant influence on the trade-off between compressor power and fan power and hence the chiller COP, and it is worth considering how the use of variable speed condenser fans can improve the COP of air-cooled chillers with water mist operating in various outdoor temperatures and load conditions. To implement variable speed control, the current configuration of condenser fans should be changed (Yu and Chan 2006b). Given that the chiller studied had two refrigeration circuits, a new condenser fan arrangement within the chiller model was proposed, under which eight groups of constant speed condenser fans were replaced by two variable speed fans, and each of

the variable speed fans consumed a rated power of 19.2 kW and provided a rated airflow of 42.76 m^3/s at the full speed of 15.8 rps. It was assumed that the variable speed drive consumed 3% of the total power of the staged condenser fans at all speeds. An algorithm to compute the speed of condenser fans staged to meet any given heat-rejection based on a set point of condensing temperature was considered.

Three operating schemes (VS1 to VS3) were considered for the chiller with variable speed condenser fans. VS1 referred to the conventional HPC without VSF and water mist pre-cooling, which served as the baseline. Schemes VS2 and VS3 referred to different strategies for the air-cooled chiller: VS2 was HPC with VSF and designed water mist generation rate; VS3 was HPC with VSF and optimal water mist generation rate. A straightforward strategy to operate the water mist system was applied by interlocking the operation of the high pressure water pumps and the chillers for schemes VS2 and VS3.

The variation of the COP under various PLRs and ambient DBT was shown in Figure 5.25 when the chiller operated with variable speed fans without water mist pre-cooling. This figure clearly demonstrated that the chiller COP varied with the staging of refrigeration circuits and the compressors in each refrigeration circuit.

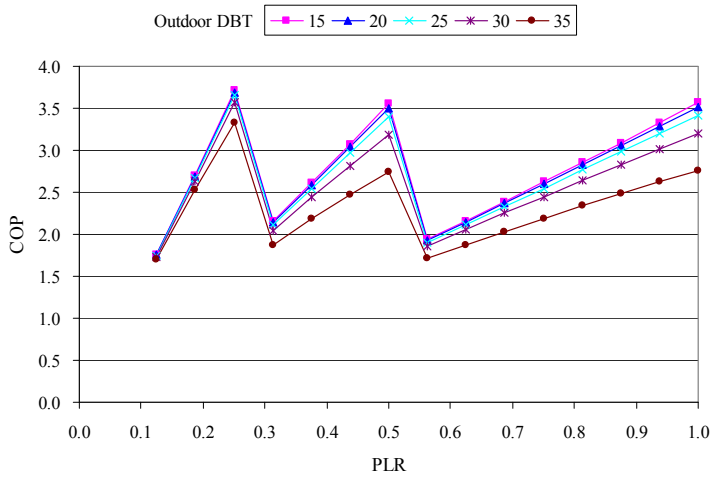

Figure 5.25 Chiller performance curves for scheme VS1

5.6.1 Thermal properties of air entering the condenser

With designed water mist generation rate, Figure 5.26 shows the temperature change of the entering condenser air due to water mist evaporative cooling. The temperature of the entering condenser air under scheme VS2 could drop by up to 8.0°C when the rotating speed of the staged condenser fans was smaller than 2.0 Hz with the designed water mist generation rate.

As shown in Figure 5.26, the wet bulb depression (WBD) of ambient air had great influence on the cooling effect of the water mist system, and the temperature of the entering condenser air could drop more with greater WBD. It should be noted that the temperature change of air entering the condenser was not only dependent on the WBD, but also on the condenser airflow rate, DBT and the water mist generation rate. When the rotating speed of the staged condenser fans (R_{cf}) was smaller than 2.0 Hz, the temperature drop of the entering condenser air was linear with the WBD for scheme VS2. As shown in Figure 5.26, the temperature drop of the entering condenser air tended to be smaller when rotating speed of the staged condenser fans was larger. Under such conditions, the airflow rate was larger, but the designed water mist generation rate was insufficient to bring the DBT of the entering condenser air to approach the WBT, hence the temperature drop was smaller.

With optimal water mist generation rate for scheme VFS3, the DBT of the entering condenser air approached to the WBT under all working conditions, taking maximum advantage of the WBD. For scheme VS3, the temperature drop of the entering condenser air could be up to 8.8°C when outdoor RH was 50%.

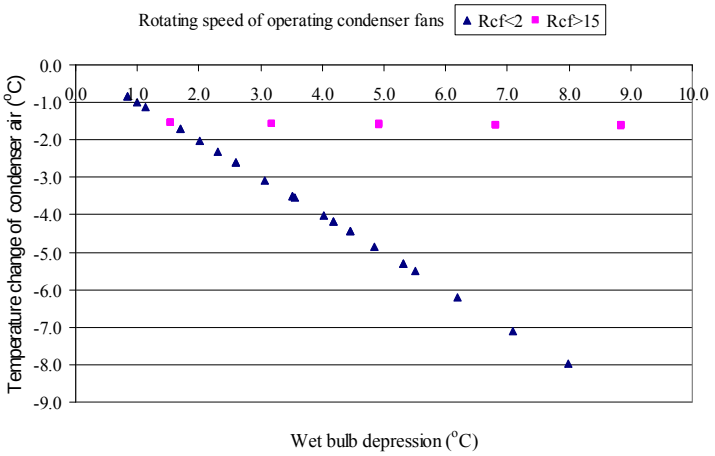

Figure 5.26 Temperature change of air entering the condenser for scheme VS2

5.6.2 Condensing temperature

It was worth investigating how the water mist affected the performance of the chiller with variable speed fans. Figures 5.27 and 5.28 illustrate the change of the condensing temperature under schemes VS2 and VS3 compared with that under scheme VS1, respectively. The condensing temperature dropped in relation to VS1 for all operating conditions, and it could drop more when the outdoor DBT was higher. The condensing temperature drop was less than 0.2°C when the outdoor DBT was less than 35°C for scheme VS2. When the outdoor DBT was 35°C, the condensing temperature could drop by up to 1.9°C, which was much smaller than that of the chiller equipped with constant speed fans. As shown in Figure 5.28 for scheme VS3, the condensing temperature drop was less than 0.5°C when the outdoor DBT was less than 35°C. When the outdoor DBT was 35°C, the condensing temperature could drop by varying degrees up to 5.1°C, which was much smaller than that of the chiller equipped with constant speed fans.

As the variable speed condenser fans allowed the heat rejection airflow to be regulated smoothly, the condensing temperature could be controlled around the set point of condensing temperature closely. When the chiller operated without water mist pre-cooling and the outdoor dry bulb temperature was 35°C, the variable speed

fans operated at their full speed to prevent the condensing temperature to exceed the high setting, but the condensing temperature was slightly above the set point (say, 45°C). As there was a dead band for the condensing temperature, under which the high setting was 52°C and the low setting was 42°C. With evaporative cooling effect, the temperature of entering condenser air decreased, and the condenser fans could operate with lower fan speed to provide the required heat rejection airflow to control the condensing temperature to the set point.

The condensing temperature change was affected by the rotating speed of the condenser fans. Figures 5.29 and 5.30 show the fan speed change due to the water mist pre-cooling, which varied with the same pattern as the condensing temperature. With higher outdoor dry bulb temperature, the rotating speed of the condenser fans reduced noticeable, especially when outdoor DBT was 35°C.

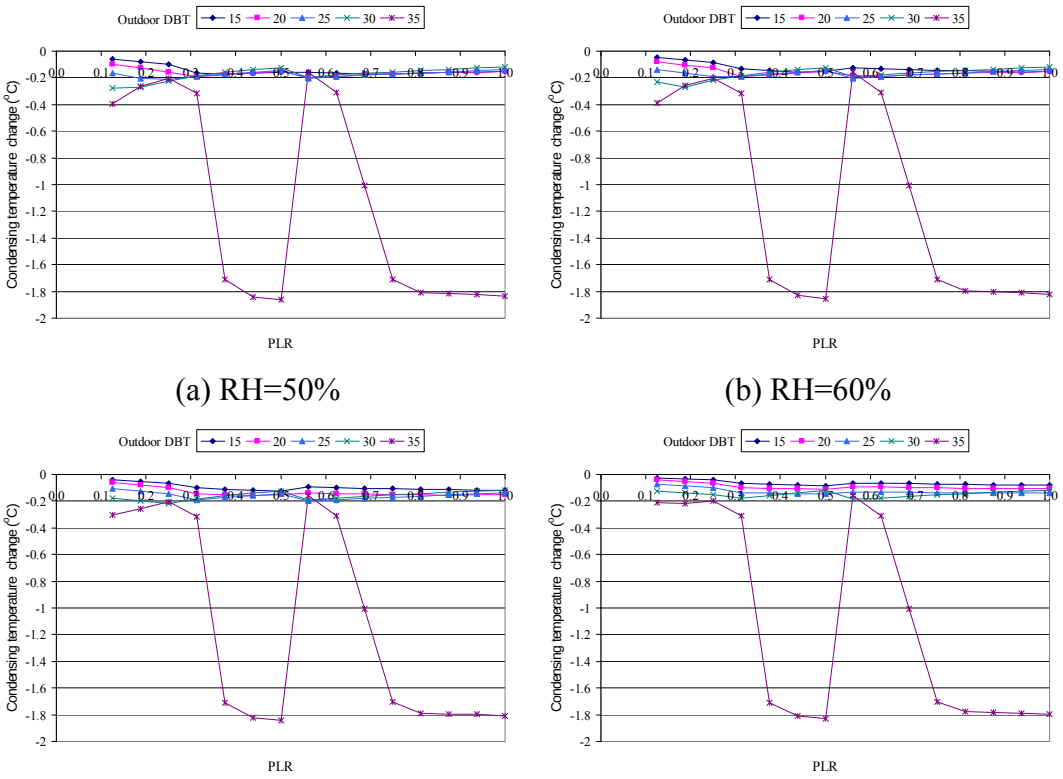

(a) RH=50% (b) RH=60%

(c) RH=70% (d) RH=80%

Figure 5.27 Condensing temperature change for scheme VS2

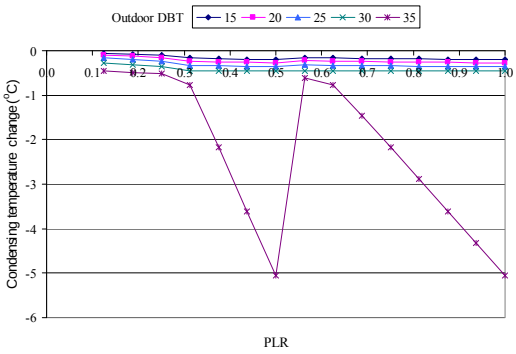

(a) RH=50%

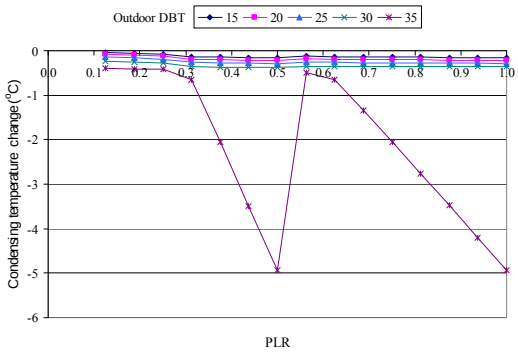

(b) RH=60%

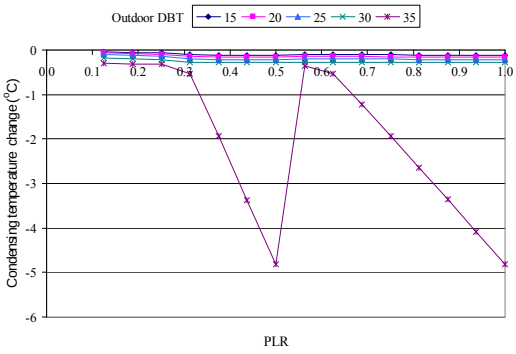

(c) RH=70%

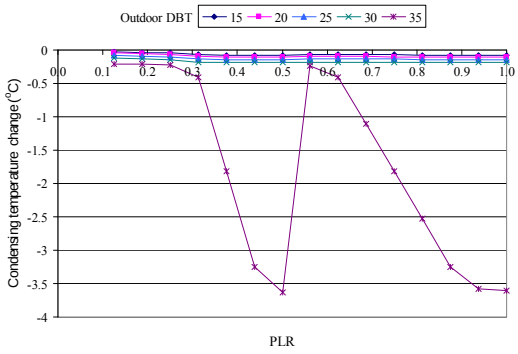

(d) RH=80%

Figure 5.28 Condensing temperature change for scheme VS3

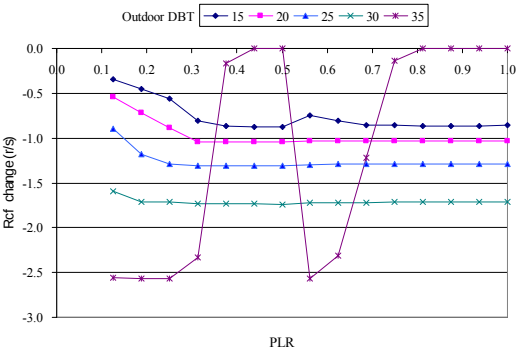

(a) RH=50%

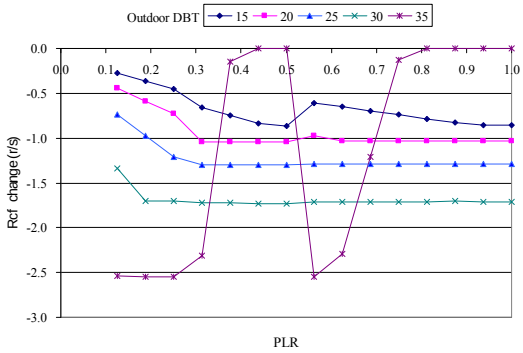

(b) RH=60%

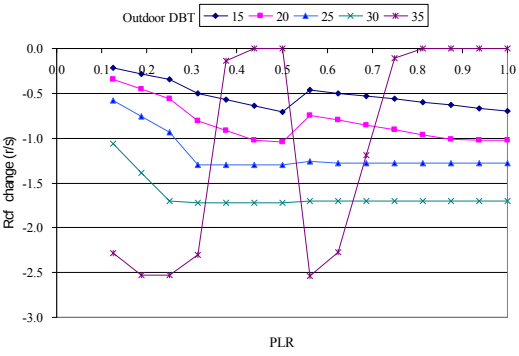

(c) RH=70%

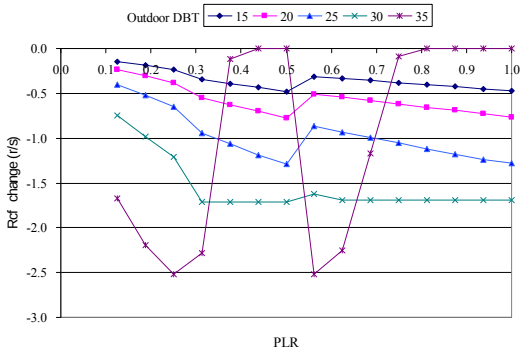

(d) RH=80%

Figure 5.29 Fan speed change for scheme VS2

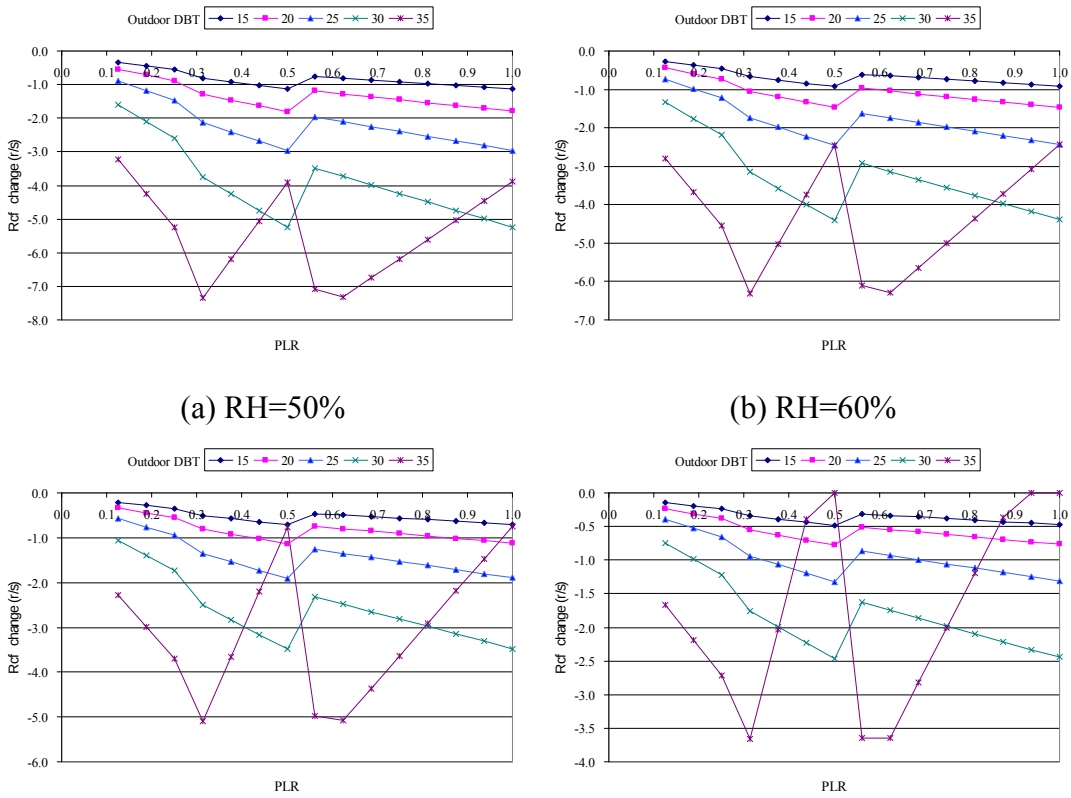

(a) RH=50%

(b) RH=60%

(c) RH=70%

(d) RH=80%

Figure 5.30 Fan speed change for scheme VS3

5.6.3 Chiller COP

With the decreased rotating speed of the condenser fans, the condenser fan power was reduced significantly. For the operating scheme VS2 with designed water mist generation rate, the percentage change of COP from the baseline under HPC was illustrated in Figure 5.31, which increased up to 5.7%. With optimal water mist generation for VS3 as shown in Figure 5.32, the chiller COP increased more up to 23.0% and 10.9% when outdoor RH was 50% and 80%, respectively. However, the chiller COP could slightly decrease in certain working conditions. The casual COP decrease resulted from the additional power for the high pressure pumps generating water mist and the variable speed drive, which consumed 3% of the total power of the staged condenser fans at all speeds.

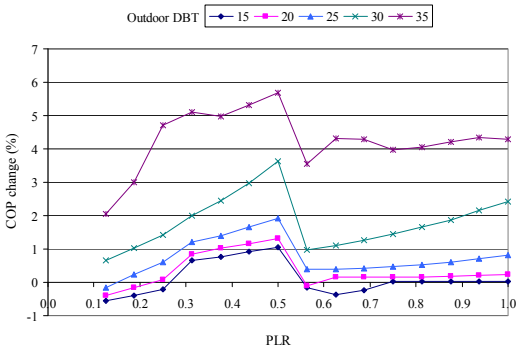

(a) RH=50%

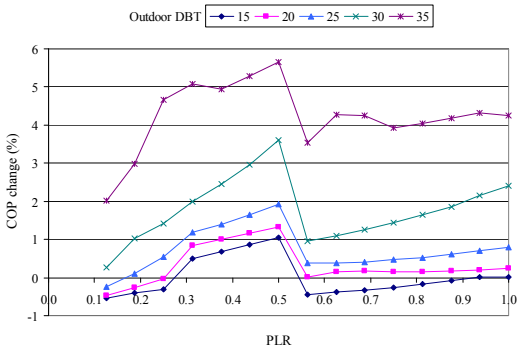

(b) RH=60%

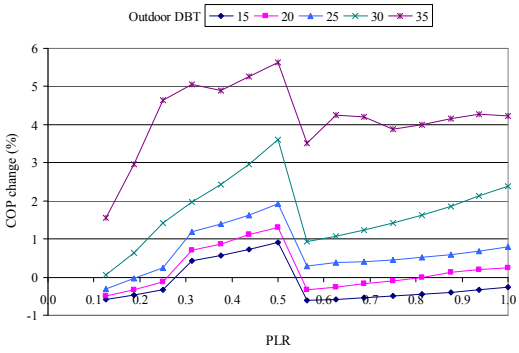

(c) RH=70%

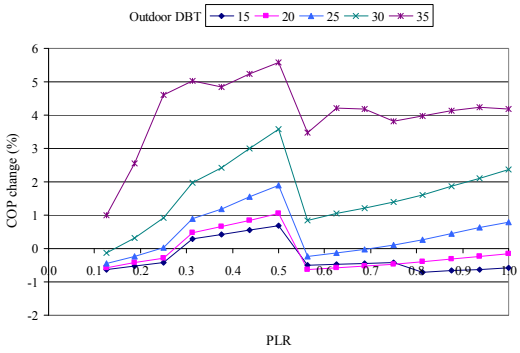

(d) RH=80%

Figure 5.31 COP change for scheme VS2

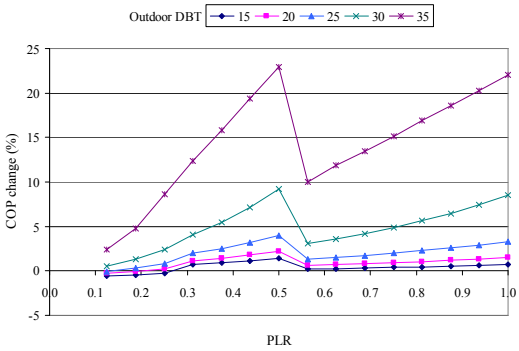

(a) RH=50%

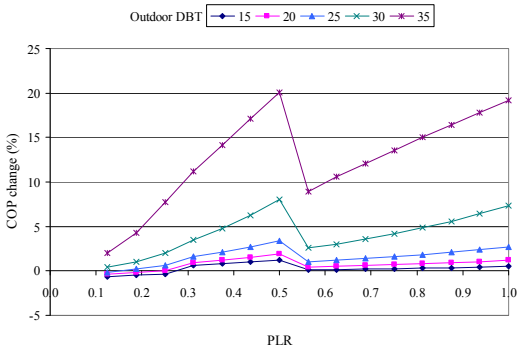

(b) RH=60%

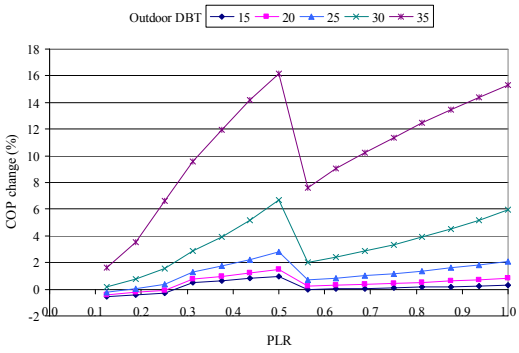

(c) RH=70%

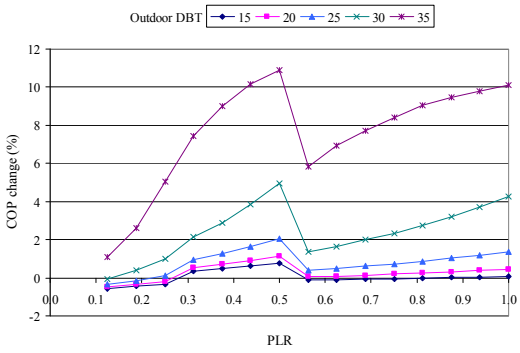

(d) RH=80%

Figure 5.32 COP change for scheme VS3

5.7 Improved chiller COP with CTC and water mist

As HPC is regarded as energy inefficient, variable condensing temperature control (CTC) is proposed as an alternative to HPC to lower the condensing temperature in response to changes of the ambient and load conditions, whereby compressor power can decrease considerably by allowing the condensing temperature to approach its lower boundary.

5.7.1 Optimal set point of condensing temperature

It has been confirmed that the use of HPC with a high set point of condensing temperature leads to a decline in chiller COP especially under partial load conditions. The use of combination of variable speed condenser fans (VSF), water mist and CTC, is a feasible means to improve the chiller COP. It is worth ascertaining the optimal set points of condensing temperature to achieve maximum chiller COP for all operating conditions.

A logical argument was included in the algorithm of controlling condenser fans when the condenser was designed with an water mist system and variable speed fans, which was to determine the optimal set point of condensing temperature ($T_{cdsp,op}$) for maximum chiller COP. For any given chiller part load ratio, it was possible to identify the $T_{cdsp,op}$ by checking the variation in chiller COP throughout the T_{cdsp} range. For each operating condition, this argument checked the difference in chiller COP when T_{cdsp} increased in steps of 0.05°C from its lower level of 20°C or (T_{cdae} + 5) °C, whichever was higher. The lower boundary was intended for ensuring proper oil viscosity for compressor lubrication (Yu, Chan et al. 2006) and the upper boundary was based on HPC. The high T_{cdsp} was 45°C which was normally used under HPC (Yu and Chan 2006b). These steps were small enough to trace the change of COP so as to identify $T_{cdsp,op}$ along with the maximum chiller COP.

Figure 5.33 illustrated how the optimum T_{cdsp} varied under different operating conditions for the air-cooled chiller with constant speed fans and designed water mist generation rate, at different combinations of outdoor dry bulb and wet bulb temperatures. It should be noted that there could be more than one set point of condensing temperature at which the local maximum COP occurred for each operating condition. This was due to the change in the number of staged condenser fans across the range of set point of condensing temperature. In Figure 5.33, just one of the set points of condensing temperature was presented at which the maximum COP was achieved for specific working condition. Figure 5.34 illustrated the variation of the temperature difference between one of the optimal set points of condensing temperature and the outdoor wet bulb temperature. The wet bulb temperature of outdoor air was generally considered as one of the parameters to specify the heat rejection capacity of condensers with evaporative cooling. As shown in Figures 5.33 and 5.34, there was no regular trend for the optimal set point(s) of condensing temperature for the chiller with constant speed fans and water mist, which fluctuated widely with chiller part load ratios and wet-bulb temperature under various operating conditions. For certain operating conditions, the optimal set point of condensing temperature increased closely with the part load ratios, as shown in Figure 5.33 (c) when the outdoor temperature was 30°C.

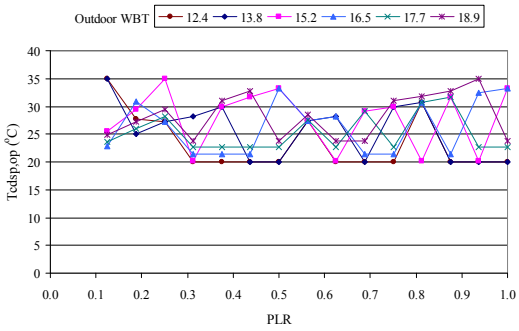

(a) T_{db}=20°C

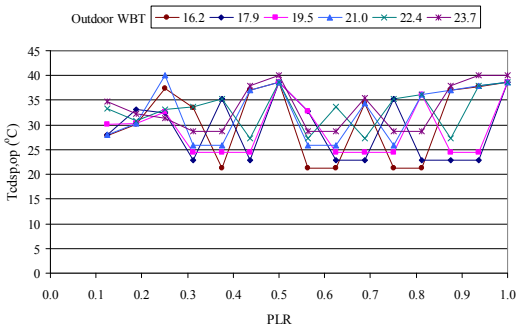

(b) T_{db}=25°C

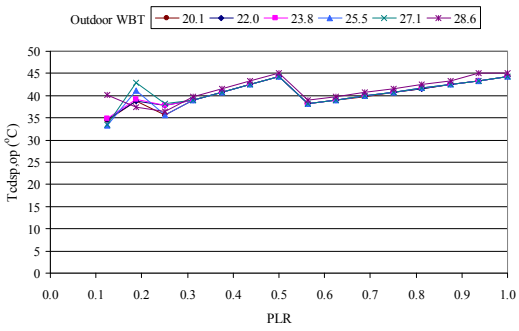

(c) T_{db}=30°C

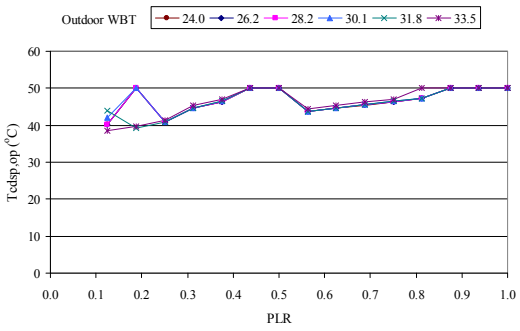

(d) T_{db}=35°C

Figure 5.33 Variations in the $T_{cdsp,op}$ with designed water mist generation rate and CSF

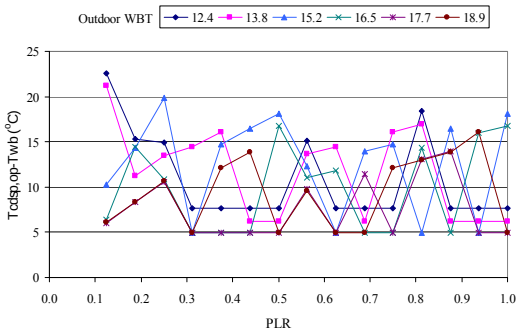

(a) T_{db}=20°C

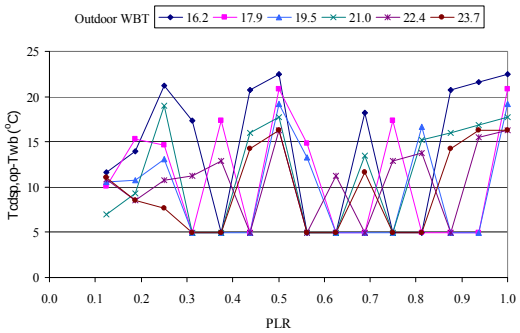

(b) T_{db}=25°C

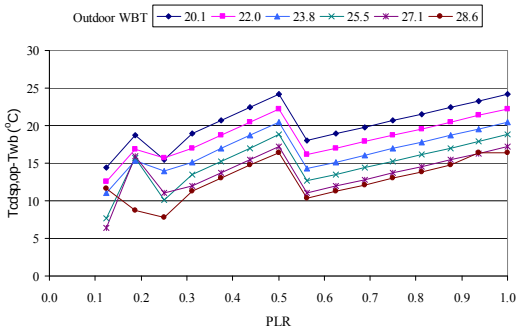

(c) T_{db}=30°C

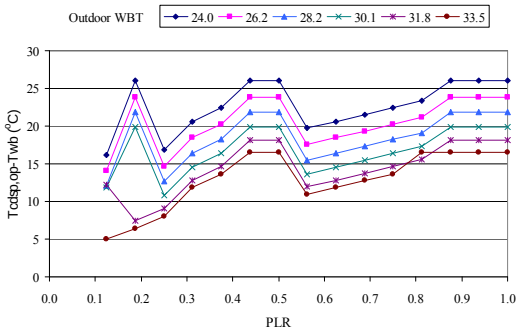

(d) T_{db}= 35°C

Figure 5.34 Variations in the difference between $T_{cdsp,op}$ and the outdoor WBT with designed water mist generation rate and CSF

When the water mist system generated designed or optimal water mist generation rate, as shown in Figures 5.35 and 5.36, respectively, the optimal set point of condensing temperature ($T_{cdsp,op}$) increased closely with the chiller part load ratio if the chiller operated with variable speed condenser fans. It should be noted that $T_{cdsp,op}$ varied with the staging of the refrigeration circuit for specific outdoor condition. The optimal set point of the condensing temperature tended to increase with the wet bulb temperature regardless of designed water mist rate or optimal water mist rate. As shown in Figure 5.35, the optimal set point of condensing temperature with designed water mist rate could be nearly described with one curve for a certain outdoor dry-bulb temperature regardless of the outdoor wet-bulb temperature. However, the optimal set point of condensing temperature with optimal water mist rate should be described with one set of curves for an outdoor dry-bulb temperature with different wet bulb temperature, as shown in Figure 5.36. The reason for that was due to the designed water mist generation rate, which was less than the required mist rate to let the dry bulb temperature to approach to the wet bulb temperature for most of the operating conditions, and there was no great difference on the temperature drop of entering condenser air. With optimal water mist generation rate, the temperature of the entering condenser air approached to the wet bulb temperature, and the temperature reduction would be considerable at a given dry bulb temperature with different wet bulb temperature, which resulted in noticeable change of the optimal set point of condensing temperature.

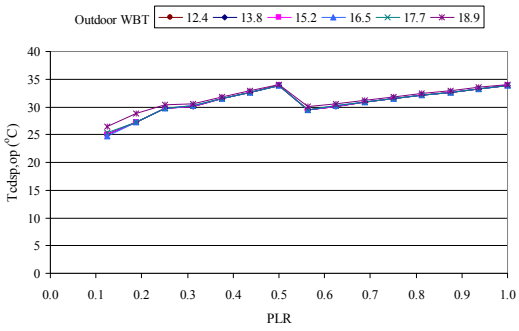

(a) T_{db}= 20°C

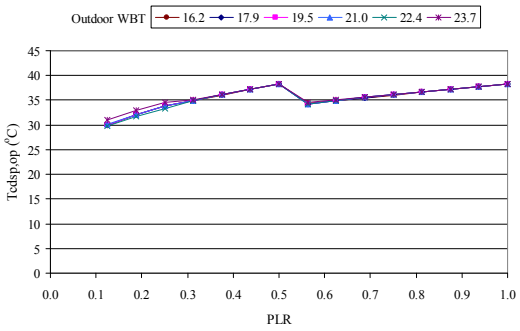

(b) T_{db}=25°C

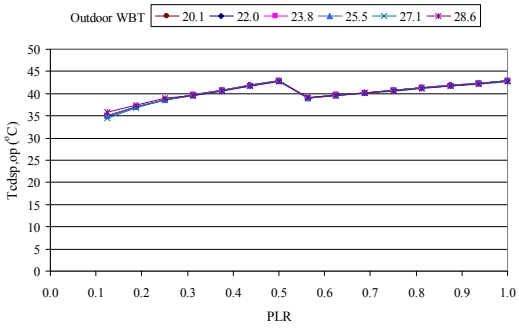

(c) T_{db}=30°C

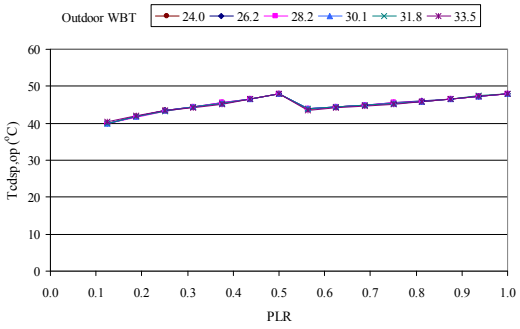

(d) T_{db}=35°C

Figure 5.35 Variations in the optimum set point of condensing temperature ($T_{cdsp,op}$) with designed water mist generation rate and VSF

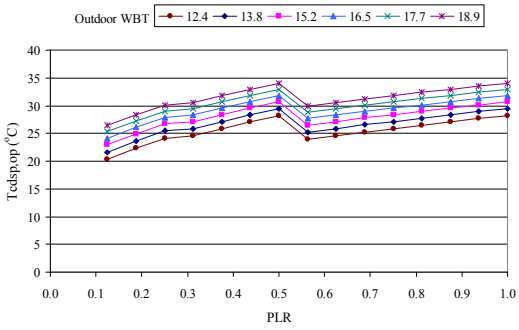

(a) T_{db}=20°C

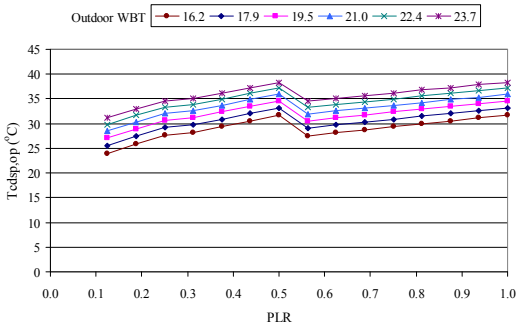

(b) T_{db}=25°C

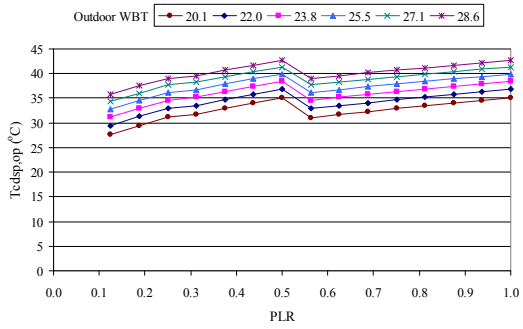

(c) T_{db}=30°C

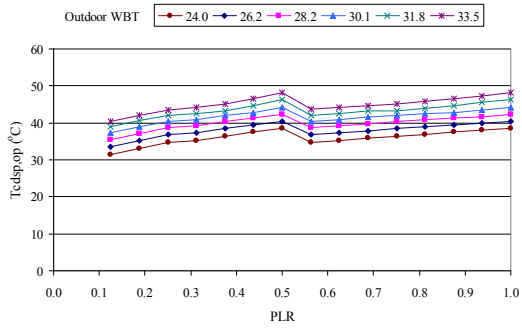

(d) T_{db}=35°C

Figure 5.36 Variations in the $T_{cdsp,op}$ with optimal water mist generation rate and VSF

Figures 5.37 and 5.38 illustrated that the temperature difference between the optimal set point of condensing temperature and the outdoor wet bulb temperature tended to increase linearly with chiller part load ratios and varied following the sequence of the refrigeration circuit, regardless of the chiller operating with designed or optimal water mist generation rate, which indicated that $T_{cdsp,op}$ should be determined based on the outdoor wet bulb temperature and the chiller part load ratio rather than on the outdoor wet-bulb temperature alone. To implement CTC, the reset strategy for set point of condensing temperature supposed by Briley (2003) was that the set point of condensing temperature should be fixed at 5°C, or somewhere between 3 and 8°C, above the wet bulb temperature of outdoor air. This strategy was straightforward, but the optimal set point of condensing temperature might not be obtained. For maximum COP, the optimum set point of condensing temperature should be expressed as a function of outdoor wet bulb temperature and chiller PLR, as described in Eq. (5.16). It should be noted that the optimal set point of condensing temperature varied with the staging of the refrigeration circuit(s).

$$T_{cdsp,op}=f(\mathrm{PLR}, T_{wb}) \tag{5.16}$$

It should be noted that the optimal set points of condensing temperature for various operating conditions were specific to a particular condenser design. When condenser fans were of the high static type requiring larger power, higher optimum set points of condensing temperature might be required to minimize the sum of compressor power and condenser fan power. The optimum set point should be calibrated against the designed difference between the condensing temperature and outdoor wet bulb temperature for an air-cooled condenser with water mist.

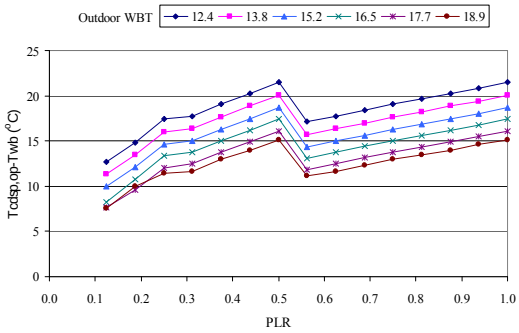

(a) T_{db}=20°C

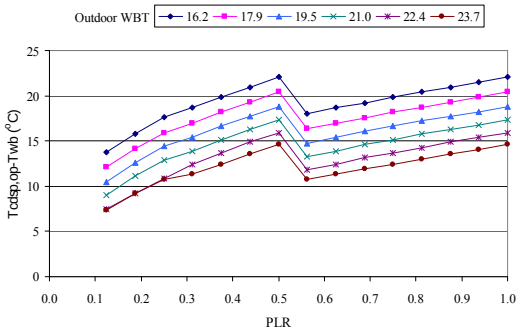

(b) T_{db}=25°C

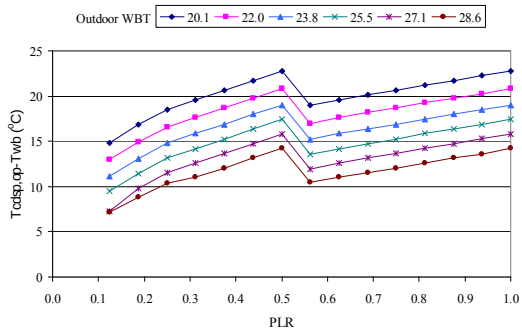

(c) T_{db}=30°C

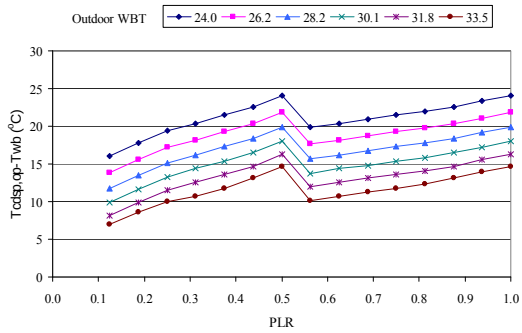

(d) T_{db}=35°C

Figure 5.37 Variations in the difference between $T_{cdsp,op}$ and the outdoor WBT with designed water mist generation rate andVSF

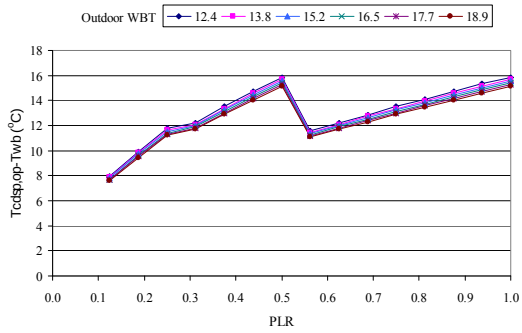

(a) T_{db}= 20°C

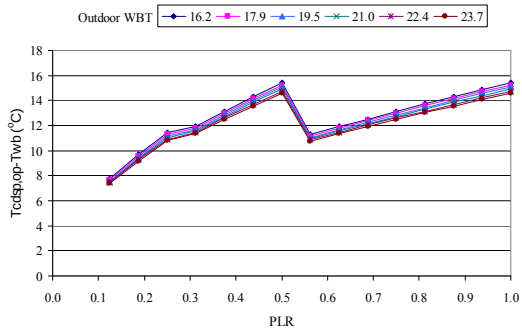

(b) T_{db}=25°C

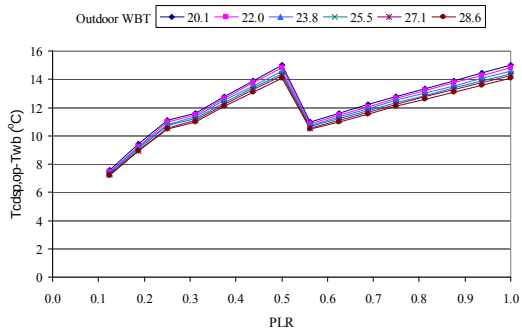

(c) T_{db}=30°C

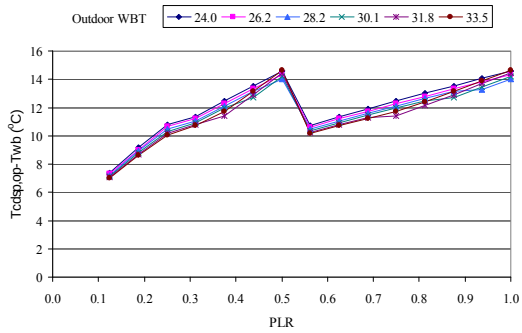

(d) T_{db}=35°C

Figure 5.38 Variations in the difference between $T_{cdsp,op}$ and the outdoor WBT with optimal water mist generation rate and VSF

5.7.2 Improved chiller COP with enhanced condenser features

After identifying the optimum set point of condensing temperature, it appeared worth assessing the potential improvements in chiller COP when the optimum set point, variable speed condenser fans and water mist pre-cooling were applied to the existing air-cooled screw chillers. The validated model was sophisticated enough to assess how the different condenser features (CTC, CSF, VSF, WM and their combinations) would influence the steady-state behaviour of chiller COP at various combinations of chiller loads and outdoor temperatures.

There is a lack of economic analysis to support the implementation of the condenser features of CTC, VSF and WM. This section focuses on evaluating the economic benefits of air-cooled chillers with the individual and mixed condenser features, including 12 cases. The detailed information about the cases was given in Table 5.2.

Table 5.2 Case study of individual and mixed condenser features

Case	*Description*
HPC (base case)	Head pressure control with constant speed condenser fans
HPC+VSF	HPC and the use of variable speed condenser fans
HPC+CSF+WM1	HPC with designed water mist generation rate
HPC+CSF+WM2	HPC with optimal water mist generation rate
HPC+VSF+WM1	HPC and the use of variable speed condenser fans with designed water mist generation rate
HPC+VSF+WM2	HPC and the use of variable speed condenser fans with optimal water mist generation rate
CTC+CSF	Condensing temperature control with constant speed condenser fans
CTC+VSF	CTC and the use of variable speed condenser fans
CTC+CSF+WM1	CTC with designed water mist generation rate
CTC+CSF+WM2	CTC with optimal water mist generation rate
CTC+VSF+WM1	CTC and the use of variable speed condenser fans with designed water mist generation rate
CTC+VSF+WM2	CTC and the use of variable speed condenser fans with optimal water mist generation rate

The part load performance curves of the model chiller operating under HPC without water mist pre-cooling were given in Figure 5.19. Based on the models, performance curves of the chiller with various condenser features were established, as shown in Figure 5.39. When the water mist system was applied, the chiller performance varied with different RH levels at certain outdoor dry bulb temperature, and 50% relative humidity level was considered to show the variation of the COP curves under various operating conditions. These COP curves clearly demonstrated the variation of chiller COP following the sequence of refrigeration circuits in the studied chiller. With HPC and CSF, the chiller COP fluctuated regardless of with water mist or without water mist pre-cooling. With VSF or CTC, the chiller COP varied regularly with the part load ratios following the staging of refrigeration circuits and the compressors in each refrigeration circuit.

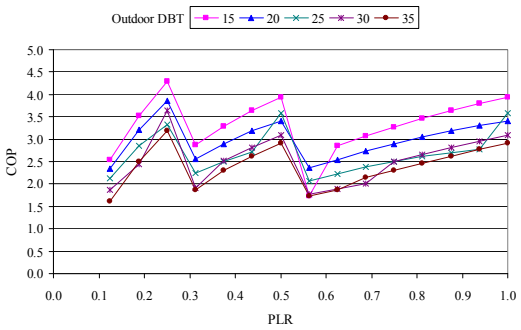

(a) HPC+CSF+WM1

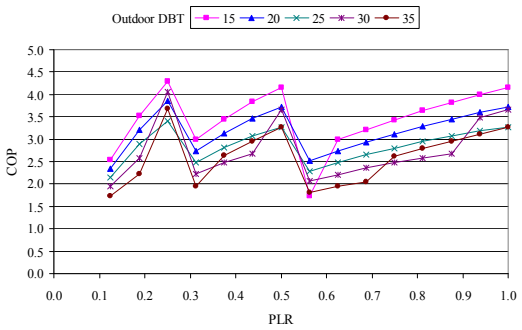

(b) HPC+CSF+WM2

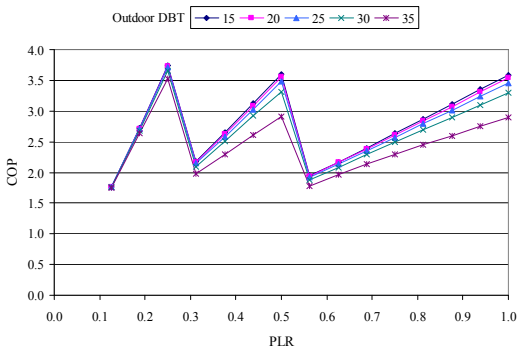

(c) HPC+VSF+WM1

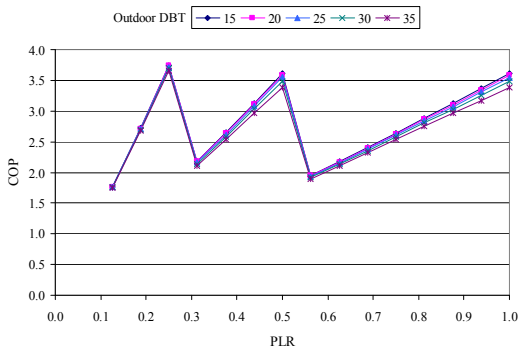

(d) HPC+VSF+WM2

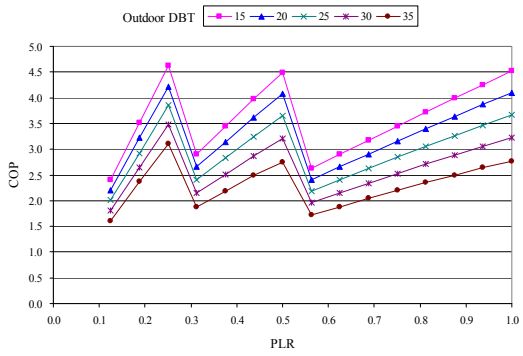

(e) CTC+CSF

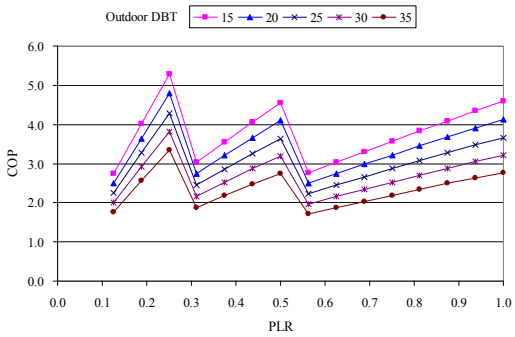

(f) CTC+VSF

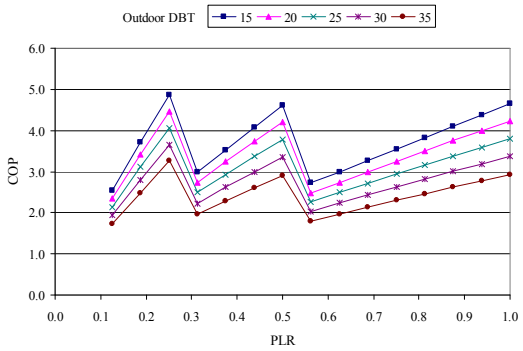

(g) CTC+CSF+WM1

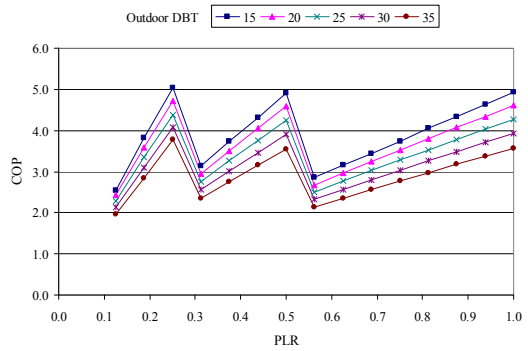

(h) CTC+CSF+WM2

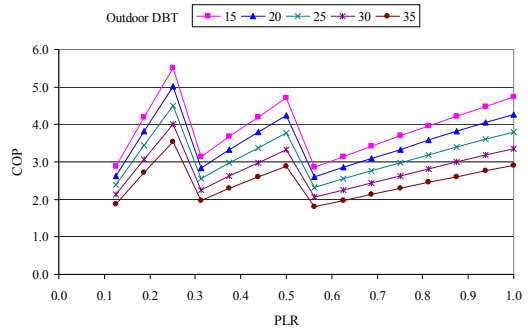

(i) CTC+VSF+WM1

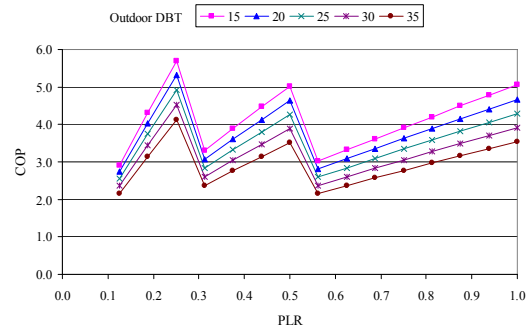

(j) CTC+VSF+WM2

Figure 5.39 COP curves of the chiller with different control strategies

The potential benefits of each condenser feature in relation to the baseline could be identified by a comparison on how the system COP varied under different control schemes. CTC, WM and VSF had different effects on the increase or decrease in the power components and the chiller COP.

Figures 5.40 and 5.41, for outdoor air RH of 50% and 80%, respectively, demonstrated the benefits of each condenser feature described by the percentage change of chiller COP. A positive percentage meant a chiller COP increase while a

negative percentage meant a chiller COP drop. The performance of chiller without water mist pre-cooling was affected by the dry bulb temperature of outdoor air, while the performance of chiller with water mist pre-cooling was affected by the wet bulb temperature of outdoor air. Both sensible and latent heat transfers took place for the air-cooled condensers with water mist pre-cooling. With lower relative humidity of the ambient air, the evaporative cooling effect would be more significant, and the chiller performance could be improved more.

Under HPC with constant speed condenser fans, when RH was 50%, the COP of the chiller with designed water mist rate and optimal water mist generation rate increased by varying degrees up to 22.6% and 26.8%, respectively. When RH was 80%, the chiller COP was improved by up to 22.1% and 24.6% for the chiller operated with designed water mist rate and optimal water mist generation rate, respectively. In such conditions, the additional power of high pressure pump generating water mist was more than offset by the reduction in compressor power due to the reduced outdoor temperature by water mist pre-cooling. As shown in Figures 5.40 and 5.41, the increase in the chiller COP could be higher when the relative humidity of outdoor air was lower.

The use of VSF has a significant influence on the trade-off between compressor power and fan power and hence the chiller COP, regardless of HPC and CTC. As shown in Figure 5.25, the chiller COP could rise almost linearly with the chiller part load ratio and varied with the refrigeration circuit sequence at any given outdoor temperature, which was different from the fluctuating COP shown in Figure 5.19. Under HPC, the COP of the chiller with VSF could increase by up to 17.1%, but it could drop by 23.1% from the base case. When the chiller operated with VSF and optimal water mist generation rate, the COP could be improved up to 23.3%.

It was observed that water mist pre-cooling had both positive and negative impacts on the chiller COP when the chiller operated under HPC. Although the chiller condensing temperature could be better managed by using variable speed fans to the set point, the COP could increase or decline comparing with the HPC case with constant speed fans in certain operating conditions. The casual decrease of the chiller COP was due to the HPC with unfavorable staging of constant speed condenser fans. In addition, the chiller COP drop was due to the fact that the variable speed drive consumed 3% of the total power of the staged condenser fans. The studied chiller was equipped with 8 groups of constant speed fans, and the condenser fans were staged group by group. To prevent the condensing temperature from exceeding the high temperature setting, one more group of condenser fans were needed to be staged than that operating with water mist due to the pre-cooling effect. When one more group of condenser fans were cycled on, the condensing temperature dropped significantly below the high setting, and could even drop below the set point. This indicated that head pressure control was energy inefficient, and it was undesirable to operate the chiller with water mist under HPC, which would result in an increase of chiller power due to an inadequate trade-off between compressor power and condenser fan power.

As HPC was considered to be energy inefficient, CTC was proposed as a desirable alternative to HPC. When the chiller operated under CTC with constant speed fans, the chiller COP was improved by up to 35.5%. When the chiller operated with VSF and CTC, the chiller COP was improved further by up to 51.8% because the compressor power dropped significantly with lower condensing temperature and the fan power dropped considerably at lower fan speed. It should be noted that there was high potential for improving the chiller COP under CTC when the outdoor temperature was low, because CTC enabled the condensing temperature to approach

the lower boundary of condensing temperature. When the chiller operated with VSF, CTC, optimal water mist generation rate and the relative humidity was 50%, the chiller COP was improved most by up to 70.8%. With lower chiller load part load ratio and lower relative humidity of the outdoor air, the degree of the COP improvement was more significant. At a low chiller load, the heat rejection airflow rate could still be high under CTC, allowing water mist to fully vaporize. This, in turn, brought a further decrease in the temperature of the entering condenser air to lower the compressor power.

Based on the analysis above, water mist pre-cooling is an effective means to improve chiller efficiency, but it is undesirable to operate the chiller with water mist under HPC. CTC should be a compulsory energy efficient measure to improve the performance of air-cooled chillers, and it is desirable to operate the air-cooled chillers with VSF, CTC and water mist pre-cooling together.

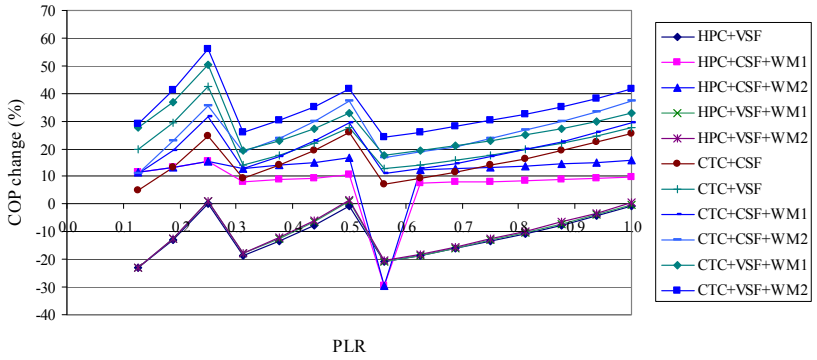

(a) T_{db}=15°C

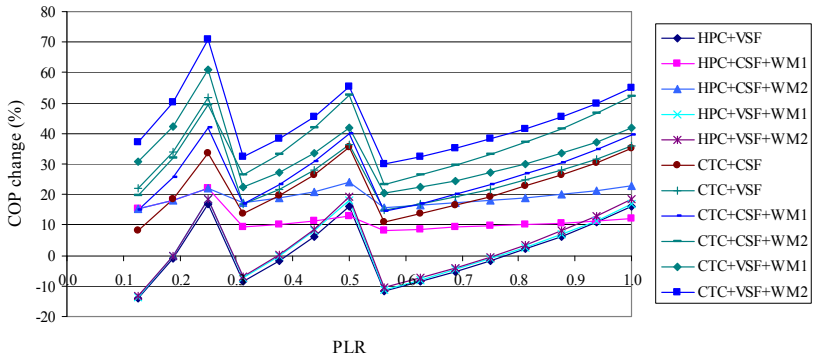

(b) T_{db}=20°C

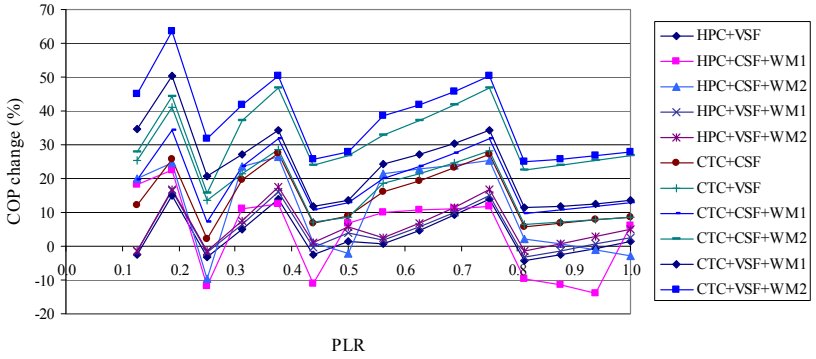

(c) T_{db}=25°C

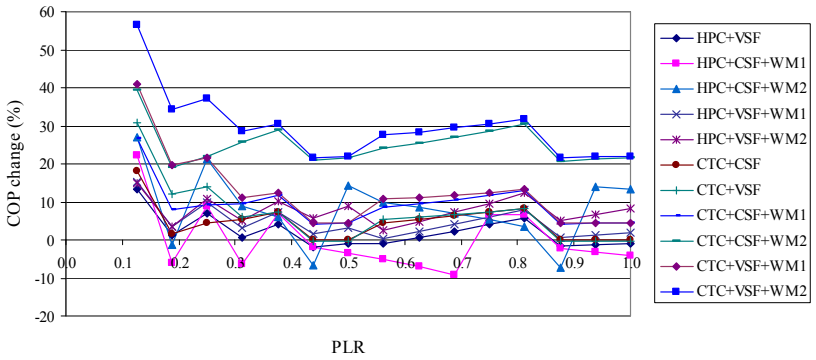

(d) T_{db}=30°C

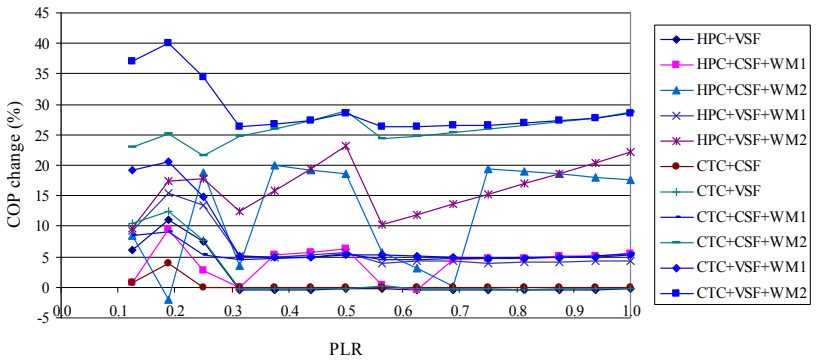

(e) T_{db}=35°C

Figure 5.40 Percentage change in chiller COP under various conditions in relation to the HPC case (RH=50%)

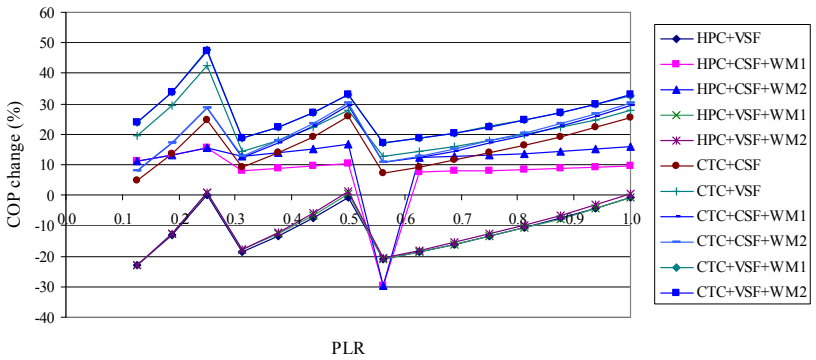

(a) T_{db}=15°C

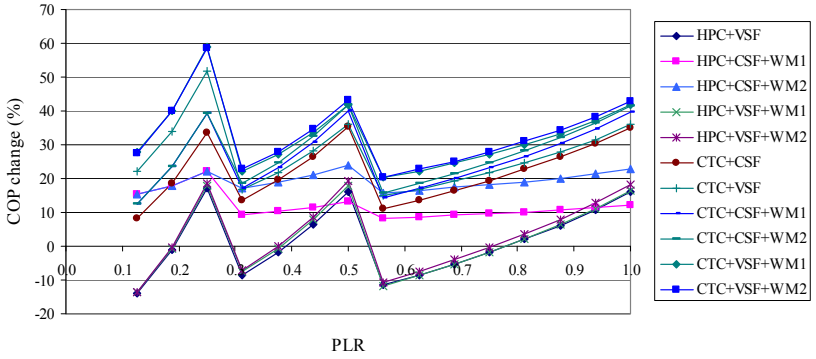

(b) T_{db}=20°C

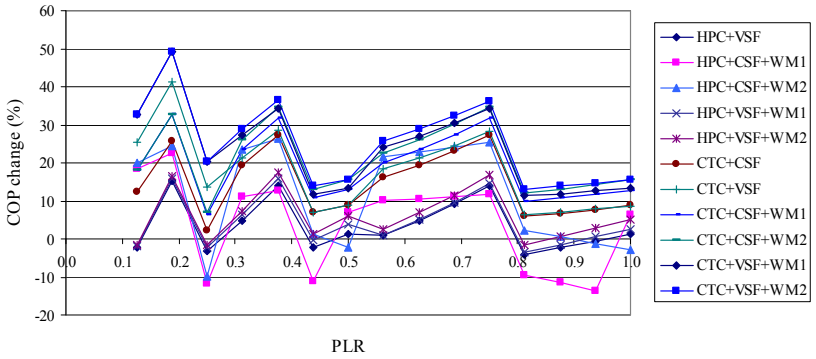

(c) T_{db}=25°C

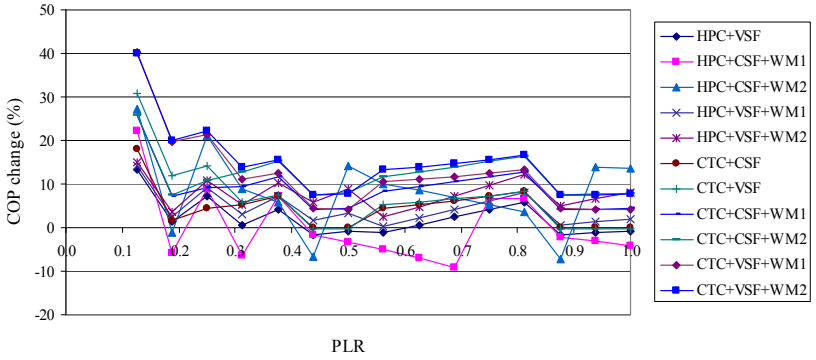

(d) T_{db}=30°C

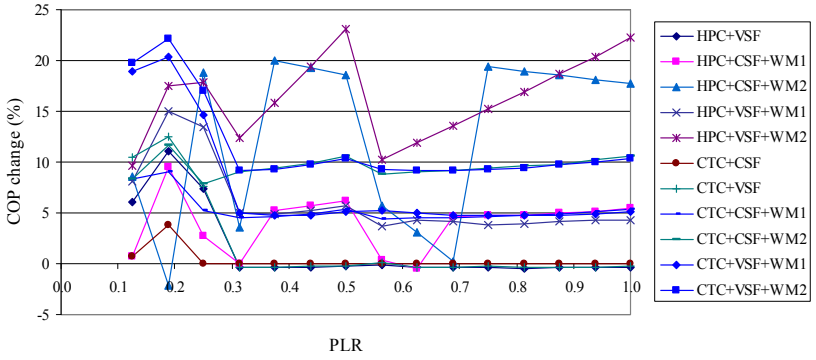

(e) T_{db}=35°C

Figure 5.41 Percentage change in chiller COP under various conditions in relation to the HPC case (RH=80%)

5.8 Energy savings of enhanced condenser features

Having identified the chiller performance under various control strategies for condenser fans, the feasibility of using composite features of CTC, VSF and water mist pre-cooling were analysed with respect to their energy savings. Chiller plants serving a representative office building and a hotel building were considered in order to investigate to what extent each condenser feature would influence the electricity consumption of the air-cooled chillers.

According to the representative building models described in Chaper 3 and the weather-load and load-frequency profiles of the reference office building and the hotel building, the number and capacity of chillers in the chilled water plants serving the two buildings could be determined. To meet the peak building cooling load of the reference buildings, the chiller plant of the office building was designed with seven identical air-cooled screw chillers, and the chiller plant of the hotel building was designed with four identical air-cooled screw chillers. Each chiller had a nominal cooling capacity of 1116 kW, which was compatible to the studied chiller reported in Chapter 4. To meet the changing building cooling load, conventional chiller sequencing was implemented. All the running chillers equally shared the cooling load, and no additional chillers started to operate until each of the running chillers was operating at full load. The schedule of staging chillers and their possible loading ranges were then determined.

Figures 5.42 and 5.43 illustrated how the chillers were staged to implement chiller sequencing when the building load reached a certain level. The number inside each column in the figures indicated the number of staged chillers at a given nominal cooling capacity. The chilled water plants of the reference buildings were designed with equally sized chillers, and one more chiller would be staged when the building

cooling load exceeded the total cooling capacity of the staged chillers. Based on this, the step of staging chillers was equal to the total number of chillers installed, and there were 7 steps and 4 steps for staging chillers with different total cooling load for the typical office building and the representative hotel building, respectively. More steps meant that the chillers could operate more frequently at higher PLR to meet various building cooling loads.When more chillers were staged to meet higher building cooling loads, each of them could operate at higher part load ratio and hence operate with higher efficiency.

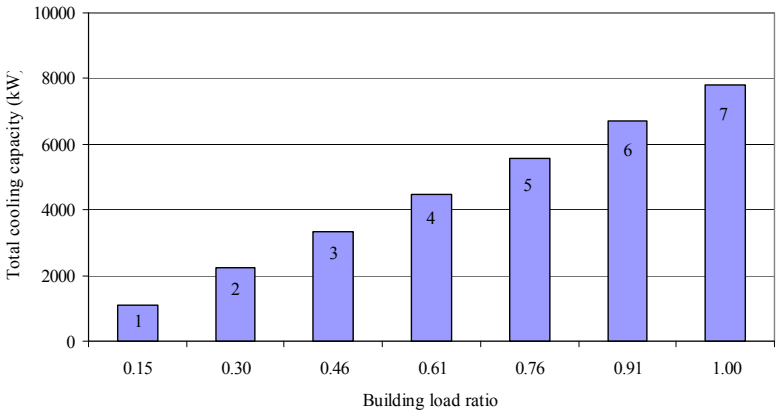

Figure 5.42 Schedule of staging chillers in the office building

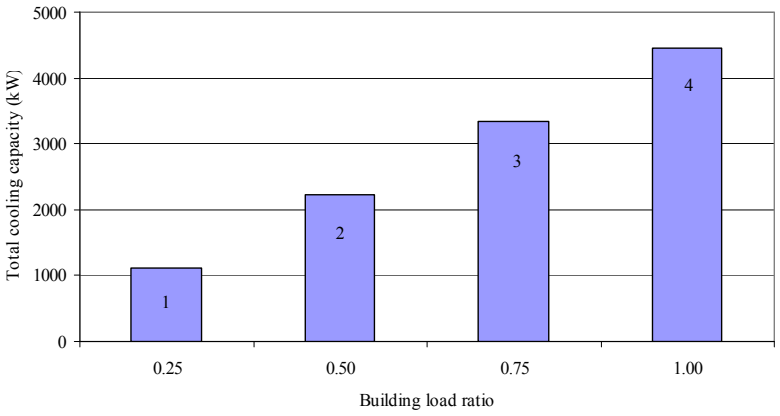

Figure 5.43 Schedule of staging chillers in the hotel building

HPC is regarded to be energy inefficient, and condensing temperature control (CTC) is proposed as a viable alternative to improve the efficiency of air-cooled chillers in

various operating conditions. The variable speed condenser fans and water mist pre-cooling can complement CTC to further improve the chiller performance. Given that the operation of chillers generally accounts for a significant percentage of the total electricity consumption of a commercial building, it is worth considering how existing chilled water plants benefit from the advanced control with enhanced condenser features in relation to head pressure control (HPC) in terms of the annual energy saving of chillers.

In view of a considerable proportion of offices and hotels in the local building sector, it was justifiable to investigate the cooling demand for these types of buildings and to examine the energy saving potential of the chilled water plants throughout a year when CTC, VSF or water mist pre-cooling was applied.

Drawing on the chiller system model, the variations in the annual electricity consumption of the chillers under different control strategies were evaluated. Figure 5.44 shows the variation of the monthly total electricity consumption, which is the sum of the compressor power, condenser fan power and high pressure pump power, for the office building and hotel building with individual and mixed condenser features of CTC, VSF and water mist. The individual and mixed features had similar effects on monthly electricity consumptions of the chillers. Distinct seasonal variations could be observed, which peaked during the hot summer months.

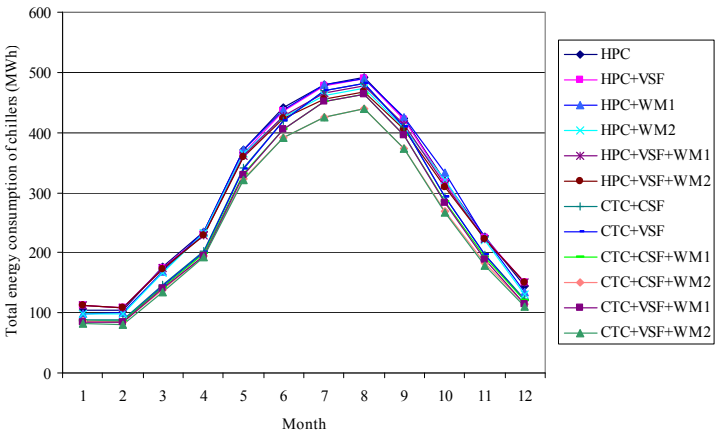

(a) Office

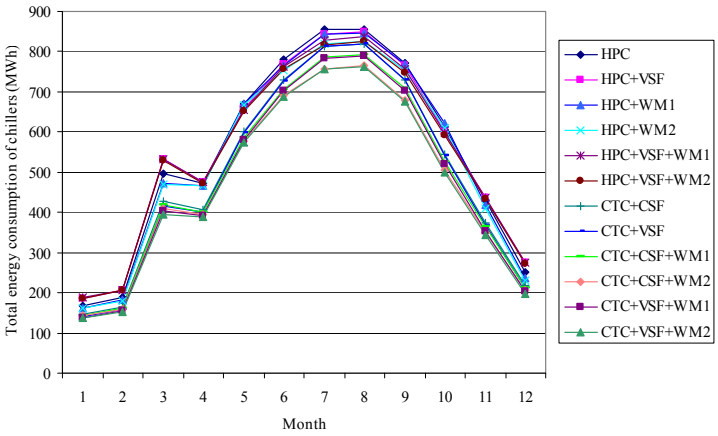

(b) Hotel

Figure 5.44 Monthly total electricity consumption of chillers serving the typical buildings with each condenser feature

Figure 5.45 shows the variation of chiller COP in the reference office building and hotel building in an example weather year for the HPC base case. This figure clearly demonstrated that the chiller COP varied with the refrigeration circuit sequence and the compressor sequence in a refrigeration circuit. The annual average COP and annual electricity consumption of chillers with each condenser feature serving the office building and hotel building were summarized in Table 5.3 and Table 5.4, respectively. It was identified that there was a small decrease on the annual chiller energy consumption with HPC and variable speed fans from the baseline, and the annual chiller energy consumption of the office building was saved by only 0.3%.

Under HPC with variable speed condenser fans for the hotel building, water mist pre-cooling could incur a 0.3% increase in the annual electricity consumption of chillers. This was because the condensing temperature was controlled by the variable speed fans around the set point, but it could not be controlled precisely at the set point for the chiller with constant speed fans. The staged constant speed condenser fans could provide more heat rejection airflow than required minimum airflow, which resulted in considerable drop of condensing temperature, and the compressor power decreased accordingly.

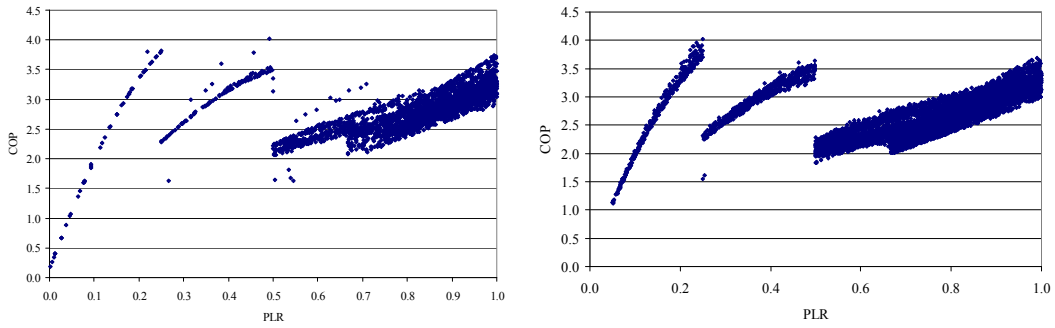

(a) Office (b) Hotel

Figure 5.45 Variation of chiller COP in reference buildings

It was also interesting to investigate whether the chillers, coupled with water mist pre-cooling, resulted in a further decrease in their annual energy consumption under local weather conditions. From Tables 5.3 and 5.4, it was observed that water mist pre-cooling had no significant impacts on the chiller annual energy consumption when the chillers operated under HPC. Under HPC, electricity consumption of chillers was saved by 0.6% and 3.3% when the water mist system generated designed and optimal water mist rate for the office building, respectively. Under HPC, electricity consumption of chillers was saved by 1.5% and 3.2% with designed and optimal water mist rate for the hotel building, respectively. The energy saving potential by coupling water mist pre-cooling with air-cooled chillers could not be effectively realized under HPC. Hence, it was not beneficial to apply water mist to

air-cooled chillers without changing the traditional head pressure control method.

When CTC replaced HPC, the chiller COP was improved noticeably, which helped reduce the annual electricity consumption. Based on the local weather, chillers operated at part load condition with an outdoor temperature of below 25°C for half of the time. Regarding this, there was a considerable scope to decrease the condensing temperature for better efficiency. For the office building, the annual chiller energy consumption under CTC could be saved by 7.3% and 7.7% when the chillers were equipped with constant speed condenser fans and variable speed fans, respectively. For the hotel building, the annual chiller energy consumption under CTC could be saved by 8.7% and 9.4% with constant speed fans and variable speed fans, respectively. When a combination of the advanced condenser features of CTC, VSF and WM were present, the annual electricity consumption of chillers decreased by 11.0% and 14.8% with designed and optimal water mist rate for the office building, and that was saved by 12.5% and 14.9% with designed and optimal water mist rate for the hotel building. These findings indicate that variable speed fan control and water mist system are favourable complements to CTC.

Water is often mistaken to be an unlimited and renewable resource. To the contrary, water resource is very limited and precious, especially for crowded cities. It was desirable to assess the water consumption by the water mist system in the different operating schemes, and the results were shown in Tables 5.3 and 5.4. For water-cooled chillers, the total water losses from cooling tower are the sum of drift losses, evaporation losses and blowdown losses. According to Standard 550/590 (ARI 2003), the total water loss can be calculated based on an assumption that the water loss accounts for 1.5% of the condenser water flow rate, which is designed at 0.054 l/s per kW cooling capacity. For a water-cooled chiller with same cooling capacity as

the studied air-cooled chiller, whose capacity is 1116 kW, the water loss is 0.91 l/s.

If water-cooled chillers were used in the representative office building, the annual total water losses from cooling towers were 3.43×10^4 m^3. Comparatively, the water consumption of the water mist system was very small, which was about 7.3%, 10.5% and 16.2% of the total water losses for open-loop cooling towers serving the water-cooled chillers for schemes HPC+CSF+WM1, HPC+CSF+WM2 and CTC+VSF+WM2, respectively. The amount of water consumption for schemes HPC+VSF+WM1, CTC+CSF+WM1 and CTC+VSF+WM1 were same as scheme HPC+CSF+WM1.

Table 5.3 Energy performance of chillers under different control strategies (Office)

Case	*S1*	*S2*	*S3*	*S4*	*S5*	*S6*
HPC (base case)	2.83	3.52×10^6	0	3.52×10^6		0
HPC+VSF	2.81	3.51×10^6	0	3.51×10^6	0.3	0
HPC+CSF+WM1	2.87	3.48×10^6	1.57×10^4	3.50×10^6	0.6	2.52×10^3
HPC+CSF+WM2	2.94	3.39×10^6	1.57×10^4	3.40×10^6	3.3	3.60×10^3
HPC+VSF+WM1	2.85	3.44×10^6	1.57×10^4	3.45×10^6	1.9	2.52×10^3
HPC+VSF+WM2	2.87	3.40×10^6	1.57×10^4	3.42×10^6	2. 9	3.28×10^3
CTC+CSF	3.13	3.26×10^6	0	3.26×10^6	7.3	0
CTC+VSF	3.16	3.25×10^6	0	3.16×10^6	7.7	0
CTC+CSF+WM1	3.23	3.14×10^6	1.57×10^4	3.16×10^6	10.2	2.52×10^3
CTC+CSF+WM2	3.36	3.01×10^6	1.57×10^4	3.02×10^6	14.1	5.57×10^3
CTC+VSF+WM1	3.28	3.12×10^6	1.57×10^4	3.13×10^6	11.0	2.52×10^3
CTC+VSF+WM2	3.40	2.98×10^6	1.57×10^4	3.00×10^6	14.8	4.91×10^3

Notes on S1 to S6:
S1: Average chiller COP
S2: Annual electricity consumption of chillers (kWh)
S3: Annual electricity consumption of high pressure pump (kWh)
S4: Annual total electricity consumption of chillers and high pressure pumps (kWh)
S5: Percentage saving in annual electricity consumption of chillers and high pressure pumps (%)
S6: Water consumption by the water mist system the chiller plant (m^3)

Table 5.4 Energy performance of chillers under different control strategies (Hotel)

Case	*S1*	*S2*	*S3*	*S4*	*S5*	*S6*
HPC (base case)	2.69	6.36×10^6	0	6.36×10^6		0
HPC+VSF	2.65	6.38×10^6	0	6.38×10^6	-0.3	0
HPC+CSF+WM1	2.75	6.24×10^6	2.89×10^4	6.27×10^6	1.5	4.65×10^3
HPC+CSF+WM2	2.79	6.13×10^6	2.89×10^4	6.16×10^6	3.2	5.21×10^3
HPC+VSF+WM1	2.66	6.31×10^6	2.89×10^4	6.34×10^6	0.3	4.65×10^3
HPC+VSF+WM2	2.68	6.25×10^6	2.89×10^4	6.28×10^6	1.3	4.58×10^3
CTC+CSF	2.99	5.81×10^6	0	5.81×10^6	8.7	0
CTC+VSF	3.03	5.77×10^6	0	5.77×10^6	9.4	0
CTC+CSF+WM1	3.08	5.62×10^6	2.89×10^4	5.64×10^6	11.3	4.65×10^3
CTC+CSF+WM2	3.16	5.45×10^6	2.89×10^4	5.48×10^6	13.9	8.54×10^3
CTC+VSF+WM1	3.13	5.54×10^6	2.89×10^4	5.57×10^6	12.5	4.65×10^3
CTC+VSF+WM2	3.22	5.39×10^6	2.89×10^4	5.42×10^6	14.9	7.17×10^3

5.9 Evaluation of chiller energy saving potential in the local building sector

The experimental and simulation results in this research confirm that variable condensing temperature control and water mist pre-cooling are promising energy efficient measures for air-cooled chillers. Having presented the methods to improve chiller efficiency, it is worth investigating how this improvement help reduce the growing electricity demand for the commercial sector.

Energy consumption statistics of the residential, commercial, industrial and transport sectors in Hong Kong are provided by the Census and Statistics Department (C&SD) and the Electrical and Mechanical Services Department (EMSD). EMSD has established an energy end-use database for the past years, which contains breakdowns of different energy end-uses for each segment in these sectors. With regard to the commercial sector, the electricity use for air-conditioning went up from 2584 to 7570 GWh (a 193% increase), and the total electricity consumption rose from 9081 to 31461 GWh (a 246% increase), over the years 1984–2009 (EMSD 2004; EMSD 2011). The commercial sector includes four segments: the office segment, the restaurant segment, the retail segment and other commercial segments.

According to the statistical data, it is possible to directly determine the overall electricity demand and the proportion taken up by air-conditioning (as one of the energy end-uses) for the office segment. Table 5.5 shows the trend of energy use of office buildings from 1985 to 2009 (EMSD 2004; EMSD 2011). EUI means the annual electricity use in kWh per unit floor area of a building in m^2. A/C EUI is the annual electricity use by air conditioning system in kWh per unit floor area of a building in m^2.

Table 5.5 Summary of energy use of office buildings from 1985 to 2009

(Source: Hong Kong Energy End-use Data, EMSD, Hong Kong)

Year	*Floor area* ($\times 10^3$ m^2)	*Total Energy use (GWh))*	*Air conditioning (GWh)*	*EUI* (kWh/m^2)	*A/C EUI* (kWh/m^2)
1984	4067.6	683	336.7	167.9	82.8
1985	4375.8	743.6	352.8	169.9	80.6
1986	4176.5	809.2	376.4	193.7	90.1
1987	4420.4	959.2	483.6	217.0	109.4
1988	4657.4	1165.3	600.8	250.2	129.0
1989	4896.8	1514.7	796.7	309.3	162.7
1990	5085.2	1691.1	864.7	332.6	170.0
1991	5541.8	1854.2	895.0	334.6	161.5
1992	6099.1	2084.4	948.1	341.8	155.4
1993	6390.8	2365.8	1054.2	370.2	165.0
1994	6849.5	2765.3	1321.7	403.7	193.0
1995	7188.6	2937.8	1403.9	408.7	195.3
1996	7416.8	3041.1	1453.1	410.0	195.9
1997	7889.3	3246.1	1551.1	411.5	196.6
1998	8603.5	3388.1	1619.4	393.8	188.2
1999	8970.9	3642.5	1741.4	406.0	194.1
2000	9085.5	3857.8	1844.4	424.6	203.0
2001	9131.9	3868.6	1850.0	423.6	202.6
2002	9286.5	3864.7	1848.1	416.2	199.0
2003	9540.7	3849.4	1840.8	403.5	192.9
2004	9794.9	3979.7	1903.1	406.3	194.3
2005	9769.7	3838.3	1986.1	392.9	203.3
2006	9812.8	3663.9	1996.1	373.4	203.4
2007	10106.7	3491.7	1936.1	345.5	191.6
2008	10392.3	3303.9	1776.1	317.9	170.9
2009	10529	3274.4	1760.3	311.0	167.2

However, a breakdown for the electricity consumption of hotels was absent, and hotels were aggregated into the other commercial segments, which included hotels, education, health, storage, and other miscellaneous commercial or public services. Extensive surveys of the electricity end-use by other researchers had shown that the electricity end-use for air-conditioning in hotels rose from 194.7 GWh in 1988 to 405.4 GWh in 2000 (Chan and Lam 2002), and this increasing rate was the same as that in the overall electricity consumption. Accordingly, the electricity end-use for air-conditioning in hotels increased by an average rate of 16.2 GWh per annum, and the average rate of increase in the total electricity consumption was 36.8 GWh per annum. The operation of chillers accounted for 24.8 to 28.6% of the overall electricity consumption of hotels (Yu and Chan 2005a). Under this scenario, the

electricity demand of chillers could grow by 9.1–10.5 GWh per annum for hotels. With these average rates of increase in electricity consumption, it was possible to forecast the growth of electricity demand for hotels in the long term.

The analysis reported in Section 5.8 showed that the annual electricity consumption of air-cooled chillers dropped by up to 14.8% and 14.9% for the typical office building and hotel building when the improved condenser features of CTC, VSF and WM were implemented together. Having identified the annual growth rate of total electricity consumption due to air-conditioning in hotels and office buildings, it was worth estimating how the improved condenser features would help reduce the electricity demand in the office and hotel sector in future. According to the simulation results of this research, when air-cooled chillers operate with the composite energy efficient measures, the EUI of the chillers was reduced from 82.1 kWh/m^2 to 70.0 kWh/m^2 for office buildings and from 139.7 kWh/m^2 to 118.9 kWh/m^2 for hotels.

Given a close relationship between the increasing stock of office and hotel premises and their growing electricity use, a forecast was made on the overall electricity demand for the local office and hotel sector in 2012–2016. Figure 5.46 illustrates the variation of the total stock of offices in Hong Kong from 1985 to 2010 referring to the past reports of Hong Kong Property Review (RVD 2011). The trend of the total stock of offices in Hong Kong could be determined with the correlation equation shown in Figure 5.46, and the prediction of the supply of the office building in terms of total floor area in a 5-year period could be obtained. The high value of the correlation coefficient (R^2=0.9833) confirmed that the agreement between the statistical data and modeling data was pretty good.

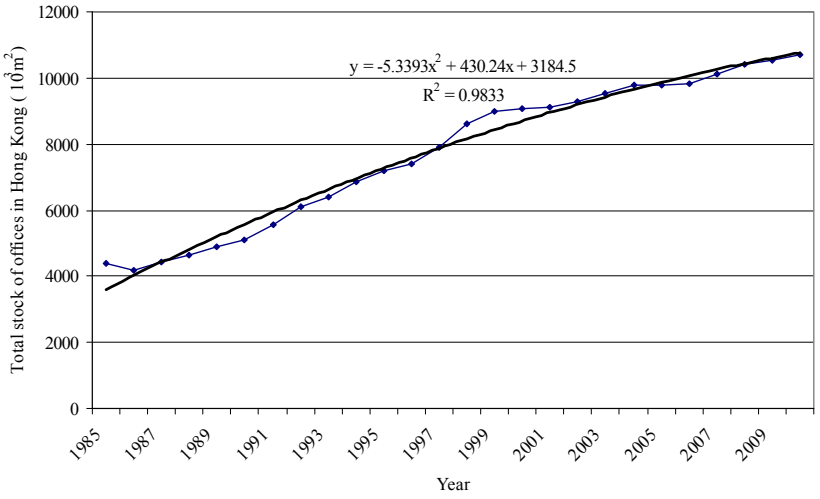

Figure 5.46 Variation of the total stock of offices in Hong Kong ($\times 10^3$ m^2)

Considering that half of the local commercial buildings were installed with air-cooled chillers, the overall annual chiller energy use was 878.5 GWh in the office segment or 348.9 GWh in the hotel segment in 2011, based on the local energy end-use database and the predicted supply of office buildings and hotels. The likely annual electricity savings of chillers in the office and hotel sector from 2012 to 2016 were calculated, as shown in Table 5.6, assuming that half of new office and hotel buildings would be installed with air-cooled chillers with the condenser features of VSF, CTC, WM or combination of them. When variable condensing temperature control was implemented, the electricity demand of air-cooled chillers in new offices and hotels could decrease by 16.3 GWh and 5.5 GWh in the next 5-year period, respectively. When the air-cooled chillers operated with CTC, VSF and optimal water mist rate, the electricity savings of air-cooled chillers in new offices and hotels could be 32.8 GWh and 9.5 GWh in the next 5-year period, respectively. It was expected that the electricity savings could be much higher if air-cooled chillers in existing office and hotel buildings would have been retrofitted with the improved condenser features.

Table 5.6 Electricity savings of air-cooled chillers in new offices and hotels due to improved condenser features in 2012-2016

Year	Estimated electricity demand (GWh)		Likely reduction of annual chiller electricity consumption (GWh)							
			CTC		CTC +VSF		CTC+CSF+WM1		CTC+VSF+WM2	
	Office	Hotel	Office	Hotel	Office	Hotel	Office	Hotel	Office	Hotel
2012	3298.4	1252.6	1.0	0.4	1.1	0.4	2.0	0.6	2.1	0.6
2013	3327.7	1286.1	2.3	0.7	2.4	0.8	4.5	1.2	4.7	1.3
2014	3349.8	1319.5	3.3	1.1	3.4	1.2	6.3	1.8	6.6	1.9
2015	3374.1	1352.9	4.3	1.5	4.6	1.6	8.4	2.4	8.7	2.5
2016	3396.3	1386.3	5.3	1.8	5.6	2.0	10.3	2.9	10.7	3.2
Accumulative reduction (GWh)			16.3	5.5	17.1	6.0	31.5	8.9	32.8	9.5

5.10 Summary

This chapter described the experiment on an air-cooled screw chiller with water mist system, and the experimental data were evaluated in detail. It then presented the methodologies of the water mist model, and the water mist model was incorporated into the chiller model developed in Chapter 4 under the TRNSYS environment. With the validated integrated chiller models, the effect of combinations of water mist pre-cooling, variable speed condenser fans and variable condensing temperature control on the air-cooled chillers was investigated. This chapter also conducted detailed analysis on the energy saving potential of the chillers serving a representative office building and a representative hotel building with improved efficiency of air-cooled chillers, and determined the potential contribution in reducing the future total electricity consumption of commercial buildings in Hong Kong.

Chapter 6 Neural Network Based Optimal Control of Air-Cooled Chillers

Chapters 4 and 5 put forward the simulation-based optimization schemes aiming to improve the air-cooled chillers with advanced condenser features, including CTC, VSF and WM. Chiller operation is vital for building energy efficiency in the commercial buildings. However, chiller operation is complicated because nonlinear relationships and interactions may occur among parameters. A different approach to optimize the chiller operation based on artificial intelligence methods is proposed here. This chapter builds on the foundation established before and demonstrates the implementation and application of the simulation-based hybrid artificial intelligence control method combining both ANN and GA. The idea is to apply genetic algorithms to find the optimum set point of condensing temperature or water mist generation rate, which will minimize the chiller energy consumption. For this purpose, ANN is used to establish a complex and non-linear function of the air-cooled chillers relative to the controlled and the uncontrolled variables.

The hybrid ANN−GA technique consists of three steps: generation of the databases, training and evaluation of ANN model, searching and evaluation of optimum using GA. The chiller database has been provided from the simulations of chiller models using TRNSYS reported in Chapters 4 and 5. This chapter first presents the ANN models for the air-cooled chillers under different operating schemes. The trained and validated ANN models are then integrated into the genetic algorithm serving as the evaluation function, and GA can search for the optimal or near-optimal controlled variables to operate the chillers efficiently. The optimization results are verified by

using the data obtained from TRNSYS simulation to ensure that the hybrid ANN−GA technique is suitable for the optimal control.

6.1 Optimization method

Due to the drawbacks of the conventional mathematical and empirical methods, in this research, a hybrid intelligent system is developed to achieve optimal control for the air-cooled chillers with advanced condenser features. The objective of optimization of the chiller operation is to select the optimal control variables under given constraints, in order to minimize the electricity consumption by chillers. The hybrid artificial intelligent control combines a BP neural network to model the air-cooled chiller and a genetic algorithm to find the optimal values for the controllable variables to reach the system objectives. The concept of a controller that applies GA to optimize the values of the controlled parameters with the neural network is shown in Figure 6.1. The intelligent controller can not only predict the chiller performance (using ANN), but also find the optimal set points of the condensing temperature and water mist generation rate that will minimize the chiller power consumption. The BP neural network works like an emulator to predict the chiller performance. Once the ANN model is developed with desired level of precision after training, the ANN model is integrated into the GA method as an evaluation function. When GA is performed, the optimal solutions can be found within the constraints, as GA employs a ‘natural selection’ guided parallel search under pre-specified constraints.

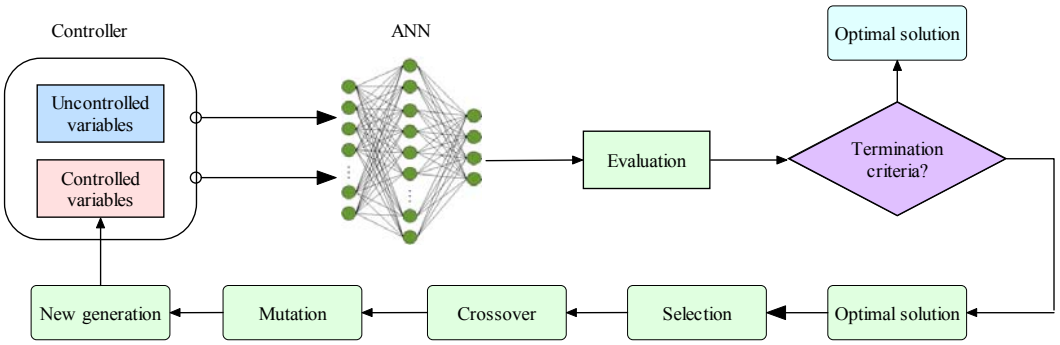

Figure 6.1 Hybrid intelligent control using ANN and GA

6.1.1 Formulation of optimization problem

The difference between normal operation and optimal operation is that in optimal operation, the system is controlled not only to satisfy certain physical constraints but also a predefined performance index or cost function is minimized or maximized at the same time, which is a function of controlled and uncontrolled variables. An optimization model consists principally of three ingredients: an objective function, variables and constraints.

Genetic algorithms search for the best solution dependent on the fitness function of each individual in the population, and hence the fitness function should reflect the individual's performance in the current problem. In terms of building energy efficiency, the most important concern is the energy consumed by the chillers to achieve the desired indoor environment, the smaller the energy use, the better it is. Therefore, the objective in this research is to minimize the total energy consumption of the chillers and the high pressure pumps generating water mist, and it is selected as the performance index for the optimization analysis.

Based on the mathematical models of related components, the operating characteristics of condenser fans and the energy efficiency of the chillers can be maximized by variable condensing temperature control and water mist pre-cooling. There are three types of devices which consume energy, including compressors,

condenser fans and high pressure pumps. To simplify the model and optimization analysis, the energy consumption by chilled water pumps is neglected. Therefore, the objective function is to minimize the total energy consumption of the compressors, condenser fans and the high pressure pumps generating water mist. In the development of optimal control strategy, quasi steady-state load is assumed during each optimization step.

6.1.2 Process of the hybrid ANN–GA optimization algorithm

Figure 6.2 illustrates the flowchart of the proposed optimization scheme based on combined ANN-GA algorithm which is used in this investigation. The optimization scheme is summarized as follows:

(1) An initial population is generated at random.

(2) The fitness function based on ANN model is used to calculate the fitness for all initial individuals. It will be assigned a fitness value for each individual by the well-trained ANN model.

(3) A population for the next generation is reproduced by the genetic operations (selection, crossover and mutation).

(4) The new individuals replace the parent individuals into the population.

(5) Steps 2 – 4 are executed until the terminating criterion has been satisfied.

MATLAB software is used to develop the above algorithm and optimize the parameters affecting the chiller performance.

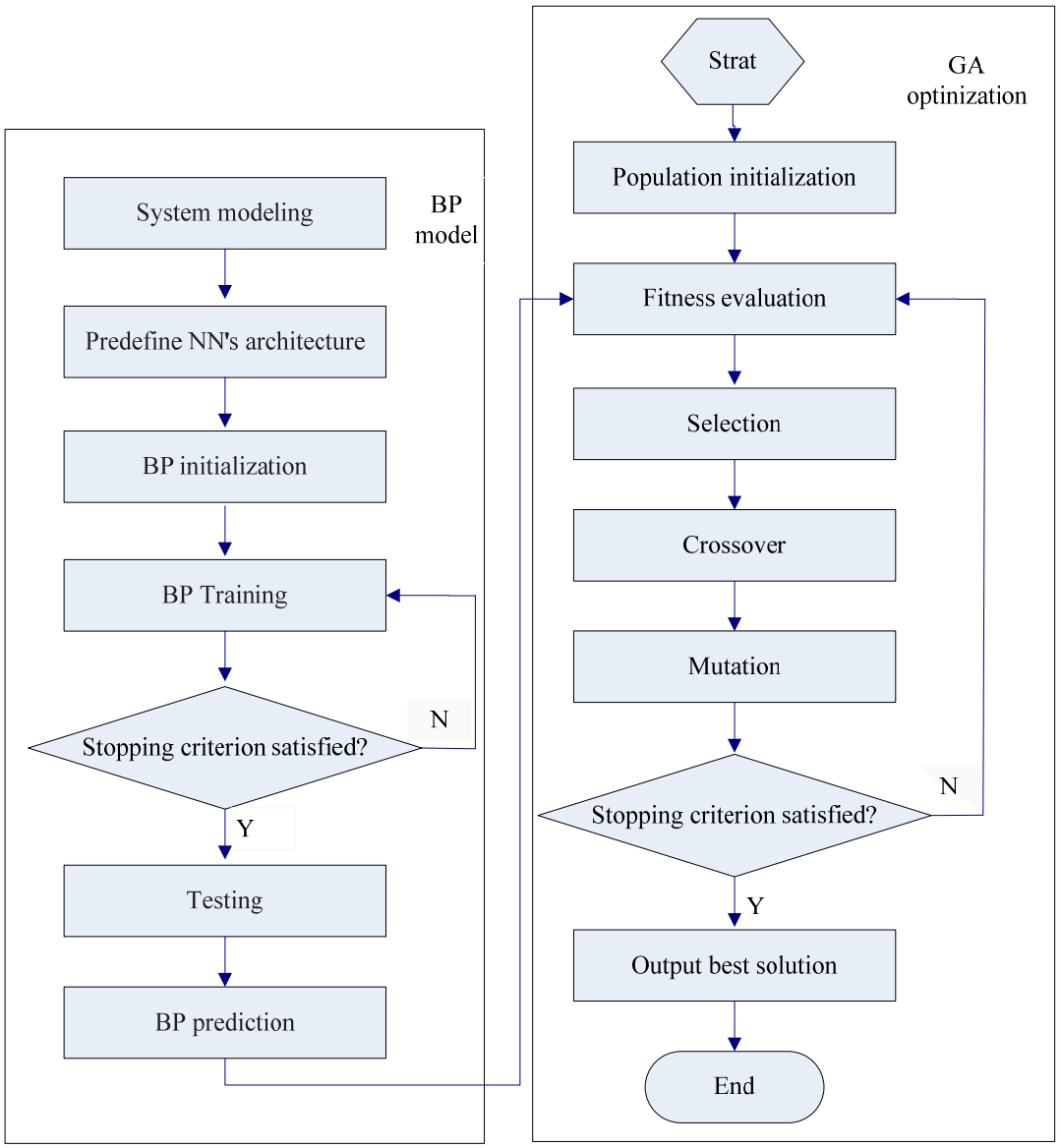

Figure 6.2 Flowchart of optimization scheme based on combined ANN-GA algorithm

6.2 Optimization case studies

There are 23 cases investigated in Chapters 4 and 5, including the conventional head pressure control (HPC), variable condensing temperature control (CTC), constant speed condenser fans (CSF), variable speed condenser fans (VSF) and water mist pre-cooling (WM). One of the main objectives is to establish the control strategy for the air-cooled chillers with advanced condenser features, and proposes a hybrid artificial intelligent technique for chiller modeling and control using neural network and genetic algorithm to optimize the chiller operation, and demonstrates this

approach with some illustrative examples. To minimize the chiller energy consumption, it is essential to set the controlled variables under certain conditions. ANN-GA technique can be considered to be a model-based method of supervisory control, in which the values of the controlled variables are obtained by solving an optimization problem using GA to obtain the desired output.

Two different cases were investigated using the proposed hybrid ANN-GA method and presented below. The desired output to be optimized in the case studies was the chiller energy consumption while the input operating parameters to be calculated were different for different cases. The global optimization of the chiller plant was not the main concern in the cases. The idea behind the proposed control strategy was to satisfy a certain chiller demand, and determine the values at which the controlled input variables had to be set to minimize the chiller energy consumption at the current ambient and working conditions. The results by ANN-GA control were compared with simulation data by TRNSYS to evaluate the accuracy of the proposed approach.

Two different cases are investigated to demonstrate the hybrid methodology: (1) variable condensing temperature control and variable speed fan control (CTC+VSF); (2) variable condensing temperature control coupling variable speed fan control and variable water mist generation rate (CTC+VSF+VWM). In Case 1 the set points of the condensing temperature of the two refrigeration circuits were the controlled input variables which were set to minimize the chiller energy consumption. In Case 2 the controlled input variables of the chiller system were the set points of the condensing temperature of the two refrigeration circuits and the optimal water mist generation rate of each water mist circuit.

6.2.1 CTC with VSF

For the air-cooled chiller equipped with variable speed condenser fans operating under variable condensing temperature control, the data for developing the chiller model were from the simulation data of chillers serving the representative office building using TRNSYS. For better developing the chiller model using ANN, a number of simulations were required. It is important to cover the lower and upper extreme conditions of the cases to be investigated, as the neural network learns all the range of possible values and hence extrapolation is not needed. For this reason, all cases were simulated for the working conditions of a typical weather year. In this way, a database was generated with the combination of the correlation of set point of condensing temperature on chiller energy consumption for various cases.

The "operating data" would be used to train, validate and test the ANN model, and there were 3051 data patterns in total for this study. From the operating data set, 60% was selected randomly for the neural network training, 20% was used for validation and the remaining 20% of the total data was employed for testing the network. When the data had been collected and arranged, the next step in training a network was to create the neural network.

6.2.1.1 Neural network construction

The model was developed with Matlab using the neural network toolbox (Beale, Hagan et al. 2011). The architecture of the three-layer BP network for this case was shown in Figure 6.3. As one hidden layer could be sufficient to map an arbitrary function to any degree of accuracy, the ANN model with just one hidden layer was investigated in this research. The input parameters of an ANN had to be selected carefully because they would significantly affect the performance of the ANN. In the present case, the inputs included the dry bulb temperature (T_{db}) of the entering

condenser air, chiller load sharing by refrigeration circuit 1 (Q_{cl1}), chiller load sharing by refrigeration circuit 2 (Q_{cl2}), temperature of supply chilled water (T_{chws}), chilled water mass flow rate (m_{chw}), degree of subcooling (T_{cdsc}), degree of superheating (T_{evsh}), set point of condensing temperature of refrigeration circuit 1 (T_{cdsp1}) and set point of condensing temperature of refrigeration circuit 2 (T_{cdsp2}). The outputs from the ANN models were the speed of the variable speed fan of refrigeration circuit 1 (V_{cf1}), the speed of the variable speed fan of refrigeration circuit 2 (V_{cf2}) and the chiller power consumption (E_{ch}). In this case, the set points of condensing temperature of refrigeration circuits 1 and 2 were the controlled input variables which were set to achieve the desired chiller energy consumption.

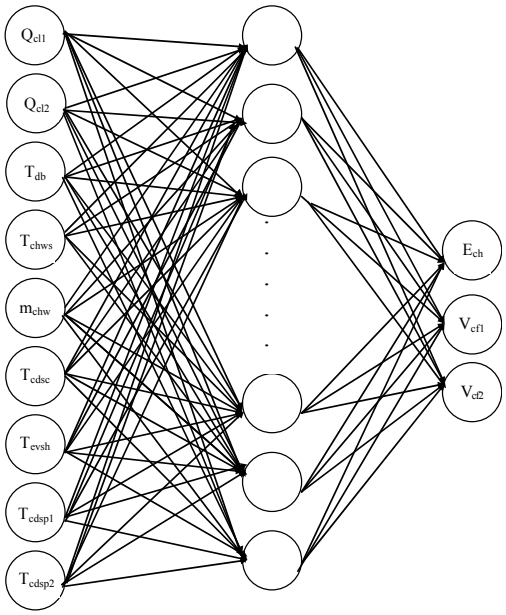

Figure 6.3 ANN architecture for Case 1

Since there was no explicit rule to determine either the number of neurons in the hidden layer or the number of hidden layers, the trial and error method was applied to find the best solution. In order to achieve the optimal result, different training algorithms and different number of neurons in the hidden layer were performed. The training algorithms included Levenberg-Marquardt backpropagation, Batch gradient descent with momentum, Variable learning rate backpropagation, BFGS quasi-

Newton backpropagation and Bayesian regulation backpropagation, which were popular training algorithms. For all BP algorithms, a three-layer ANN with a sigmoid transfer function in the hidden layer and a linear transfer function in the output layer was developed.

In this research, an iterative process for the proper selection of the number of neurons in the hidden layer was carried out. It started with a reduced number of neurons, and then increased this number by one at a time until the addition of a new neuron did not further improve the performance of the neural network. Eqs. (2.9-2.13) in Chapter 2 were introduced for estimating the optimal number of hidden neurons in the ANN model. Although these five formulas suggested different optimal number of hidden neurons in the feed-forward neural network, they could provide the possible range of the optimal number of hidden neurons. According to these equations, it was recommended that the range of the neuron nodes in the hidden layer for this case was from 4 to 13. To be sure to achieve the optimal network architecture, the neurons in the hidden layer varied in larger range from 3 to 15, covering the recommended range of the neurons in the hidden layer. The results for finding the optimal number of neurons in a single hidden layer by trial and error were shown in Table 6.1, and the statistical values of MSE, r, R^2 and the training time were given for different training algorithms with 3-15 neurons in the hidden layer.

It could be identified in all cases that the training accuracy improved by increasing the number of hidden neurons, as indicated by the smaller MSE and r values and R^2 values approaching to 1. However, when the number of hidden neurons was greater than a certain value, the training errors and the testing errors began to increase, and the ANN with larger number of hidden neurons became more complex.

Compared with the different training algorithms with different neurons in the hidden

layer, the best one with minimum mean square absolute error was selected, which was the Bayesian regularization backpropagation with 11 neurons in the hidden layer and the minimum MSE was 0.002. For the Bayesian regularization backpropagation in this research, it was applied in combination with Levenberg-Marquardt training (in conjunction with early stopping technique). Bayesian regularization minimizes a linear combination of squared errors and weights, and then determines the correct combination so as to produce a neural network with noticeable advantage over other training algorithms on generalization, especially when the data sets are smaller. The Bayesian regularization has higher stability together with excellent training performance and testing performance. However, Bayesian regularization method generally takes longer to converge. Levenberg-Marquardt algorithm has faster convergence rate than other training algorithm. To make fully use of their advantages, Bayesian regularization with Levenberg–Marquardt algorithm was selected to act as the training function in this research, which updated the weight and bias values according to Levenberg-Marquardt optimization.

Table 6.1 Comparison of the candidate network structures

BP algorithms	*Neurons*	*Time(s)*	*MSE*	*r*			R^2		
				E_{ch}	R_{cf1}	R_{cf2}	E_{ch}	R_{cf1}	R_{cf2}
Levenberg-Marquardt backpropagation	3	14.53	2.4852	0.9997	0.9994	0.9998	0.9988	0.9994	0.9995
	4	45.25	0.5542	0.9995	0.9988	0.9999	0.9969	0.9990	0.9997
	5	11.97	0.6846	0.9998	0.9998	0.9998	0.9996	0.9996	0.9997
	6	9.42	0.0979	0.9999	0.9999	0.9998	0.9999	0.9998	0.9997
	7	20.41	0.2193	1.0000	1.0000	1.0000	1.0000	1.0000	1.0000
	8	11.75	0.0608	0.9994	0.9994	1.0000	0.9987	0.9989	0.9999
	9	14.08	0.1817	0.9983	0.9979	1.0000	0.9964	0.9956	1.0000
	10	18.51	0.0396	1.0000	1.0000	1.0000	1.0000	1.0000	1.0000
	11	16.81	0.0155	1.0000	1.0000	1.0000	1.0000	1.0000	1.0000
	12	18.40	0.0551	0.9999	0.9999	1.0000	0.9999	0.9999	1.0000
	13	14.05	0.0715	1.0000	1.0000	1.0000	1.0000	0.9999	1.0000
	14	18.88	0.1391	1.0000	1.0000	1.0000	0.9999	1.0000	1.0000
	15	14.05	0.2791	1.0000	1.0000	1.0000	1.0000	0.9999	1.0000
Batch gradient descent with momentum	3	72.17	174.6957	0.9090	0.8833	0.9200	0.8251	0.7601	0.8448
	4	74.22	73.75852	0.9690	0.7916	0.9966	0.9330	0.5232	0.9910
	5	81.00	156.1097	0.9124	0.9553	0.9506	0.8286	0.9078	0.9022
	6	336.76	112.5037	0.9405	0.9254	0.9751	0.8831	0.8377	0.9491
	7	76.80	248.0053	0.8707	0.8012	0.9688	0.7577	0.5629	0.9383
	8	79.36	124.771	0.9120	0.7599	0.9458	0.8281	0.5024	0.8936
	9	82.15	65.57768	0.9697	0.8823	0.9419	0.9352	0.7687	0.8846
	10	85.19	146.1974	0.9300	0.8152	0.9651	0.8553	0.5192	0.9286
	11	81.68	77.22071	0.9610	0.9041	0.9803	0.9235	0.7885	0.9593
	12	91.94	102.7911	0.9355	0.8881	0.9743	0.8744	0.7517	0.9492
	13	84.94	44.10117	0.9795	0.9116	0.9892	0.9530	0.7888	0.9758
	14	85.83	85.83246	0.9674	0.9398	0.9951	0.9291	0.8768	0.9893
	15	91.57	31.50485	0.9856	0.9219	0.9744	0.9708	0.8455	0.9466
Variable learning rate backpropagation	3	9.94	136.0684	0.9538	0.8736	0.9901	0.8926	0.7590	0.9800
	4	10.62	14.83162	0.9939	0.9828	0.9971	0.9875	0.9558	0.9941
	5	11.89	32.00292	0.9880	0.9875	0.9959	0.9754	0.9703	0.9918
	6	11.72	20.72765	0.9907	0.9845	0.9951	0.9816	0.9685	0.9903
	7	12.53	36.13948	0.9855	0.9763	0.9973	0.9707	0.9479	0.9945
	8	12.09	29.10651	0.9869	0.9799	0.9976	0.9699	0.9548	0.9951
	9	12.53	17.19014	0.9930	0.9702	0.9975	0.9857	0.9409	0.9946
	10	15.45	16.74292	0.9931	0.9230	0.9956	0.9862	0.8469	0.9908
	11	12.80	27.63442	0.9880	0.9796	0.9974	0.9759	0.9488	0.9949
	12	14.06	27.81523	0.9887	0.9054	0.9933	0.9726	0.7879	0.9859
	13	14.56	32.15606	0.9860	0.9858	0.9983	0.9722	0.9694	0.9965
	14	11.50	16.28079	0.9897	0.9776	0.9880	0.9793	0.9554	0.9747
	15	11.98	11.93889	0.9948	0.9306	0.9911	0.9887	0.8653	0.9811
BFGS quasi-Newton backpropagation	3	10.50	11.4720	0.9955	0.9912	0.9992	0.9911	0.9821	0.9984
	4	13.12	8.9750	0.9970	0.9953	0.9997	0.9933	0.9905	0.9994
	5	12.35	6.8020	0.9971	0.9902	0.9996	0.9941	0.9799	0.9992
	6	12.22	6.7807	0.9972	0.9889	0.9997	0.9941	0.9774	0.9994
	7	21.44	0.6432	0.9997	0.9994	0.9999	0.9992	0.9987	0.9998
	8	15.96	3.0147	0.9982	0.9973	0.9996	0.9961	0.9942	0.9992
	9	13.49	6.6763	0.9969	0.9934	0.9998	0.9938	0.9865	0.9996
	10	12.70	0.9841	0.9994	0.9967	0.9996	0.9987	0.9927	0.9993
	11	13.48	1.7153	0.9989	0.9973	0.9992	0.9978	0.9946	0.9984
	12	15.67	2.0228	0.9992	0.9992	0.9997	0.9982	0.9983	0.9994
	13	17.40	1.3470	0.9995	0.9985	0.9997	0.9989	0.9970	0.9994
	14	15.85	2.0604	0.9991	0.9980	0.9997	0.9980	0.9959	0.9994
	15	17.44	0.7312	0.9997	0.9995	0.9997	0.9994	0.9987	0.9995
Bayesian regulation backpropagation	3	39.62	3.2791	0.9982	0.9979	0.9998	0.9963	0.9950	0.9997
	4	28.79	1.2250	0.9985	0.9989	0.9997	0.9968	0.9974	0.9995
	5	22.36	0.8443	0.9999	0.9999	0.9999	0.9998	0.9997	0.9997
	6	31.06	0.5517	0.9999	0.9999	1.0000	0.9998	0.9997	1.0000
	7	41.74	0.4336	1.0000	1.0000	1.0000	1.0000	0.9999	1.0000
	8	66.26	0.0750	1.0000	0.9999	1.0000	0.9999	0.9999	1.0000
	9	20.80	0.1895	1.0000	1.0000	1.0000	1.0000	1.0000	1.0000
	10	24.25	0.1355	0.9999	1.0000	1.0000	0.9999	0.9999	1.0000
	11	135.52	**0.0020**	1.0000	1.0000	1.0000	1.0000	1.0000	1.0000
	12	42.72	0.1358	0.9999	0.9997	1.0000	0.9997	0.9994	1.0000
	13	42.06	0.0511	0.9999	0.9998	1.0000	0.9997	1.0000	1.0000
	14	120.38	0.2869	1.0000	1.0000	1.0000	0.9999	0.9999	1.0000
	15	58.26	0.2660	1.0000	1.0000	1.0000	1.0000	0.9999	1.0000

The number of neurons in a hidden layer greatly influences the network performance.

Figure 6.4 demonstrated how the neural network performance MSE varied with the number of neurons in the hidden layer for the Bayesian regularization with Levenberg–Marquardt algorithm. The optimal architecture of the ANN model could be determined based on the minimum value of the MSE of the training and testing set. As shown in Figure 6.4, the MSE of the network was much greater (MSE 3.2791) for the ANN with 3 hidden neurons, and MSE decreased with more neurons in the hidden layer, and MSE reached its minimum value of 0.002 with 11 hidden neurons. When the number of neurons was greater than 11, MSE showed a gradual increase from 0.0551 to 0.2869. Hence, the Bayesian regularization in combination with Levenberg–Marquardt algorithm with 11 neurons in the hidden layer appeared to be most optimal topology for this case. That is, in this case, the best ANN model had 9-11-3 architecture, which meant that there were 9, 11, and 3 neurons in the input, hidden, and output layers, respectively. Figure 6.3 shows the architecture of the ANN used for this case.

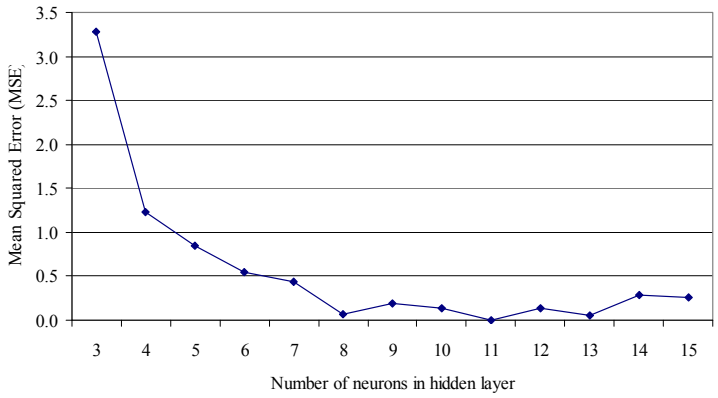

Figure 6.4 The networks performance MSE against neurons in the hidden layer

6.2.1.2 Performance analysis of MLP neural network

When the architecture of the ANN model was determined, the neural network model employing backpropagation was trained, validated and tested with the training set, validation set and the test set, respectively. Then, an analysis on the training

performance and testing performance of the neural network was examined. The neural network would find the input–output map by analyzing the training data set repeatedly. The neural network's weights were updated during the network training phase, which was needed to monitor how well the neural network was learning. As the Bayesian regularization with Levenberg–Marquardt algorithm was applied in this research, the generalized error function was used as the performance indicators of the neural network.

The curves of the generalized error of the neural network for this case versus iteration were shown in Figure 6.5. As the neural network learned, the error was converging to zero. The training was considered to have reached convergence if both the sum of squared error (SSE) and the sum of squared weights (SSW) stabilized after the iterations. The generalized errors in the validation set and the testing set were also shown on the same figure. As could be identified from Figure 6.5, the training error, validation error and the testing error decreased similarly.

When the training was completed, it was necessary to check the network performance and determine if any changes were needed for the training process, the network architecture or the data sets. During the training, critical observations were the performance, the magnitude of the gradient and the number of validation checks. The magnitude of the gradient and the number of validation checks were used to terminate the training. The number of validation checks represented the number of successive iterations that the validation performance failed to decrease. When this number reached 6 (the default value), the training would stop (Beale, Hagan et al. 2011), as shown in Figure 6.6. Figure 6.6 was the training state plot showing the progress of other training variables, including the gradient magnitude and the number of validation checks. The validation error reduced in the early phase of training,

similar to the training set error. However, the error on the validation set would begin to increase when the neural network tended to overfit the data (Haykin 1999). Figure 6.5 illustrates the changes in the error level for training, validation and testing during the iterations. The training stopped after 625 iterations for the Bayesian regularization in combination with Levenberg–Marquardt algorithm after 6 validation checks. The validation performance reached a minimum at the 619th iteration. The training continued for 6 more iterations as the differences between the training error and the validation error started to increase.

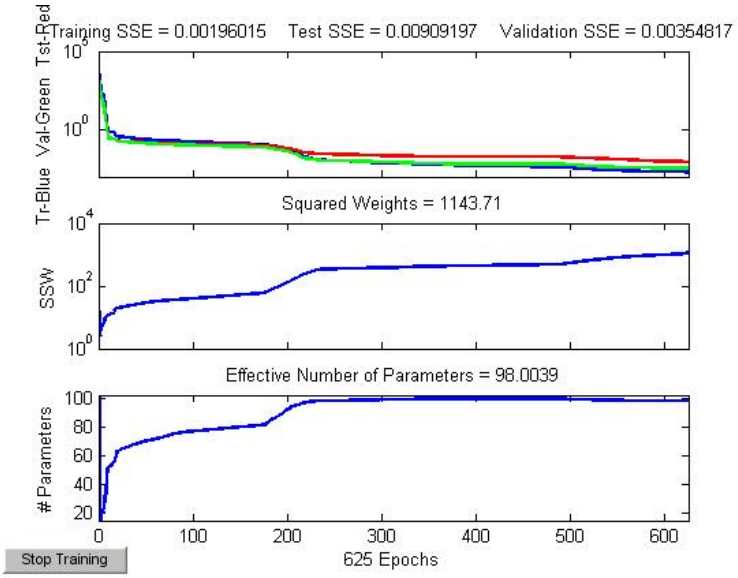

Figure 6.5 The converging trends of training, validation and testing subsets

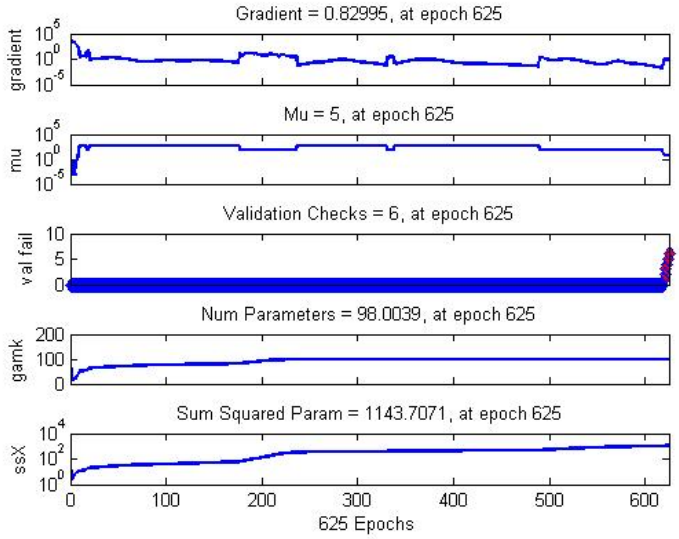

Figure 6.6 Training state of the ANN model

After training, the trained neural network was capable of giving a certain output whenever input factors were offered. The next step was to validate the trained neural network. The performance of a trained network could be assessed to some extent by the errors on the training, validation and test sets as shown in Figure 6.5, and it was also useful to investigate the network response in more detail. One option was to perform a regression analysis between the outputs of the network and the corresponding targets, which was one of the most popular techniques for data analysis. If the training was perfect, the network outputs and the targets would be exactly equal. The regression correlation coefficient (*R*-value) between the network outputs and the corresponding TRNSYS simulation results were shown in Figure 6.7 for training, validation, testing and the whole datasets. The dashed line in each axis represented a perfect matching, where the outputs were equal to targets. The solid line represented the best fit linear regression line between outputs and targets. *R*-values of 1, 0.9999, 0.9999 and 0.9999 were obtained for the training, validation, testing and the whole datasets, respectively. This demonstrated that the ANN

predicted values were very close to the actual values for all the datasets, and there was an exact linear relationship between outputs and targets.

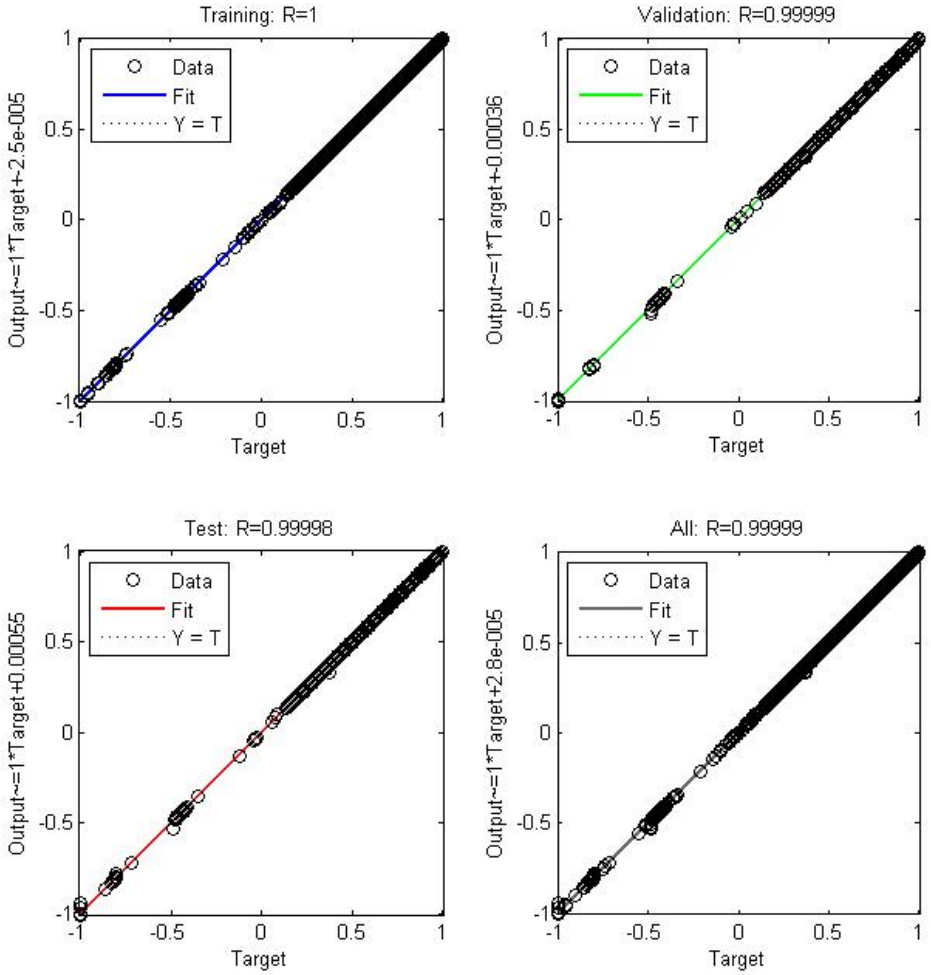

Figure 6.7 Performance of the ANN model (Case 1)

The regression analysis results of each output between the ANN predicted values and the simulated values by TRNSYS were shown in Figure 6.8 for this case, including the chiller power consumption, speeds of condenser fans in the refrigeration circuit 1 and refrigeration circuit 2. It should be noted that the comparisons in Figure 6.8 were made using values only from the test data set, which was not introduced to the ANN model during the training process. All graphics were provided with a correlation line indicating the curve fit and a ±5% error band.

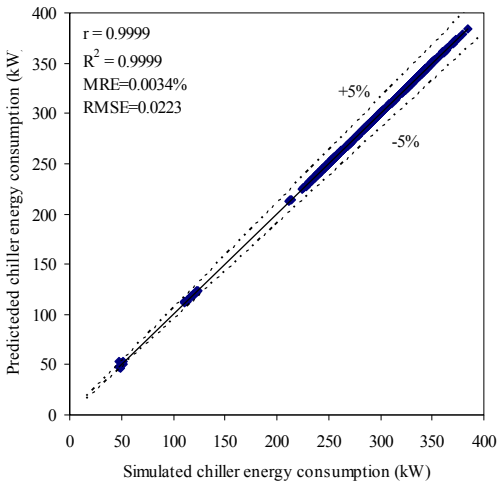

(a) Chiller power consumption

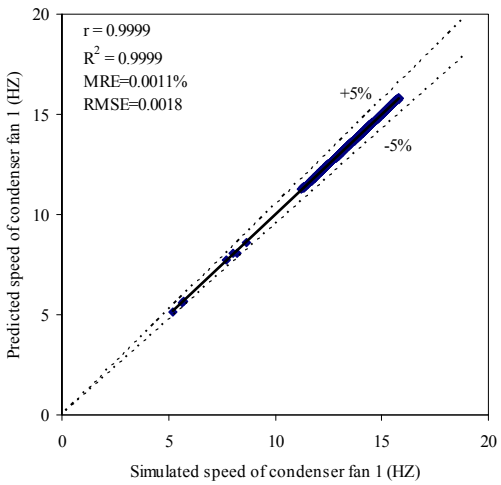

(b) Condenser fan speed (Circuit 1)

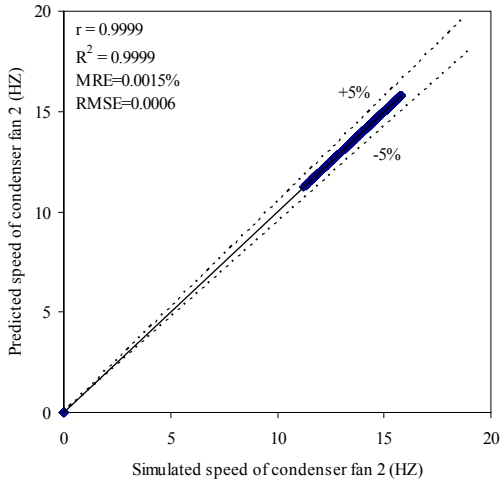

(c) Condenser fan speed (Circuit 2)

Figure 6.8 Comparison of ANN modeled and TRNSYS simulated values for Case 1

As shown in Figure 6.8(a), the ANN predictions for the chiller power yielded a correlation coefficient (R) of 0.9999, a coefficient of determination (R^2) of 0.9999, a mean relative error (MRE) of 0.0034% and a root mean square error (RMSE) of 0.0223 kW with the simulated data by TRNSYS. These values revealed that the ANN predicted chiller power consumption very well in a wide range of operating conditions. For the speed of the condenser fans, the statistical performances of the predictions were almost as good as those obtained in chiller power consumption predictions, as shown in Figure 6.8(b). The ANN predictions for this parameter could

achieve an R value of 0.9999, a R^2 of 0.9999, a MRE of 0.0011% and a RMSE of 0.0018 HZ. The results demonstrated that the predictions of ANN to the speed of the variable speed condenser fan were quite accurate and had good agreement according to the characteristic parameter R, R^2 and RMSE, as shown in Figure 6.8.

As indicated in Figures 6.7 and 6.8, a close linear relationship was observed between outputs and targets simulated by TRNSYS, and hence the well trained ANN could be regarded to have achieved the ability to accurately map the chiller performance. The performance map based on the ANN would be used as the objective function of the optimization problem.

6.2.1.3 Formulation of optimization problem

In this study, an optimization problem could be formulated to find the solutions (optimal set points of condensing temperature for two refrigeration circuits) that would minimize the chiller energy consumption, when the other input parameters were specified. In addition to the energy use, the operation of the chiller system was subjected to constraints for proper operation of the mechanical system and constraints for maintaining indoor thermal comfort. The chilled water supply temperature T_{chws} should be set properly to avoid freezing in the evaporator and to provide dehumidification of the air in the cooling coil. For cooling and dehumidification purpose, the minimum and maximum perturbations of T_{chws} were 5 and 9°C, respectively (Fong, Lee et al. 2010; Yu and Chan 2006b). The possible variations in the degree of subcooling (T_{cdsc}) and the degree of superheat (T_{evsh}) were 1–6°C and 4–9.5°C, respectively (Yu and Chan 2006b).

Mathematically the optimal operation problem was stated as follows:

$$Min \qquad J = E_{cc} + E_{cf} \tag{6.10}$$

subject to: $20 \le T_{cdsp1} \le 45$

$20 \le T_{cdsp2} \le 45$

$T_{chwr,low} \le T_{chwr} \le T_{chwr,high}$

$T_{cdsc,low} \le T_{cdsc} \le T_{cdsc,high}$

$T_{evsh,low} \le T_{evsh} \le T_{evsh,high}$

Since the aim was to find a feasible optimal solution, penalty functions were used to penalize infeasible solution for handling the nonlinear constraints whenever one or more constraints were violated. The penalty was imposed when the set point of condensing temperature was not within [20, 45]. When this condition occurred, the objective was penalized for the individual. The fitness function of GA was revised to accommodate the penalty and was expressed in the following equation.

$$Min \qquad J = E_{cc} + E_{cf} + C \tag{6.11}$$

In Eq. (6.11), C is a positive constant and should be large enough to avoid the corresponding chromosome being selected as the optimal value. It is defined as follow:

$$C = \begin{cases} 500 & \text{If } T_{cdsp} > 45 \text{ or } T_{cdsp} < 20 \\ 0 & \text{If } 20 \le T_{cdsp} \le 45 \end{cases}$$

6.2.1.4 Optimization results by GA

A key feature of this work was that the optimal set points of the condensing temperature were obtained from the AI controller based on the specified values for the other 7 uncontrolled input variables. The AI controller applied GA to find the optimal set points of the condensing temperature to minimize the chiller energy consumption. Each input parameter was specified within a pre-determined range based on the chiller operation. Therefore, the optimization problem was to find the

optimal set points of the condensing temperature for the two refrigeration circuits, while the chiller system satisfied the chiller load with the least compressor and condenser fan energy consumption. The outline of the hybrid optimization algorithm using ANN and GA was given in Figure 6.2.

In this stage, GA was performed to optimize the fitness function for obtaining the optimal response and the corresponding combination values of the control variables within the feasible solution space of the system. Herein, a possible solution represented a chromosome; a performance index was served as the fitness value of the GA. Genes in the chromosome were formed by the values of the controlled variables and uncontrolled variables, which were set as continuous and fell in the specified range. The parameter bounds and the precision were determined according to the characteristics of the system.

There were a large number of conditions for the chiller operating under CTC for one year in the current study. As one of the objectives of this research was to investigate the possibility of artificial intelligent control combing ANN and GA to improve the chiller performance, several working conditions were considered to optimize the chiller operation as shown in Table 6.2, which were not used for developing the chiller model. When part load ratio was 0.5, one refrigeration circuit was full loaded. When the chiller operated at full load, both of the two refrigeration circuits were full loaded. For these two working conditions, the states of the staged refrigeration circuit(s) were similar, and hence the comparison between TRNSYS and ANN at part load ratio of 0.5 was not conducted.

The problem defined in Section 6.3.1.3 was optimized by real-coded GA. The population size was 50, and the maximum number of generations was 100. The crossover rate p_c was 0.80, and the mutation rate p_m was 0.085. The objective

function was a minimum problem of the chiller energy consumption. Figure 6.9 shows the evolution of the generations for one of the working conditions in Table 6.2, Test 7. Through the performance map model based on ANN, the predicted optimal set points of condensing temperature were obtained by GA. Table 6.2 listed the predicted optimal set points of condensing temperature and the corresponding values of variable combination.

6.2.1.5 Verification of the optimization result

There would be some differences between ANN outputs and the simulation results by TRNSYS, even if the ANN was properly trained. Therefore, using hybrid ANN-GA methodology, it was important to verify the optimal solutions using TRNSYS to ensure whether the solutions were acceptable.

Simulation by TRNSYS was carried out for the working conditions in Table 6.2. With the simulation results, the chiller electricity consumption obtained with the hybrid ANN-GA technique was compared with that obtained in the simulation. Table 6.2 shows the comparison between the TRNSYS simulated values and the parameters estimated by ANN-GA methodology for 12 data sets.

Mathematical validation demonstrated that the comparison between the artificial control and simulation data had a discrepancy lower than 5.8% in the worst case for the set point of condensing temperature. For the chiller power consumption, the discrepancy between the artificial control and simulation data was less than 4.5%. From this comparison, it demonstrated that the solutions by AI controller were near optimal.

The CPU runtime for GA to search for the optimal solutions was calculated by MATLAB, and all tests performed on a same computer, in the absence of any other major activity. The computer used was equipped with a Genuine Intel(R) CPU

E6750 @2.66GHz, 4GB of RAM; MATLAB version used is 7.0. Each test was performed three times for each function and for each algorithm studied. The CPU time was shown in Table 6.2. The small relative errors for the variables in conjunction with a computing time of about 80 s indicated that this strategy could be applied with a high level of confidence for the on-line control of the chiller system.

For the purpose of benchmarking, this study conducted a comparison on the chiller electricity consumption between the traditional head pressure control and the proposed advanced control. Table 6.2 revealed that the proposed approach outperformed the traditional HPC in terms of the chiller energy consumption, and it could be improved up to 21.5% for the listed conditions in Table 6.2.

Table 6.2 Comparison of ANN-GA with TRNSYS results (Case 1)

Test No.	*1*	*2*	*3*	*4*	*5*	*6*	*7*	*8*	*9*	*10*	*11*	*12*
PLR	0.25	0.25	0.25	0.25	0.75	0.75	0.75	0.75	1.0	1.0	1.0	1.0
T_{db} (°C)	20	25	30	35	20	25	30	35	20	25	30	35
m_{chw} (l/s)	53.3	53.3	53.3	53.3	53.3	53.3	53.3	53.3	53.3	53.3	53.3	53.3
T_{cdsc} (°C)	8	8	8	8	8	8	8	8	8	8	8	8
T_{evsh} (°C)	3	3	3	3	3	3	3	3	3	3	3	3
T_{cdsp1} (°C)	31.7	35.7	40.3	44.8	32.8	37.3	41.9	45.0	35.0	39.5	44.3	45.0
$^{*}T_{cdsp1}$ (°C)	32.6	35.1	41.3	43.9	31.6	37.9	41.5	44.7	33.5	37.3	42.1	44.1
Error (%)	2.8	-1.7	2.5	-2.1	-3.7	1.6	-1.0	-0.7	-4.3	-5.6	-4.9	-2.0
T_{cdsp2} (°C)	-	-	-	-	32.8	37.3	41.9	45.0	35.0	39.5	44.3	45.0
$^{*}T_{cdsp2}$ (°C)					30.9	37.4	41.6	44.8	33.6	38.3	40.3	43.9
Error (%)					-5.8	0.3	-0.7	-0.4	-4.0	-3.0	-4.5	-2.3
E_{ch} (kW)	58.3	65.1	73.3	83.5	260.3	291.9	331.3	381.3	270.7	304.5	346.8	403.5
$^{*}E_{ch}$ (kW)	59.6	64.3	75.1	81.7	253.3	291.7	331.6	382.9	258.6	299.0	338.9	387.8
Error (%)	2.2	-1.2	2.5	-2.2	-2.7	-0.1	0.1	0.4	-4.5	-1.8	-2.3	-3.9
$^{**}E_{ch}$ (kW)	*75.6*	76.4	78.1	83.7	322.7	328.6	341.6	382.1	317.3	326.6	348.7	404.3
Sav.(%)	*21.2*	15.8	3.8	2.3	21.5	11.2	2.9	0.2	18.5	8.5	2.8	4.1
t (s)	*81.3*	81.6	81.3	84.1	81.5	81.2	81.6	81.7	81.8	81.5	80.6	81.5

Note: * Values from AI controller;
** Chiller power consumption under head pressure control.

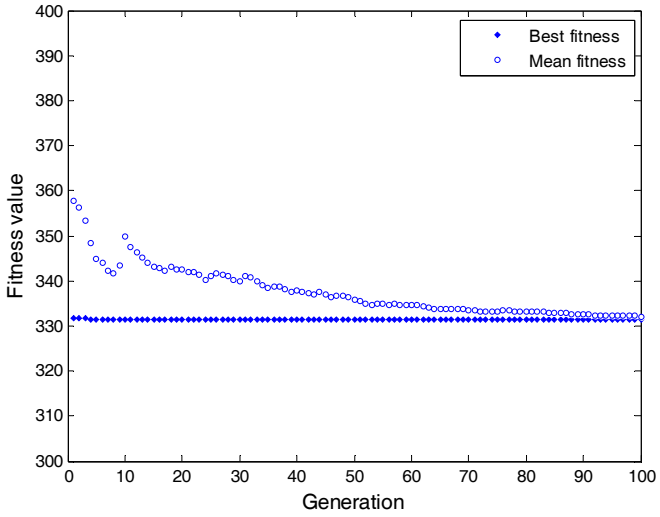

Figure 6.9 The convergence curve of the GA search for case 1

6.2.2 CTC with VSF and optimal waster mist

For the air-cooled chiller equipped with variable speed condenser fans and water mist pre-cooling operating under variable condensing temperature control, the data for developing the chiller model were generated from the simulation data of chillers serving the representative office building using TRNSYS in Chapter 5. The difference between this case and Case 1 was that the chiller energy consumption was controlled by not only the set points of condensing temperature of refrigeration circuits 1 and 2, but also the water mist generation rate of each water mist circuits.

6.2.2.1 Neural network construction

For the air-cooled chiller under CTC with optimal water mist generation rate, its performance map model was constructed by a BP neural network. The "operating data" simulated by TRNSYS would be used to train, validate and test the ANN model, and there were 3051 data patterns in total for this case. From the chiller operating data set, 60% were selected randomly for the neural network training, 20% were used for validation and the remaining 20% of the total data were employed for

testing the network. All the input–output data pairs were normalized to fall in the interval [−1, 1] in order to improve the predicted agreement.

As one hidden layer could be sufficient to map an arbitrary function to any degree of accuracy, the ANN model with just one hidden layer was investigated for this case. In the present case, the inputs included the dry bulb temperature (T_{db}) and RH of the entering condenser air, chiller load sharing by refrigeration circuit 1 (Q_{cl1}), chiller load sharing by refrigeration circuit 2 (Q_{cl2}), temperature of supply chilled water (T_{chws}), chilled water mass flow rate (m_{chw}), degree of subcooling (T_{cdsc}), degree of superheating (T_{evsh}), set point of condensing temperature of refrigeration circuit 1 (T_{cdsp1}), set point of condensing temperature of refrigeration circuit 2 (T_{cdsp2}), water mist generation rate of water mist circuit 1 (m_{wm1}) and water mist generation rate of water mist circuit 1 (m_{wm2}). The outputs from the ANN models were the condenser fan speed of refrigeration circuit 1 (V_{cf1}), the condenser fan speed of refrigeration circuit 2 (V_{cf2}), the chiller power consumption (E_{ch}) and the power consumption of high pressure pumps (E_{ch}). In this case, to minimize the chiller energy consumption, the controlled variables included the set points of condensing temperature of refrigeration circuits 1 and 2, the water mist generation rate of each water mist circuit.

Bayesian regularization with Levenberg–Marquardt algorithm was selected to act as the training function. Sigmoid transfer function was used as the activation function for the hidden layers, and linear function was used for the output layers. The neuron number of the hidden layer was determined by trial and error with different ANN configurations. Eqs. (2.9-2.13) in Chapter 2 were also introduced for estimating the optimal number of hidden neurons in the ANN model. Although these formulas suggested different optimal number of hidden neurons in the ANN model, they could provide the possible range of the optimal number of hidden neurons, and the

recommended range of optimal node number in the hidden layer from 4 to 14 for this case. By comparing the performance of the ANN model with different ANN configurations, the ANN model with 13 neurons in the hidden layer appeared to be the most optimal topology for this case, and hence the neural network structure 12-13-4 with testing RMSE, 0.0776, was selected to obtain a better performance, as shown in Figure 6.10. The tan-sigmoid transfer function was used as the activation function for the hidden layer, and linear transfer function was used as the activation function for the output layer.

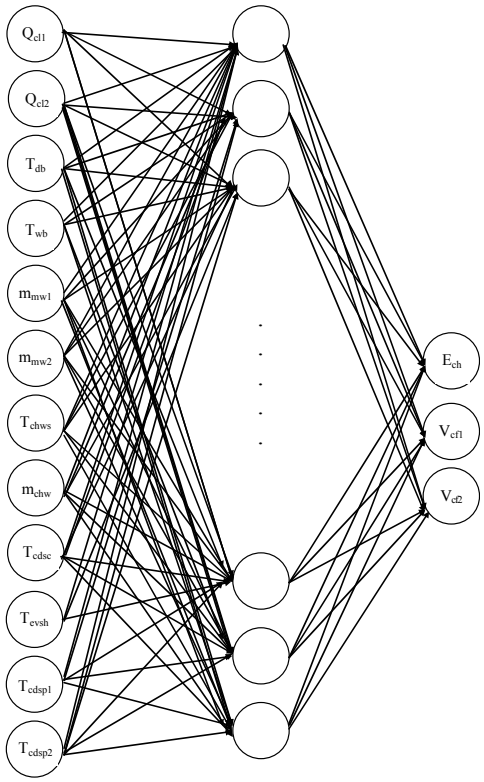

Figure 6.10 ANN architecture for Case 2

6.2.2.2 Performance analysis of MLP neural network

When the architecture of the ANN model was determined, the neural network model was trained, validated and tested with the training set, validation set and the test set, respectively. Figure 6.11 illustrates the convergence for training, validation and testing during the iterations. The training was stopped after 224 iterations for the

Bayesian regularization in combination with Levenberg–Marquardt algorithm after 6 validation checks, as shown in Figure 6.12.

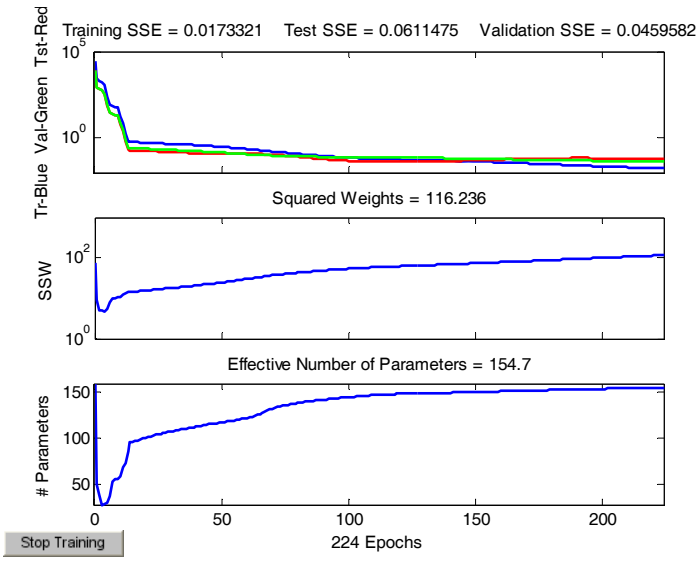

Figure 6.11 Convergence of training, validation and testing subsets for Case 2

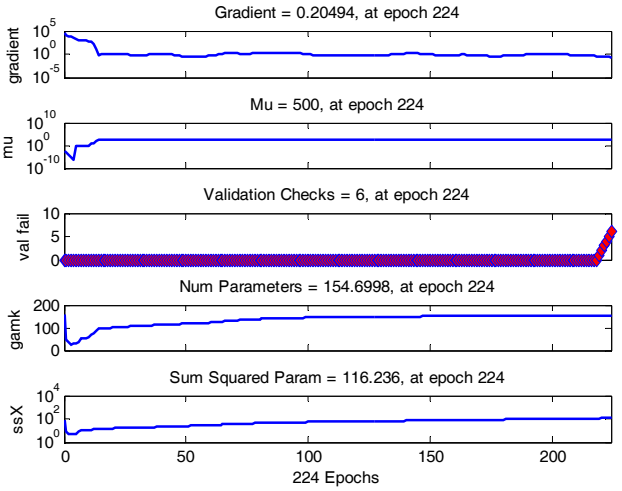

Figure 6.12 Training state of the ANN model for Case 2

Regression analysis was performed between the outputs of the network and the corresponding targets, which were the corresponding TRNSYS simulation outputs for this case, on the training, validation, testing and whole datasets as shown in Figure 6.13. The dashed line in each axis represented the perfect result, where the outputs were equal to targets. The solid line represented the best fit linear regression line between outputs and targets. For this case, *R*-values of 1, 0.9999, 0.9999 and

0.9999 were obtained for the training, validation, testing and the whole datasets, respectively. This demonstrated that the ANN could predict the chiller performance with higher confidence level.

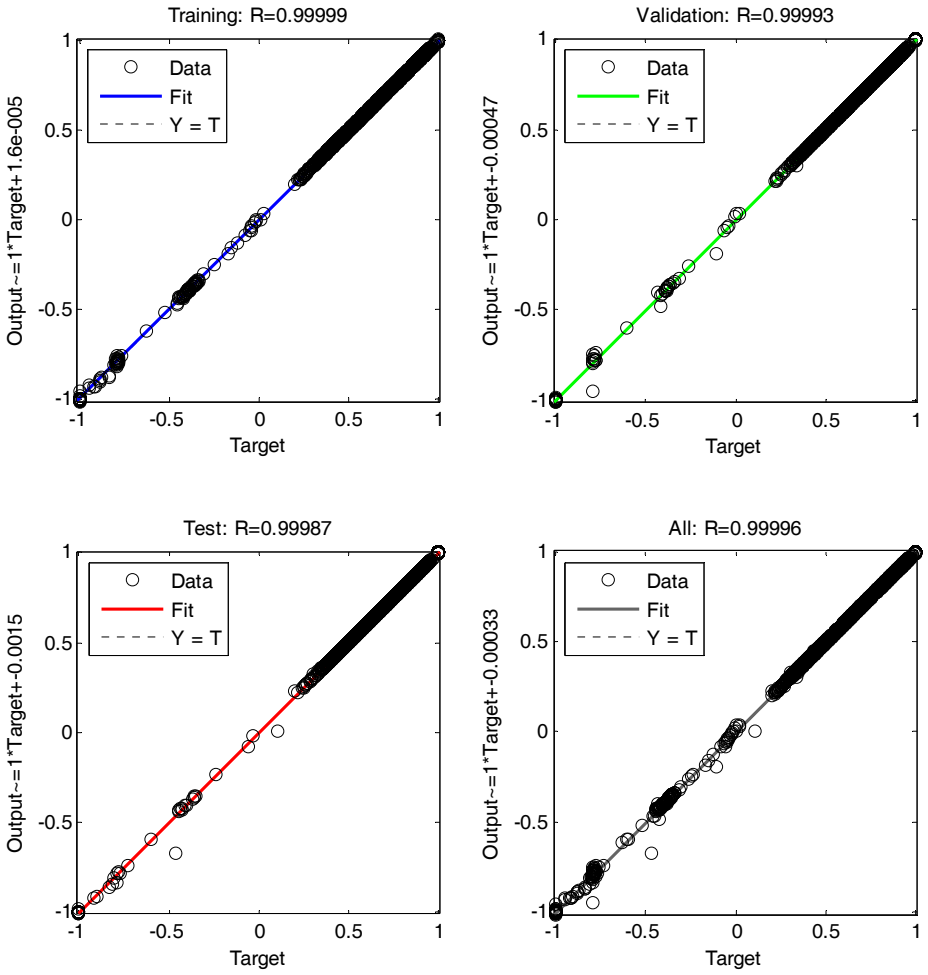

Figure 6.13 Performance of the ANN model (Case 2)

The regression analysis results of each output between the ANN predicted values and the simulated values by TRNSYS were shown in Figure 6.14 for this case, including the chiller power consumption, high pressure pump power consumption, speed of condenser fans in the refrigeration circuit 1 and refrigeration circuit 2. The comparisons in Figure 6.14 were made using values only from the test data set, which was not introduced to the ANN model during the training process. All graphics were provided with a correlation line indicating the curve fit and a ±5%

error band. For all the four output parameters, the correlation coefficient (R) was greater than 0.999, and the MRE was less than 0.05%, which confirmed that the agreement between outputs and targets was very good, and hence the well trained ANN could accurately map the chiller performance in wide ranges of operating conditions. The performance map based on the ANN would be used as the objective function of the optimization problem.

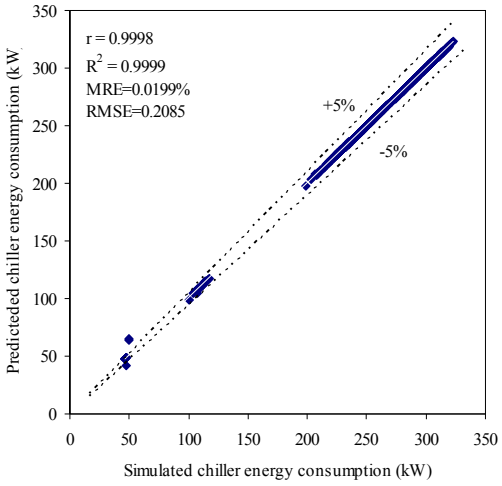

(a) Chiller power consumption

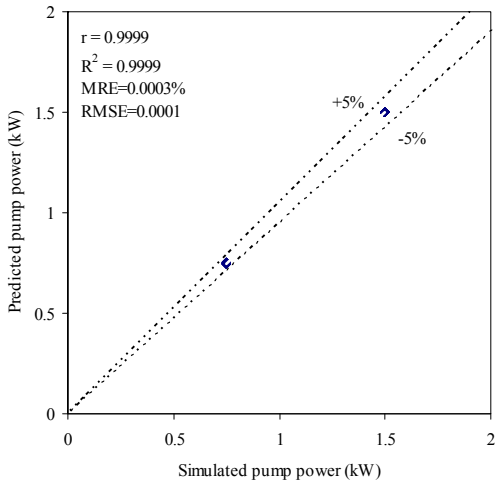

(b) High pressure pump power

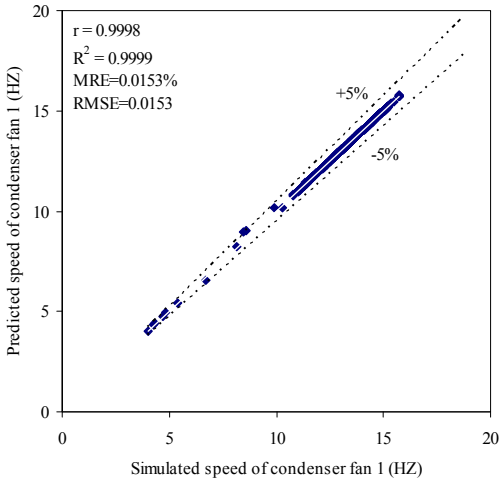

(c) Speed of condenser fan 1

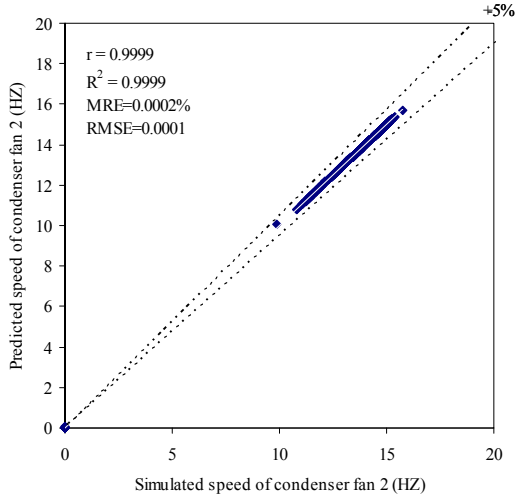

(d) Speed of condenser fan 2

Figure 6.14 Comparison of ANN modeled and TRNSYS simulated values for Case 2

6.2.2.3 Formulation of optimization problem

For this case, an optimization problem could be formulated to find the solutions (optimal set points of condensing temperature for two refrigeration circuits and water mist generation rate of each water mist circuit) that would minimize the energy consumption by chillers and high pressure pumps, under given working conditions. In addition to the energy use, the operation of the chiller system was subjected to constraints for proper operation of the mechanical system and constraints for maintaining indoor thermal comfort. The optimal operation problem for this case is stated as follows:

$$\textit{Min} \qquad J = E_{cc} + E_{cf} + E_{pump} \tag{6.12}$$

subject to:

$$20 \le T_{cdsp1} \le 45$$

$$20 \le T_{cdsp2} \le 45$$

$$T_{chwr,low} \le T_{chwr} \le T_{chwr,high}$$

$$T_{cdsc,low} \le T_{cdsc} \le T_{cdsc,high}$$

$$T_{evsh,low} \le T_{evsh} \le T_{evsh,high}$$

Since the aim was to find a feasible optimal solution, penalty functions were applied to penalize infeasible solution whenever one or more constraints were violated. The set point of condensing temperature should be within [20, 45]. When any constraints were violated, the objective was penalized for the individual. The fitness function of GA was accordingly revised to accommodate the penalty expressed as follow.

$$\textit{Min} \qquad J = E_{cc} + E_{cf} + E_{pump} + C \tag{6.13}$$

where C had the same meaning as defined in Eq. (6.11).

6.2.2.4 Optimization results by GA

With the trained ANN model, the artificial intelligent controller applied GA to find the optimal set points of the condensing temperature and water mist generation rate to minimize the energy consumption by chillers and high pressure pumps, while the chiller system satisfied the chiller load. GA was performed to optimize the fitness function for obtaining the optimal response and the corresponding combination values of the control variables within the feasible solution space of the system. A possible solution represented a chromosome, and a performance index was the fitness value of the GA. Genes in the chromosome were formed by the values of the controlled variables and the values of the uncontrolled variables, which were set as continuous and fell in the specified range.

As in the previous cases, several working conditions were considered to optimize the chiller operation as shown in Table 6.3, which were not used for developing the chiller model. The problem of this case was optimized by real-coded GA. The population size was 50, and the maximum number of generations was 100. The crossover rate p_c was 0.80, and the mutation rate p_m was 0.085. Figure 6.15 illustrates the evolution of the generations for Test 13 in Table 6.3. Through the performance map model based on ANN, the predicted optimal set points of condensing temperature and water mist generation rate were obtained for the corresponding values of variable combination, as shown in Table 6.3.

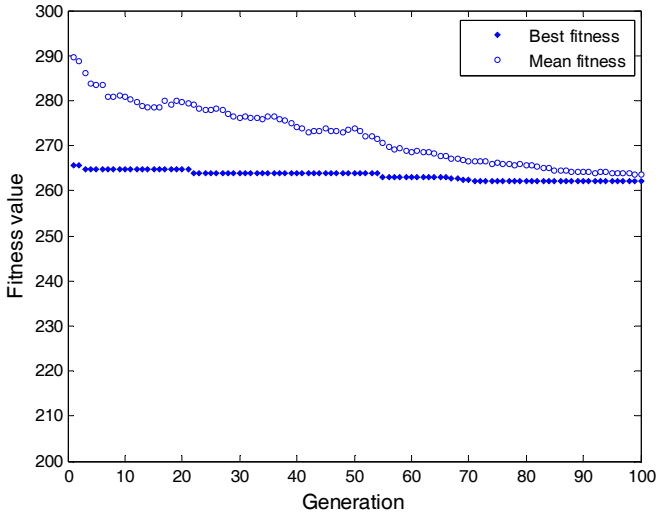

Figure 6.15 The convergence curve of the GA search for case 2

6.2.2.5 Verification of the optimization result

In order to test the AI control strategy, the results by AI control were compared with the simulation data by TRNSYS. Again, the mathematical validation of the AI control strategy demonstrated very satisfactory with the simulation data, as shown in Table 6.3. The percentage error compared to the simulation data was, as in Case 1, less than 10% for most conditions. The CPU runtime for GA to search for the optimal solutions was calculated by MATLAB, shown in Table 6.3. As expected, this methodology took longer time, above 90 s, to find the optimal parameters, but it was still acceptable for implementation in on-line control.

From the above two cases, the mathematical validation showed that the AI control, comparing to the simulation data, had a discrepancy less than 10% for most conditions. It is affirmed that this artificial intelligent methodology using ANN and GA can be successfully implemented in the chiller systems as an on-line control strategy.

Table 6.3 Comparison of ANN-GA with TRNSYS results (Case 2)

Test No.	*1*	*2*	*3*	*4*	*5*	*6*	*7*	*8*	*9*	*10*	*11*	*12*
PLR	0.25	0.25	0.25	0.25	0.25	0.25	0.25	0.25	0.75	0.75	0.75	0.75
T_{db} (°C)	20	20	25	25	30	30	35	35	20	20	25	25
RH (%)	50%	80%	50%	80%	50%	80%	50%	80%	50%	80%	50%	80%
m_{chw} (l/s)	53.3	53.3	53.3	53.3	53.3	53.3	53.3	53.3	53.3	53.3	53.3	53.3
T_{cdsc} (°C)	8	8	8	8	8	8	8	8	8	8	8	8
T_{evsh} (°C)	3	3	3	3	3	3	3	3	3	3	3	3
T_{cdsp1} (°C)	25.5	29.0	29.2	33.3	32.9	37.7	36.8	42.0	27.2	30.7	30.9	35.0
$^{*}T_{cdsp1}$ (°C)	26.3	27.8	28.3	33.9	32.1	36.9	37.5	41.1	27.9	31.6	30.1	33.8
Error (%)	3.1	-4.1	-3.0	1.8	-2.4	-2.1	1.9	-2.1	2.6	2.9	-2.6	-3.4
T_{cdsp2} (°C)	-	-	-	-	-	-	-	-	27.1	30.7	30.9	35.0
$^{*}T_{cdsp2}$ (°C)									27.8	29.1	29.9	35.7
Error (%)									2.6	-5.2	-3.2	2.0
m_{wm1}(l/s)	0.072	0.029	0.086	0.034	0.102	0.040	0.118	0.047	0.101	0.040	0.120	0.048
$^{*}m_{wm1}$(l/s)	0.068	0.031	0.081	0.038	0.106	0.037	0.111	0.051	0.107	0.036	0.127	0.049
Error (%)	-5.6	6.9	-5.8	11.7	3.9	-7.5	-5.9	8.5	5.9	-9.8	5.8	2.1
m_{wm2}(l/s)	-	-	-	-	-	-	-	-	0.100	0.040	0.120	0.048
$^{*}m_{wm2}$(l/s)									0.103	0.043	0.115	0.049
Error (%)									3.0	7.5	-4.1	2.1
E_{ch} (kW)	51.8	55.8	56.0	61.5	60.9	68.3	66.9	76.8	229.3	248.1	249.1	274.8
$^{*}E_{ch}$(kW)	53.6	53.7	54.1	65.3	58.5	66.1	69.3	73.6	233.7	253.8	241.9	260.3
Error (%)	3.5	-3.8	-3.4	6.2	-3.9	-3.2	3.6	-4.2	1.9	2.3	-2.9	-5.3
E_{ch} (kW)	*75.6*	*75.6*	76.4	76.4	78.1	78.1	83.7	83.7	322.7	322.7	328.6	328.6
Sav.(%)	29.1	29.0	29.2	14.5	25.1	15.4	17.2	12.1	27.6	21.4	26.4	20.8
t (s)	*90.9*	90.8	90.4	91.9	90.5	89.7	90.2	91.3	90.5	90.3	91.1	90.5

Table 6.3 cont. Comparison of ANN-GA with TRNSYS results (Case 2)

Test No.	*13*	*14*	*15*	*16*	*17*	*18*	*19*	*20*	*21*	*22*	*23*	*24*
PLR	0.75	0.75	0.75	0.75	1.0	1.0	1.0	1.0	1.0	1.0	1.0	1.0
T_{db} (°C)	30	30	35	35	20	20	25	25	30	30	35	35
RH (%)	50%	80%	50%	80%	50%	80%	50%	80%	50%	80%	50%	80%
m_{chw} (l/s)	53.3	53.3	53.3	53.3	53.3	53.3	53.3	53.3	53.3	53.3	53.3	53.3
T_{cdsc} (°C)	8	8	8	8	8	8	8	8	8	8	8	8
T_{evsh} (°C)	3	3	3	3	3	3	3	3	3	3	3	3
T_{cdsp1} (°C)	34.7	39.3	38.5	43.2	29.5	32.9	33.1	37.1	36.8	41.3	40.5	45
$^{*}T_{cdsp1}$ (°C)	36.9	41.6	37.6	42.5	31.3	34.1	31.5	35.5	37.3	43.9	43.6	43.3
Error (%)	6.3	5.9	-2.3	-1.6	6.1	3.6	-4.8	-4.3	1.4	6.3	7.7	-3.8
T_{cdsp2} (°C)	34.7	39.3	38.5	43.6	29.5	32.9	33.1	37.1	36.8	41.3	40.5	45
$^{*}T_{cdsp2}$ (°C)	36.6	41.3	38.8	42.6	31.5	33.8	31.0	35.3	38.1	43.1	44.1	43.7
Error (%)	5.5	5.1	0.8	-2.3	6.8	2.7	-6.3	-4.9	3.5	4.4	8.9	-2.9
m_{wm1}(l/s)	0.141	0.056	0.166	0.068	0.109	0.043	0.130	0.051	0.153	0.061	0.179	0.068
$^{*}m_{wm1}$(l/s)	0.131	0.061	0.156	0.077	0.116	0.049	0.121	0.053	0.151	0.067	0.168	0.073
Error (%)	-7.1	8.9	-6.0	13.2	6.4	14.0	-6.9	3.9	-1.3	9.8	-6.1	7.4
m_{wm2}(l/s)	0.141	0.056	0.166	0.068	0.109	0.043	0.130	0.051	0.153	0.061	0.179	0.068
$^{*}m_{wm2}$(l/s)	0.143	0.059	0.16	0.071	0.113	0.047	0.123	0.055	0.156	0.066	0.166	0.075
Error (%)	1.4	5.4	-3.6	4.4	3.7	9.3	-5.4	7.8	2.0	8.2	-7.3	10.3
E_{ch} (kW)	272.5	307.7	300.6	348.3	237.5	257.5	258.7	286.2	283.7	321.3	313.7	365.2
$^{*}E_{ch}$(kW)	282.3	323.3	293.6	334.6	251.8	269.1	243.9	271.5	293.9	339.5	336.2	380.1
Error (%)	3.6	5.1	-2.3	-3.9	6.0	4.5	-5.7	-5.1	3.6	5.7	7.2	4.1
E_{ch} (kW)	341.6	341.6	382.1	382.1	317.3	317.3	326.6	326.6	348.7	348.7	404.3	404.3
Sav.(%)	17.4	5.4	23.2	12.4	20.6	15.2	25.3	16.9	15.7	2.6	16.8	6.0
t (s)	*91.3*	93.8	92.9	92.7	90.5	89.9	90.3	90.6	90.5	91.1	91.3	90.8

Note: * Values from AI controller;
** Chiller power consumption under head pressure control.

6.3 Sensitivity analysis

As shown in Tables 6.2 and 6.3, the chiller efficiency might in fact be very sensitive to particular operating parameters, which need to be given particular attention during operation. Therefore, in order to improve the chiller efficiency, sensitivity analysis is conducted to identify the most influential factors that affect the energy consumption of the chiller system.

Sensitivity analysis consists of quantitative comparison of changes in outputs to changes in inputs (Lam and Hui 1996). In this study, the main output was the chiller COP while the inputs were eight parameters that were individually varied to reflect the impact of the variables on the chiller performance. Tables 6.4 and 6.5 summarize the considered inputs with their initial values used in the base case model and the possible range over which they were varied, when the chiller was operating at full load and at a part load ratio of 0.3, respectively. Upon the base model, the input variables were then adjusted individually to examine the effect of each factor on the chiller performance.

The temperature of the supply chilled water (T_{chws}) could deviate by 1 °C from its nominal set point of 7 °C , so its minimum and maximum perturbations were 6 and 8 °C, respectively (Yu, Chan et al. 2006). Outdoor dry bulb temperature ($T_{db)}$ could vary from 15 to 35 °C, and the outdoor relative humidity (RH) could vary from 40% to 100% for chillers operating in Hong Kong. The range of the chilled water flow rate (m_w) is related to its lower and upper limits given in the chiller specifications. The mist systems were designed to provide a mist generation rate of 0.0335 l/s for each refrigeration circuit, and 0,067 l/s for each refrigeration circuit was computed based on the calculation of peak mist generation rate. The degree of evaporator superheat (T_{evsh}) and that of condenser subcooling (T_{cdsc}) were assumed to be 6°C

and 3°C in the base case, as the possible variations for T_{evsh} and T_{cdsc} were 4–8°C and 1–6°C, respectively (Yu and Chan 2006b). In this study, the set point of the condensing temperature (T_{cdsp}) is 45°C, which is normally used under HPC. The lower limit for T_{cdsp} is 20 °C or (T_{cdae} + 5) °C, whichever is higher, and the highest T_{cdsp} is 50°C (Yu and Chan 2006b).

After completion of the analysis, the sensitivity influence coefficients (IC) were calculated to quantitatively measure the sensitivity of the models to changes in the inputs presented in Tables 6.4 and 6.5. IC is a ratio of the percentage change in output to the percentage change in input as shown in Eq. (6.14) (Lam and Hui 1996; Lam, Wan et al. 2008), where OP_{BC} and IP_{BC} are the base case output and input values, respectively, and ΔOP is the change in output resulting from a ΔIP change in input.

$$IC = \frac{\Delta OP / OP_{BC}}{\Delta IP / IP_{BC}} \tag{6.14}$$

Tables 6.4 and 6.5 show the sensitivity analysis results for various operating conditions, and Figure 6.16 shows the sensitivity influence coefficients of the eight studied operating parameters in terms of chiller performance, which indicate a high consistency in the outputs at full load and part load conditions. The negative IC values for $T_{db,}$, RH, T_{evsh}, m_{chw} and T_{cdsp1} suggest that chiller efficiency would decrease as these factors increase.

Outdoor dry bulb temperature has a dominating influence on the performance of air-cooled chillers with high values for both full load and part load conditions. It is ascertained that chiller efficiency tends to be sensitive to the set point of the condensing temperature. T_{cdsp} is responsible for 14.3% of the chiller performance at full load when the outdoor temperature is 35°C. When the outdoor temperature is 28°C and the part load ratio is 0.3, T_{cdsp} is responsible for 27.2% of the chiller

performance. It reveals that the variable set point of the condensing temperature is significant to improve the chiller performance, especially when the chillers are operating at part load ratio with mild weather conditions. For the air-cooled chillers with water mist pre-cooling, RH is also an important factor affecting the chiller performance, which is responsible for 9.5% and 5.8% of the chiller performance when the outdoor temperature is 35°C and 28°C, respectively. It reveals that water mist pre-cooling effect would be more significant with higher outdoor dry bulb temperature and lower relative humidity.

Table 6. 4 Variable list and input ranges for sensitivity analysis and IC (PLR=1).

Input Parameters	Base case value	Range	Sensitivity influence coefficient
T_{db} (°C)	33	15-35	-0.297
RH (%)	60	40-100	-0.051
T_{chws} (°C)	7	6-8	0.029
T_{cdsc} (°C)	3	1-6	-0.027
T_{evsh} (°C)	6	4-8	0.012
m_{chw} (l/s)	53.3	23.0-91.9	-0.019
m_{wm1} (l/s)	0.0335	0-0.067	0.022
m_{wm2} (l/s)	0.0335	0-0.067	0.022
T_{cdsp1} (°C)	45	38-50	-0.076
T_{cdsp2} (°C)	45	38-50	-0.076

Table 6.5 Variable list and input ranges for sensitivity analysis and IC (PLR=0.3).

Input Parameters	Base case value	Range	Sensitivity influence coefficient
T_{db} (°C)	28	15-35	-0.104
RH (%)	60	40-100	-0.016
T_{chws} (°C)	7	6-8	0.031
T_{cdsc} (°C)	3	1-6	-0.021
T_{evsh} (°C)	6	4-8	0.012
m_{chw} (l/s)	53.3	23.0-91.9	-0.013
m_{wm1} (l/s)	0.0335	0-0.067	0.007
m_{wm2} (l/s)	0.0335	0-0.067	0.007
T_{cdsp1} (°C)	45	33-50	-0.076
T_{cdsp2} (°C)	45	33-50	-0.076

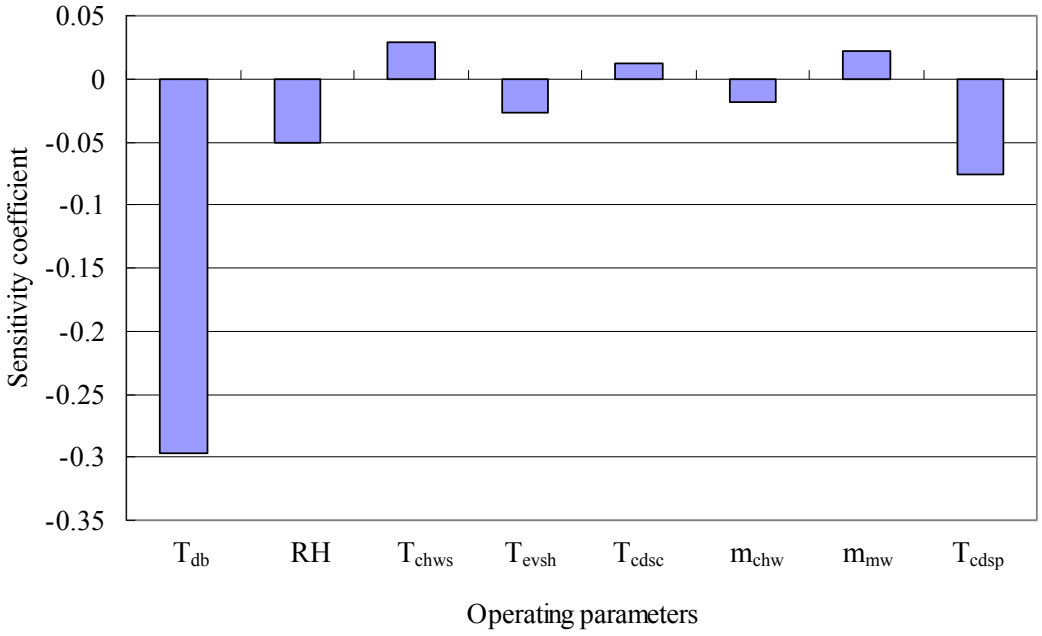

(a) Full load conditions

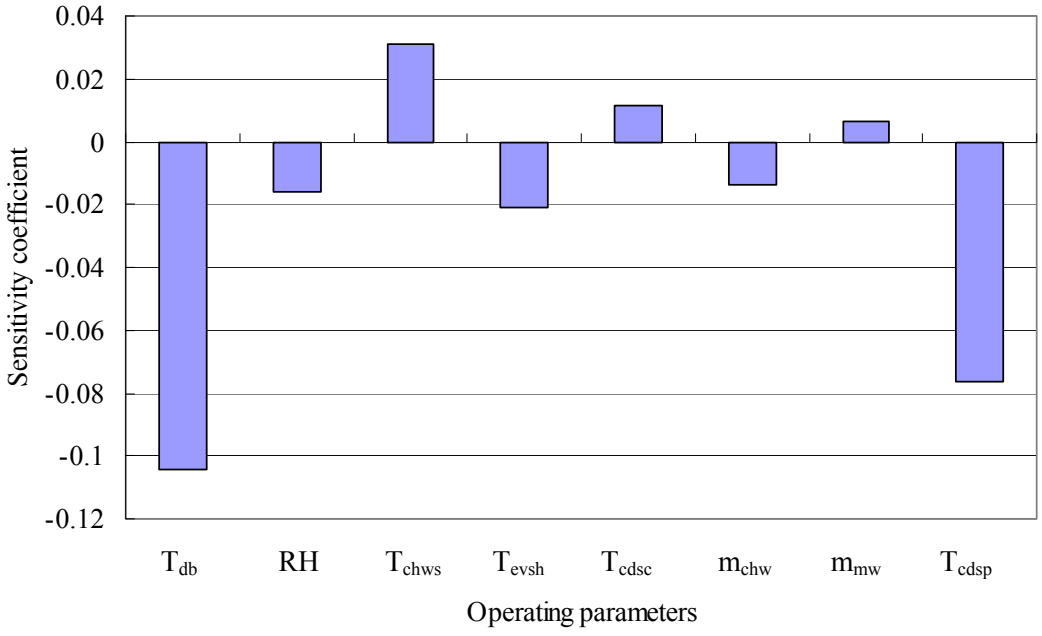

(b) Part load conditions (PLR=0.3)

Figure 6.16 Sensitivity influence coefficients

6.4 Summary

An approach to optimize the chiller operation based on artificial intelligence methods

was reported in this chapter. This chapter demonstrated the implementation of the simulation-based hybrid artificial intelligence control method combining ANN and GA. ANN was used to construct the performance map model of a chiller, and GA was then applied to find the parameter settings with an optimal response based on the ANN models.

The chiller database was generated from the simulation of chiller models using TRNSYS in Chapters 4 and 5. To demonstrate the possibility of artificial intelligent control combing ANN and GA to improve the chiller performance, two different cases were considered. The ANN models for the air-cooled chillers under different operating schemes were developed. The trained and validated ANN models were then integrated into the genetic algorithm serving as the evaluation function, and GA could search for the optimal or near-optimal controlled variables to operate the chillers efficiently. The optimization results were verified with simulation data using TRNSYS, and it confirmed that the hybrid ANN−GA technique was suitable for the optimal control for the air-cooled chillers.

Chapter 7 Conclusions and Recommendations

This chapter draws conclusions on the field investigation, experimentation and simulation for air-cooled chillers with advanced condenser features, including variable condensing temperature control, variable speed condenser fan control and water mist pre-cooling. A variety of studies have been performed, which has proved the promising application of the advanced condenser features. This research has also affirmed the feasibility of the hybrid intelligent control using ANN and GA for optimal control of air-cooled chillers for energy efficiency. The contributions of this research are summarized, and some research works requiring further investigations in the future are suggested.

7.1 Conclusions

Air-cooled chillers are widely used to provide space cooling in air-conditioned buildings due to their flexibility. The operation of chillers usually takes up the highest proportion of the total electricity consumption of buildings in regions of hot or warm climate. Low operational efficiency and undesirable control are part of the reasons for such high energy consumption. The deficient performance of air-cooled chillers is mainly due to the traditional head pressure control (HPC) under which the condensing temperature is kept high. New methods for improving chiller operation and energy efficiency are necessary.

This research focused on the optimal operation of air-cooled chillers with variable condensing temperature control (CTC) to lower the condensing pressure and reduce chiller power. The optimization problem was formulated and solved to find the optimal set point of condensing temperature and optimal water mist generation rate

under various conditions with least chiller energy consumption. To achieve this objective, a combination of field investigation, experimentation and system simulation was conducted. Through this research, how the operational efficiency of air-cooled chillers could be improved was demonstrated, and the implication of this improvement on the energy saving in the commercial building sector was assessed.

Field investigation has been conducted to identify the operating characteristics and energy performance of two existing chiller plants with and without water mist pre-cooling. Based on the detailed evaluation of the existing chilled water plants in the PolyU campus, it has been found that the condensing temperature fluctuates widely under traditional head pressure control, which results in an inadequate control of chiller operation. An experiment has been conducted on an air-cooled chiller with water mist system. When the water mist system was coupled to the air-cooled chillers, the condensing temperature dropped by up to 7.2°C, and the chiller COP could be improved in varying degrees by up to 18.6 during the experimental period. This affirms the benefit of applying water mist pre-cooling in the subtropical climate, let alone the hot and dry climate.

With the operating characteristics of the studied chillers, the thermodynamic models for the air-cooled chillers with twin refrigeration circuits with or without water mist system were developed using TRNSYS and validated using a wide range of operating data. Within the chiller models, the mass balance of refrigerant and energy balance are satisfied and the mechanistic relations between chiller components are taken into account. An algorithm is introduced to compute the number and speed of staged condenser fans by a set point of condensing temperature for the chiller operating under variable condensing temperature control or head pressure control. The integrated model for the chiller with water mist pre-cooling is sophisticated and

capable of controlling the optimal set point of condensing temperature and optimal water mist generation rate. With the aid of TRNSYS, extensive simulations were performed for various operating schemes, and the chiller performance was analyzed.

Under HPC with constant speed condenser fans, water mist pre-cooling enabled the condensing temperature drop by up to 7.8°C and 8.8°C with designed and optimal water mist generation rate, respectively. When RH was 50%, the COP of the chiller with designed and optimal water mist generation rate increased by varying degrees up to 22.6% and 26.8%, respectively. When the chiller operated under HPC but with VSF and optimal water mist generation rate, the COP could be improved up to 23.3%. When the chiller operated under CTC with constant speed condenser fans, the chiller COP could be improved in all operating conditions up to 35.4%. The use of variable speed condenser fans and CTC enabled the chiller COP to be improved further up to 51.8%.

It was noted that there were casual occurrences of decreased chiller COP due to unfavourable fan staging under HPC and extra pump power consumed for generating water mist. This indicated that it was undesirable to operate the chiller with water mist under HPC. To take full advantage of the water mist, HPC should be replaced by CTC and VSF. When the chiller operated with VSF, CTC, optimal water mist generation rate and the relative humidity was 50%, the chiller COP was improved most by up to 70.8%. The water consumption of the water mist system was small comparing to the total water losses for an open-loop cooling tower system with equivalent heat rejection capacity. This research demonstrates that a combination of CTC, VSF and water mist system coupled to air-cooled chillers is an energy-efficient and environmentally green technique.

The building and air-conditioning system of the representative office and hotel

buildings in Hong Kong have been developed using EnergyPlus. Simulation analyses were carried out to assess the electricity savings and cost effectiveness of individual and mixed uses of the measures, including variable condensing temperature control, variable speed condenser fans and water mist pre-cooling for the entering condensers air. The simulation results showed that the annual electricity consumption of air-cooled chillers dropped by up to 14.8% and 14.9% for the typical office building and hotel building when the improved condenser features of CTC, VSF and WM were implemented together. These energy effective measures would yield a long-term significance on reducing the electricity consumption by the commercial sector.

Many air-cooled chillers are designed with multiple refrigeration circuits connected in parallel to enhance the reliability improve the chiller performance, for which proper control for load sharing in the refrigeration circuits (CLS) is critical. Optimal CLS enabled the total electricity consumption of the chillers to drop by 4.2% under HPC. Under CTC with optimal CLS, the annual power consumption by chillers serving the typical office building could be saved by 9.6%.

Due to the complex nonlinear characteristics of chiller systems, an intelligent control technique, including neural network and genetic algorithm, was adopted in this research for the optimal control of the air-cooled chillers under various operating conditions. The neural network was applied to map the chiller performance, and genetic algorithm was adopted in searching optimal set points of condensing temperature and optimal water mist generation rate based on the predicted fitness values. The ANN predictions for the chiller power yielded a correlation coefficient (R) and coefficient of determination (R^2) greater than 0.99, which demonstrated that the predictions of ANN model were quite accurate. The chiller energy consumption could be saved up to 21.5% when CTC and VSF were applied. The saving was

further improved to 29.2% when CTC, VSF and optimal water mist generation rate were implemented. The results reveal that the hybrid ANN-GA approach is workable, and it outperforms the conventional HPC in achieving chiller energy saving. This intelligent control technique enables optimal condensing temperature control successfully, and the energy consumed by the compressors, condenser fans and high pressure pumps generating water mist can be minimized. The control performance is superior to the conventional head pressure control.

7.2 Recommendations

Major efforts of this study are made on the development of the variable condensing temperature control to improve the efficiency of air-cooled chillers. It would be desirable and valuable to make further efforts on the following three related aspects.

Experiment on water mist pre-cooling

The criteria for operating air-cooled chillers with water mist system for optimal efficiency should be investigated further with more experiments conducted at various combinations of chiller part load ratio, weather conditions, water mist generation rates and droplet sizes. Droplet sizes and distance between the nozzles and the condenser face shall be investigated in details in the future research work.

In the condenser air stream, the water mist generated may not fully evaporate before entering the condenser coil, and the unevaporized or excessive mist may cause damping of the condenser fins and coil. On the other hand, any presence of water mist in the air stream passing through the condenser coil may provide further evaporation and reject more heat from the refrigerant. This is an unknown process which deserves further research.

Experiment on variable condensing temperature control

The analyses performed in this research show that it is viable to implement variable condensing temperature control with regard to the potential of energy savings. Experimental tests should be carried out by the chiller manufactures to analyse how the control of condensing temperature with variable set points interacts with the capacity control, refrigerant flow control, condensing fan operation and compressor lubrication. It is important to ascertain the likely effects of lowering the condensing temperature on the precision of controlling the chilled water supply temperature and degree of superheat at compressor suction, and on the viscosity of lubricant to ensure proper compressor lubrication. In-site implementation and validation of the proposed variable condensing temperature control on chiller system are needed. More sophisticated control logic may be required to ensure stable operation with more precise control of the parameters in response to various ambient and load conditions.

Experiment on application of the hybrid ANN-GA control strategy

In this research, a hybrid artificial intelligent control using ANN and GA was proposed, and satisfactory preliminary results were achieved. The future work will be to refine the AI controller design and apply it to the control of an actual air-cooled condenser, and compare its performance with the one of the conventional controller. The experimental tests and field investigation will determine the applicability of the AI controller when applied to different chillers operating under conventional head pressure control. The AI controller in this research was developed based on the simulation data by TRNSYS. The benefit of the research work presented, however, will be realized when the neural network is initially trained by manufacturer's measured data, while subsequent on-line training will allow for continuous improvement of the desired condenser features through optimal control.

Appendix A - Chiller Model under HPC

```
      SUBROUTINE TYPE391 (TIME,XIN,OUT,T,DTDT,PAR,INFO,ICNTRL,*)
C**********************************************************************
C*   Developer:      Yang Jia
C*                   Department of Building Services Engineering
C*                   The Hong Kong Polytechnic University
C**********************************************************************
C*    PROGRAM:   TYPE 391
C*    PURPOSE:    Parameter evaluation of screw chiller
C**********************************************************************
C*
C* INPUT VARIABLE
C* Ifluid      Selection of the refrigerant                (-)
C*            If Ifluid
C*            =1: Refrigerant 12
C*            =2: Refrigerant 134a
C*            =3: Refrigerant 114
C*            =4: Refrigerant 22
C*            =5: Refrigerant 502
C*            =6: Refrigerant 717 (Ammonia)
C* Fw          Chilled water mass flow rate                (kg/s)
C* N           Number of operating conditions              (-)
C* PLR         Part load ratio of a chiller                (-)
C* Tcdae       Outdoor temperature (dry bulb)              (oC)
C* Tcdsc       Degree of subcooling                        (oC)
C* Tcdsp       Set point of condensing temperature         (oC)
C* Tchws       Supply chilled water Temperature            (oC)
C* Tevsh       Degree of superheat                         (oC)
C*
C*    REFRIGERANT PROPERTIES
C* Acl         First coefficient in the Clausius-Clapeyron quation (-)
C* Bcl         Second coefficient in the Clausius-Clapeyron equation (K)
C* b           Coefficient used in the calculation of the aporization enthalpy (-)
C* cpliq       Mean specific heat in saturated liquid state (J/kg/K)
C* cpvap       Mean specific heat at constant pressure     (J/kg/K)
C*             in superheated vapor state for saturation temperatures ranging from 253 K to 283 K
C* cpvapcd     Mean specific heat at constant pressure     (J/kg/K)
C*             in superheated vapor state for saturation temperatures ranging from 303 K to 333 K
C* Gamma       Mean isentropic coefficient                 (-)
C* hfgb        Vaporization enthalpy at standard boiling point (101325 Pa) (J/kg)
C* hfo         Enthalpy of the saturated liquid at the reference temperature (J/kg)
C* r           Gas constant                                (J/kg/K)
C* Tb          Standard boiling temperature                (K)
C* Tc          Critical temperature                        (K)
C* To          Reference temperature                       (K)
C* Zeta        Mean compressibility factor for saturation  (-)
C*             temperatures ranging from 253 K to 283 K
C* Zetacd      Mean compressibility factor for saturation temperatures ranging from 303 K to 333 K (-)
C**********************************************************************
C* OUTPUT VARIABLES
C* AUcd        Condenser heat transfer coefficient         (kW/oC)
C* AUev        Evaporator heat transfer coefficient        (kW/oC)
C* CR          Compression ratio                           (-)
C* Ecc         Compressor power                            (kW)
C* ecd         Condenser heat exchange effectiveness       (-)
C* Ecf         Total condenser fan power                   (kW)
C* Ech         Total chiller power                         (kW)
```

```
C* eev        Evaporator heat exchanger effectiveness          (-)
C* Effcc      Combined motor and transmission efficiency       (-)
C* Effis      Isentropic efficiency                            (-)
C* Effv       Volumetric efficiency                            (-)
C* Frtot      Total refrigerant mass flow                      (kg/s)
C* h1         Refrigerant enthalpy at compressor suction       (kJ/kg)
C* h2         Refrigerant enthalpy at compressor discharge     (kJ/kg)
C* h3         Refrigerant enthalpy at condenser discharge      (kJ/kg)
C* kton       Chiller operating efficiency in kW/kW            (kW/kW)
C* Pcd        Saturated condensing pressure                    (kPa)
C* Pev        Saturated evaporating pressure                   (kPa)
C* Qcd        Total heat rejection                             (kW)
C* Qcl        Cooling capacity                                 (kW)
C* qrf        Refrigeration effect                             (kJ/kg)
C* Tcd        Saturated condensing temperature                 (oC)
C* Tcdal      Leaving condenser air temperature                (oC)
C* Tchwr      Return chilled water temperature                 (oC)
C* Tev        Saturated evaporating temperature                (oC)
C* Va         Heat rejection airflow                           (m3/s)
C* win        Indicated work done by a compressor              (kJ/kg)
C* Xcc        Number of operating compressors                  (-)
C* Xcf        Number of operating condenser fans               (-)
C*********************************************************************
C* CONSTANT PARAMETERS
C* Cpa        Specific heat of outdoor air                     (kJ/kg/K)
C* Cpw        Specific heat of liquid water                    (kJ/kg/K)
C* Dena       Density of air                                   (kg/m3)
C* Ecfr       Rated total condenser fan power                  (kW)
C* Nccr       Maximum number of compressors                    (-)
C* Ncfr       Maximum number of condenser fans                 (-)
C* ni         Index of reversible polytropic expansion process (-)
C* Qcr        Rated cooling capacity                           (kW)
C* Tcdr       Maximum condensing temperature                   (oC)
C* Var        Rated heat rejection airflow                     (m3/s)
C* Vp         Piston displacement of each compressor           (m3/s)
C*********************************************************************

      INTEGER*4 INFO
      Integer Iter1,Iter2,Iter3,Iter4,Iter5,Iter6,Iter7,Iter8
      DOUBLE PRECISION XIN,out
      PARAMETER (M=8760)
      REAL Ifluid,N,Vp,Den1,ni,Cpw,Cpa,Dena,v1
      REAL Qcr,Var,Ncfr,Ecfr,Nccr,Tcdr,Tcdrlow,hX,Tcdsp,Tcd,Xcf

      DIMENSION PLR(M),PLR1(M),PLR2(M),PLR11(M),PLR12(M),PLR21(M)
      DIMENSION PLR22(M),Tcdae(M),Fw(M),Tchws1(M),Tchwr1(M),Tchwr11(M)
      DIMENSION Tcdsc(M),Qcl(M),Qcl1(M),Qcl2(M),Tev(M),Tev1(M),Tev2(M)
      DIMENSION Pev1(M),Pev2(M),AUev11(M),AUev12(M),AUev2(M),eev11(M)
      DIMENSION eev12(M),eev2(M),Fr11(M),Fr12(M),Fr21(M),Fr22(M)
      DIMENSION EFFv1(M),EFFv2(M),EFFis1(M),EFFis2(M),Fr1(M),Fr2(M)
      DIMENSION EFFcc1(M),EFFcc2(M),CR1(M),CR2(M),Xcc(M),Xcc1(M),Xcc2(M)
      DIMENSION Ecc(M),Ecc1(M),Ecc2(M),Tcd1(M),Tcd2(M),Xcc11(M),Xcc12(M)
      DIMENSION Tcdal1(M),Tcdal2(M),Qcd1(M),Qcd2(M),AUcd1(M),AUcd2(M)
      DIMENSION Va1(M),Va2(M),Xcf1(M),Xcf2(M),Ecf(M),Ecf1(M),Ecf2(M)
      DIMENSION qrf1(M),qrf2(M),Ech(M),Ech1(M),Ech2(M),h11(M),h21(M)
      DIMENSION Tchwr(M),Frtot1(M),Frtot2(M),win1(M),win2(M),Fcc(M)
      DIMENSION Tcdsp(M),Pcd1(M),Pcd2(M),h31(M),h12(M),h22(M),h32(M)
      DIMENSION Tchws(M), COP1(M),COP2(M),Tevsh(M),ecd1(M),ecd2(M)
      DIMENSION Xcf(M),Ts1(M),Effcc11(M),Effcc12(M),Effcc21(M),COP(M)
      DIMENSION Effcc22(M),Ecc11(M),Ecc12(M),Ecc21(M),Ecc22(M),Qcl11p(M)
      DIMENSION Qcl11(M),Qcl12(M),Qcl21(M),Qcl22(M),Tev1p(M),AUev1(M)
      DIMENSION Ma1(M),Ma2(M)
```

```
      DIMENSION PAR(14),XIN(8),out(60),INFO(15)

      COMMON /LUNITS/ LUR,LUW,IFORM,LUK
      COMMON /SIM/ TIME0,TFINAL,DELT,IWARN
      COMMON /CONFIG/ TRNEDT,PERCOM,HEADER,PRTLAB,LNKCHK,PRUNIT,IOCHEK,
     &               PRWARN

      INFO(6)=60


C1*** PARAMETERS

      ITIME=INT(TIME)
      N=par(1)
      Cpw=par(2)
      Cpa=par(3)
      Dena=par(4)
      ni=par(5)
      Qcr=par(6)
      Vp=par(7)
      Var=par(8)
      Ncfr=par(9)
      Ecfr=par(10)
      Nccr=par(11)
      Tcdr=par(12)
      Tcdrlow=par(13)

C1*** For each operating condition:

      DO 60 L=1,N
      Ifluid= xin (1)
      PLR(L)=xin(2)
      Tcdae(L)=xin(3)
      Tchws(L)=xin(4)
      Fw(L)=xin(5)
      Tevsh(L)=xin(6)
      Tcdsc(L)=xin(7)
      Tcdsp(L)=xin(8)

C2*** Selection of the refrigerant

      CALL PROPERTY (Ifluid,To,cpliq,hfo,cpvap,cpvapcd,hfgb,Tb,Tc,
     &               b,r,Zeta,Zetacd,Gamma,Acl,Bcl,*10)
10    CONTINUE

C1***Compute operating parameters at evaporator side

200   Qcl(L)=PLR(L)*Qcr

C*** Load sharing strategy

      IF (Qcl(L).GT.0.5*Qcr) THEN
        Qcl1(L)=0.5*Qcl(L)
        Qcl2(L)=Qcl(L)-Qcl1(L)
        ELSE
         Qcl1(L)=Qcl(L)
         Qcl2(L)=0
      ENDIF

      PLR1(L)=Qcl1(L)/(0.5*Qcr)
      PLR2(L)=Qcl2(L)/(0.5*Qcr)
```

```
C     Chilled water return temperaturte

      Tchwr(L)=Tchws(L)+Qcl(L)/Fw(L)/Cpw

      It3=0

      Qcl11(L)=0.5*Qcl1(L)

C1*** Calculate the cooling capacity of section 2 of circuit A
11    Qcl12(L)=Qcl1(L)-Qcl11(L)

C*** Calculate the evaporator effectivenesses
      AUev11(L)=1/(0.027*Fw(L)**(-0.8)+0.934*Qcl11(L)**(-0.745))
      eev11(L)=1-EXP(-AUev11(L)/Fw(L)/Cpw)
      AUev12(L)=1/(0.027*Fw(L)**(-0.8)+0.934*Qcl12(L)**(-0.745))
      eev12(L)=1-EXP(-AUev12(L)/Fw(L)/Cpw)

C2*** calculate the chilled water temperature entering circuit B
      Tchwr1(L)=Tchwr(L)-Qcl11(L)/Fw(L)/Cpw

C2*** Calculate the chilled water temperature leaving circuit B

      Tchws1(L)=Tchwr1(L)-Qcl2(L)/Fw(L)/Cpw

C1*** Calculate the evaporating temperature
      Tev1(L)=Tchws1(L)-Qcl12(L)/Fw(L)/Cpw/eev12(L)

C1*** Recalculate the cooling capacity of section 1 of circuit A
       Qcl11p(L)=eev11(L)*Fw(L)*Cpw*(Tchwr(L)-Tev1(L))

       IF (Qcl11p(L).GT.0.5*Qcl1(L)) THEN
       Qcl11p(L)=0.5*Qcl1(L)
       ELSE
       CONTINUE
       ENDIF

      IF(abs((Qcl11p(L)-Qcl11(L))/Qcl11(L)).GT.0.01)THEN
      Qcl11(L)=Qcl11p(L)
       GOTO 11
       ELSE
       CONTINUE
       ENDIF

C*** Calculate the evaporator effectivenesses
C1*** Calculate the refrigerant state 1at the evaporator exhaust
      dhfg1=(hfgb/1000)*((Tc-(Tev1(L)+273.15))/(Tc-Tb))**b
      hX1=(hfo/1000)+(cpliq/1000)*(Tev1(L)+273.15-T0)+dhfg1
      h11(L)=hX1+(cpvap/1000)*Tevsh(L)
      v11=Zeta*r*(Tev1(L)+273.15)/(Pev1(L)*1000)
      Den11=1/v11-(-.0007+.0002*Pev1(L))*Tevsh(L)

       Iter1=1
       Tcd01=55

C*** Calculate the condensing pressure
52    Pcd1(L)=EXP(Acl+Bcl/(Tcd01+273.15))

C1***Compute operating parameters at compressor
      h31(L)=(hfo/1000)+(cpliq/1000)*(Tcd01+273.15-T0-Tcdsc(L))
      qrf1(L)=hX1-h31(L)
```

```
      CR1(L)=Pcd1(L)/Pev1(L)
      Effv1(L)=.925-.009*CR1(L)
      Effis11=-.0316958*Tcd01**2+2.90112*Tcd01-.0296849*Tev1(L)**2
      Effis21=-1.45279*Tev1(L)+.000321176*Tcd01**2*Tev1(L)
      Effis31=.00683086*Tcd01*Tev1(L)+.0170575*0.5*Qcr-16.5018
      Effis1(L)=(Effis11+Effis21+Effis31)/80

      Fr1(L)=Effv1(L)*Den11*Vp
     Xcc1(L)=INT(Qcl1(L)/Fr1(L)/qrf1(L)+0.95))

     IF (Xcc1(L).LT.1) THEN
       Xcc1(L)=1
     ENDIF

     IF (Xcc1(L).GT.(0.5*Nccr)) THEN
       Xcc1(L)=0.5*Nccr
     ENDIF

C***  Loading sharing between compressors
     IF (PLR1(L).LE.0.5) THEN
      Xcc1(L)=1
      ELSE
      Xcc1(L)=0.5*Nccr
      ENDIF
C***  Equally shared
     IF (PLR1(L).LE.0.5) THEN
      PLR11(L)=Qcl1(L)/(0.25*Qcr)
      PLR12(L)=0
      ELSE
      PLR11(L)=0.5*Qcl1(L)/(0.25*Qcr)
      PLR12(L)=PLR11(L)
      ENDIF

C1*** Calculate the refrigerant mass flow rate
     Frtot1(L)=Qcl1(L)/qrf1(L)

C1*** Calculate the refrigerant mass flow rate
     Fr11(L)=PLR11(L)*0.25*Qcr/qrf1(L)

C1*** Calculate the refrigerant mass flow rate
     Fr12(L)=PLR12(L)*0.25*Qcr/qrf1(L)

C1*** Calculate the internal compression power
     win1(L)=Pev1(L)/Den11*(ni/(ni-1))*(CR1(L)**(1-1/ni)-1)

C***  compressor efficiency
     Effcc11(L)=0.0258+0.8214*PLR11(L)+0.1932*PLR11(L)**2
     Effcc12(L)=0.0258+0.8214*PLR12(L)+0.1932*PLR12(L)**2

     IF (PLR11(L).GT.0) THEN
      Ecc11(L)=Fr11(L)*win1(L)/Effis1(L)/Effcc11(L)
      ELSE
      Ecc11(L)=0
      ENDIF

     IF (PLR12(L).GT.0) THEN
      Ecc12(L)=Fr12(L)*win1(L)/Effis1(L)/Effcc12(L)
      ELSE
      Ecc12(L)=0
      ENDIF

     Ecc1(L)=Ecc11(L)+Ecc12(L)
```

```
C1***Compute operating parameters at condenser side
     Qcd1(L)=Qcl1(L)+Frtot1(L)*(cpvap/1000)*Tevsh(L)+Ecc1(L)

     IF (Tcdsp(L).LE.Tcdae(L)) THEN
       Xcf1(L)=0.5*Ncfr
       GOTO 51
     ENDIF

      Ncfr1=0.5*Ncfr
      Xcf1(L)=INT(Qcd1(L)*Ncfr/(Var*Dena*Cpa*(Tcdsp(L)-Tcdae(L)))+0.5)

      IF (Xcf1(L).GT.Ncfr1) THEN
         Xcf1(L)=Ncfr1
         GOTO 51
     ENDIF

     DO 80 P=1,INT(Ncfr1)
       IF (Xcf1(L).LE.P) THEN
          Xcf1(L)=P
          GOTO 51
     ENDIF
80   CONTINUE

     Xcf1(L)=Ncfr1

      Iter3=0
      Iter4=0

51    Va1(L)=Xcf1(L)*(Var/Ncfr)

     Tcdal1(L)=Tcdae(L)+Qcd1(L)/(Va1(L)*Dena*Cpa)

     IF (Tcdal1(L).GT.Tcdr.AND.Xcf1(L).LT.Ncfr1) THEN
       Xcf1(L)=Xcf1(L)+1
     GOTO 51
     ENDIF

C1*** Calculate the condenser effectivenesses
     AUcd1(L)=1/(0.049*Va1(L)**-.5+.006*Frtot1(L)**-.8)
     ecd1(L)=1-EXP(-AUcd1(L)/Va1(L)/Dena/Cpa)

C1*** Calculate the condensing temperature
     Tcd1(L)=Tcdae(L)+(Tcdal1(L)-Tcdae(L))/ecd1(L)

     IF (Tcd1(L).GT.Tcd01) THEN
           Xcf1(L)=Xcf1(L)+1
           GOTO 51
      ENDIF

     IF ((Tcd01-Tcd1(L)).GT.0.05) THEN
           Tcd01=Tcd1(L)
           GOTO 52
         ENDIF

     IF (Tcd1(L).GT.Tcdr) THEN
           Xcf1(L)=Xcf1(L)+1
           GOTO 51
         ENDIF

C1*** Calculate the power consumed by the condenser fans of circuit A
           Ecf1(L)=Xcf1(L)*Ecfr/Ncfr
```

```
C1*** Calculate the power consumed by the circuit A
          Ech1(L)=Ecc1(L)+Ecf1(L)

C1*** Calculate the coefficient of performance
           COP1(L)=Qcl1(L)/Ech1(L)

      IF (Qcl2(L).LE.0.0) THEN
         Xcf2(L)=0
         Ecf2(L)=0
         Ech2(L)=0
         Tchwr1(L)=Tchwr1(L)
         Tev2(L)=0
         AUev2(L)=0
         Frtot2(L)=0
         Effv2(L)=0
         Effis2(L)=0
         Effcc2(L)=0
         Xcc2(L)=0
         win2(L)=0
         Ecc2(L)=0
         Tcd2(L)=0
         Pcd2(L)=0
         Tcdal2(L)=Tcdae(L)
         Qcd2(L)=0
         AUcd2(L)=0
         Va2(L)=0
         COP2(L)=0
         GOTO 29
       ELSE
        CONTINUE
    ENDIF

C1****Cir B

C1*** Calculate the evaporator effectivenesses
      AUev2(L)=1/(0.027*Fw(L)**(-0.8)+0.934*Qcl2(L)**(-0.745))
      eev2(L)=1-EXP(-AUev2(L)/Fw(L)/Cpw)

C1*** Calculate the evaporating temperature
      Tev2(L)=Tchwr1(L)-Qcl2(L)/Fw(L)/Cpw/eev2(L)

C1*** Calculate the evaporating pressure
      Pev2(L)=EXP(Acl+Bcl/(Tev2(L)+273.15))

C1***refrigerant state 1
      dhfg2=(hfgb/1000)*((Tc-(Tev2(L)+273.15))/(Tc-Tb))**b
      hX2=(hfo/1000)+(cpliq/1000)*(Tev2(L)+273.15-T0)+dhfg2
      h12(L)=hX2+(cpvap/1000)*Tevsh(L)
      v12=Zeta*r*(Tev2(L)+273.15)/(Pev2(L)*1000)
      Den12=1/v12-(-.0007+.0002*Pev2(L))*Tevsh(L)

C1***Compute operating parameters at compressor
      Iter2=1
      Tcd02=55

53  Pcd2(L)=EXP(Acl+Bcl/(Tcd02+273.15))
      h32(L)=(hfo/1000)+(cpliq/1000)*(Tcd02+273.15-T0-Tcdsc(L))
      qrf2(L)=hX2-h32(L)

      CR2(L)=Pcd2(L)/Pev2(L)
      Effv2(L)=.925-.009*CR2(L)
```

```
      Effis12=-.0316958*Tcd02**2+2.90112*Tcd02-.0296849*Tev2(L)**2
      Effis22=-1.45279*Tev2(L)+.000321176*Tcd02**2*Tev2(L)
      Effis32=.00683086*Tcd02*Tev2(L)+.0170575*0.5*Qcr-16.5018
      Effis2(L)=(Effis12+Effis22+Effis32)/80

      Fr2(L)=Effv2(L)*Den12*Vp

      Xcc12(L)=Qcl2(L)/Fr2(L)/qrf2(L)+0.95
      Xcc2(L)=INT(Xcc12(L))

       IF (Xcc2(L).LT.1) THEN
         Xcc2(L)=1
      ENDIF

      IF (Xcc2(L).GT.(0.5*Nccr)) THEN
        Xcc2(L)=0.5*Nccr
      ENDIF

C***  Loading sharing between compressors
      IF (PLR2(L).LE.0.5) THEN
       Xcc2(L)=1
       ELSE
       Xcc2(L)=0.5*Nccr
       ENDIF

C***  Equally shared
      IF (PLR2(L).LE.0.5) THEN
       PLR21(L)=Qcl2(L)/(0.25*Qcr)
        PLR22(L)=0
       ELSE
       PLR21(L)=0.5*Qcl2(L)/(0.25*Qcr)
       PLR22(L)=PLR21(L)
       ENDIF

C***  Loading shared
      Qcl21(L)=PLR21(L)*Qcr/4
      Qcl22(L)=PLR22(L)*Qcr/4

C1*** Calculate the refrigerant mass flow rate
      Frtot2(L)=Qcl2(L)/qrf2(L)

C1*** Calculate the refrigerant mass flow rate
      Fr21(L)=Qcl21(L)/qrf2(L)

C1*** Calculate the refrigerant mass flow rate
      Fr22(L)=Qcl22(L)/qrf2(L)

C1*** Calculate the internal compression power
      win2(L)=Pev2(L)/Den12*(ni/(ni-1))*(CR2(L)**(1-1/ni)-1)

C***  compressor efficiency
      Effcc21(L)=0.0258+0.8214*PLR21(L)+0.1932*PLR21(L)**2
      Effcc22(L)=0.0258+0.8214*PLR22(L)+0.1932*PLR22(L)**2

     IF (PLR21(L).GT.0) THEN
       Ecc21(L)=Fr21(L)*win2(L)/Effis2(L)/Effcc21(L)
       ELSE
       Ecc21(L)=0
     ENDIF

     IF (PLR22(L).GT.0) THEN
       Ecc22(L)=Fr22(L)*win2(L)/Effis2(L)/Effcc22(L)
```

```
      ELSE
      Ecc22(L)=0
     ENDIF

     Ecc2(L)=Ecc21(L)+Ecc22(L)

C1***Compute operating parameters at condenser side
     Qcd2(L)=Qcl2(L)+Frtot2(L)*(cpvap/1000)*Tevsh(L)+Ecc2(L)

     IF (Tcdsp(L).LE.Tcdae(L)) THEN
       Xcf2(L)=0.5*Ncfr
       GOTO 54
     ENDIF

      Ncfr2=0.5*Ncfr
      Xcf2(L)=INT(Qcd2(L)*Ncfr/(Var*Dena*Cpa*(Tcdsp(L)-Tcdae(L)))+0.5)

      IF (Xcf2(L).GT.Ncfr2) THEN
         Xcf2(L)=Ncfr2
         GOTO 54
     ENDIF

     DO 90 P=1,INT(Ncfr2)
       IF (Xcf2(L).LE.P) THEN
          Xcf2(L)=P
          GOTO 54
     ENDIF
90    CONTINUE

     Xcf2(L)=Ncfr2

      Iter5=0
      Iter6=0

54    Va2(L)=Xcf2(L)*(Var/Ncfr)
     Tcdal2(L)=Tcdae(L)+Qcd2(L)/(Va2(L)*Dena*Cpa)

     IF (Tcdal2(L).GT.Tcdr.AND.Xcf2(L).LT.Ncfr2) THEN
       Xcf2(L)=Xcf2(L)+1
     GOTO 54
     ENDIF

C1*** Calculate the condenser effectivenesses
     AUcd2(L)=1/(0.049*Va2(L)**-.5+.006*Frtot2(L)**-.8)
     ecd2(L)=1-EXP(-AUcd2(L)/Va2(L)/Dena/Cpa)

C1*** Calculate the condensing temperature
     Tcd2(L)=Tcdae(L)+(Tcdal2(L)-Tcdae(L))/ecd2(L)

     IF (Tcd2(L).GT.Tcd02) THEN
           Xcf2(L)=Xcf2(L)+1
           GOTO 54
      ENDIF

     IF ((Tcd02-Tcd2(L)).GT.0.05) THEN
           Tcd02=Tcd2(L)
           GOTO 53
         ENDIF

     IF (Tcd2(L).GT.Tcdr) THEN
           Xcf2(L)=Xcf2(L)+1
           GOTO 54
```

```
          ENDIF

C1*** Calculate the power consumed by the condenser fans of circuit B
       Ecf2(L)=Xcf2(L)*Ecfr/Ncfr

C1*** Calculate the power consumed by the circuit B
      Ech2(L)=Ecc2(L)+Ecf2(L)

C1*** Calculate the coefficient of performance of Circuit B
      COP2(L)=Qcl2(L)/Ech2(L)

C1*** Calculate the coefficient of performance
29    Ecf(L)=Ecf1(L)+Ecf2(L)
       Ech(L)=Ech1(L)+Ech2(L)
      Xcf(L)=Xcf1(L)+Xcf2(L)
      COP(L)=Qcl(L)/Ech(L)

C***  Outputs of 30 operating variables

       out(1)=DBLE(Qcl(L))
       out(2)=DBLE(Tchwr(L))
       out(3)=DBLE(Qcl1(L))
       out(4)=DBLE(Tev1(L))
       out(5)=DBLE(Tchwr1(L))
       out(6)=DBLE(Tchws1(L))
       out(7)=DBLE(AUev11(L))
       out(8)=DBLE(Frtot1(L))
       out(9)=DBLE(Xcc1(L))
       out(10)=DBLE(Ecc1(L))
       out(11)=DBLE(Tcd01)
       out(12)=DBLE(Tcdal1(L))
       out(13)=DBLE(AUcd1(L))
       out(14)=DBLE(Tcd1(L))
       out(15)=DBLE(Va1(L))
       out(16)=DBLE(2*Xcf1(L))
       out(17)=DBLE(Ecf1(L))
       out(18)=DBLE(Frtot2(L))
       out(19)=DBLE(Tev2(L))
       out(20)=DBLE(AUev2(L))
       out(21)=DBLE(Xcc2(L))
       out(22)=DBLE(Ecc2(L))
       out(23)=DBLE(Tcd02)
       out(24)=DBLE(Tcd2(L))
       out(25)=DBLE(AUcd2(L))
       out(26)=DBLE(Va2(L))
       out(27)=DBLE(Tcdal2(L))
       out(28)=DBLE(2*Xcf2(L))
       out(29)=DBLE(Ecf2(L))
       out(30)=DBLE(Ech(L))

60    CONTINUE

       RETURN 1

       END



SUBROUTINE PROPERTY (Ifluid,To,cpliq,hfo,cpvap,cpvapcd,hfgb,Tb,Tc,
     &                b,r,Zeta,Zetacd,Gamma,Acl,Bcl,*)
```

```
REAL Ifluid

To=233.15

IF (Ifluid.EQ.1) THEN
  cpliq=917
  hfo=0
  cpvap=641.6
  cpvapcd=779
  hfgb=165300
  Tb=243.4
  Tc=385.2
  b=0.37
  r=68.7539
  Zeta=0.9403
  Zetacd=0.8670
  Gamma=1.086
  Acl=14.669
  Bcl=-2443.13
ENDIF


IF (Ifluid.EQ.2) THEN
  cpliq=1265
  hfo=0
  cpvap=892.5
  cpvapcd=1144
  hfgb=215100
  Tb=246.9
  Tc=374.3
  b=0.376
  r=81.4899
  Zeta=0.9411
  Zetacd=0.8610
  Gamma=1.072
  Acl=15.489
  Bcl=-2681.99
ENDIF

IF (Ifluid.EQ.3) THEN
  cpliq=925
  hfo=0
  cpvap=693.6
  cpvapcd=784
  hfgb=136100
  Tb=276.9
  Tc=418.9
  b=0.359
  r=48.6393
  Zeta=0.9757
  Zetacd=0.9260
  Gamma=1.056
  Acl=15.107
  Bcl=-2908.73
ENDIF

IF (Ifluid.EQ.4) THEN
  cpliq=1144
  hfo=0
  cpvap=710.4
  cpvapcd=936
  hfgb=233700
```

```
  Tb=232.4
  Tc=369.2
  b=0.369
  r=96.1426
  Zeta=0.9300
  Zetacd=0.8440
  Gamma=1.114
  Acl=15.070
  Bcl=-2421.94
ENDIF

IF (Ifluid.EQ.5) THEN
  cpliq=1090
  hfo=0
  cpvap=732
  cpvapcd=965
  hfgb=172500
  Tb=227.8
  Tc=355.4
  b=0.374
  r=74.4752
  Zeta=0.9130
  Zetacd=0.8150
  Gamma=1.065
  Acl=14.809
  Bcl=-2312.21
ENDIF

IF (Ifluid.EQ.6) THEN
  cpliq=4575
  hfo=0
  cpvap=2447.1
  cpvapcd=3159
  hfgb=1372900
  Tb=239.8
  Tc=405.6
  b=0.396
  r=488.2214
  Zeta=0.9570
  Zetacd=0.8960
  Gamma=1.230
  Acl=16.204
  Bcl=-2772.39
ENDIF

RETURN 1

END
```

Appendix B - Chiller Model under CTC with Water Mist Pre-cooling

```
      SUBROUTINE TYPE411 (TIME,XIN,OUT,T,DTDT,PAR,INFO,ICNTRL,*)
C**********************************************************************
C*   Developer:      Yang Jia
C*                   Department of Building Services Engineering
C*                   The Hong Kong Polytechnic University
C**********************************************************************
C*    PROGRAM:   TYPE 411
C*    PURPOSE:     Parameter evaluation of screw chiller under CTC with water mist
C**********************************************************************
C*
C*   INPUT VARIABLE
C*   Ifluid      Selection of the refrigerant                    (-)
C*             If Ifluid
C*             =1: Refrigerant 12
C*             =2: Refrigerant 134a
C*             =3: Refrigerant 114
C*             =4: Refrigerant 22
C*             =5: Refrigerant 502
C*             =6: Refrigerant 717 (Ammonia)
C*   N           Number of operating conditions              (-)
C*   PLR         Part load ratio of a chiller                (-)
C*   Tcdae       Outdoor dry bulb temperature                (oC)
C*   Twb         Outdoor wet bulb temperature                (oC)
C*   Tchws       Supply chilled water Temperature            (oC)
C*   Fw          Chilled water mass flow rate                (kg/s)
C*   Tevsh       Degree of superheat                         (oC)
C*   Tcdsc       Degree of subcooling                        (oC)
C*   Tcdsp       Set point of condensing temperature         (oC)
C*
C*    REFRIGERANT PROPERTIES
C* Acl          First coefficient in the Clausius-Clapeyron quation (-)
C* Bcl          Second coefficient in the Clausius-Clapeyron equation (K)
C* b            Coefficient used in the calculation of the aporization enthalpy (-)
C* cpliq        Mean specific heat in saturated liquid state (J/kg/K)
C* cpvap       Mean specific heat at constant pressure      (J/kg/K)
C*               in superheated vapor state for saturation temperatures ranging from 253 K to 283 K
C* cpvapcd     Mean specific heat at constant pressure      (J/kg/K)
C*               in superheated vapor state for saturation temperatures ranging from 303 K to 333 K
C* Gamma      Mean isentropic coefficient                  (-)
C* hfgb       Vaporization enthalpy at standard boiling point (101325 Pa) (J/kg)
C* hfo        Enthalpy of the saturated liquid at the reference temperature (J/kg)
C* r          Gas constant                                 (J/kg/K)
C* Tb         Standard boiling temperature                 (K)
C* Tc         Critical temperature                         (K)
C* To         Reference temperature                        (K)
C* Zeta       Mean compressibility factor for saturation   (-)
C*               temperatures ranging from 253 K to 283 K
C* Zetacd     Mean compressibility factor for saturation temperatures ranging from 303 K to 333 K (-)
C**********************************************************************
C* OUTPUT VARIABLES
C* AUcd        Condenser heat transfer coefficient         (kW/oC)
C* AUev        Evaporator heat transfer coefficient        (kW/oC)
C* CR          Compression ratio                           (-)
```

```
C* Ecc        Compressor power                          (kW)
C* ecd        Condenser heat exchange effectiveness     (-)
C* Ecf        Total condenser fan power                 (kW)
C* Ech        Total chiller power                       (kW)
C* eev        Evaporator heat exchanger effectiveness   (-)
C* Effcc      Combined motor and transmission efficiency (-)
C* Effis      Isentropic efficiency                     (-)
C* Effv       Volumetric efficiency                     (-)
C* Frtot      Total refrigerant mass flow               (kg/s)
C* h1         Refrigerant enthalpy at compressor suction (kJ/kg)
C* h2         Refrigerant enthalpy at compressor discharge (kJ/kg)
C* h3         Refrigerant enthalpy at condenser discharge (kJ/kg)
C* kton       Chiller operating efficiency in kW/kW     (kW/kW)
C* Pcd        Saturated condensing pressure             (kPa)
C* Pev        Saturated evaporating pressure            (kPa)
C* Qcd        Total heat rejection                      (kW)
C* Qcl        Cooling capacity                          (kW)
C* qrf        Refrigeration effect                      (kJ/kg)
C* Tcd        Saturated condensing temperature          (oC)
C* Tcdal      Leaving condenser air temperature         (oC)
C* Tchwr      Return chilled water temperature          (oC)
C* Tev        Saturated evaporating temperature         (oC)
C* Va         Heat rejection airflow                    (m3/s)
C* win        Indicated work done by a compressor       (kJ/kg)
C* Xcc        Number of operating compressors           (-)
C* Xcf        Number of operating condenser fans        (-)
C*********************************************************************
C* CONSTANT PARAMETERS
C* Cpa        Specific heat of outdoor air              (kJ/kg/K)
C* Cpw        Specific heat of liquid water             (kJ/kg/K)
C* Dena       Density of air                            (kg/m3)
C* Ecfr       Rated total condenser fan power           (kW)
C* Nccr       Maximum number of compressors             (-)
C* Ncfr       Maximum number of condenser fans          (-)
C* ni         Index of reversible polytropic expansion process (-)
C* Qcr        Rated cooling capacity                    (kW)
C* Tcdr       Maximum condensing temperature            (oC)
C* Var        Rated heat rejection airflow              (m3/s)
C* Vp         Piston displacement of each compressor    (m3/s)
C*********************************************************************

      INTEGER*4 INFO
      Integer Iter1,Iter2,Iter3,Iter4,Iter5,Iter6,Iter7,Iter8
      DOUBLE PRECISION XIN,out
      PARAMETER (M=8760)
      REAL Ifluid,N,Vp,Den1,ni,Cpw,Cpa,Dena,v1
      REAL Qcr,Var,Ncfr,Ecfr,Nccr,Tcdr,Tcdrlow,hX,Tcdsp,Tcd,Xcf

      DIMENSION PLR(M),PLR1(M),PLR2(M),PLR11(M),PLR12(M),PLR21(M)
      DIMENSION PLR22(M),Tcdae(M),Fw(M),Tchws1(M),Tchwr1(M),Tchwr11(M)
      DIMENSION Tcdsc(M),Qcl(M),Qcl1(M),Qcl2(M),Tev(M),Tev1(M),Tev2(M)
      DIMENSION Pev1(M),Pev2(M),AUev11(M),AUev12(M),AUev2(M),eev11(M)
      DIMENSION eev12(M),eev2(M),Fr11(M),Fr12(M),Fr21(M),Fr22(M)
      DIMENSION EFFv1(M),EFFv2(M),EFFis1(M),EFFis2(M),Fr1(M),Fr2(M)
      DIMENSION EFFcc1(M),EFFcc2(M),CR1(M),CR2(M),Xcc(M),Xcc1(M),Xcc2(M)
      DIMENSION Ecc(M),Ecc1(M),Ecc2(M),Tcd1(M),Tcd2(M),Xcc11(M),Xcc12(M)
      DIMENSION Tcdal1(M),Tcdal2(M),Qcd1(M),Qcd2(M),AUcd1(M),AUcd2(M)
      DIMENSION Va1(M),Va2(M),Xcf1(M),Xcf2(M),Ecf(M),Ecf1(M),Ecf2(M)
      DIMENSION qrf1(M),qrf2(M),Ech(M),Ech1(M),Ech2(M),h11(M),h21(M)
      DIMENSION Tchwr(M),Frtot1(M),Frtot2(M),win1(M),win2(M),Fcc(M)
      DIMENSION Tcdsp(M),Pcd1(M),Pcd2(M),h31(M),h12(M),h22(M),h32(M)
      DIMENSION Tchws(M), COP1(M),COP2(M),Tevsh(M),ecd1(M),ecd2(M)
```

```
      DIMENSION Xcf(M),Ts1(M),Effcc11(M),Effcc12(M),Effcc21(M),COP(M)
      DIMENSION Effcc22(M),Ecc11(M),Ecc12(M),Ecc21(M),Ecc22(M),Qcl11p(M)
      DIMENSION Qcl11(M),Qcl12(M),Qcl21(M),Qcl22(M),Tev1p(M),AUev1(M)
      DIMENSION Twb(M),Fm1(M),Fm2(M),Wdb(M),Pws(M),Wdbp1(M),Wdbp2(M)
      DIMENSION Tcdaep1(M),Tcdaep2(M),Pt(M),RH(M),Hdb(M)
      DIMENSION DeltaW1(M),DeltaW2(M),RH1(M),RH2(M)
      DIMENSION Pwswb(M),Wswb(M),Wcdaep1(M),Wcdaep2(M),Pws1(M),Pws2(M)
      DIMENSION Wscdaep1(M),Wscdaep2(M),DOS1(M),DOS2(M),Pw1(M),Pw2(M)
      DIMENSION Ma1(M),Ma2(M)

      DIMENSION PAR(14),XIN(13),out(60),INFO(15)

     COMMON /LUNITS/ LUR,LUW,IFORM,LUK
     COMMON /SIM/ TIME0,TFINAL,DELT,IWARN
     COMMON /CONFIG/ TRNEDT,PERCOM,HEADER,PRTLAB,LNKCHK,PRUNIT,IOCHEK,
    &               PRWARN

     INFO(6)=60

C1*** PARAMETERS

     ITIME=INT(TIME)
     N=par(1)
     Cpw=par(2)
     Cpa=par(3)
     Dena=par(4)
     ni=par(5)
     Qcr=par(6)
     Vp=par(7)
     Var=par(8)
     Ncfr=par(9)
     Ecfr=par(10)
     Nccr=par(11)
     Tcdr=par(12)
     Tcdrlow=par(13)

C1*** For each operating condition:

     DO 60 L=1,N
     Ifluid= xin (1)
     PLR(L)=xin(2)
     Twb(L)=xin(3)
     Fm1(L)=xin(4)
     Fm2(L)=xin(5)
     RH(L)=xin(6)
     Pt(L)=xin(7)
     Tcdae(L)=xin(8)
     Tchws(L)=xin(9)
     Fw(L)=xin(10)
     Tevsh(L)=xin(11)
     Tcdsc(L)=xin(12)
     Tcdsp(L)=xin(13)

C2*** Selection of the refrigerant

     CALL PROPERTY (Ifluid,To,cpliq,hfo,cpvap,cpvapcd,hfgb,Tb,Tc,
    &               b,r,Zeta,Zetacd,Gamma,Acl,Bcl,*10)
10   CONTINUE


C1***Compute operating parameters at evaporator side
```

```
200   Qcl(L)=PLR(L)*Qcr
C     Qcl=Qcl(L)

C*** load sharing strategy

      IF (Qcl(L).GT.0.5*Qcr) THEN
        Qcl1(L)=0.5*Qcl(L)
              Qcl2(L)=Qcl(L)-Qcl1(L)
        ELSE
         Qcl1(L)=Qcl(L)
               Qcl2(L)=0
      ENDIF

      PLR1(L)=Qcl1(L)/(0.5*Qcr)
      PLR2(L)=Qcl2(L)/(0.5*Qcr)

C     chilled water return temperaturte

      Tchwr(L)=Tchws(L)+Qcl(L)/Fw(L)/Cpw

      Qcl11(L)=0.5*Qcl1(L)

C1*** Calculate the cooling capacity of section 2 of circuit A
11          Qcl12(L)=Qcl1(L)-Qcl11(L)

C*** Calculate the evaporator effectivenesses
      AUev11(L)=1/(0.027*Fw(L)**(-0.8)+0.934*Qcl11(L)**(-0.745))
      eev11(L)=1-EXP(-AUev11(L)/Fw(L)/Cpw)

      AUev12(L)=1/(0.027*Fw(L)**(-0.8)+0.934*Qcl12(L)**(-0.745))
      eev12(L)=1-EXP(-AUev12(L)/Fw(L)/Cpw)

C2*** calculate the chilled water temperature entering circuit B
      Tchwr1(L)=Tchwr(L)-Qcl11(L)/Fw(L)/Cpw

C2*** Calculate the chilled water temperature leaving circuit B

      Tchws1(L)=Tchwr1(L)-Qcl2(L)/Fw(L)/Cpw

C1*** Calculate the evaporating temperature
      Tev1(L)=Tchws1(L)-Qcl12(L)/Fw(L)/Cpw/eev12(L)

C1*** Recalculate the cooling capacity of section 1 of circuit A
       Qcl11p(L)=eev11(L)*Fw(L)*Cpw*(Tchwr(L)-Tev1(L))

     IF (Qcl11p(L).GT.0.8*Qcl1(L)) THEN
        Qcl11p(L)=0.5*Qcl1(L)
        ELSE
        CONTINUE
      ENDIF

      IF(abs((Qcl11p(L)-Qcl11(L))/Qcl11(L)).GT.0.01)THEN
            Qcl11(L)=Qcl11p(L)
            GOTO 11
            ELSE
            CONTINUE
      ENDIF

C1*** Calculate the evaporating pressure
      Pev1(L)=EXP(Acl+Bcl/(Tev1(L)+273.15))

C1****Cir A
```

```
C1*** Refrigerant state 1 at the evaporator exhaust
     dhfg1=(hfgb/1000)*((Tc-(Tev1(L)+273.15))/(Tc-Tb))**b
     hX1=(hfo/1000)+(cpliq/1000)*(Tev1(L)+273.15-T0)+dhfg1
     h11(L)=hX1+(cpvap/1000)*Tevsh(L)
     v11=Zeta*r*(Tev1(L)+273.15)/(Pev1(L)*1000)
     Den11=1/v11-(-.0007+.0002*Pev1(L))*Tevsh(L)

C1***Compute operating parameters at compressor
     Iter1=1
     Tcd01=55
     Ech1opt=500

    Tcdsp1(L)=Tcdae(L)+15

    IF (Tcdsp1(L).LT.20) THEN
        Tcdsp1(L)=20
   ENDIF

   Tcdaep1(L)=Twb(L)

C*** Calculate the condensing pressure

52    Pcd1(L)=EXP(Acl+Bcl/(Tcd01+273.15))

     h31(L)=(hfo/1000)+(cpliq/1000)*(Tcd01+273.15-T0-Tcdsc(L))
     qrf1(L)=hX1-h31(L)

     CR1(L)=Pcd1(L)/Pev1(L)
     Effv1(L)=.925-.009*CR1(L)
     Effis11=-.0316958*Tcd01**2+2.90112*Tcd01-.0296849*Tev1(L)**2
     Effis21=-1.45279*Tev1(L)+.000321176*Tcd01**2*Tev1(L)
     Effis31=.00683086*Tcd01*Tev1(L)+.0170575*0.5*Qcr-16.5018
     Effis1(L)=(Effis11+Effis21+Effis31)/80

     Fr1(L)=Effv1(L)*Den11*Vp

     Xcc11(L)=Qcl1(L)/Fr1(L)/qrf1(L)+0.95
     Xcc1(L)=INT(Xcc11(L))

     IF (Xcc1(L).LT.1) THEN
       Xcc1(L)=1
     ENDIF

     IF (Xcc1(L).GT.(0.5*Nccr)) THEN
       Xcc1(L)=0.5*Nccr
     ENDIF

     IF (PLR1(L).LE.0.5) THEN
      Xcc1(L)=1
           ELSE
           Xcc1(L)=0.5*Nccr
           ENDIF
C***  Equally shared
     IF (PLR1(L).LE.0.5) THEN
         PLR11(L)=Qcl1(L)/(0.25*Qcr)
         PLR12(L)=0
           ELSE
           PLR11(L)=0.5*Qcl1(L)/(0.25*Qcr)
           PLR12(L)=PLR11(L)
    ENDIF

C1*** Calculate the refrigerant mass flow rate
```

```
      Frtot1(L)=Qcl1(L)/qrf1(L)

C1*** Calculate the refrigerant mass flow rate
      Fr11(L)=PLR11(L)*0.25*Qcr/qrf1(L)

C1*** Calculate the refrigerant mass flow rate
      Fr12(L)=PLR12(L)*0.25*Qcr/qrf1(L)

C1*** Calculate the internal compression power
      win1(L)=Pev1(L)/Den11*(ni/(ni-1))*(CR1(L)**(1-1/ni)-1)

C***  compressor efficiency

       Effcc11(L)=0.0258+0.8214*PLR11(L)+0.1932*PLR11(L)**2
       Effcc12(L)=0.0258+0.8214*PLR12(L)+0.1932*PLR12(L)**2

      IF (PLR11(L).GT.0) THEN
            Ecc11(L)=Fr11(L)*win1(L)/Effis1(L)/Effcc11(L)
            ELSE
            Ecc11(L)=0
      ENDIF

      IF (PLR12(L).GT.0) THEN
            Ecc12(L)=Fr12(L)*win1(L)/Effis1(L)/Effcc12(L)
            ELSE
            Ecc12(L)=0
     ENDIF

      Ecc1(L)=Ecc11(L)+Ecc12(L)

C1***Compute operating parameters at condenser side

      Qcd1(L)=Qcl1(L)+Frtot1(L)*(cpvap/1000)*Tevsh(L)+Ecc1(L)

      IF (Tcdsp1(L).LE.Twb(L)) THEN
        Xcf1(L)=0.5*Ncfr
        GOTO 51
      ENDIF

      Ncfr1=0.5*Ncfr
     Xcf1(L)=INT(Qcd1(L)*Ncfr/(Var*Dena*Cpa*(Tcdsp1(L)-Tcdaep1(L)))+0.5)

      IF (Xcf1(L).GT.Ncfr1) THEN
          Xcf1(L)=Ncfr1
          GOTO 51
      ENDIF

      DO 80 P=1,INT(Ncfr1)
      IF (Xcf1(L).LE.P) THEN
           Xcf1(L)=P
           GOTO 51
      ENDIF
80      CONTINUE

      Xcf1(L)=Ncfr1

      Iter3=0
      Iter4=0

51    Va1(L)=Xcf1(L)*(Var/Ncfr)

C     Evaporative cooling
```

```
      DeltaW1(L)=Fm1(L)/(Va1(L)*Dena)

C     The saturation pressure of water vapor
      C1=-5.8002206*10**3
      C2=1.3914993
      C3=-4.8640239*0.01
      C4=4.1764768*0.00001
      C5=-1.4452093*0.00000001
      C6=6.5459673
      Pws(L)=exp(C1/(Tcdae(L)+273.15)+C2+C3*(Tcdae(L)+273.15)
     &+C4*(Tcdae(L)+273.15)**2+C5*(Tcdae(L)+273.15)**3
     &+C6*LOG((Tcdae(L)+273.15)))

C     the increased moisture content Wdb'
      Wdb(L)=0.622*RH(L)*Pws(L)/(Pt(L)-RH(L)*Pws(L))
      Wdbp1(L)=Wdb(L)+DeltaW1(L)

C     The moist air specific enthalpy in kJ/kgda is
      Hdb(L)=1.006*Tcdae(L)+Wdb(L)*(2501+1.86*Tcdae(L))

C     The temperature of the air at the inlet of condensing ciol
      Tcdaep1(L)=(Hdb(L)-2501*Wdbp1(L))/(1.006+1.86*Wdbp1(L))

C     Pws (twb)
      Pswsb(L)=exp(C1/(Twb(L)+273.15)+C2+C3*(Twb(L)+273.15)
     &+C4*(Twb(L)+273.15)**2+C5*(Twb(L)+273.15)**3
     &+C6*LOG((Twb(L)+273.15)))

C     Humidity ratio W at twb
      Wswb(L)=0.622*Pswsb(L)/(Pt(L)-Pswsb(L))

C     Humidity ratio W at tcdaep
      Wcdaep1(L)=((2501-2.326*Twb(L))*Wswb(L)-1.006*(Tcdaep1(L)-Twb(L)))
     &/(2501+1.86*Tcdaep1(L)-4.186*Twb(L))

C     The saturation pressure of water vapor at Tcdaep1
      Pws1(L)=exp(C1/(Tcdaep1(L)+273.15)+C2+C3*(Tcdaep1(L)+273.15)
     &+C4*(Tcdaep1(L)+273.15)**2+C5*(Tcdaep1(L)+273.15)**3
     &+C6*LOG((Tcdaep1(L)+273.15)))

C     Humidity ratio W at saturation of tcdaep
      Wscdaep1(L)=0.622*Pws1(L)/(Pt(L)-Pws1(L))

C     Degreee of saturation
      DOS1(L)=Wcdaep1(L)/Wscdaep1(L)

C     Pw
      Pw1(L)=Pt(L)*Wcdaep1(L)/(0.622+Wcdaep1(L))

C     RH1
      RH1(L)=DOS1(L)/(1-(1-DOS1(L))*(Pw1(L)/Pt(L)))


      IF(RH1(L).GE.1.or.Tcdaep1(L).LE.Twb(L)) THEN
        Tcdaep1(L)=Twb(L)
        RH1(L)=1
      ENDIF

      Tcdal1(L)=Tcdaep1(L)+Qcd1(L)/(Va1(L)*Dena*Cpa)

      IF (Tcdal1(L).GT.Tcdr.AND.Xcf1(L).LT.Ncfr1) THEN
        Xcf1(L)=Xcf1(L)+1
```

```
        GOTO 51
      ENDIF

C1*** Calculate the condenser effectivenesses
      AUcd1(L)=1/(0.049*Va1(L)**-.5+.006*Frtot1(L)**-.8)
      ecd1(L)=1-EXP(-AUcd1(L)/Va1(L)/Dena/Cpa)

C1*** Calculate the condensing temperature
      Tcd1(L)=Tcdaep1(L)+(Tcdal1(L)-Tcdaep1(L))/ecd1(L)

      IF (Tcd1(L).GT.Tcd01) THEN
            Xcf1(L)=Xcf1(L)+1
            GOTO 51
       ENDIF

      IF ((Tcd01-Tcd1(L)).GT.0.05) THEN
            Tcd01=Tcd1(L)
            GOTO 52
     ENDIF

C1*** Compare Tcd(L) with Tcdr and Tcdrlow
      IF (Tcd1(L).GT.Tcdr) THEN
            Xcf1(L)=Xcf1(L)+1
            GOTO 51
      ENDIF

C1*** Calculate the power consumed by the condenser fans of circuit A
           Ecf1(L)=Xcf1(L)*Ecfr/Ncfr

C1*** Calculate the power consumed by the circuit A
           Ech1(L)=Ecc1(L)+Ecf1(L)

C1*** Calculate the coefficient of performance
          COP1(L)=Qcl1(L)/Ech1(L)

      IF (Ech1(L).LE.Ech1opt(L)) THEN
         Ech1opt(L)=Ech1(L)
         Qcl1opt(L)=Qcl1(L)
         Tchwr1opt(L)=Tchwr1(L)
         Tchws1opt(L)=Tchws1(L)
         Tev1opt(L)=Tev1(L)
         Pev1opt(L)=Pev1(L)
         AUev11opt(L)=AUev11(L)
         AUev12opt(L)=AUev12(L)
         eev11opt(L)=eev11(L)
         eev12opt(L)=eev12(L)
         Frtot1opt(L)=Frtot1(L)
         Effv1opt(L)=Effv1(L)
         Effis1opt(L)=Effis1(L)
         Effcc11opt(L)=Effcc11(L)
         Effcc12opt(L)=Effcc12(L)
         CR1opt(L)=CR1(L)
         Xcc1opt(L)=Xcc1(L)
         win1opt(L)=win1(L)
         Ecc1opt(L)=Ecc1(L)
         Tcd1opt(L)=Tcd1(L)
         Pcd1opt(L)=Pcd1(L)
         Tcdal1opt(L)=Tcdal1(L)
         Qcd1opt(L)=Qcd1(L)
         AUcd1opt(L)=AUcd1(L)
         ecd1opt(L)=ecd1(L)
         Va1opt(L)=Va1(L)
```

```
          Xcf1opt(L)=Xcf1(L)
          Vcf1opt(L)=Vcf1(L)
          Ecf1opt(L)=Ecf1(L)
          Ech1opt(L)=Ech1(L)
          COP1opt(L)=COP1(L)
          qrf1opt(L)=qrf1(L)
          Tcdaep1opt(L)=Tcdaep1(L)
          RH1opt(L)=RH1(L)
          Tcdsp1opt(L)=Tcdsp1(L)
        ENDIF

        a1=max(Twb(L)+5,20.05)

        IF (Tcdsp1opt(L).LT.a1) THEN
                goto 55
        ENDIF

        IF (Tcdsp1(L).GT.a1) THEN
              Tcdsp1(L)=Tcdsp1(L)-0.05
              goto 52
         ENDIF

55      IF (Qcl2(L).LE.0.0) THEN
        Tchwr1opt(L)=Tchwr1(L)
        Ech2opt(L)=0
        Qcl2opt(L)=0
        Tev2opt(L)=0
        Pev2opt(L)=0
        AUev2opt(L)=0
        eev2opt(L)=0
        Frtot2opt(L)=0
        Effv2opt(L)=0
        Effis2opt(L)=0
        Effcc21opt(L)=0
        Effcc22opt(L)=0
        CR2opt(L)=0
        Xcc2opt(L)=0
        win2opt(L)=0
        Ecc2opt(L)=0
        Tcd2opt(L)=0
        Pcd2opt(L)=0
        Tcdal2opt(L)=Tcdae(L)
        Qcd2opt(L)=0
        AUcd2opt(L)=0
        ecd2opt(L)=0
        Va2opt(L)=0
        Xcf2opt(L)=0
        Ecf2opt(L)=0
        Ech2opt(L)=0
        COP2opt(L)=0
        qrf2opt(L)=0
       Tcdsp2opt(L)=0
       Vcf2opt(L)=0
         GOTO 29
          ELSE
           CONTINUE
      ENDIF

C1****Cir B

C1*** Calculate the evaporator effectivenesses
66      AUev2(L)=1/(0.027*Fw(L)**(-0.8)+0.934*Qcl2(L)**(-0.745))
```

```
      eev2(L)=1-EXP(-AUev2(L)/Fw(L)/Cpw)

C1*** Calculate the evaporating temperature
      Tev2(L)=Tchwr1(L)-Qcl2(L)/Fw(L)/Cpw/eev2(L)

C1*** Calculate the evaporating pressure
      Pev2(L)=EXP(Acl+Bcl/(Tev2(L)+273.15))

C1***refrigerant state 1

      dhfg2=(hfgb/1000)*((Tc-(Tev2(L)+273.15))/(Tc-Tb))**b
      hX2=(hfo/1000)+(cpliq/1000)*(Tev2(L)+273.15-T0)+dhfg2
      h12(L)=hX2+(cpvap/1000)*Tevsh(L)
      v12=Zeta*r*(Tev2(L)+273.15)/(Pev2(L)*1000)
      Den12=1/v12-(-.0007+.0002*Pev2(L))*Tevsh(L)

C1***Compute operating parameters at compressor

         Iter2=1
         Tcd02=55
         Ech2opt=500
         Tcdsp2(L)=Tcdae(L)+15

         IF (Tcdsp2(L).LT.20) THEN
            Tcdsp2(L)=20
         ENDIF

      Tcdaep2(L)=Twb(L)

53  Pcd2(L)=EXP(Acl+Bcl/(Tcd02+273.15))
      h32(L)=(hfo/1000)+(cpliq/1000)*(Tcd02+273.15-T0-Tcdsc(L))
      qrf2(L)=hX2-h32(L)

      CR2(L)=Pcd2(L)/Pev2(L)
      Effv2(L)=.925-.009*CR2(L)
      Effis12=-.0316958*Tcd02**2+2.90112*Tcd02-.0296849*Tev2(L)**2
      Effis22=-1.45279*Tev2(L)+.000321176*Tcd02**2*Tev2(L)
      Effis32=.00683086*Tcd02*Tev2(L)+.0170575*0.5*Qcr-16.5018
      Effis2(L)=(Effis12+Effis22+Effis32)/80

      Fr2(L)=Effv2(L)*Den12*Vp


      Xcc12(L)=Qcl2(L)/Fr2(L)/qrf2(L)+0.95
      Xcc2(L)=INT(Xcc12(L))

      IF (Xcc2(L).LT.1) THEN
        Xcc2(L)=1
      ENDIF

      IF (Xcc2(L).GT.(0.5*Nccr)) THEN
        Xcc2(L)=0.5*Nccr
      ENDIF

C***  Loading sharing between compressors
      IF (PLR2(L).LE.0.5) THEN
          Xcc2(L)=1
            ELSE
            Xcc2(L)=0.5*Nccr
      ENDIF

C***  Equally shared
```

```
      IF (PLR2(L).LE.0.5) THEN
         PLR21(L)=Qcl2(L)/(0.25*Qcr)
         PLR22(L)=0
       ELSE
          PLR21(L)=0.5*Qcl2(L)/(0.25*Qcr)
          PLR22(L)=PLR21(L)
      ENDIF

C***  Loading shared
      Qcl21(L)=PLR21(L)*Qcr/4
            Qcl22(L)=PLR22(L)*Qcr/4

C1*** Calculate the refrigerant mass flow rate
      Frtot2(L)=Qcl2(L)/qrf2(L)

C1*** Calculate the refrigerant mass flow rate
      Fr21(L)=Qcl21(L)/qrf2(L)

C1*** Calculate the refrigerant mass flow rate
      Fr22(L)=Qcl22(L)/qrf2(L)

C1*** Calculate the internal compression power
      win2(L)=Pev2(L)/Den12*(ni/(ni-1))*(CR2(L)**(1-1/ni)-1)

C***  compressor efficiency
       Effcc21(L)=0.0258+0.8214*PLR21(L)+0.1932*PLR21(L)**2
       Effcc22(L)=0.0258+0.8214*PLR22(L)+0.1932*PLR22(L)**2

      IF (PLR21(L).GT.0) THEN
            Ecc21(L)=Fr21(L)*win2(L)/Effis2(L)/Effcc21(L)
            ELSE
            Ecc21(L)=0
      ENDIF

      IF (PLR22(L).GT.0) THEN
            Ecc22(L)=Fr22(L)*win2(L)/Effis2(L)/Effcc22(L)
            ELSE
            Ecc22(L)=0
     ENDIF

      Ecc2(L)=Ecc21(L)+Ecc22(L)

C1***Compute operating parameters at condenser side

      Qcd2(L)=Qcl2(L)+Frtot2(L)*(cpvap/1000)*Tevsh(L)+Ecc2(L)

      IF (Tcdsp2(L).LE.Twb(L)) THEN
        Xcf2(L)=0.5*Ncfr
        GOTO 54
      ENDIF

     Ncfr2=0.5*Ncfr

     Xcf2(L)=INT(Qcd2(L)*Ncfr/(Var*Dena*Cpa*(Tcdsp2(L)-Tcdaep2(L)))+0.5)

      IF (Xcf2(L).GT.Ncfr2) THEN
         Xcf2(L)=Ncfr2
         GOTO 54
      ENDIF


      DO 90 P=1,INT(Ncfr2)
```

```
      IF (Xcf2(L).LE.P) THEN
          Xcf2(L)=P
          GOTO 54
      ENDIF
90    CONTINUE

      Xcf2(L)=Ncfr2

      Iter5=0
      Iter6=0

54    Va2(L)=Xcf2(L)*(Var/Ncfr)

C     Evaporative cooling
      DeltaW2(L)=Fm2(L)/(Va2(L)*Dena)

C     The saturation pressure of water vapor
      C1=-5.8002206*10**3
      C2=1.3914993
      C3=-4.8640239*0.01
      C4=4.1764768*0.00001
      C5=-1.4452093*0.00000001
      C6=6.5459673
      Pws(L)=exp(C1/(Tcdae(L)+273.15)+C2+C3*(Tcdae(L)+273.15)
     &+C4*(Tcdae(L)+273.15)**2+C5*(Tcdae(L)+273.15)**3
     &+C6*LOG((Tcdae(L)+273.15)))

C     the increased moisture content Wdb'
      Wdb(L)=0.622*RH(L)*Pws(L)/(Pt(L)-RH(L)*Pws(L))
      Wdbp2(L)=Wdb(L)+DeltaW2(L)

C     The moist air specific enthalpy in kJ/kgda is
      Hdb(L)=1.006*Tcdae(L)+Wdb(L)*(2501+1.86*Tcdae(L))

C     The temperature of the air at the inlet of condensing ciol
      Tcdaep2(L)=(Hdb(L)-2501*Wdbp2(L))/(1.006+1.86*Wdbp2(L))

C     Pws (twb)
      Pswsb(L)=exp(C1/(Twb(L)+273.15)+C2+C3*(Twb(L)+273.15)
     &+C4*(Twb(L)+273.15)**2+C5*(Twb(L)+273.15)**3
     &+C6*LOG((Twb(L)+273.15)))

C     Humidity ratio W at twb
      Wswb(L)=0.622*Pswsb(L)/(Pt(L)-Pswsb(L))

C     Humidity ratio W at tcdaep
      Wcdaep2(L)=((2501-2.326*Twb(L))*Wswb(L)-1.006*(Tcdaep2(L)-Twb(L)))
     &/(2501+1.86*Tcdaep2(L)-4.186*Twb(L))

C     The saturation pressure of water vapor at Tcdaep1
      Pws2(L)=exp(C1/(Tcdaep2(L)+273.15)+C2+C3*(Tcdaep2(L)+273.15)
     &+C4*(Tcdaep2(L)+273.15)**2+C5*(Tcdaep2(L)+273.15)**3
     &+C6*LOG((Tcdaep2(L)+273.15)))

C     Humidity ratio W at saturation of tcdaep
      Wscdaep2(L)=0.622*Pws2(L)/(Pt(L)-Pws2(L))

C     Degreee of saturation
      DOS2(L)=Wcdaep2(L)/Wscdaep2(L)

C     Pw
      Pw2(L)=Pt(L)*Wcdaep2(L)/(0.622+Wcdaep2(L))
```

```
C     RH2
      RH2(L)=DOS2(L)/(1-(1-DOS2(L))*(Pw2(L)/Pt(L)))

      IF(RH2(L).GE.1.or.Tcdaep2(L).LE.Twb(L)) THEN
      Tcdaep2(L)=Twb(L)
      RH2(L)=1
      ENDIF

      Tcdal2(L)=Tcdaep2(L)+Qcd2(L)/(Va2(L)*Dena*Cpa)

      IF (Tcdal2(L).GT.Tcdr.AND.Xcf2(L).LT.Ncfr2) THEN
        Xcf2(L)=Xcf2(L)+1
      GOTO 54
      ENDIF

C1*** Calculate the condenser effectivenesses
      AUcd2(L)=1/(0.049*Va2(L)**-.5+.006*Frtot2(L)**-.8)
      ecd2(L)=1-EXP(-AUcd2(L)/Va2(L)/Dena/Cpa)

C1*** Calculate the condensing temperature
      Tcd2(L)=Tcdaep2(L)+(Tcdal2(L)-Tcdaep2(L))/ecd2(L)

       IF (Tcd2(L).GT.Tcd02) THEN
             Xcf2(L)=Xcf2(L)+1
             GOTO 54
       ENDIF

      IF ((Tcd02-Tcd2(L)).GT.0.05) THEN
             Tcd02=Tcd2(L)
             GOTO 53
      ENDIF

      IF (Tcd2(L).GT.Tcdr) THEN
             Xcf2(L)=Xcf2(L)+1
             GOTO 54
      ENDIF

C1*** Calculate the power consumed by the condenser fans of circuit B
             Ecf2(L)=Xcf2(L)*Ecfr/Ncfr

C1*** Calculate the power consumed by the circuit B
            Ech2(L)=Ecc2(L)+Ecf2(L)

C1*** Calculate the coefficient of performance of Circuit B
           COP2(L)=Qcl2(L)/Ech2(L)

    IF (Ech2(L).LE.Ech2opt(L)) THEN
      Ech2opt(L)=Ech2(L)
      Qcl2opt(L)=Qcl2(L)
      Tev2opt(L)=Tev2(L)
      Pev2opt(L)=Pev2(L)
      AUev2opt(L)=AUev2(L)
      eev2opt(L)=eev2(L)
      Frtot2opt(L)=Frtot2(L)
      Effv2opt(L)=Effv2(L)
      Effis2opt(L)=Effis2(L)
      Effcc21opt(L)=Effcc21(L)
      Effcc22opt(L)=Effcc22(L)
      CR2opt(L)=CR2(L)
      Xcc2opt(L)=Xcc2(L)
      win2opt(L)=win2(L)
```

```
      Ecc2opt(L)=Ecc2(L)
      Tcd2opt(L)=Tcd2(L)
      Pcd2opt(L)=Pcd2(L)
      Tcdal2opt(L)=Tcdal2(L)
      Qcd2opt(L)=Qcd2(L)
      AUcd2opt(L)=AUcd2(L)
      ecd2opt(L)=ecd2(L)
      Va2opt(L)=Va2(L)
      Xcf2opt(L)=Xcf2(L)
      Vcf2opt(L)=Vcf2(L)
      Ecf2opt(L)=Ecf2(L)
      Ech2opt(L)=Ech2(L)
      COP2opt(L)=COP2(L)
      qrf2opt(L)=qrf2(L)
      Tcdaep2opt(L)=Tcdaep2(L)
      RH2opt(L)=RH2(L)
      Tcdsp2opt(L)=Tcdsp2(L)
     ENDIF

      a2=max(Twb(L)+5,20.05)

      IF (Tcdsp2opt(L).LT.a2) THEN
                goto 29
      ENDIF

      IF (Tcdsp2(L).GT.a2) THEN
            Tcdsp2(L)=Tcdsp2(L)-0.05
            goto 53
      ENDIF


C1*** Calculate the coefficient of performance

29    Ecfopt(L)=Ecf1opt(L)+Ecf2opt(L)
      Echopt(L)=Ech1opt(L)+Ech2opt(L)
      Xcfopt(L)=Xcf1opt(L)+Xcf2opt(L)
      COP(L)=Qcl(L)/Echopt(L)

C***    OUTPUTS 30

      out(1)=DBLE(Qcl(L))
      out(2)=DBLE(Tchwr(L))
      out(3)=DBLE(Qcl1opt(L))
      out(4)=DBLE(Tev1opt(L))
      out(5)=DBLE(Tchwr1opt(L))
      out(6)=DBLE(Tchws1opt(L))
      out(7)=DBLE(AUev11opt(L))
      out(8)=DBLE(Frtot1opt(L))
      out(9)=DBLE(Xcc1opt(L))
      out(10)=DBLE(Tcdaep1opt(L))
      out(11)=DBLE(Tcdsp1opt(L))
      out(12)=DBLE(Tcdal1opt(L))
      out(13)=DBLE(AUcd1opt(L))
      out(14)=DBLE(Tcd1opt(L))
      out(15)=DBLE(RH1opt(L))
      out(16)=DBLE(2*Xcf1opt(L))
      out(17)=DBLE(Ecc1opt(L))
      out(18)=DBLE(Frtot2opt(L))
      out(19)=DBLE(Tev2opt(L))
      out(20)=DBLE(AUev2opt(L))
      out(21)=DBLE(Xcc2opt(L))
      out(22)=DBLE(Tcdaep2opt(L))
```

```
      out(23)=DBLE(Tcdsp2opt(L))
      out(24)=DBLE(Tcd2opt(L))
      out(25)=DBLE(AUcd2opt(L))
      out(26)=DBLE(RH2opt(L))
      out(27)=DBLE(Tcdal2opt(L))
      out(28)=DBLE(2*Xcf2opt(L))
      out(29)=DBLE(Ecc2opt(L))
      out(30)=DBLE(Echopt(L))

60    CONTINUE

      RETURN 1

      END




SUBROUTINE PROPERTY (Ifluid,To,cpliq,hfo,cpvap,cpvapcd,hfgb,Tb,Tc,
     &                b,r,Zeta,Zetacd,Gamma,Acl,Bcl,*)
      REAL Ifluid

      To=233.15

      IF (Ifluid.EQ.1) THEN
        cpliq=917
        hfo=0
        cpvap=641.6
        cpvapcd=779
        hfgb=165300
        Tb=243.4
        Tc=385.2
        b=0.37
        r=68.7539
        Zeta=0.9403
        Zetacd=0.8670
        Gamma=1.086
        Acl=14.669
        Bcl=-2443.13
      ENDIF


      IF (Ifluid.EQ.2) THEN
        cpliq=1265
        hfo=0
        cpvap=892.5
        cpvapcd=1144
        hfgb=215100
        Tb=246.9
        Tc=374.3
        b=0.376
        r=81.4899
        Zeta=0.9411
        Zetacd=0.8610
        Gamma=1.072
        Acl=15.489
        Bcl=-2681.99
      ENDIF

      IF (Ifluid.EQ.3) THEN
```

```
  cpliq=925
  hfo=0
  cpvap=693.6
  cpvapcd=784
  hfgb=136100
  Tb=276.9
  Tc=418.9
  b=0.359
  r=48.6393
  Zeta=0.9757
  Zetacd=0.9260
  Gamma=1.056
  Acl=15.107
  Bcl=-2908.73
ENDIF

IF (Ifluid.EQ.4) THEN
  cpliq=1144
  hfo=0
  cpvap=710.4
  cpvapcd=936
  hfgb=233700
  Tb=232.4
  Tc=369.2
  b=0.369
  r=96.1426
  Zeta=0.9300
  Zetacd=0.8440
  Gamma=1.114
  Acl=15.070
  Bcl=-2421.94
ENDIF

IF (Ifluid.EQ.5) THEN
  cpliq=1090
  hfo=0
  cpvap=732
  cpvapcd=965
  hfgb=172500
  Tb=227.8
  Tc=355.4
  b=0.374
  r=74.4752
  Zeta=0.9130
  Zetacd=0.8150
  Gamma=1.065
  Acl=14.809
  Bcl=-2312.21
ENDIF

IF (Ifluid.EQ.6) THEN
  cpliq=4575
  hfo=0
  cpvap=2447.1
  cpvapcd=3159
  hfgb=1372900
  Tb=239.8
  Tc=405.6
  b=0.396
  r=488.2214
  Zeta=0.9570
  Zetacd=0.8960
```

```
  Gamma=1.230
  Acl=16.204
  Bcl=-2772.39
ENDIF

RETURN 1

END
```

References

Al-Rabghi, O. M. and D. C. Hittle (2001). Energy simulation in buildings: overview and BLAST example. *Energy Conversion and Management* **42**(13): 1623-1635.

Al-Shareef, A., E. Mohamed and E. Al-Judaibi (2008). One Hour Ahead Load Forecasting Using Artificial Neural Network for the Western Area of Saudi Arabia. *International Journal of Electrical Systems Science and Engineering* **3**(1): 35-40.

Allen, B., M. Savard-Goguen and L. Gosselin (2009). Optimizing heat exchanger networks with genetic algorithms for designing each heat exchanger including condensers. *Applied Thermal Engineering* **29**(16): 3437-3444.

Alsultanny, Y. A. and M. M. Aqel (2003). Pattern recognition using multilayer neural-genetic algorithm. *Neurocomputing* **51**(0): 237-247.

Andolsun, S., C. H. Culp, J. Haberl, et al. (2011). EnergyPlus vs. DOE-2.1e: The effect of ground-coupling on energy use of a code house with basement in a hot-humid climate. *Energy and Buildings* **43**(7): 1663-1675.

Anijdan, S. H. M., A. Bahrami, H. R. M. Hosseini, et al. (2006). Using genetic algorithm and artificial neural network analyses to design an Al–Si casting alloy of minimum porosity. *Materials & Design* **27**(7): 605-609.

Aprea, C., R. Mastrullo, C. Renno, et al. (2004). An evaluation of R22 substitutes performances regulating continuously the compressor refrigeration capacity. *Applied Thermal Engineering* **24**(1): 127-139.

ARI (1998). *Refrigeration and air conditioning*. NJ: Prentice Hall, Upper Saddle River.

ARI (2003). ARI Standard 550/590: Performance rating of water chilling packages using the vapour compression cycle. Arlington, VA: Air-Conditioning, Heating and Refrigeration Institute.

ASHRAE (2009). *ASHRAE Handbook – Fundamentals*. American Society of Heating, Refrigerating and Air-conditioning Engineers, Inc. , Atlanta, GA.

ASHRAE (2010). *ASHRAE Guideline 2, Engineering analysis of experimental data*. American Society of Heating, Refrigerating and Air Conditioning Engineers, Inc., Atlanta, GA, USA.

ASHRAE. (2007). *ASHRAE Handbook – HVAC applications*. American Society of Heating, Refrigerating and Air-conditioning Engineers, Inc. , Atlanta, GA.

Azadeh, A., S. F. Ghaderi, S. Tarverdian, et al. (2007). Integration of artificial neural networks and genetic algorithm to predict electrical energy consumption. *Applied Mathematics and Computation* **186**(2): 1731-1741.

Basheer, I. A. and M. Hajmeer (2000). Artificial neural networks: fundamentals, computing, design, and application. *Journal of Microbiological Methods* **43**(1): 3-31.

Beale, M. H., M. T. Hagan and H. B. Demuth (2011). Neural Network Toolbox™ 7 User's Guide. Natick, MA: The MathWorks, Inc.

Bechtler, H., M. W. Browne, P. K. Bansal, et al. (2001a). Neural networks—a new approach to model vapour-compression heat pumps. *International Journal of Energy Research* **25**(7): 591-599.

Bechtler, H., M. W. Browne, P. K. Bansal, et al. (2001b). New approach to dynamic modelling of vapour-compression liquid chillers: artificial neural networks. *Applied Thermal Engineering* **21**(9): 941-953.

Besaw, L. E., D. M. Rizzo, P. R. Bierman, et al. (2010). Advances in ungauged streamflow prediction using artificial neural networks. *Journal of Hydrology* **386**(1-4): 27-37.

Bom, G. J., R. Foster, E. Dijkstra, et al. (1999). *Evaporative air-conditioning: Applications for environmentally friendly cooling* World Bank, Washington, DC.

Booker, L. B. and R. B. Riolo (2000). Introduction to the Special Issue: Advances in Genetic Algorithms - Research Trends and Perspectives. *Evolutionary Computation* **8**(4): 3-4.

Bourdouxhe, J., M. Grodent and J. Lebrun (1999). A Toolkit for Primary HVAC System Energy Calculation. Atlanta, GA.: ASHRAE.

Briley, G. C. (2003). Energy conservation in industrial refrigeration systems. *ASHRAE Journal* **45**(6): 46–47.

Browne, M. W. and P. K. Bansal (1998). Challenges in modeling vapor-compression liquid chillers. *ASHRAE Transactions* **104**(1A): 474-486.

Browne, M. W. and P. K. Bansal (1998). Steady state model of centrifugal liquid chillers. *International Journal of Refrigeration* **21**(5): 343-358.

Browne, M. W. and P. K. Bansal (2001a). Different modelling strategies for in situ liquid chillers. *Proceedings of the Institution of Mechanical Engineers Part A:ournal of Power and Energy* **215**(A3): 357-374.

Browne, M. W. and P. K. Bansal (2001b). An elemental NTU-ε model for vapour-compression liquid chillers. *International Journal of Refrigeration* **24**: 612-627.

Browne, M. W. and P. K. Bansal (2002). Transient simulation of vapour-compression packaged liquid chillers. *International Journal of Refrigeration* **25**(5): 597-610.

Brownell, K. A. (1998). Fixed and floating head pressure comparison for Madison Ice Arena. E. C. o. Wisconsin. Madison.

Brownell, K. A., S. A. Klein and D. T. Reindl (1999). Refrigeration system malfunctions. *ASHRAE Journal* **41**(2): 40-46.

Caldas, L. G. and L. K. Norford (2002). A design optimization tool based on a genetic algorithm. *Automation in Construction* **11**(2): 173-184.

Chan, C. W. and G. H. Huang (2003). Artificial intelligence for management and control of pollution minimization and mitigation processes. *Engineering Applications of Artificial Intelligence* **16**(2): 75-90.

Chan, K. T. and W. K. Chow (1998). Energy impact of commercial-building envelopes in the sub-tropical climate. *Applied Energy* **60**(1): 21-39.

Chan, K. T. and F. W. Yu (2002). Applying condensing-temperature control in air-cooled reciprocating water chillers for energy efficiency. *Applied Energy* **72**(3-4): 565-581.

Chan, K. T. and F. W. Yu (2006). Thermodynamic-behaviour model for air-cooled screw chillers with a variable set-point condensing temperature. *Applied Energy* **83**(3): 265-279.

Chan, W. W. and J. C. Lam (2002). Prediction of pollutant emission through electricity consumption by the hotel industry in Hong Kong. *International Journal of Hospitality Management* **21**(4): 381-391.

Chang, Y.-C., T.-S. Chan and W.-S. Lee (2010). Economic dispatch of chiller plant by gradient method for saving energy. *Applied Energy* **87**(4): 1096-1101.

Chang, Y. C. (2005). Genetic algorithm based optimal chiller loading for energy conservation. *Applied Thermal Engineering* **25**(17-18): 2800-2815.

Chen, Q., K. Worden, P. Peng, et al. (2007). Genetic algorithm with an improved fitness function for (N)ARX modelling. *Mechanical Systems and Signal Processing* **21**(2): 994-1007.

Cheung, N., C. A. Santos, J. A. Spim, et al. (2006). Application of a heuristic search technique for the improvement of spray zones cooling conditions in continuously cast steel billets. *Applied Mathematical Modelling* **30**(1): 104-115.

Chi, H.-M., O. K. Ersoy, H. Moskowitz, et al. (2007). Modeling and optimizing a vendor managed replenishment system using machine learning and genetic algorithms. *European Journal of Operational Research* **180**(1): 174-193.

Chipperfield, A., P. Fleming, H. Pohlheim, et al. (2001). *Genetic Algorithm Toolbox User's Guide*. University of Sheffield.

Chow, T. T., G. Q. Zhang, Z. Lin, et al. (2002). Global optimization of absorption chiller system by genetic algorithm and neural network. *Energy and Buildings* **34**(1): 103-109.

Chow, W. K. and K. T. Chan (1995). Parameterization study of the overall thermal-transfer value equation for buildings. *Applied Energy* **50**(3): 247-268.

Cook, D. F., C. T. Ragsdale and R. L. Major (2000). Combining a neural network with a genetic algorithm for process parameter optimization. *Engineering Applications of Artificial Intelligence* **13**(4): 391-396.

Costelloe, B. and D. Finn (2007). Thermal effectiveness characteristics of low approach indirect evaporative cooling systems in buildings. *Energy and Buildings* **39**(12): 1235-1243.

Crawley, D. B., L. K. Lawrie, F. C. Winkelmann, et al. (2001). EnergyPlus: creating a new-generation building energy simulation program. *Energy and Buildings* **33**(4): 319-331.

Deng, S.-M. and J. Burnett (2000). A study of energy performance of hotel buildings in Hong Kong. *Energy and Buildings* **31**(1): 7-12.

Diakaki, C., E. Grigoroudis and D. Kolokotsa (2008). Towards a multi-objective optimization approach for improving energy efficiency in buildings. *Energy and Buildings* **40**(9): 1747-1754.

Ding, G.-l. (2007). Recent developments in simulation techniques for vapour-compression refrigeration systems. *International Journal of Refrigeration* **30**(7): 1119-1133.

Ding, G. L. and L. Fu (2005). Performance analysis and improvement of air-to-water chiller for application in wide ambient temperature range. *Applied Thermal Engineering* **25**(1): 135-145.

Dossat, R. J. and T. J. Horan (2002). *Principles of refrigeration* NJ: Prentice Hall, Upper Saddle River.

Dounis, A. I. (2010). Artificial intelligence for energy conservation in buildings. *Advances in building energy research* **4**(1): 267 -299.

Edison, S. C. (2007). "Evaporative and Air-Cooled Condensers ", from www.sce.com/RebatesandSavings/DesignandEngineering/RTTC/ResearchProjects/SupermarketSummaries/RTTC_Project7.htm.htm.

Ekici, B. B. and U. T. Aksoy (2009). Prediction of building energy consumption by using artificial neural networks. *Advances in Engineering Software* **40**(5): 356-362.

EMSD (2004). *Hong Kong Energy End-use Data (1992-2002)*. Electrical and Mechanical Services Department, Hong Kong.

EMSD (2007). *Performance-based Building Energy Code 2007 Edition*. Electrical & Mechanical Services Department (EMSD), Hong Kong.

EMSD (2008). Scheme for wider use of fresh water in evaporative cooling towers for energy-efficient air conditioning systems. Hong Kong: Electrical and Mechanical Services Department, the Government of the Hong Kong Special Administrative Region.

EMSD (2011). *Hong Kong Energy End-use Data 2011*. Electrical and Mechanical Services Department, Hong Kong.

Esen, H., M. Inalli, A. Sengur, et al. (2008). Performance prediction of a ground-coupled heat pump system using artificial neural networks. *Expert Systems with Applications* **35**(4): 1940-1948.

Fast, M., M. Assadi and S. De (2009). Development and multi-utility of an ANN model for an industrial gas turbine. *Applied Energy* **86**(1): 9-17.

Finn, D. P. and C. J. Doyle (2000). Control and optimization issues associated with algorithm-controlled refrigerant throttling devices. *ASHRAE Transactions.* **106**(1): 524-533.

Fong, K. F., V. I. Hanby and T. T. Chow (2009). System optimization for HVAC energy management using the robust evolutionary algorithm. *Applied Thermal Engineering* **29**(11-12): 2327-2334.

Fong, K. F., C. K. Lee, T. T. Chow, et al. (2010). Solar hybrid air-conditioning system for high temperature cooling in subtropical city. *Renewable Energy* **35**(11): 2439-2451.

Gan, A. I., S. A. Klein and D. T. Reindl (2000). Analysis of refrigerator / freezer appliances having dual refrigeration cycles. *Ashrae Transactions* **106**(2): 185-191.

Gandhidasan, P. and M. A. Mohandes (2011). Artificial neural network analysis of liquid desiccant dehumidification system. *Energy* **36**(2): 1180-1186.

Garrett, J. H. (1994). Where and why artificial neural networks are applicable in civil engineering. *Journal of Computing in Civil Engineering* **8**(2): 129-130.

Gibson, G. L. (1997). A supervisory controller for optimization of building central cooling systems. *Ashrae Transactions* **103**(1): 486-493.

Goldberg, D. E. (1989). *Genetic Algorithms in Search, Optimization and Machine Learning*. Addison-Wesley Longman Publishing Co., Inc., Boston, MA, USA.

Haberschill, P., L. Gay, P. Aubouin, et al. (2003). Dynamic Model of a Vapor-Compression Refrigerating Machine Using R-407C. *HVAC&R Research* **9**(4): 451-466.

Haider, S. S. and X.-J. Zeng (2009). Simplified neural networks algorithm for function approximation on discrete input spaces in high dimension-limited sample applications. *Neurocomputing* **72**(4-6): 1078-1083.

Hajidavalloo, E. and H. Eghtedari (2010). Performance improvement of air-cooled refrigeration system by using evaporatively cooled air condenser. *International Journal of Refrigeration* **33**(5): 982-988.

Hartman, T. (2001). All-variable speed centrifugal chiller plants. *Ashrae Journal* **43**(9): 43-51.

Haykin, S. (1999). *Neural networks: A comprehensive foundation*. Prentice Hall, Upper Saddle River, N.J.

Henze, G. P. and J. Schoenmann (2003). Evaluation of reinforcement learning control for thermal energy storage systems. *HVACR Research* **9**(3): 259-275.

Holden, G. (2005). "The benefits of inverter control in air-cooled condensers." from http://www.modbs.co.uk/news/fullstory.php/aid/893.

Holland, J. H. (1992). *Adaptation in Natural and Artificial Systems*. MIT Press, Cambridge, MA, USA

Hosoz, M. and H. M. Ertunc (2006). Modelling of a cascade refrigeration system using artificial neural network. *International Journal of Energy Research* **30**(14): 1200-1215.

Hosoz, M., H. M. Ertunc and H. Bulgurcu (2007). Performance prediction of a cooling tower using artificial neural network. *Energy Conversion and Management* **48**(4): 1349-1359.

Hosoz, M., H. M. Ertunc and A. F. Ozguc (2008). Modelling of a direct evaporative air cooler using artificial neural network. *International Journal of Energy Research* **32**(1): 83-89.

Hsieh, C. C. and S. C. Yao (2006). Evaporative heat transfer characteristics of a water spray on micro-structured silicon surfaces. *International Journal of Heat and Mass Transfer* **49**(5-6): 962-974.

Hu, Y.-C. (2005). Finding useful fuzzy concepts for pattern classification using genetic algorithm. *Information Sciences* **175**(1–2): 1-19.

Huang, W. and H. N. Lam (1997). Using genetic algorithms to optimize controller parameters for HVAC systems. *Energy and Buildings* **26**(3): 277-282.

Iannella, N. and A. D. Back (2001). A spiking neural network architecture for nonlinear function approximation. *Neural Networks* **14**(6-7): 933-939.

Ilhan, B. (2012). Computational simulation methods for vehicle thermal management. *Applied Thermal Engineering* **36**(0): 325-329.

Jia, Y. Z. and T. A. Reddy (2003). Characteristic physical parameter approach to modeling chillers suitable for fault detection, diagnosis, and evaluation. *Journal of Solar Energy Engineering-Transactions of the Asme* **125**(3): 258-265.

Kalogirou, S. A. (2003). Artificial intelligence for the modeling and control of combustion processes: a review. *Progress in Energy and Combustion Science* **29**(6): 515-566.

Kalogirou, S. A. (2004). Optimization of solar systems using artificial neural-networks and genetic algorithms. *Applied Energy* **77**(4): 383-405.

Kamei, K. and M. Ishikawa (2006). Reduction of computational cost in optimization of parameter values in reinforcement learning by a genetic algorithm. *International Congress Series* **1291**(0): 185-188.

Kavchak, M. and H. Budman (1999). Adaptive neural network structures for non-linear process estimation and control. *Computers and Chemical Engineering* **23**(9): 1209-1228.

Khan, J.-u.-R. and S. M. Zubair (1999). Design and performance evaluation of reciprocating refrigeration systems. *International Journal of Refrigeration* **22**(3): 235-243.

Khattar, M. K. and H. I. Henderson (2000). Experiences with modeling supermarket energy use and performance. *IEA Supermarket Refrigeration Workshop*. Stockholm, Sweden.

King, D. J. and R. A. Potter (1998). Description of a Steady-State Cooling Plant Model Developed for Use in Evaluating Optimal Control of Ice Thermal Energy Storage Systems. *ASHRAE Transactions* **104**(1A): 42-53.

Koonce, D. A. and S. C. Tsai (2000). Using data mining to find patterns in genetic algorithm solutions to a job shop schedule. *Computers & Industrial Engineering* **38**(3): 361-374.

Koulouriotis, D. E. and A. Xanthopoulos (2008). Reinforcement learning and evolutionary algorithms for non-stationary multi-armed bandit problems. *Applied Mathematics and Computation* **196**(2): 913-922.

Koury, R. N. N., L. Machado and K. A. R. Ismail (2001). Numerical simulation of a variable speed refrigeration system. *International Journal of Refrigeration* **24**: 192-200.

Kusiak, A. and M. Li (2010). Cooling output optimization of an air handling unit. *Applied Energy* **87**(3): 901-909.

Lam, J. C. and S. C. M. Hui (1996). Sensitivity analysis of energy performance of office buildings. *Building and Environment* **31**(1): 27-39.

Lam, J. C. (2000). Energy analysis of commercial buildings in subtropical climates. *Building and Environment* **35**(1): 19-26.

Lam, J. C., D. H. W. Li and S. O. Cheung (2003). An analysis of electricity end-use in air-conditioned office buildings in Hong Kong. *Building and Environment* **38**(3): 493-498.

Lam, J. C., K. K. W. Wan, et al. (2008). Sensitivity analysis and energy conservation measures implications. *Energy Conversion and Management* **49**(11): 3170-3177.

Lee, S. H., F. W. H. Yik, J. H. K. Lai, et al. (2010). Performance modelling of air-cooled twin-circuit screw chiller. *Applied Thermal Engineering* **30**(10): 1179-1187.

Lee, W. L. and F. W. H. Yik (2002). Regulatory and voluntary approaches for enhancing energy efficiencies of buildings in Hong Kong. *Applied Energy* **71**(4): 251-274.

Li, K. and H. Su (2010). Forecasting building energy consumption with hybrid genetic algorithm-hierarchical adaptive network-based fuzzy inference system. *Energy and Buildings* **42**(11): 2070-2076.

Lin, D., M.-Q. Li and J.-S. Kou (2000). On the convergence of real-coded genetic algorithms. *Journal of Computer Research and Development* **37**(11): 1321-1327.

Lipowski, A. and D. Lipowska (2012). Roulette-wheel selection via stochastic acceptance. *Physica A: Statistical Mechanics and its Applications* **391**(6): 2193-2196.

Liu, S. and G. P. Henze (2006). Experimental analysis of simulated reinforcement learning control for active and passive building thermal storage inventory: Part 1. Theoretical foundation. *Energy and Buildings* **38**(2): 142-147.

Love, R. J., D. J. Cleland, I. Merts, et al. (2005). What is the optimum compressor discharge pressure set point for condensers. *EcoLibrium* **4**(7): 24-29.

Lu, L., W. Cai, Y. C. Soh, et al. (2005a). Global optimization for overall HVAC systems--Part II problem solution and simulations. *Energy Conversion and Management* **46**(7-8): 1015-1028.

Lu, L., W. Cai, L. Xie, et al. (2005b). HVAC system optimization--in-building section. *Energy and Buildings* **37**(1): 11-22.

Maass, W. (1997). Fast sigmoidal networks via spiking neurons. *Neural computation* **9**(2): 279-304.

Magnier, L. and F. Haghighat (2010). Multiobjective optimization of building design using TRNSYS simulations, genetic algorithm, and Artificial Neural Network. *Building and Environment* **45**(3): 739-746.

Manske, K. A., D. T. Reindl and S. A. Klein (2001). Evaporative condenser control in industrial refrigeration systems. *International Journal of Refrigeration* **24**(7): 676-691.

Massie, D. D., K. D. White and S. F. Daly (2002). Application of neural networks to predict ice jam occurrence. *Cold Regions Science & Technology* **35**(2): 115-122.

McCord-Nelson, M. and W. T. Illingworth (1991). *A practical guide to neural nets*. Addison-Wesley Longman Publishing Co., Inc. , Boston, MA, USA

Mellit, A. and S. A. Kalogirou (2008). Artificial intelligence techniques for photovoltaic applications: A review. *Progress in Energy and Combustion Science* **34**(5): 574-632.

Mellit, A., S. A. Kalogirou and M. Drif (2010). Application of neural networks and genetic algorithms for sizing of photovoltaic systems. *Renewable Energy* **35**(12): 2881-2893.

Mellit, A., S. A. Kalogirou, L. Hontoria, et al. (2009). Artificial intelligence techniques for sizing photovoltaic systems: A review. *Renewable and Sustainable Energy Reviews* **13**(2): 406-419.

Mitchell, M. (1996). *An Introduction to Genetic Algorithms*. MIT Press, Cambridge MA.

Mohanraj, M., S. Jayaraj and C. Muraleedharan (2012). Applications of artificial neural networks for refrigeration, air-conditioning and heat pump systems—A review. *Renewable and Sustainable Energy Reviews* **16**(2): 1340-1358.

Morimoto, T., J. De Baerdemaeker and Y. Hashimoto (1997). An intelligent approach for optimal control of fruit-storage process using neural networks and genetic algorithms. *Computers and Electronics in Agriculture* **18**(2-3): 205-224.

Mossolly, M., K. Ghali and N. Ghaddar (2009). Optimal control strategy for a multi-zone air conditioning system using a genetic algorithm. *Energy* **34**(1): 58-66.

Nannariello, J. and F. R. Fricke (2001). Introduction to neural network analysis and its application to building services engineering. *Building Services Engineering Research and Technology* **22**(1): 58-68.

Nassif, N., S. Kajl and R. Sabourin (2005). Optimization of HVAC control system strategy using two-objective genetic algorithm. *HVAC&R Research* **11**(3): 459-486.

Negnevitsky, M. (2005). *Artificial intelligence: A guide to intelligent systems*. Addison-Wesley.

Nguyen, H. H. and C. W. Chan (2006). Applications of artificial intelligence for optimization of compressor scheduling. *Engineering Applications of Artificial Intelligence* **19**(2): 113-126.

Nguyen, M. H., H. A. Abbass and R. I. McKay (2005). Stopping criteria for ensemble of evolutionary artificial neural networks. *Applied Soft Computing* **6**(1): 100-107.

Ning, M. and M. Zaheeruddin (2010). Neuro-optimal operation of a variable air volume HVAC&R system. *Applied Thermal Engineering* **30**(5): 385-399.

Ooka, R. and K. Komamura (2009). Optimal design method for building energy systems using genetic algorithms. *Building and Environment* **44**(7): 1538-1544.

Oswaldo, V.-L. (2005). Genetic algorithms in oil industry: An overview. *Journal of Petroleum Science and Engineering* **47**(1-2): 15-22.

Outtagarts, A., P. Haberschill and M. Lallemand (1997). The transient response of an evaporator fed through an electronic expansion valve. *International Journal of Energy Research* **21**(9): 793-807.

P.N, S. (2002). Structural pattern recognition using genetic algorithms. *Pattern Recognition* **35**(9): 1883-1893.

Peng, Y., Y. Zhang and L. Wang (2010). Artificial intelligence in biomedical engineering and informatics: an introduction and review. *Artificial Intelligence in Medicine* **48**(2-3): 71-73.

Pham, D. T. and P. T. N. Pham (1999). Artificial intelligence in engineering. *International Journal of Machine Tools and Manufacture* **39**(6): 937-949.
Phelan, J., M. J. Brandemuehl and M. Krarti (1997). In-situ performance testing of chillers for energy analysis *ASHRAE Transactions* **103**(1): 290-302.
Polat, Ö. and T. Yıldırım (2008). Genetic optimization of GRNN for pattern recognition without feature extraction. *Expert Systems with Applications* **34**(4): 2444-2448.
Priddy, K. and P. Keller (2005). *Artificial neural networks: an introduction*. The International Society for Optical Engineering, Bellingham, Washington.
Qureshi, T. Q. and S. A. Tassou (1996). Variable-speed capacity control in refrigeration systems. *Applied Thermal Engineering* **16**(2): 103-113.
Randy, L. H. and E. H. Sue (2004). *Practical genetic algorithms* John Wiley & Sons, Inc., Hoboken, New Jersey.
Reddy, T. A. and K. K. Andersen (2002). An evaluation of classical steady-state off-line linear parameter estimation methods applied to chiller performance data. *HVAC&R Research* **8**(1): 101-124.
Richard M, G. (1997). Exploring the Diversity of Artificial Neural Network Architectures. Review of Neural Networks: A Comprehensive Foundation,by Simon Haykin. *Journal of Mathematical Psychology* **41**(3): 287-292.
Roper, M. A. (2000). *Energy Efficient Chiller Control(Technical note TN 16/2000)*. Bracknell: Building Services Research and Information Association.
RVD (2011). *Hong Kong Property Review 2011*. Rating and Valuation Department, Hong Kong.
Sarkar, B. K., S. S. Sana and K. Chaudhuri (2011). Selecting informative rules with parallel genetic algorithm in classification problem. *Applied Mathematics and Computation* **218**(7): 3247-3264.
Sette, S. and L. Boullart (2000). An implementation of genetic algorithms for rule based machine learning. *Engineering Applications of Artificial Intelligence* **13**(4): 381-390.
Shen, C., L. Wang and Q. Li (2007). Optimization of injection molding process parameters using combination of artificial neural network and genetic algorithm method. *Journal of Materials Processing Technology* **183**(2-3): 412-418.
Shin, S. (1998). Constructive function-approximation by three-layer artificial neural networks. *Neural Networks* **11**(6): 1049-1058.
Sikora, R. and S. Piramuthu (2007). Framework for efficient feature selection in genetic algorithm based data mining. *European Journal of Operational Research* **180**(2): 723-737.
Singh, A. (2007). "Optimum refrigeration control with E2™." from http://www.emersonclimate.com/White%20Papers/Optimum-Refrigeration-Control-with-E2.pdf.
Smith, M. and G. King (1998). Energy saving controls for air-cooled water chillers. *Building Services Journal* **4**: 47-48.
Solar-Energy-Laboratory (2000). TRNSYS: A Transient System Simulation Program: University of Wisconsin-Madison.
Solati, B., R. Zmeureanu and F. Haghighat (2003). Correlation based models for the simulation of energy performance of screw chillers. *Energy Conversion and Management* **44**(12): 1903-1920.
Song, K.-B., Y. S. Baek, D. H. Hong, et al. (2005). Short-term load forecasting for the holidays using fuzzy linear regression method. *IEEE Transactions on Power Systems* **20**(1): 96-101.

Sörensen, K. and G. K. Janssens (2003). Data mining with genetic algorithms on binary trees. *European Journal of Operational Research* **151**(2): 253-264.
Soteris A, K. (2000). Applications of artificial neural-networks for energy systems. *Applied Energy* **67**(1-2): 17-35.
Soteris A, K. (2004). Optimization of solar systems using artificial neural-networks and genetic algorithms. *Applied Energy* **77**(4): 383-405.
Sun, J., L. Fang and J. Han (2010). Optimization of concrete hollow brick using hybrid genetic algorithm combining with artificial neural networks. *International Journal of Heat and Mass Transfer* **53**(23-24): 5509-5518.
Swider, D. J. (2003). A comparison of empirically based steady-state models for vapor-compression liquid chillers. *Applied Thermal Engineering* **23**(5): 539-556.
Swider, D. J., M. W. Browne, P. K. Bansal, et al. (2001). Modelling of vapour-compression liquid chillers with neural networks. *Applied Thermal Engineering* **21**(3): 311-329.
Tassou, S. A. and H. O. Al-Nizari (1993). Effect of refrigerant flow control on the thermodynamic performances of reciprocating chillers. *Applied Energy* **45**(2): 101-116.
Tassou, S. A. and T. Q. Qureshi (1998). Comparative performance evaluation of positive displacement compressors in variable-speed refrigeration applications. *International Journal of Refrigeration* **21**(1): 29-41.
Tissot, J., P. Boulet, F. Trinquet, et al. (2011). Air cooling by evaporating droplets in the upward flow of a condenser. *International Journal of Thermal Sciences* **50**(11): 2122-2131.
Tiwari, G. N., S. Dubey and J. C. H. FRS (2009). *Fundamentals of Photovoltaic Modules and their Applications*. Royal Society of Chemistry.
Uraikul, V., C. W. Chan and P. Tontiwachwuthikul (2007). Artificial intelligence for monitoring and supervisory control of process systems. *Engineering Applications of Artificial Intelligence* **20**(2): 115-131.
Varun and Siddhartha (2010). Thermal performance optimization of a flat plate solar air heater using genetic algorithm. *Applied Energy* **87**(5): 1793-1799.
Walczak, S. and N. Cerpa (1999). Heuristic principles for the design of artificial neural networks. *Information and Software Technology* **41**(2): 107-117.
Wang, L. (2005). A hybrid genetic algorithm-neural network strategy for simulation optimization. *Applied Mathematics and Computation* **170**(2): 1329-1343.
Wang, S. W. (1998). Dynamic simulation of a building central chilling system and evaluation of EMCS on-line control strategies. *Building and Environment* **33**(1): 1-20.
Wang, S.W. and Z.J. Ma (2008). Supervisory and Optimal Control of Building HVAC Systems: A Review. *HVAC&R Research* **14**(1): 3-32.
Wang, S. W. and Y. M. Chen (2002). Fault-tolerant control for outdoor ventilation air flow rate in buildings based on neural network. *Building and Environment* **37**(7): 691-704.
Wang, S. W. and X. Q. Jin (2000). Model-based optimal control of VAV air-conditioning system using genetic algorithm. *Building and Environment* **35**(6): 471-487.
Wang, S. W., J. Wang and J. Burnett (2000). Mechanistic model of centrifugal chillers for HVAC system dynamics simulation. *Building Services Engineering Research & Technology* **21**(2): 73-83.

Wang, S. W. and X. H. Xu (2006). Parameter estimation of internal thermal mass of building dynamic models using genetic algorithm. *Energy Conversion and Management* **47**(13-14): 1927-1941.

Wang, W., R. Zmeureanu and H. Rivard (2005). Applying multi-objective genetic algorithms in green building design optimization. *Building and Environment* **40**(11): 1512-1525.

Wright, J. A. and V. I. Hanby (1987). The formulation, characteristics and solution of HVAC system optimized design problems. *ASHRAE Transactions* **93**(2): 2133-2145.

Wright, J. A., H. A. Loosemore and R. Farmani (2002). Optimization of building thermal design and control by multi-criterion genetic algorithm. *Energy and Buildings* **34**(9): 959-972.

Wu, J., G. Zhang, Q. Zhang, et al. (2011). Artificial neural network analysis of the performance characteristics of a reversibly used cooling tower under cross flow conditions for heat pump heating system in winter. *Energy and Buildings* **43**(7): 1685-1693.

Xie, G. N., B. Sunden and Q. W. Wang (2008). Optimization of compact heat exchangers by a genetic algorithm. *Applied Thermal Engineering* **28**(8-9): 895-906.

Xie, Q. S. (2003). *Neural Net Method in Mechanical Engineering*. China Machine Press, Beijing.

Xin, F. (2000). *Basic theory and method of neural net intelligence*. Southwest Jiaotong University Press, Chengdu.

Xin, L. (1996). Simultaneous approximations of multivariate functions and their derivatives by neural networks with one hidden layer. *Neurocomputing* **12**(4): 327-343.

Xu, S. and L. Chen (2008). A novel approach for determining the optimal number of hidden layer neurons for FNN's and its application in data mining. *5th International Conference on Information Technology and Applications (ICITA 2008)*. Cairns, Queensland, Australia**:** 683-686

Yamany, S. M., K. J. Khiani and A. A. Farag (1997). Application of neural networks and genetic algorithms in the classification of endothelial cells. *Pattern Recognition Letters* **18**(11–13): 1205-1210.

Yao, Y. and J. Chen (2010). Global optimization of a central air-conditioning system using decomposition–coordination method. *Energy and Buildings* **42**(5): 570-583.

Yao, Y. B. and J. L. Wang (2002). Research on raising BP network training speed. *Information Technology* **1**: 4-6 (in Chinese).

Yik, F. W. (2001). A climatic variable for constructing thermal performance lines for air-conditioned commercial buildings in Hong Kong. *Building Services Engineering Research & Technology* **22**(4): 219-236.

Yik, F. W. H., J. Burnett and I. Prescott (2001). Predicting air-conditioning energy consumption of a group of buildings using different heat rejection methods. *Energy and Buildings* **33**(2): 151-166.

Yik, F. W. H. and V. K. C. Lam (1998). Chiller models for plant design studies. *Building Services Engineering Research and Technology* **19**(4): 233-241

Yip, P. C. and S. C. M. Hui (1991). Selection of heat rejection methods for air conditioning systems in Hong Kong. *Procedding of the CIBSE National Conference 1991*: University of Kent, Canterbury**:** 73-89.

Yu, F. W. and K. T. Chan (2005a). Electricity end-use characteristics of air-cooled chillers in hotels in Hong Kong. *Building and Environment* **40**(1): 143-151.

Yu, F. W. and K. T. Chan (2005b). Application of direct evaporative coolers for improving the energy efficiency of air-cooled chillers. *Journal of Solar Energy Engineering-Transactions of the Asme* **127**(3): 430-433.

Yu, F. W. and K. T. Chan (2006a). Life cycle analysis of enhanced condenser features for air-cooled chillers serving air-conditioned buildings. *Building and Environment* **41**(8): 981-991.

Yu, F. W. and K. T. Chan (2006b). Modelling of the coefficient of performance of an air-cooled screw chiller with variable speed condenser fans. *Building and Environment* **41**(4): 407-417.

Yu, F. W. and K. T. Chan (2007). Part load performance of air-cooled centrifugal chillers with variable speed condenser fan control. *Building and Environment* **42**(11): 3816-3829.

Yu, F. W. and K. T. Chan (2009). Modelling of improved energy performance of air-cooled chillers with mist pre-cooling. *International Journal of Thermal Sciences* **48**(4): 825-836.

Yu, F. W., K. T. Chan and H. Y. Chu (2006). Constraints of using thermostatic expansion valves to operate air-cooled chillers at lower condensing temperatures. *Applied Thermal Engineering* **26**(17-18): 2470-2478.

Zhang, H., S. You, H. Yang, et al. (2000). Enhanced performance of air-cooled chillers using evaporative cooling. *Building Services Engineering Research and Technology* **21**(4): 213-217

Zhang, J. and A. J. Morris (1998). A sequential learning approach for single hidden layer neural networks. *Neural Networks* **11**(1): 65-80.

Zhang, Y., Y. Fang, X. Huang, et al. (2007). Experimental study of the interation between the water mists and PVC fire. *Process Safety and Environmental Protection* **85**(1): 39-44.

Zhou, L. and F. Haghighat (2009). Optimization of ventilation system design and operation in office environment, Part I: Methodology. *Building and Environment* **44**(4): 651-656.

Znouda, E., N. Ghrab-Morcos and A. Hadj-Alouane (2007). Optimization of Mediterranean building design using genetic algorithms. *Energy and Buildings* **39**(2): 148-153.